Dissertation

Studies of multiple scattering in low-dimensional sytems

ausgeführt zum Zwecke der Erlangung des akademischen Grades
eines Doktors der Naturwissenschaften

unter der Leitung von
Ao.Univ.Prof.i.R. Dipl.-Ing. Dr.techn. Peter Kasperkovitz
Institut für Theoretische Physik (136)

eingereicht an der Technischen Universität Wien,
Fakultät für Physik

von
Dipl.-Ing. Martin Nigsch
Martikelnummer 9525720
Danhausergasse 9/1
1040 Wien

Wien, am 8. Februar 2006

Kurzfassung

In dieser Arbeit werden drei Modelle in Zusammenhang mit zeitunabhängiger sowie zeitabhängiger Streuung an mehreren Objekten analytisch und numerisch diskutiert. Für diese Modelle wurden Programme entwickelt, die numerische Näherungen für die Lösungen der entsprechenden Gleichungen produzieren. Allen Systemen gemeinsam ist eine mathematische Beschreibung, mit der die erhaltenen Ergebnisse im Rahmen der Maxwell-Theorie, der Akustik oder der Quantenmechanik interpretiert werden können.

Das erste System ist ein zweidimensionales System, welches aus elliptischen nicht überlappenden Zylindern besteht, die in einem homogenen Medium eingebettet sind, wobei die Anzahl der Zylinder, ihre Position und Geometrie sowie ihre Materialkonstanten frei gewählt werden können. Die Lösung des entsprechenden zeitunabhängigen Streuproblems liefert die asymptotische Winkelabhängigkeit der Intensitätsverteilung der gestreuten Welle, wobei auf die Interferenz mit der einfallenden Welle nicht näher eingegangen wird. Diese Lösung wird mit einem Separationsansatzes in elliptischen Koordinaten zuerst für einen Zylinder erhalten. Um diese Lösungen für einen elliptischen Zylinder darstellen zu können, sind spezielle Funktionen notwendig, die sogenannten Mathieufunktionen. Diese sind zwar in der einschlägigen Literatur zu finden, sind aber im Allgemeinen eher wenig bekannt. Die Streuung an einem einzelnen elliptischen Zylinder kann noch mit den Mathieufunktionen berechnet werden, die in öffentlich verfügbaren Bibliotheken erhältlich sind. Um die Streuung an mehreren solchen Objekten zu berechnen, ist die numerische Beherrschung des Additionstheorems für Mathieufunktionen notwendig. Von diesem existiert derzeit keine allgemein verfügbare Implementierung. Darüber hinaus stellte sich heraus, dass es für die numerische Konvergenz in dem gewünschten Parameterbereich notwendig war, die Mathieufunktionen mit weitaus größerer Präzision zu berechnen als dies die oben erwähnten Programme tun. Es war somit eine Hauptaufgabe dieser Dissertation, ein Programmpaket zur Berechnung der Mathieufunktionen und dem zugeordneten inneren Additionstheorem in beliebiger Präzision zu erstellen und zu testen.

Aus einer Überlagerung von zeitunabhängigen Lösungen mit einem geeigneten Gewichtsfaktor erhält man eine zeitabhängige Version des Streuproblems, in welchem ein zunächst freies Wellenpaket auf die Streuer trifft. In der Nähe der Streuer treten dann Interferenzeffekte auf, welche mit der zeitunabhängigen Theorie nicht beschrieben werden können. Lange nach dem Streuprozess nähert sich dann die zeitabhängige Lösung der schon vorhin berechneten zeitunabhängigen an. Die numerische Berechnung dieser zeitabhängigen Lösungen erwies sich

als sehr aufwändig: die erwähnte Überlagerung der zeitunabhängigen Lösungen muss für eine sehr grosse Zahl von Richtungen und Wellenlängen durchgeführt werden, was das Interesse an der praktischen Anwendung dieser numerischen Lösung begrenzt. Da sie allerdings mit beliebiger Präzision für beliebige Zeiten berechnet werden kann, ist das erstellte Programm als Refernz für Vergleiche mit anderen Methoden durchaus interessant. Weiters ist mit der Weiterentwicklung der Computertechnik zu erwarten, dass das Programm in der heutigen Form in einiger Zeit durchaus auch dazu verwendet werden kann, physikalische Anwendungen wie photonische Kristalle zu simulieren.

Das zweite System besteht ebenfalls aus zweidimensionalen Dirichlet-Streuern, diesmal von beliebiger Form, die sich in einem durch Dirichlet-Randbedingungen gegebenen Wellenleiter befinden. In diesem Modell können größere Anordnungen von Streuern betrachtet werden, insbesonders dann, wenn sie regelmäßig wiederkehren, da freie Lösungen an verschiedenen Querschnitten des Wellenleiters immer mittels der sogenannten Transfermatrix miteinander in Beziehung gebracht werden können. Ein Programm wurde erstellt, welches die zeitunabhängige Lösung für eine Anordnung von gleichen, durch eine geschlossene Kurve parametrisierbare Streuern berechnet. Mit diesem Programm sollen in Zukunft Lokalisierungseffekte in zwei Dimensionen gesucht werden.

Um diese Lokalisierungseffekte besser zu verstehen, wurde die Untersuchung des dritten Modells gestartet: dieses ist ein eindimensionales Modell, welches aus einem Dirac-Kamm besteht, bei dem nur endlich viele Potenziale ungleich Null sind; es kann als einfaches Modell für einen unvollkommenen eindimensionalen Kristall gesehen werden. Wenn die Potenzialverteilung symmetrisch ist, so können lokalisierte Zustände sowohl analytisch wie auch numerische gefunden werden. Das neue an diesem Zugang ist, dass analytisch der Zusammenhang zwischen Transmissionskoeffizient und einem in dieser Arbeit definierten Lokalisierungsmaß hergeleitet wurde. Des weiteren wurde in einer zeitabhängigen Rechnung ein Wellenpaket simuliert, welches ausserhalb des endlichen „Kristalles" startet, in diesen eindringt, zum Teil reflektiert oder transmittiert wird, zum anderen Teil aber relativ lange im Kristall eingeschlossen bleibt, bevor es langsam wieder herausfliesst.

Abstract

In this thesis three models related to time-independent and time-dependent scattering at several obstacles are discussed both analytically and numerically. Programs which produce numerical approximations to the solutions were developped for these three models. All systems have in common that they are described in a framework which permits to interpret the results obtained in Maxwell theory, in acoustics, and in quantum mechanics.

The first system is a two-dimensional one which consists of elliptical, non-overlapping cylinders embedded in a homogeneous medium. The number of cylinders, their relative positions and geometries as well a their material constants are parameters which may be freely choosen. The solution of the corresponding time-independent scattering problem yields the asymptotic angular dependence of the scattered wave but does not provide information on its interaction with the incident wave. This solution is first obtained for one cylinder using the separation of variables technique in an elliptical coordinate system. To express these solutions for one elliptical cylinder one needs special functions, the so-called Mathieu functions: although they can be found in literature, their knowledge and use is not widespread. Scattering at one single elliptical cylinder may be calculated with a numerical implementation of Mathieu functions which are publicly available. For the same calculation with several objects, a reliable implementation of the addition theorem for Mathieu functions is needed; presently, no such library is available. During the implementation, it was found that in order to obtain numerical convergence of this addition theorem for the desired parameter range, it was necessary to know the Mathieu functions with a much greater precision than provided by already existing and available implementations. Therefore, one of the principal tasks of this thesis was to produce and test a software package which provides reliable approximations for Mathieu functions and the corresponding inner addition theorem. This required the implementation of an internal part of the calculation in arbitrary precision arithmetic.

In the sequel time-dependent solutions of the scattering process were obtained by superposition of time-independent solutions with appropriate weight factors. In these time-dependent solutions, a free wave packet which is free in the beginning hits the scatterers. In the vicinity of the scatterers, interference effects occur which cannot be described by time-independent theory. A long time after the scattering process, the time-dependent solution converges asymptotically to the already calculated time-independent solution. The numerical

calculation of this time-dependent solutions turned out to be very expensive in terms of computational cost: the superposition of the time-independent solutions has to be performed for a large number of directions and wavelengths. This limits the possibility of an application of this numerical scheme to physical problems of practical interest. However, as the solution can be calculated with arbitrary precision for arbitrary times, the program should be of interest as a reference for comparison with other methods. As well, one can expect that with ongoing development of computer technology it will become possible to use the program in its present form to simulate physical devices like photonic crystals.

The second system studied consists of Dirichlet scatterers of arbitrary shape which are placed in a waveguide given by Dirichlet boundary conditions. In this model, one can study more extended structures of scatterers, in particular regular arrays, because free solutions at different cross sections in the waveguide can be related with the transfer matrix technique. A repetition of this process yields a repetition of the structure; the numerical realisation of this is computationally very cheap. A program has been written which calculates a time-independent solution of a given structure of identical scatterers which may be described by a closed curve. With this program, it is intended to study localisation effects in two dimensions.

In order to get more insight into localisation effects in two and three dimensions, the analysis of a third model was undertaken. This model consists of a Dirac comb in one dimension with only a finite number of non-zero potentials. It may be seen as a simple model for an imperfect one-dimensional crystal. If the potential distribution is symmetrical, localised states can be found analytically and numerically. An interesting result is the fact that maxima of the transmission and localisation (in a measure defined in this work) are related to each other. As well, in a time-dependent simulation, a wave packet was simulated which starts from outside of this finite "crystal", enters the crystal, is partially reflected or transmitted, but in part also kept enclosed in the crystal for a relatively long time before it dissipates slowly.

To Ingeborg

Acknowledgements

Special and sincere thanks go first of all to my supervisor Professor Peter Kasperkovitz, with whom it has been a privilege to work, for his guidance and insight, his constant willingness to help me, and his patience.

Moreover, I am most grateful to Professor Angus MacKinnon from the Condensed Matter Theory Group at Imperial College, London, who kindly accepted me as an academic visitor during the final phase of my thesis.

Furthermore, I am much obliged to the Center for Computational Materials Science who financed this thesis as well as my stay in London. In particular, my sincere thanks go to Professor Rainer Dirl who was very helpful during the last three years.

Further thanks go to all my friends and colleagues who supported this work in multifarious ways in Vienna as well as in London. In particular, I would like to express my thanks to Bernhard Petersch, Severin Puschkarski, Arnold Rofner, Markus Demetz, Christian Tutschka, Harald Stockinger, Wayne Williams, Nicholas Hine, Jonathan Le Page, Ben Wood, Oliva Garcia Cantú Ros, and Sabrina Rabello.

Extraordinary thanks go to my dear darling Ingeborg for her invaluable wholehearted support day after day and for enduring me smilingly in the last phase of this thesis.

For always being here for me when I need them, particular thanks go to my family: my aunt, Ella, my cousin, Markus, and my brothers, Florian and Eduard.

Most of all, I am formidably thankful to my parents Otto and Waltraud, who helped me morally, culinarily, and financially over the last three years. Thank you in particular for inciting me to continue this work when I was about to lose my enthusiasm – this thesis would not have been possible without you. Danke!

Contents

List of Figures

List of Tables

Chapter 1

Introduction

The physical problem considered in this thesis is multiple scattering [1] of waves, i.e., scattering in one and two dimensions by finite arrays of objects with various boundary conditions. In this context, *scattering* means the interaction of an incident field with one or more obstacles. The solution of this problem is theoretically interesting and important in many areas of physics, whence it is a classical topic of research. The solution of the problem of many scatterers is more complex than for one and thus it took longer to understand it: one of the first papers on multiple scattering was written by Záviška in 1913 [2]; for recent research see, e.g., [3], where a problem similar to the one studied in chapter 3 is discussed. The notion of multiple scattering refers to a recursive way of solving the problem of scattering by several objects: the mathematical description of the physical process starts by ignoring completely the interaction between the waves of the individual obstacles, then introduces various 'orders of scattering' by taking the scattered waves from every obstacle as new incoming waves. This process eventually leads to a converging series and is one way to treat scattering by several objects.

In this thesis, we consider several models. In all of them it is assumed that the reaction of the objects to the incoming field may be described by linear response theory. The first model considered is scattering of electrodynamic, acoustical or quantum mechanical waves by elliptical cylinders. The necessary mathematical framework is formulated in chapter 2 along with the boundary conditions and asymptotic conditions at infinity which allow one to obtain a unique solution of the problem. The reason why elliptical cylinders were chosen is that it provides for each obstacle two more degrees of freedom than in the simplest model (cylindrical obstacles): the ratio of the axes and the orientation may be varied for each cylidner. Formally this problem is closely related to the three-dimensional problem of scattering by ellipsoids. Despite of the general analogy and the close relation of the special functions involved the treatment in two dimensions is much simpler because only one scalar function of two variables has to be computed. Thus it seemed to be reasonable to study this

problem first.

The time-independent scattered fields are calculated in chapter 3 using the separation of variables technique for an arbitrary number of scatterers with given positions, geometries and material constants. The separation of variables technique is based on the choice of the 'right' coordinate system in which the Helmholtz equation is solved; it anticipates the fact that in the following the vacuum does not fill the whole space but only the exterior of one or more regions which have a simple geometrical form in an appropriately chosen coordinate system. The scattered wave is then expanded in eigenfunctions of the Helmholtz equations. To determine the yet unknown coefficients of the expansion of the scattered wave, we employ the boundary conditions described in chapter 2. During this process, the field inside the scatterer is calculated, too.

If two or more scatterers are present it is not possible to solve the scattering problem by simply adding the scattering waves of the isolated single scatterers to the incident plane wave. The first-order multiple scattering approximation is obtained if the response of the second cylinder to the primary scattering wave of the first cylinder is added to the primary scattering wave of the second cylinder, and vice versa. This yields the already mentioned iteration scheme which converges to the solution of the multiple scattering problem: the incoming plane wave plus an outgoing scattering wave for each scatterer. The mathematical tool needed to realise this program is the so-called addition theorem where an outgoing wave related to one coordinate system is expressed as superposition of regular partial waves related to another coordinate system.

The second model is described in chapter 4: the physical process of scattering is now taking place in the interior of a waveguide with Dirichlet boundary conditions. The waveguide has the advantage that by means of the transfer matrix method, which relates free solutions at two cross sections of the waveguide, calculations for bigger structures or even a periodic structure are easier performed. The solution is based on the Green's function method for an arbitrary number of Dirichlet scatterers of arbitrary shape.

One application of multiple scattering is to understand localisation effects due to constructive and destructive interference. The concepts for these localisation phenomena are discussed in chapter 5 with a one-dimensional model system based on a transfer matrix approach. This approach turns out to be useful for finite structures, both regular and irregular ones. In the first ones, the concept of bands and gaps can be introduced with great advantage: they express the fact that, depending on their wavelengths, some waves can penetrate the structure in question while others cannot. An interesting phenomenon is localisation, in particular time-dependent localisation which is not so commonly studied. In chapter five, the situation of a wave packet entering a finite one-dimensional crystal described by a Dirac comb is discussed in detail and related to 'localised states'.

In order to proceed from the time-independent solutions already found to time-dependent ones, we introduce in chapter 6 a weighted integral over two-dimensional k space which yields a time-dependent solution. Here, the choice of an efficient integration method is crucial for the numerical approximation. Details of this choice are given in chapter 8.

In chapter seven, Mathieu functions are described in detail. They are special functions analogous to sine and cosine, with the difference that the underlying coordinate system is not circular but elliptical. These functions were used in chapter 3 for time-independent scattering by elliptical scatterers embedded in vacuum.

In chapter 8, the chosen numerical implementation of the formulas presented in the previous chapters is described in some detail. Chapter 9 presents numerical results obtained with the code written during this thesis, and finally, chapter 10 summarises, concludes and gives an outlook.

Chapter 2

Formulation of the problem

In this chapter, the physical problems and the equations used to describe them are presented. In particular, a common framework is formulated for electromagnetic, quantum mechanical, and acoustical scattering problems. We start by explaining what is meant by scattering and then introduce the mathematical framework we are working with, the meaning of the parameters entering there, and the boundary conditions needed to obtain a unique solution of the given problem.

2.1 Introduction to scattering

Fig. 2.1 shows a schematic view of the scattering problem considered here. An *incident field* u^{in} interacts with a *scatterer* which occupies a bounded region O with surface ∂O in two-dimensional space $\mathbb{R}^2$. The *total field* u^{tot} in the

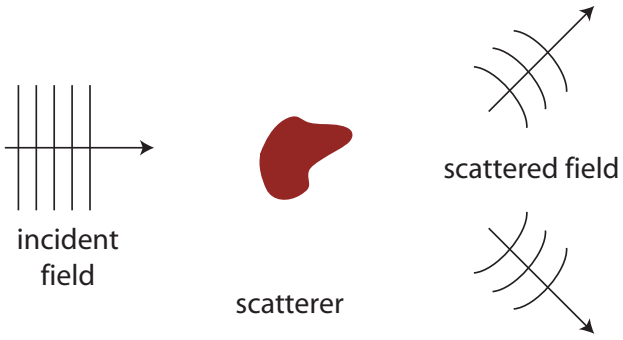

Figure 2.1: Schematic scattering process

surrounding medium $\mathbb{R}^2 \setminus O$ is equal to the sum of the incident and the *scattered field*, i.e. $u^{\text{tot}} = u^{\text{in}} + u^{\text{sc}}$. The field inside the scatterer is called the *internal field* u^{int}. The problem is to determine the unknown scattered and internal fields in

terms of the known incident fields. The mathematical formulation is based on Helmholtz equations in $\mathbb{R}^2 \setminus O$ and O, boundary conditions on ∂O that depend on the physical nature of the field (electromagnetism, quantum mechanics, and acoustics), and an asymptotic boundary condition far away from the scatterer which we introduce in chapter 3. We show that with certain assumptions, we can find the same basic equations regardless of the theory we are working with. Thus, it is possible to interpret the results obtained in this thesis as solutions of electrodynamic, quantum mechanical, and acoustical problems.

Figure 2.2: Schematic evolution of a free wave packet

The *time-dependent scattering* process for one scatterer is sketched here in order to illustrate time-dependent scattering and also to relate it to *time-independent scattering*. In Fig. 2.2 a free gaussian wave packet moves upwards with constant velocity, its horizontal extension being essential given by the two branches of a hyperbola (cf. chapter 6). If a scatterer is placed at the center of this hyperbola, the initial evolution of the wave packet is the same as long as the packet is sufficiently far away from the obstacle (Fig. 2.3). Long after scattering process the wave packet is concentrated in a ring which moves outwards from the scatterer with constant velocity. The wave packet is given

Figure 2.3: Schematic evolution of a scattered wave packet long before and long after the scattering process

by the superposition of the original *free wave packet* and a *scattering wave packet* both located within the ring. The angular dependence of the scattering wave packet is usually determined by time-independent scattering theory. Note that within the hyperbola the two packets interfere, reducing the intensity in the forward direction. This corresponds to the shadow caused by the obstacle. Information about the scattering process, e.g., the structure of the wave packet in the vicinity of the scatterer, is implicitly fixed by time-independent theory but cannot be easily deduced from this theory.

The time-dependent general equation is

$$\left(\Delta - \frac{1}{c^2(\mathbf{x})}\frac{\partial^2}{\partial t^2}\right) u(\mathbf{x},t) = 0, \tag{2.1}$$

where we assume that

$$\lim_{|\mathbf{x}|\to\infty} c(\mathbf{x}) = c_0. \tag{2.2}$$

The Fourier transform

$$u(\mathbf{x},t) = \frac{1}{2\pi}\int_{-\infty}^{\infty} u(\mathbf{x},\omega)e^{-i\omega t}\,\mathrm{d}\omega \tag{2.3}$$

and its inverse

$$u(\mathbf{x},\omega) = \int_{-\infty}^{\infty} u(\mathbf{x},t)e^{i\omega t}\,\mathrm{d}t \tag{2.4}$$

yield a time-independent version of (2.1) for every value of ω:

$$\left(\Delta + \gamma^2 k^2\right) u(\mathbf{x}) = 0, \tag{2.5}$$

with

$$c_0 k = \omega, \qquad \gamma(\mathbf{x}) = \frac{c_0}{c(\mathbf{x})}. \tag{2.6}$$

$\gamma(\mathbf{x})$ is a function whose meaning depends on the underlying physical theory. In our models, $\gamma(\mathbf{x})$ is constant inside and outside the obstacle with different values.

$$\gamma(\mathbf{x}) = \begin{cases} 1 & \mathbf{x} \in \mathbb{R}^2 \setminus O \\ \gamma \neq 1 & \mathbf{x} \in O \end{cases} \tag{2.7}$$

It will be specified later on for the three theories under consideration. We will only consider boundary conditions at the surface ∂O which can be put into the following general form[1].

$$u(\mathbf{x})\big|_{\mathbf{x}\in\partial O^+} = \gamma_0 u(\mathbf{x})\big|_{\mathbf{x}\in\partial O^-} \tag{2.8}$$

$$\frac{\partial}{\partial \mathbf{n}} u(\mathbf{x})\big|_{\mathbf{x}\in\partial O^+} = \gamma_1 \frac{\partial}{\partial \mathbf{n}} u(\mathbf{x})\big|_{\mathbf{x}\in\partial O^-} \tag{2.9}$$

Eqns. (2.7) and (2.8) may be generalised in an obvious way for any finite number of obstacles.

[1] This means that we do not consider acoustical impedance boundary conditions

2.2 Electromagnetism

In SI units, the Maxwell equations in a medium read as follows.

$$\begin{aligned} \operatorname{div} \mathbf{D} &= \rho && (2.10)\\ \operatorname{rot} \mathbf{E} + \frac{\partial \mathbf{B}}{\partial t} &= \mathbf{0} && (2.11)\\ \operatorname{div} \mathbf{B} &= 0 && (2.12)\\ \operatorname{rot} \mathbf{H} - \frac{\partial \mathbf{D}}{\partial t} &= \mathbf{J} && (2.13) \end{aligned}$$

$\mathbf{J}$ and ρ denote the free current density and the free charges. They are sources which are independent of the materials, i.e., all the induced currents and charges are included in the fields $\mathbf{H}$ and $\mathbf{D}$. The medium is characterised by two macroscopic fields: the *polarisation density* $\mathbf{P}$ and the *magnetisation density* $\mathbf{M}$, which are related to the fields $\mathbf{D}$, $\mathbf{E}$, $\mathbf{B}$ and $\mathbf{H}$ by [4]

$$\begin{aligned} \mathbf{D} &= \epsilon_0 \mathbf{E} + \mathbf{P} = (1 + \chi_e\ )\, \epsilon_0 \mathbf{E} = \epsilon_r \epsilon_0 \mathbf{E} = \epsilon \mathbf{E}, && (2.14)\\ \mathbf{B} &= \mu_0\, (\mathbf{H} + \mathbf{M}) = (1 + \chi_m\ )\, \mu_0 \mathbf{H} = \mu_r \mu_0 \mathbf{H} = \mu \mathbf{H}. && (2.15) \end{aligned}$$

In these formulas, the quantities characterising the materials are called as follows: χ_e is the *electrical susceptibility*, χ_m the *magnetic susceptibility*, ϵ is called *electrical permittivity*, and finally μ is known as the *magnetic permeability*. The constants ϵ_0 and μ_0 are the vacuum values of ϵ and μ. They are related to the vacuum velocity of light c_0 by the relation

$$\epsilon_0 \mu_0 = \frac{1}{c_0^2}. \tag{2.16}$$

We limit ourselves to isotropic, homogeneous materials, i.e., ϵ_r and μ_r are scalar quantities whose magnitude does not depend on the field strengths, but may depend on the position in space. In this case Maxwell's equations reduce to

$$\begin{aligned} \operatorname{div} \mathbf{E} &= \frac{\rho}{\epsilon_r \epsilon_0}, && (2.17)\\ \operatorname{rot} \mathbf{E} + \frac{\partial \mathbf{B}}{\partial t} &= \mathbf{0}, && (2.18)\\ \operatorname{div} \mathbf{B} &= 0, && (2.19)\\ \operatorname{rot} \mathbf{B} - \frac{\epsilon_r \mu_r}{c_0^2} \frac{\partial \mathbf{E}}{\partial t} &= \mu_r \mu_0 \mathbf{J}. && (2.20) \end{aligned}$$

Note that the frequency dependence of ϵ and μ is neglected in these equations, although every real material exhibits such a dependence. However, this dependence is not crucial for our purposes. In the following, we will limit ourselves to a material with all the restrictions mentioned so far. Using the equality

$$\operatorname{rot} \operatorname{rot} \mathbf{A} = \operatorname{grad} \operatorname{div} \mathbf{A} - \Delta \mathbf{A} \tag{2.21}$$

we get by straightforward combination of Maxwell equations the inhomogeneous vector Helmholtz equation

$$\Delta \mathbf{E} - \frac{\epsilon_r \mu_r}{c_0^2} \frac{\partial^2 \mathbf{E}}{\partial t^2} = \mu_r \mu_0 \mathbf{J}. \tag{2.22}$$

Boundary conditions

If a change in the material constants occurs – caused by the obstacle O with surface ∂O that we intend to study – the normal components of $\mathbf{D}$ and $\mathbf{B}$ and the tangential components of $\mathbf{E}$ and $\mathbf{H}$ on either side of the obstacle are related according to [4]

$$\begin{aligned} \mathbf{n} \cdot (\mathbf{D}_2 - \mathbf{D}_1) &= \sigma, & (2.23)\\ \mathbf{n} \times (\mathbf{E}_2 - \mathbf{E}_1) &= \mathbf{0}, & (2.24)\\ \mathbf{n} \cdot (\mathbf{B}_2 - \mathbf{B}_1) &= 0, & (2.25)\\ \mathbf{n} \times (\mathbf{H}_2 - \mathbf{H}_1) &= \mathbf{K}. & (2.26) \end{aligned}$$

$\mathbf{n}$ denotes the normal vector on ∂O. Here, it is assumed that the external charge density ρ is singular at the interface and may therefore be interpreted as an idealised surface charge density σ. As well, $\mathbf{K}$ is the idealised surface current flowing on ∂O. Note that these still are the external sources and not any induced charges or induced current densities. The induced charges and currents are reflected in the discontinuities at ∂O of the normal component of $\mathbf{E}$ and the tangential component of $\mathbf{B}$.

Harmonic time dependence

Fields with a harmonic time dependence $e^{-i\omega t}$, where $\omega = kc_0$, lead to the following Fourier decomposition of the Maxwell equations.

$$\begin{aligned} \operatorname{div} \mathbf{E}_k &= \frac{\rho}{\epsilon_r \epsilon_0} & (2.27)\\ \operatorname{rot} \mathbf{E}_k - i\omega \mathbf{B}_k &= \mathbf{0} & (2.28)\\ \operatorname{div} \mathbf{B}_k &= 0 & (2.29)\\ \operatorname{rot} \mathbf{B}_k + i\omega \frac{\epsilon_r \mu_r}{c_0^2} \mathbf{E}_k &= \mu_r \mu_0 \mathbf{J}_k. & (2.30) \end{aligned}$$

With $\frac{\omega^2}{c_0^2} = k^2$ the wave equations for the electric and the magnetic field become

$$\begin{aligned} \left(\Delta + \epsilon_r \mu_r k^2\right) \mathbf{E}_k &= \frac{1}{\epsilon_r \epsilon_0} \operatorname{grad} \rho - i\omega \mu_r \mu_0 \mathbf{J}_k, & (2.31)\\ \left(\Delta + \epsilon_r \mu_r k^2\right) \mathbf{B}_k &= -\mu_r \mu_0 \operatorname{rot} \mathbf{J}_k. & (2.32) \end{aligned}$$

The model studied

In the following, we assume that ϵ_r and μ_r are piecewise constant functions inside and outside the obstacles.

$$\epsilon_r(\mathbf{x}) = \begin{cases} 1 & \mathbf{x} \notin O \\ \epsilon_r \neq 1 & \mathbf{x} \in O \end{cases} \tag{2.33}$$

$$\mu_r(\mathbf{x}) = \begin{cases} 1 & \mathbf{x} \notin O \\ \mu_r \neq 1 & \mathbf{x} \in O \end{cases} \tag{2.34}$$

We further assume that free charges and currents do not exist within a finite distance of the obstacles.

$$\mathbf{J} = \mathbf{0} \tag{2.35}$$

$$\mathbf{K} = \mathbf{0} \tag{2.36}$$

$$\rho = 0 \tag{2.37}$$

$$\sigma = 0 \tag{2.38}$$

We then obtain the wave equations (2.1) and (2.5) with

$$\gamma = \epsilon_r \mu_r. \tag{2.39}$$

Two-dimensional problems

Next we assume that the problem considered is two-dimensional, i.e., that all planes parallel to a chosen axis – say the z axis – are physically equivalent: the field vectors do not depend on z, and the obstacle is a cylinder with arbitrary cross section whose axis is parallel to the z axis. The Maxwell equations then simplify in the following way [5]: They decouple and we obtain two cases of different *polarisation*, one called the *transversal electric* (TE) and the other *transversal magnetic* (TM). Note that the terminology used for these two cases is not unique [6]. The $\mathbf{k}$ vector of the incident field lies in the x-y plane. The TE polarisation then refers to the situation where the incident electric field is transverse to the x-y plane, i.e., $\mathbf{E}(\mathbf{x}) = E(x, y)\mathbf{e}_z$. As this means that the electric field is parallel to the obstacle, we will call this the $\mathbf{E}_\parallel$-case. Similarly, the TM polarised case refers to an incident wave with magnetic field $\mathbf{H}(\mathbf{x}) = H(x, y)\mathbf{e}_z$. As this implies that $E_z(x, y) \equiv 0$, we refer to this as the $\mathbf{E}_\perp$-case.

2.2.1 General equation and boundary conditions

We further have to specify the boundary conditions on the surface ∂O of the obstacle O for the two cases. That is, the constants γ_0 and γ_1 vary depending on whether we consider the $\mathbf{E}_\parallel$ or the $\mathbf{E}_\perp$ case.

The $\mathbf{E}_\parallel$-case

We set $\mathbf{E}_k(\mathbf{x}) = u(\mathbf{x})\mathbf{e}_z$, i.e., the incident electric field is parallel to the cylinder axis z, and the magnetic field is normal to the cylinder. We then get the following coefficients for the boundary conditions (2.8) and (2.9)

$$\gamma_0 = 1 \qquad \mathbf{E}^{\text{tang}} \text{ continuous,} \tag{2.40}$$

$$\gamma_1 = \frac{1}{\mu_r} \qquad \mathbf{H}^{\text{tang}} \text{ continuous.} \tag{2.41}$$

In the limit of the perfectly conducting cylinder ($\epsilon_r \to \infty$, $\mu_r \to 0$, $\epsilon_r\mu_r =$ const.) we get only one boundary condition, namely

$$u(\mathbf{x})\big|_{\mathbf{x}\in\partial O} = 0. \tag{2.42}$$

The $\mathbf{E}_\perp$-case

Similarly, we set $\mathbf{B}_k(\mathbf{x}) = u(\mathbf{x})\mathbf{e}_z$ here; now we get from Maxwell equations and the boundary conditions the following relation for general boundary conditions and material constants.

$$\gamma_0 = \frac{1}{\mu_r} \qquad \mathbf{H}^{\text{tang}} \text{ continuous} \tag{2.43}$$

$$\gamma_1 = \frac{1}{\epsilon_r\mu_r} \qquad \mathbf{E}^{\text{tang}} \text{ continuous} \tag{2.44}$$

In the limit of the perfectly conducting cylinder ($\epsilon_r \to \infty$, $\mu_r \to 0$, $\epsilon_r\mu_r =$ const.) we now get the boundary condition

$$\frac{\partial}{\partial \mathbf{n}} u(\mathbf{x})\big|_{\mathbf{x}\in\partial O} = 0. \tag{2.45}$$

2.3 Quantum Mechanics

The situation in quantum mechanics is less complex. We want to solve the one-particle Schrödinger equation [7]

$$i\hbar\frac{\partial\psi(\mathbf{x},t)}{\partial t} = -\frac{\hbar^2}{2m}\Delta\psi(\mathbf{x},t) + V(\mathbf{x})\psi(\mathbf{x},t), \tag{2.46}$$

whose time-independent form is obtained with the ansatz $\psi(\mathbf{x},t) = u(\mathbf{x})e^{-\frac{i}{\hbar}Et}$:

$$-\frac{\hbar^2}{2m}\Delta u(\mathbf{x}) + V(\mathbf{x})u(\mathbf{x}) = Eu(\mathbf{x}). \tag{2.47}$$

The model studied

In the following, we assume that $V(\mathbf{x})$ is a piecewise constant function inside and outside the obstacles.

$$V(\mathbf{x}) = \begin{cases} 0 & \mathbf{x} \notin O \\ V \neq 1 & \mathbf{x} \in O \end{cases} \tag{2.48}$$

2.3.1 General equation and boundary conditions

Again, we obtain the general time-independent and time-dependent wave equations (2.5) and (2.1). If, k^2 and $\gamma^2(\mathbf{x})$ are given by

$$k^2 = \frac{2m}{\hbar^2}E, \tag{2.49}$$

$$\gamma^2(\mathbf{x})k^2 = \frac{2m}{\hbar^2}\left(E - V(\mathbf{x})\right). \tag{2.50}$$

The boundary conditions at ∂O are determined by the fact that the wave function and its normal derivative have to be continuous. Thus, the coefficients for (2.8) and (2.9) are

$$\gamma_0 = 1 \qquad u(\mathbf{x}) \text{ continuous}, \tag{2.51}$$

$$\gamma_1 = 1 \qquad \frac{\partial}{\partial \mathbf{n}}u(\mathbf{x}) \text{ continuous}. \tag{2.52}$$

In the limit $V \to \infty$, the derivative of the wave function jumps and we get the Dirichlet boundary condition

$$u(\mathbf{x})\big|_{\mathbf{x}\in\partial O} = 0. \tag{2.53}$$

2.4 Acoustics

The wave equation for a homogeneous, lossless, source-free medium at rest is given by the familiar wave equation for the density [8]

$$c^2(\mathbf{x})\Delta\rho(\mathbf{x},t) - \frac{\partial^2\rho(\mathbf{x},t)}{\partial t^2} = 0. \tag{2.54}$$

However, as the boundary conditions introduced below will depend on normal velocity and pressure, this is a too general equation. Thus, we introduce the further assumption that, in the equilibrium state, the fluid is at rest and that the acoustical changes are isentropic. In this case, the relation between the acoustical pressure and its equilibrium value is given by

$$\frac{P}{P_0} = \left(\frac{\rho}{\rho_0}\right)^{\gamma},$$

where γ is the ratio of the specific heats. Linearisation yields the following relations between the acoustical pressure $p = P - P_0$, the acoustical density $\delta = \rho - \rho_0$, and the speed of sound c_0. The index 0 denotes equilibrium quantities.

$$p = c_0^2\delta \tag{2.55}$$

$$c_0^2 = \frac{\gamma P_0}{\rho_0} \tag{2.56}$$

Eventually, we get a more specialised version of the wave equation which is expressed in terms of pressure and thus expressed in the desired quantity, suitable for simple application of the boundary conditions.

$$\Delta p(\mathbf{x},t) - \frac{1}{c^2(\mathbf{x})}\frac{\partial^2 p(\mathbf{x},t)}{\partial t^2} = 0 \tag{2.57}$$

A quantity that we will need further on is the velocity

$$\mathbf{u}(\mathbf{x},t) = -\frac{1}{\rho_0}\int \operatorname{grad} p(\mathbf{x},t)\,\mathrm{d}t. \tag{2.58}$$

Harmonic time dependence

Assuming again harmonic time dependence, i.e.,

$$p(\mathbf{x},t) = p(\mathbf{x})e^{-i\omega t}, \tag{2.59}$$

we obtain the now already familiar form of the wave equation when $kc_0 = \omega$

$$\Delta p(\mathbf{x}) + \frac{c_0^2}{c^2(\mathbf{x})}k^2 p(\mathbf{x}) = 0. \tag{2.60}$$

The harmonic and linearised expression for the velocity (2.58) is

$$\mathbf{u}(\mathbf{x}) = \frac{1}{ik\rho_0 c_0}\operatorname{grad} p(\mathbf{x}). \tag{2.61}$$

The model studied

We assume in the following that $c(\mathbf{x})$ and $\rho(\mathbf{x})$ describe two different media.

$$c(\mathbf{x}) = \begin{cases} c^+ & \mathbf{x} \notin O \\ c^- & \mathbf{x} \in O \end{cases} \tag{2.62}$$

$$\rho(\mathbf{x}) = \begin{cases} \rho^+ & \mathbf{x} \notin O \\ \rho^- & \mathbf{x} \in O \end{cases} \tag{2.63}$$

Boundary conditions

The boundary conditions on the surfaces of obstacles are: both the normal velocity through the boundary surface and the pressure across the surface have to be continuous.

$$p(\mathbf{x})\big|_{\mathbf{x}\in\partial O^+} = p(\mathbf{x})\big|_{\mathbf{x}\in\partial O^-} \tag{2.64}$$

$$\frac{1}{\rho_0^+}\frac{\partial}{\partial \mathbf{n}}p(\mathbf{x})\big|_{\mathbf{x}\in\partial O^+} = \frac{1}{\rho_0^-}\frac{\partial}{\partial \mathbf{n}}p(\mathbf{x})\big|_{\mathbf{x}\in\partial O^-} \tag{2.65}$$

The speed of sound $c(\mathbf{x})$ does not appear in (2.65) because it has no effect in the order considered in the linearised theory. Two limits to these boundary

conditions exist: the *acoustically soft* case where the pressure vanishes on the surface

$$p(\mathbf{x})\big|_{\mathbf{x}\in\partial O} = 0, \tag{2.66}$$

and the *acoustically hard* case, where the normal velocity, and thus in our model the normal derivative of the pressure, vanishes on the surface.

$$\frac{\partial}{\partial \mathbf{n}} p(\mathbf{x})\big|_{\mathbf{x}\in\partial O} = 0 \tag{2.67}$$

2.4.1 General equation and boundary conditions

Again, the equation has the desired form for the pressure $p(\mathbf{x}) = u(\mathbf{x})$. With the equilibrium speed of sound c_0, we get the following expressions for k^2 and γ^2:

$$k^2 = \frac{\omega^2}{c_0^2}, \tag{2.68}$$

$$\gamma^2(\mathbf{x}) = \frac{c_0^2}{c^2(\mathbf{x})}. \tag{2.69}$$

Finally, the γ coefficients for (2.8) and (2.9) are

$$\gamma_0 = 1 \qquad p(\mathbf{x}) \text{ continuous}, \tag{2.70}$$

$$\gamma_1 = \frac{\rho_0^+}{\rho_0^-} \qquad \mathbf{u}(\mathbf{x}) \text{ continuous}. \tag{2.71}$$

2.5 Summary

In this chapter, we introduced the Helmholtz equation and the corresponding boundary conditions for two-dimensional electromagnetic, quantum mechanical and acoustical problems. The meaning of the constants has been given for each of these theories. These equations, supplemented by suitable asymptotic boundary conditions, are the mathematical framework used to discuss various scattering problems.

Chapter 3

Scattering in vacuum

In this chapter we discuss solutions of the time-independent Helmholtz equation in an infinite domain in which an array of cylinders is embedded.

$$\left(\Delta + k^2\right) u(\mathbf{x}) = 0, \qquad \text{for } x \in \mathbb{R}^2 \setminus O \tag{3.1a}$$

$$\left(\Delta + \gamma_i^2 k^2\right) u(\mathbf{x}) = 0, \qquad \text{for } x \in O_i \tag{3.1b}$$

Here, O is the union of several bounded regions ('scatterers') $O_i \subset \mathbb{R}^2$

$$O = \bigcup_i O_i, \qquad O_i \cap O_j = \emptyset. \tag{3.2}$$

We will use the separation of variables technique for elliptical cylinder geometry. A review of other methods commonly used to solve scattering problems may be found in [9]. It is well known [10] that the Helmholtz equation plus boundary conditions at the scatterer are not sufficient to obtain a unique solution of the time-independent scattering problem. This question has been investigated by Sommerfeld [11] in connection with the Green function of the Helmholtz equation for spaces of infinite extent: a supplementary condition has to be added in order to uniquely specify the scattering problem in an infinite domain. This condition is called *radiation condition*.

Formulation of the time-independent scalar scattering problem

The function $u(\mathbf{x}) = u^{\text{in}}(\mathbf{x}) + u^{\text{sc}}(\mathbf{x})$, whose physical meaning was discussed in chapter 2, is uniquely determined [12] if the following conditions are fulfilled.

(a) $u(\mathbf{x})$ satisfies (3.1a) and (3.1b).

(b) $u(\mathbf{x})$ satisfies homogeneous boundary conditions of the type

$$u(\mathbf{x})\big|_{\mathbf{x}\in\partial O_i^+} = \gamma_0^{(i)} u(\mathbf{x})\big|_{\mathbf{x}\in\partial O_i^-} \tag{3.3}$$

$$\frac{\partial}{\partial \mathbf{n}} u(\mathbf{x})\big|_{\mathbf{x}\in\partial O_i^+} = \gamma_1^{(i)} \frac{\partial}{\partial \mathbf{n}} u(\mathbf{x})\big|_{\mathbf{x}\in\partial O_i^-} \tag{3.4}$$

where $\gamma_0^{(i)}$ and $\gamma_1^{(i)}$ are constants or specified functions of position.

(c) For $r = |\mathbf{x}|$, the scattering wave $u^{\mathrm{sc}}(\mathbf{x})$ fulfills the *radiation condition*

$$\lim_{r\to\infty} r^{\frac{1}{2}} \left(\frac{\partial u^{\mathrm{sc}}(\mathbf{x})}{\partial r} - iku^{\mathrm{sc}}(\mathbf{x}) \right) = 0. \tag{3.5}$$

The sense of the $-$ sign in the radiation condition will become more evident in chapter 6, where time-dependent scattering is introduced.

Separation of variables method

The basic idea of the separation of variables method [9] is to make a *separation ansatz* for the solution of the scalar Helmholtz equation (3.1a, 3.1b) and to obtain from the scalar Helmholtz equation a set of differential equations for each component. In order to make this happen, we first have to formulate the partial differential equation in a coordinate system adapted to the geometry of the problem. Then, in this particular coordinate system, we have to separate the equation into as many ordinary differential equations as there are dimensions to the problem. The solutions of these equations are finally used as building blocks for the construction of an unique solution that fulfills the boundary conditions [13].

The separation of variables method is very useful if the shape of the scatterer may be described by a simple geometric form. There exist (at least) eleven coordinate systems called *separable coordinate systems* for which this method works for the Helmholtz equation [14]. These coordinate systems allow families of separated solutions from which all solutions of the Helmholtz equation can be built up.

3.1 Scattering by one elliptical cylinder

First, we solve the scattering problem for one elliptical cylinder as sketched in Fig. 3.1. Now we are looking for a function $u_{\mathbf{k}}$ fulfilling the scalar Helmholtz equations

$$\left(\Delta + k^2\right) u_{\mathbf{k}}(\xi,\eta) = 0 \qquad \xi > \xi_0 \tag{3.6}$$

$$\left(\Delta + \gamma^2 k^2\right) u_{\mathbf{k}}(\xi,\eta) = 0 \qquad \xi < \xi_0 \tag{3.7}$$

in the implicitly defined elliptical coordinate system

$$(x,y) = \mathbf{x} = (h\cosh\xi\cos\eta, h\sinh\xi\sin\eta) = \mathbf{X}(h,\boldsymbol{\xi}) \tag{3.8}$$

$$(\xi,\eta) = \boldsymbol{\xi} = \left(\cosh^{-1}\sqrt{\frac{s_{h,x,y}+\sqrt{t_{h,x,y}}}{2h^2}}, \sigma(x,y) + \cos^{-1}\sqrt{\frac{s_{h,x,y}-\sqrt{t_{h,x,y}}}{2h^2}} \right) = \boldsymbol{\Xi}(h,\mathbf{x}) \tag{3.9}$$

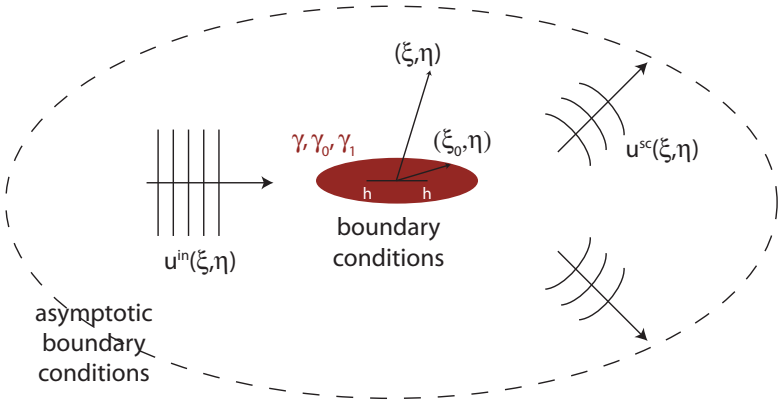

Figure 3.1: Scattering by one elliptic cylinder

where the $\sigma(x,y)$ depends on the quadrant containing (x,y) in the following way.

$$\sigma(x,y) = \begin{cases} 0 & x>0, y>0 \\ \frac{\pi}{2} & x<0, y>0 \\ \pi & x<0, y<0 \\ \frac{3\pi}{2} & x>0, y<0 \end{cases} \tag{3.10}$$

Finally, $2h$ is the distance between the two focal points and

$$s_{h,x,y} = h^2 + x^2 + y^2, \tag{3.11}$$

$$t_{h,x,y} = 4h^2y^2 + \left(x^2 + y^2 - h^2\right)^2. \tag{3.12}$$

In the coordinate system (3.8), the Laplacian reads [14]

$$\Delta = \frac{2}{h^2\left[\cosh 2\xi - \cos 2\eta\right]}\left(\frac{\partial^2}{\partial\xi^2} + \frac{\partial^2}{\partial\eta^2}\right). \tag{3.13}$$

In addition to (3.6) and (3.7) we impose the following conditions.

1. Continuity of $u_{\mathbf{k}}(\xi,\eta)$ and $\operatorname{grad} u_{\mathbf{k}}(\xi,\eta)$ for $x \notin \partial O$. As we see from (3.9), necessary conditions for smoothness of $u_{\mathbf{k}}(\xi,\eta)$ are

$$\lim_{\epsilon\to 0}\left[u_{\mathbf{k}}(\xi,\epsilon) - u_{\mathbf{k}}(\xi,2\pi-\epsilon)\right] = 0, \tag{3.14}$$

$$\lim_{\epsilon\to 0}\left[\frac{\partial}{\partial\eta}u_{\mathbf{k}}(\xi,\epsilon) - \frac{\partial}{\partial\eta}u_{\mathbf{k}}(\xi,2\pi-\epsilon)\right] = 0\ , \tag{3.15}$$

$$\lim_{\epsilon\to 0}\left[u_{\mathbf{k}}(\epsilon,\eta) - u_{\mathbf{k}}(\epsilon,2\pi-\eta)\right] = 0, \tag{3.16}$$

$$\lim_{\epsilon\to 0}\left[\frac{\partial}{\partial\xi}u_{\mathbf{k}}(\epsilon,\eta) + \frac{\partial}{\partial\xi}u_{\mathbf{k}}(\epsilon,2\pi-\eta)\right] = 0. \tag{3.17}$$

2. Radiation condition in elliptical coordinates

$$\lim_{\xi\to\infty}\sqrt{he^{\xi}}\left(\frac{1}{he^{\xi}}\frac{\partial}{\partial\xi}-ik\right)\left[u_{\mathbf{k}}(\xi,\eta)-u_{\mathbf{k}}^{\text{in}}(\xi,\eta)\right]=0 \tag{3.18}$$

where $u_{\mathbf{k}}^{\text{in}}(\xi,\eta)$ is the incoming wave $e^{i\mathbf{k}\cdot\mathbf{x}}$ in elliptical coordinates.

$$\mathbf{k} = (k\cos\beta, k\sin\ \beta)^T \tag{3.19}$$

$$u_{\mathbf{k}}^{\text{in}}(\xi,\eta) = e^{i\mathbf{k}\cdot\mathbf{x}} = \sum_{p=-\infty}^{\infty} e_p(\beta;q_k)\mathrm{M}_p^{(1)}(\xi;q_k)\mathrm{me}_p(\eta;q_k), \tag{3.20}$$

$$e_p(\beta;q_k) = \begin{cases} i^p\mathrm{me}_p(\beta;q_k) & p\geq 0 \\ -(i^p)\mathrm{me}_p(\beta;q_k) & p<0. \end{cases} \tag{3.21}$$

In these equations

$$q_k=\frac{k^2h^2}{4} \tag{3.22}$$

and the functions $\mathrm{M}_p^{(1)}(\xi;q_k)$ and $\mathrm{me}_p(\eta;q_k)$ are Mathieu functions and Modified Mathieu functions in the notation of chapter 7.

3. Boundary conditions at $\xi=\xi_0$.

$$\lim_{\epsilon\to 0}\Big[u_{\mathbf{k}}(\xi_0+\epsilon,\eta)-\gamma_0 u_{\mathbf{k}}(\xi_0-\epsilon,\eta)\Big]=0 \tag{3.23}$$

$$\lim_{\epsilon\to 0}\Big[\frac{\partial}{\partial\xi}u_{\mathbf{k}}(\xi_0+\epsilon,\eta)-\gamma_1\frac{\partial}{\partial\xi}u_{\mathbf{k}}(\xi_0-\epsilon,\eta)\Big]=0 \tag{3.24}$$

The constants γ_0 and γ_1 are discussed in chapter 2.

General solution

Solutions of (3.6) are products of Mathieu functions $\mathrm{me}_m(\eta;q)$ in the 'angular' variable η and modified Mathieu functions $\mathrm{M}_p^{(j)}(\xi;q)$ in the 'radial' variable ξ (cf. chapter 7). There exist two linearly independent modified Mathieu functions which we characterize by their behaviour when the ellipse becomes a cylinder ($h\to 0$). The first one, $\mathrm{M}_p^{(1)}(\xi;q)$, becomes the Bessel function and the second one, $\mathrm{M}_p^{(2)}(\xi;q)$, the Neumann function; moreover $\mathrm{M}_p^{(3)}=\mathrm{M}_p^{(1)}+i\mathrm{M}_p^{(2)}$ and $\mathrm{M}_p^{(4)}=\mathrm{M}_p^{(1)}-i\mathrm{M}_p^{(2)}$. These functions and their properties will be discussed in chapter 7. The products of angular and radial Mathieu functions are called 'partial waves' related to a certain $\mathbf{k}$. $\mathrm{M}_p^{(3)}(\xi;q_k)\mathrm{me}_p(\eta;q_k)$ is called an 'outgoing' partial wave in the sense of (3.5) and $\mathrm{M}_p^{(1)}(\xi;q_k)\mathrm{me}_p(\eta;q_k)$ a 'regular' partial wave because it is smooth. A general solution $u_{\mathbf{k}}(\xi,\eta)$ of equations (3.6) and (3.7) is

$$u_{\mathbf{k}}(\xi,\eta)=\begin{cases} u_{\mathbf{k}}^{(i)}(\xi,\eta) & \text{for } \xi<\xi_0 \\ u_{\mathbf{k}}^{(e)}(\xi,\eta) & \text{for } \xi>\xi_0 \end{cases} \tag{3.25}$$

where

$$ {}^{i}u_{\mathbf{k}}(\xi,\eta) = \sum_{p=-\infty}^{\infty} a_p \mathrm{M}_p^{(1)}(\xi;\gamma^2 q_k)\mathrm{me}_p(\eta;\gamma^2 q_k) \tag{3.26} $$

and

$$ {}^{e}u_{\mathbf{k}}(\xi,\eta) = \sum_{p=-\infty}^{\infty} \left[c_p \mathrm{M}_p^{(1)}(\xi;q_k) + d_p \mathrm{M}_p^{(3)}(\xi;q_k)\right] \mathrm{me}_p(\eta;q_k). \tag{3.27} $$

Asymptotic boundary condition

The radiation condition (3.18) implies that

$$ c_p = e_p = e_p(\beta, q_k). \tag{3.28} $$

Boundary condition at the obstacle

With (3.28), the boundary conditions at $\xi = \xi_0$ become

$$ \sum_{p=-\infty}^{\infty} \left[e_p \mathrm{M}_p^{(1)}(\xi_0;q_k) + d_p \mathrm{M}_p^{(3)}(\xi_0;q_k)\right] \mathrm{me}_p(\eta;q_k) = \gamma_0 \sum_{p=-\infty}^{\infty} a_p \mathrm{M}_p^{(1)}(\xi_0;\gamma^2 q_k)\mathrm{me}_p(\eta;\gamma^2 q_k) \tag{3.29} $$

and

$$ \sum_{p=-\infty}^{\infty} \left[e_p \frac{\mathrm{dM}_p^{(1)}}{\mathrm{d}\xi}(\xi_0;q_k) + d_p \frac{\mathrm{dM}_p^{(3)}}{\mathrm{d}\xi}(\xi_0;q_k)\right] \mathrm{me}_p(\eta;q_k) = \gamma_1 \sum_{p=-\infty}^{\infty} a_p \frac{\mathrm{dM}_p^{(1)}}{\mathrm{d}\xi}(\xi_0;\gamma^2 q_k)\mathrm{me}_p(\eta;\gamma^2 q_k). \tag{3.30} $$

Solution of the truncated set of linear equations

Since the parameters in the Mathieu functions are q_k on the left hand side and $\gamma^2 q_k$ on the right hand side, the situation is more complicated than for circular cylinders where the same angular functions appear on both sides. With

$$ A_{pr}(q_1,q_2) = \int_0^{2\pi} \mathrm{me}_p(\eta;q_1)\mathrm{me}_r(\eta;q_2)\,\mathrm{d}\eta \tag{3.31} $$

eqs. (3.29) and (3.30) become by integration over $\int_0^{2\pi} \mathrm{me}_r(\eta; q_k)\,\mathrm{d}\eta$

$$d_r \mathrm{M}_r^{(3)}(\xi_0; q_k) - \gamma_0 \sum_{p=-\infty}^{\infty} \mathrm{M}_p^{(1)}(\xi_0; \gamma^2 q_k) A_{pr}(q_k; \gamma^2 q_k) a_p = -e_r \mathrm{M}_r^{(1)}(\xi_0; q_k), \tag{3.32}$$

$$d_r \frac{\mathrm{dM}_r^{(3)}}{\mathrm{d}\xi}(\xi_0; q_k) - \gamma_1 \sum_{p=-\infty}^{\infty} \frac{\mathrm{dM}_p^{(1)}}{\mathrm{d}\xi}(\xi_0; \gamma^2 q_k) A_{pr}(q_k; \gamma^2 q_k) a_p = -e_r \frac{\mathrm{dM}_r^{(1)}}{\mathrm{d}\xi}(\xi_0; q_k). \tag{3.33}$$

For actual calculation, this linear system has to be truncated with $-P \le p \le P$ and $-R \le r \le R$ (cf. section 8.3 for the details on the truncation procedure). In order to formulate these equations as a linear system which can be solved by standard methods, we introduce the following matrices. We use the notation $\mathrm{Diag}\,(d_1, d_2, \ldots, d_N)$ for diagonal matrices with the entries $d_1, d_2, \ldots, d_N$.

$$\mathsf{A}_{R\times P}(q_k, \gamma^2 q_k) = \begin{pmatrix} A_{-R,-P}(q_k; \gamma^2 q_k) & \cdots & A_{-R,P}(q_k; \gamma^2 q_k) \\ \vdots & & \vdots \\ A_{R,-P}(q_k; \gamma^2 q_k) & \cdots & A_{R,P}(q_k; \gamma^2 q_k) \end{pmatrix} \tag{3.34}$$

$$\mathsf{M}_{R\times R} = \mathrm{Diag}\left(\frac{\mathrm{M}_{-R}^{(3)}(\xi_0; q_k)}{\mathrm{M}_{-R}^{(1)}(\xi_0; q_k)}, \cdots, \frac{\mathrm{M}_{R}^{(3)}(\xi_0; q_k)}{\mathrm{M}_{R}^{(1)}(\xi_0; q_k)} \right) \tag{3.35}$$

$$\mathsf{M}^{\partial}_{R\times R} = \mathrm{Diag}\left(\frac{\frac{\partial}{\partial\xi}\mathrm{M}_{-R}^{(3)}(\xi_0; q_k)}{\frac{\partial}{\partial\xi}\mathrm{M}_{-R}^{(1)}(\xi_0; q_k)}, \cdots, \frac{\frac{\partial}{\partial\xi}\mathrm{M}_{R}^{(3)}(\xi_0; q_k)}{\frac{\partial}{\partial\xi}\mathrm{M}_{R}^{(1)}(\xi_0; q_k)} \right) \tag{3.36}$$

$${}^{d}\mathsf{M}_{R\times R} = \mathrm{Diag}\left(\frac{1}{\mathrm{M}_{-R}^{(1)}(\xi_0; q_k)}, \cdots, \frac{1}{\mathrm{M}_{R}^{(1)}(\xi_0; q_k)} \right) \tag{3.37}$$

$${}^{d}\mathsf{M}^{\partial}_{R\times R} = \mathrm{Diag}\left(\frac{1}{\frac{\partial}{\partial\xi}\mathrm{M}_{-R}^{(1)}(\xi_0; q_k)}, \cdots, \frac{1}{\frac{\partial}{\partial\xi}\mathrm{M}_{R}^{(1)}(\xi_0; q_k)} \right) \tag{3.38}$$

$${}^{i}\mathsf{M}_{P\times P} = \mathrm{Diag}\left(\mathrm{M}_{-P}^{(1)}\left(\xi_0; \gamma^2 q_k\right), \cdots, \mathrm{M}_{P}^{(1)}\left(\xi_0; \gamma^2 q_k\right) \right) \tag{3.39}$$

$${}^{i}\mathsf{M}^{\partial}_{P\times P} = \mathrm{Diag}\left(\frac{\partial}{\partial\xi}\mathrm{M}_{-P}^{(1)}\left(\xi_0; \gamma^2 q_k\right), \cdots, \frac{\partial}{\partial\xi}\mathrm{M}_{P}^{(1)}\left(\xi_0; \gamma^2 q_k\right) \right) \tag{3.40}$$

A vector $\mathbf{x}_R$ with index R means that the vector $\mathbf{x}$ which has an infinite number of components is truncated to

$$\mathbf{x}_R = (x_{-R}, x_{-R+1}, \ldots, x_{R-1}, x_R)\,. \tag{3.41}$$

We now reformulate the equations (3.32) and (3.33) in the following way.

$$\mathsf{M}_{R\times R}\,\mathbf{d}_R = -\,\mathbf{e}_R + \gamma_0\; {}^{d}\mathsf{M}_{R\times R}\,\mathsf{A}_{R\times P}\left(q_k; \gamma^2 q_k\right)\; {}^{i}\mathsf{M}_{P\times P}\,\mathbf{a}_P \tag{3.42}$$

$$\mathsf{M}^{\partial}_{R\times R}\,\mathbf{d}_R = -\,\mathbf{e}_R + \gamma_1\; {}^{d}\mathsf{M}^{\partial}_{R\times R}\,\mathsf{A}_{R\times P}\left(q_k; \gamma^2 q_k\right)\; {}^{i}\mathsf{M}^{\partial}_{P\times P}\,\mathbf{a}_P \tag{3.43}$$

If we eliminate $\mathbf{a}_P$, we obtain

$$\mathsf{X}\mathbf{d}_R = -\mathsf{Y}\mathbf{e}_R \tag{3.44}$$

with

$$\mathsf{X} = \left[\frac{1}{\gamma_0}\left({}^{d}\mathsf{M}_{R\times R}\mathsf{A}_{R\times P}(q_k;\gamma^2 q_k)\ {}^{i}\mathsf{M}_{P\times P}\right)^{-1}\mathsf{M}_{R\times R}\left(\xi_0;q_k\right) - \frac{1}{\gamma_1}\left({}^{d}\mathsf{M}^{\partial}_{R\times R}\mathsf{A}_{R\times P}(q_k;\gamma^2 q_k)\ {}^{i}\mathsf{M}^{\partial}_{P\times P}\right)^{-1}\mathsf{M}^{\partial}_{R\times R}\left(\xi_0;q_k\right)\right], \tag{3.45}$$

$$\mathsf{Y} = \left[\frac{1}{\gamma_0}\left({}^{d}\mathsf{M}_{R\times R}\mathsf{A}_{R\times P}(q_k;\gamma^2 q_k)\ {}^{i}\mathsf{M}_{P\times P}\right)^{-1} - \frac{1}{\gamma_1}\left({}^{d}\mathsf{M}^{\partial}_{R\times R}\mathsf{A}_{R\times P}(q_k;\gamma^2 q_k)\ {}^{i}\mathsf{M}^{\partial}_{P\times P}\right)^{-1}\right]. \tag{3.46}$$

Note that for the inverse of the matrices to exist, we must demand $R = P$. If we do not wish to set $R = P$ or if, in a possible evaluation scheme, matrix inversion is not the preferred method of solution, it is more convenient to join the two vectors $\mathbf{d}_R$ and $\mathbf{a}_P$ into one single vector called $\mathbf{v}_{R+P}$:

$$\mathbf{v}_{R+P} = (\mathbf{d}_{-R},\ldots,\mathbf{d}_R,\mathbf{a}_{-P},\ldots,\mathbf{a}_P)\,. \tag{3.47}$$

Then, we obtain, with the $2R\times(R+S)$ matrix

$$\mathsf{U} = \begin{bmatrix} -\mathsf{M}_{R\times R} & \gamma_0\ {}^{d}\mathsf{M}_{R\times R}\,\mathsf{A}_{R\times P}\left(q_k;\gamma^2 q_k\right)\ {}^{i}\mathsf{M}_{P\times P} \\ -\mathsf{M}^{\partial}_{R\times R} & \gamma_1\ {}^{d}\mathsf{M}^{\partial}_{R\times R}\,\mathsf{A}_{R\times P}\left(q_k;\gamma^2 q_k\right)\ {}^{i}\mathsf{M}^{\partial}_{P\times P} \end{bmatrix} \tag{3.48}$$

and the vector

$$\mathbf{e}_{R+P} = (\mathbf{e}_{-R},\ldots,\mathbf{e}_R,\mathbf{e}_{-P},\ldots,\mathbf{e}_P) \tag{3.49}$$

the set of linear equations

$$\mathsf{U}\mathbf{v}_{R+P} = \mathbf{e}_{R+P}. \tag{3.50}$$

As we will see, it is also more convenient to demand $R = P$ in this formulation.

Limiting cases

Note that in the limit of Dirichlet boundary conditions at ∂O and $u = 0$ in O (e.g., ideally conducting cylinder for the $\mathbf{E}_{\|}$ case, soft acoustic obstacle) (3.29) and (3.30) become, according to chapter 2, $a_m = 0$ and

$$\sum_{p=-\infty}^{\infty}\left[c_p\mathrm{M}_p^{(1)}(\xi_0;q_k) + d_p\mathrm{M}_p^{(3)}(\xi_0;q_k)\right]\mathrm{me}_p(\eta;q_k) = 0 \tag{3.51}$$

with the solution

$$d_p(\alpha,q_k) = -\frac{\mathrm{M}_p^{(1)}(\xi_0;q_k)}{\mathrm{M}_p^{(3)}(\xi_0;q_k)}e_p(\alpha,q_k)\,. \tag{3.52}$$

Figure 3.2: Multiple scattering by elliptical cylinders

Similarly, the Neumann limit (e.g., ideally conducting cylinder for the $\mathbf{E}_\perp$ case, hard acoustic obstacle) leads to the boundary conditon

$$\sum_{p=-\infty}^{\infty}\left[c_p\frac{\mathrm{dM}_p^{(1)}}{\mathrm{d}\xi}(\xi_0;q_k)+d_p\frac{\mathrm{dM}_p^{(3)}}{\mathrm{d}\xi}(\xi_0;q_k)\right]\mathrm{me}_p(\eta;q_k)=0 \tag{3.53}$$

with the solution

$$d_p(\alpha,q_k)=-\frac{\frac{\mathrm{dM}_p^{(1)}}{\mathrm{d}\xi}(\xi_0;q_k)}{\frac{\mathrm{dM}_p^{(3)}}{\mathrm{d}\xi}(\xi_0;q_k)}e_p(\alpha,q_k)\,. \tag{3.54}$$

3.2 Scattering by several elliptical cylinders

Next we consider time-independent scattering of electromagnetic waves by an array of elliptical cylinders. If $N>1$ scatterers are present it is not possible to solve the scattering problem by simply adding the scattering waves of the isolated single scatterers ('primary scattering waves') to the incoming plane wave. This is an approximation which only makes sense if the distances between any two scatterers exceeds a critical value that depends on the wave length of the incoming wave and the related cross section of the single scatterers. If this condition is not satisfied one has to take into account that a scattering wave which emerges from one cylinder modifies the regular field in the vicinity of another cylinder. As illustrated in Fig. 3.2, no a priori limitations are imposed on the number of scatterers, on the geometric parameters that fix their elliptical form, on their orientation, on their relative positions (except that overlap is forbidden), and on their material constants.

To describe non-confocal elliptical coordinates labelled with an index l we use the following implicitly defined excentric coordinate system.

$$x=\rho^{(l)}\cos\psi^{(l)}+h^{(l)}\left(\cosh\xi^{(l)}\cos\eta^{(l)}\cos\alpha^{(l)}-\sinh\xi^{(l)}\sin\eta^{(l)}\sin\alpha^{(l)}\right) \tag{3.55}$$

$$y=\rho^{(l)}\sin\psi^{(l)}+h^{(l)}\left(\cosh\xi^{(l)}\cos\eta^{(l)}\sin\alpha^{(l)}+\sinh\xi^{(l)}\sin\eta^{(l)}\cos\alpha^{(l)}\right) \tag{3.56}$$

With (3.8) and (3.9), we can write this as follows.

$$\mathbf{x} = \mathbf{x}^{(l)} + \mathsf{D}(\alpha^{(l)})\mathbf{X}\left(h^{(l)}, \boldsymbol{\xi}^{(l)}\right) = \mathbf{X}^{(l)}\left(\boldsymbol{\xi}^{(l)}\right) \tag{3.57}$$

$$\boldsymbol{\xi}^{(l)} = \boldsymbol{\Xi}\left(h^{(l)}, \mathsf{D}(-\alpha^{(l)})(\mathbf{x} - \mathbf{x}^{(l)})\right) = \boldsymbol{\xi}^{(l)}(\mathbf{x}) \tag{3.58}$$

$$\mathsf{D}(\alpha) = \begin{pmatrix} \cos\alpha & -\sin\alpha \\ \sin\alpha & \cos\alpha \end{pmatrix} \tag{3.59}$$

Besides $\rho^{(l)}$, $\psi^{(l)}$, $\alpha^{(l)}$ and $h^{(l)}$, the parameters of the l'th cylinder are its radius $\xi_{l,0}$ and the material constants $\gamma^{(l)}, \gamma_0^{(l)}$, and $\gamma_1^{(l)}$. The area covered by the l'th cylinder is denoted by $O_l \subset \mathbb{R}^2$, bounded by the ellipse ∂O_l which is parametrised by $\boldsymbol{\xi}_0^{(l)} = \left(\xi_{l,0}^{(l)}, \eta^{(l)}\right)$. If a quantity is cylinder-dependent, its cylinder number is added as a superscript in parentheses. An exception to this rule is $\boldsymbol{\xi}_{l,0}^{(m)} = \boldsymbol{\xi}^{(m)}(\mathbf{X}^{(l)}(\boldsymbol{\xi}_0^{(l)}))$ meaning the 'elliptic' radius of the l'th cylinder expressed in the coordinate system of the m'th cylinder.

General solution

Let $u_{\mathbf{k}}^{(l)}(\xi^{(l)}, \eta^{(l)})$ be the incoming wave expressed in the coordinates of the l'th cylinder, ${}^{i}u_{\mathbf{k}}^{(m)}(\xi^{(m)}, \eta^{(m)})$ the interal wave of the m'th cylinder, and ${}^{e}u_{\mathbf{k}}^{(m)}(\xi^{(m)}, \eta^{(m)})$ the outgoing (scattering) wave from the same cylinder. The superscript (l) in ξ and η denotes the fact that these are local coordinates relative to the coordinate system of the l'th cylinder as defined in (3.55) and (3.56). They are given by

$${}^{e}u_{\mathbf{k}}^{(m)}(\xi, \eta) = \sum_{p=-\infty}^{\infty} d_p^{(m)} \mathrm{M}_p^{(3)}\left(\xi; q_k^{(m)}\right) \mathrm{me}_p\left(\eta; q_k^{(m)}\right) \qquad \text{for } \xi > \xi_{m,0}, \tag{3.60}$$

$${}^{i}u_{\mathbf{k}}^{(m)}(\xi, \eta) = \sum_{p=-\infty}^{\infty} a_p^{(m)} \mathrm{M}_p^{(1)}\left(\xi; {\gamma^{(m)}}^2 q_k^{(m)}\right) \mathrm{me}_p\left(\eta; {\gamma^{(m)}}^2 q_k^{(m)}\right) \quad \text{for } \xi < \xi_{m,0}, \tag{3.61}$$

where

$$q_k^{(l)} = \frac{k^2 {h^{(l)}}^2}{4}. \tag{3.62}$$

The total wave function is

$$u_{\mathbf{k}}(\mathbf{x}) = u_{\mathbf{k}}^{\mathrm{in}}(\mathbf{x}) + \sum_{m=1}^{N} {}^{e}u_{\mathbf{k}}^{(m)}\left(\boldsymbol{\xi}^{(m)}(\mathbf{x})\right) \qquad \text{for } \mathbf{x} \notin \bigcup_m O_m \tag{3.63}$$

$$u_{\mathbf{k}}(\mathbf{x}) = {}^{i}u_{\mathbf{k}}^{(l)}(\boldsymbol{\xi}^{(l)}(\mathbf{x})) \qquad \text{for } \mathbf{x} \in O_l \tag{3.64}$$

Plane wave

If the origin of the l'th coordinate system is denoted by $\mathbf{r}_0^{(l)}$, the incoming wave function in this coordinate system may be expressed with the help of the two-dimensional rotation matrix $\mathsf{D}(\alpha)$ given in (3.59) as follows. Note that $\mathbf{k}\cdot\mathsf{D}(\alpha^{(l)})\mathbf{x} = \mathsf{D}(-\alpha^{(l)})\mathbf{k}\cdot\mathbf{x}$.

$$u_{\mathbf{k}}^{\mathrm{in},(l)}(\mathbf{r}_0^{(l)},\alpha^{(l)};\xi^{(l)},\eta^{(l)}) = e^{i\mathbf{k}\cdot\mathbf{r}_0^{(l)}} e^{i\mathbf{k}\cdot\mathsf{D}(\alpha^{(l)})\mathbf{x}_l} = e^{i\mathbf{k}\cdot\mathbf{r}_0^{(l)}} u^{\mathrm{in}}_{\mathsf{D}(-\alpha^{(l)})\mathbf{k}}(\xi^{(l)},\eta^{(l)}) \quad (3.65)$$

$$= e^{i\mathbf{k}\cdot\mathbf{r}_0^{(l)}} \sum_{p=-\infty}^{\infty} e_p(\beta-\alpha^{(l)};q_k^{(l)})\mathrm{M}_p^{(1)}(\xi^{(l)};q_k^{(l)})\mathrm{me}_p(\eta^{(l)};q_k^{(l)}) \quad (3.66)$$

For the definition of β see (3.19).

Boundary conditions at the obstacles

The N boundary conditions for the obstacles labelled by $1 \le l \le N$ read as follows.

$$u_{\mathbf{k}}^{\mathrm{in},(l)}(\mathbf{r}_0^{(l)},\alpha^{(l)};\boldsymbol{\xi}_{l,0}^{(l)}) + \sum_{m=1}^{N} {}^{e}u_{\mathbf{k}}^{(m)}(\boldsymbol{\xi}_{l,0}^{(m)}) = \gamma_0^{(l)}\ {}^{i}u_{\mathbf{k}}^{(l)}(\boldsymbol{\xi}_{l,0}^{(l)}) \quad (3.67)$$

$$\frac{\partial}{\partial\xi^{(l)}}u_{\mathbf{k}}^{\mathrm{in},(l)}(\mathbf{r}_0^{(l)},\alpha^{(l)};\boldsymbol{\xi}_{l,0}^{(l)}) + \sum_{m=1}^{N}\frac{\partial}{\partial\xi^{(l)}}\ {}^{e}u_{\mathbf{k}}^{(m)}(\boldsymbol{\xi}_{l,0}^{(m)}) = \gamma_1^{(l)}\frac{\partial}{\partial\xi^{(l)}}\ {}^{i}u_{\mathbf{k}}^{(l)}(\boldsymbol{\xi}_{l,0}^{(l)}) \quad (3.68)$$

If we consider the boundary equations at a given cylinder with index l, the first step is now to express all the outgoing fields from all other cylinders with index $m \neq l$ with the help of the addition theorem.

Addition theorem

To solve these equations, we have to express an outgoing partial wave related to one coordinate system (index l) as superposition of regular partial waves related to another coordinate system (index m) as sketched in Fig. 3.3. This may be done with the so-called *addition theorem for Mathieu functions*.

$$\mathrm{M}_p^{(j)}(\xi^{(l)};q_k^{(l)})\mathrm{me}_p(\eta^{(l)};q_k^{(l)}) = \sum_{r=-\infty}^{\infty} B_{r,p}^{(j)}(\boldsymbol{\rho}^{lm},\alpha^{(l)}-\alpha^{(m)},k,q_k^{(l)},q_k^{(m)})\times$$
$$\mathrm{M}_r^{(1)}(\xi^{(m)};q_k^{(m)})\mathrm{me}_r(\eta^{(m)};q_k^{(m)}) \quad (3.69)$$

The addition theorem and its coefficients $B_{r,p}^{(j)}(\mathbf{v},\alpha,k,q_1,q_2)$ are described in detail in chapter 7.

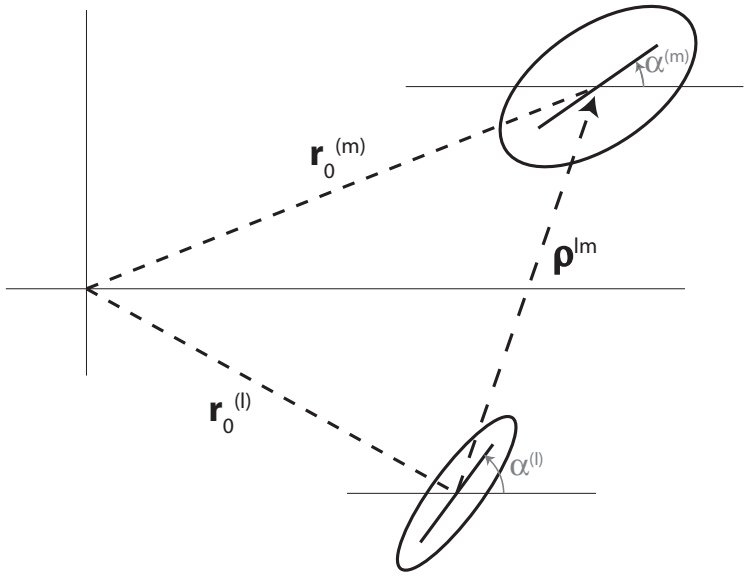

Figure 3.3: Two elliptical coordinate systems

The set of linear equations

The transformed equations (3.67) and (3.68) read as follows.

$$\begin{aligned}
&\sum_{p=-\infty}^{\infty} e_p^{(l)} \mathrm{M}_p^{(1)}\left(\xi_{l,0}^{(l)}; q_k^{(l)}\right) \mathrm{me}_p\left(\eta^{(l)}; q_k^{(l)}\right) + \sum_{\substack{m=1\\ m\neq l}}^{N} \sum_{p=-\infty}^{\infty} d_p^{(m)} \times \\
&\sum_{r=-\infty}^{\infty} B_{r,p}^{(3)}(\boldsymbol{\rho}^{lm}, \alpha_m - \alpha^{(l)}, k, q_k^{(m)}, q_k^{(l)}) \mathrm{M}_r^{(1)}(\xi_{l,0}^{(l)}; q_k^{(l)}) \mathrm{me}_r(\eta^{(l)}; q_k^{(l)}) \\
&+ \sum_{p=-\infty}^{\infty} d_p^{(l)} \mathrm{M}_p^{(3)}\left(\xi_{l,0}^{(l)}; q_k^{(l)}\right) \mathrm{me}_p\left(\eta^{(l)}; q_k^{(l)}\right) \\
=&\gamma_0^{(l)} \sum_{m=1}^{N} a_p^{(l)} \mathrm{M}_p^{(1)}\left(\xi_{l,0}^{(l)}; {\gamma^{(l)}}^2 q_k^{(l)}\right) \mathrm{me}_p\left(\eta^{(l)}; {\gamma^{(l)}}^2 q_k^{(l)}\right)
\end{aligned} \tag{3.70}$$

$$\begin{aligned}
&\sum_{p=-\infty}^{\infty} e_p^{(l)} \frac{\partial}{\partial \xi^{(l)}} \mathrm{M}_p^{(1)}\left(\xi_{l,0}^{(l)}; q_k^{(l)}\right) \mathrm{me}_p\left(\eta^{(l)}; q_k^{(l)}\right) + \sum_{\substack{m=1\\ m\neq l}}^{N} \sum_{p=-\infty}^{\infty} d_p^{(m)} \times \\
&\frac{\partial}{\partial \xi^{(l)}} \sum_{r=-\infty}^{\infty} B_{r,p}^{(3)}(\boldsymbol{\rho}^{lm}, \alpha_m - \alpha^{(l)}, k, q_k^{(m)}, q_k^{(l)}) \mathrm{M}_r^{(1)}(\xi_{l,0}^{(l)}; q_k^{(l)}) \mathrm{me}_r(\eta^{(l)}; q_k^{(l)}) \\
&+ \frac{\partial}{\partial \xi^{(l)}} \sum_{p=-\infty}^{\infty} d_p^{(l)} \mathrm{M}_p^{(3)}\left(\xi_{l,0}^{(l)}; q_k^{(l)}\right) \mathrm{me}_p\left(\eta^{(l)}; q_k^{(l)}\right) \\
=&\gamma_1^{(l)} \sum_{p=-\infty}^{\infty} a_p^{(l)} \frac{\partial}{\partial \xi^{(l)}} \mathrm{M}_p^{(1)}\left(\xi_{l,0}^{(l)}; {\gamma^{(l)}}^2 q_k^{(l)}\right) \mathrm{me}_p\left(\eta^{(l)}; {\gamma^{(l)}}^2 q_k^{(l)}\right)
\end{aligned} \tag{3.71}$$

Truncated set of linear equations

We multiply the equations we obtained in this way with $\mathrm{me}_r\left(\eta^{(l)};q_k^{(l)}\right)$ and integrate them over $\eta^{(l)}$ from 0 to 2π. This yields, using (3.31)

$$\frac{\mathrm{M}_{r_l}^{(3)}\left(\xi_{l,0}^{(l)};q_k^{(l)}\right)}{\mathrm{M}_{r_l}^{(1)}\left(\xi_{l,0}^{(l)};q_k^{(l)}\right)}d_{r_l}^{(l)} = -e_{r_l}^{(l)} - \sum_{\substack{m=1\\m\neq l}}^{N}\sum_{p_m=-\infty}^{\infty} d_{p_m}^{(m)} B_{r_l,p_m}^{(3)}(\boldsymbol{\rho}^{lm},\alpha_m-\alpha^{(l)},k,q_k^{(m)},q_k^{(l)}) + \\ + \gamma_0^{(l)}\sum_{p_l=-\infty}^{\infty} a_{p_l}^{(l)}\frac{\mathrm{M}_{p_l}^{(1)}\left(\xi_{l,0}^{(l)};{\gamma^{(l)}}^2 q_k^{(l)}\right)}{\mathrm{M}_{r_l}^{(1)}\left(\xi_{l,0}^{(l)};q_k^{(l)}\right)}A_{r_l,p_l}\left(q_k^{(l)};{\gamma^{(l)}}^2 q_k^{(l)}\right) \tag{3.72}$$

$$\frac{\frac{\partial}{\partial\xi^{(l)}}\mathrm{M}_{r_l}^{(3)}\left(\xi_{l,0}^{(l)};q_k^{(l)}\right)}{\frac{\partial}{\partial\xi^{(l)}}\mathrm{M}_{r_l}^{(1)}\left(\xi_{l,0}^{(l)};q_k^{(l)}\right)}d_{r_l}^{(l)} = -e_{r_l}^{(l)} - \sum_{\substack{m=1\\m\neq l}}^{N}\sum_{p_m=-\infty}^{\infty} d_{p_m}^{(m)} B_{r_l,p_m}^{(3)}(\boldsymbol{\rho}^{lm},\alpha^{(l)}-\alpha^{(m)},k,q_k^{(l)},q_k^{(m)}) + \\ + \gamma_1^{(l)}\sum_{p_l=-\infty}^{\infty} a_{p_l}^{(l)}\frac{\frac{\partial}{\partial\xi^{(l)}}\mathrm{M}_{p_l}^{(1)}\left(\xi_{l,0}^{(l)};{\gamma^{(l)}}^2 q_k^{(l)}\right)}{\frac{\partial}{\partial\xi^{(l)}}\mathrm{M}_{r_l}^{(1)}\left(\xi_{l,0}^{(l)};q_k^{(l)}\right)}A_{r_l,p_l}\left(q_k^{(l)};{\gamma^{(l)}}^2 q_k^{(l)}\right) \tag{3.73}$$

In order to write this equation in matrix form, we introduce the following notation. Assume that vectors $\mathbf{d}^{(l)}$ and $\mathbf{a}^{(l)}$ are truncated according to chapter 8.3. Their components are $\left(\mathbf{d}^{(l)}\right)_{r_l}$, $-R_l < r_l < R_l$ and $\left(\mathbf{a}^{(l)}\right)_{p_l}$, $-P_l < p_l < P_l$. We introduce the following matrices.

$$\mathsf{M}^{(l)} = \mathrm{Diag}\left(\frac{\mathrm{M}_{-R_l}^{(3)}\left(\xi_{l,0}^{(l)};q_k^{(l)}\right)}{\mathrm{M}_{-R_l}^{(1)}\left(\xi_{l,0}^{(l)};q_k^{(l)}\right)},\cdots,\frac{\mathrm{M}_{R_l}^{(3)}\left(\xi_{l,0}^{(l)};q_k^{(l)}\right)}{\mathrm{M}_{R_l}^{(1)}\left(\xi_{l,0}^{(l)};q_k^{(l)}\right)}\right) \tag{3.74}$$

$$\mathsf{M}^{(l)\partial} = \mathrm{Diag}\left(\frac{\frac{\partial}{\partial\xi^{(l)}}\mathrm{M}_{-R_l}^{(3)}\left(\xi_{l,0}^{(l)};q_k^{(l)}\right)}{\frac{\partial}{\partial\xi^{(l)}}\mathrm{M}_{-R_l}^{(1)}\left(\xi_{l,0}^{(l)};q_k^{(l)}\right)},\cdots,\frac{\frac{\partial}{\partial\xi^{(l)}}\mathrm{M}_{R_l}^{(3)}\left(\xi_{l,0}^{(l)};q_k^{(l)}\right)}{\frac{\partial}{\partial\xi^{(l)}}\mathrm{M}_{R_l}^{(1)}\left(\xi_{l,0}^{(l)};q_k^{(l)}\right)}\right) \tag{3.75}$$

$${}^{d}\mathsf{M}^{(l)} = \mathrm{Diag}\left(\frac{1}{\mathrm{M}_{-R_l}^{(1)}\left(\xi_{l,0}^{(l)};q_k^{(l)}\right)},\cdots,\frac{1}{\mathrm{M}_{R_l}^{(1)}\left(\xi_{l,0}^{(l)};q_k^{(l)}\right)}\right) \tag{3.76}$$

$${}^{d}\mathsf{M}^{(l)\partial} = \mathrm{Diag}\left(\frac{1}{\frac{\partial}{\partial\xi^{(l)}}\mathrm{M}_{-R_l}^{(1)}\left(\xi_{l,0}^{(l)};q_k^{(l)}\right)},\cdots,\frac{1}{\frac{\partial}{\partial\xi^{(l)}}\mathrm{M}_{R_l}^{(1)}\left(\xi_{l,0}^{(l)};q_k^{(l)}\right)}\right) \tag{3.77}$$

$${}^{i}\mathsf{M}^{(l)n} = \mathrm{Diag}\left(\mathrm{M}_{-P_l}^{(1)}\left(\xi_{l,0}^{(l)};{\gamma^{(l)}}^2 q_k^{(l)}\right),\cdots,\mathrm{M}_{P_l}^{(1)}\left(\xi_{l,0}^{(l)};q_k^{(l)}\right)\right) \tag{3.78}$$

$${}^{i}\mathsf{M}^{(l)n\partial} = \mathrm{Diag}\left(\frac{\partial}{\partial\xi^{(l)}}\mathrm{M}_{-P_l}^{(1)}\left(\xi_{l,0}^{(l)};{\gamma^{(l)}}^2 q_k^{(l)}\right),\cdots,\frac{\partial}{\partial\xi^{(l)}}\mathrm{M}_{P_l}^{(1)}\left(\xi_{l,0}^{(l)};q_k^{(l)}\right)\right) \tag{3.79}$$

As well, let $\mathsf{T}^{(l,m)}$ be defined by

$$\mathsf{T}^{(l,m)} = \begin{pmatrix} B^{(3)}_{-R_l,-R_m}(\cdot) & \dots & B^{(3)}_{-R_l,+R_m}(\cdot) \\ \vdots & & \vdots \\ B^{(3)}_{R_l,-R_m}(\cdot) & \dots & B^{(3)}_{R_l,+R_m}(\cdot) \end{pmatrix} \tag{3.80}$$

where

$$B^{(j)}_{m,n}(\cdot) \equiv B^{(j)}_{m,n}(\boldsymbol{\rho}^{lm}, \alpha^{(l)} - \alpha^{(m)}, k, q^{(l)}_k, q^{(m)}_k). \tag{3.81}$$

This yields the following equations.

$$\mathsf{M}^{(l)}\mathbf{d}^{(l)} = -\mathbf{e}^{(l)} - \sum_{\substack{m=1 \\ m\neq l}} \mathsf{T}^{(l,m)}\mathbf{d}^{(m)} + \gamma_0^{(l)}\ {}^{d}\mathsf{M}^{(l)}\mathsf{A}\left(q_k^{(l)}; {\gamma^{(l)}}^2 q_k^{(l)}\right)\ {}^{i}\mathsf{M}^{(l)}\mathbf{a}^{(l)} \tag{3.82}$$

$$\mathsf{M}^{(l)\partial}\mathbf{d}^{(l)} = -\mathbf{e}^{(l)} - \sum_{\substack{m=1 \\ m\neq l}} \mathsf{T}^{(l,m)}\mathbf{d}^{(m)} + \gamma_1^{(l)}\ {}^{d}\mathsf{M}^{(l)\partial}\mathsf{A}\left(q_k^{(l)}; {\gamma^{(l)}}^2 q_k^{(l)}\right)\ {}^{i}\mathsf{M}^{(l)\partial}\mathbf{a}^{(l)} \tag{3.83}$$

Elimination of $\mathbf{a}^{(l)}$ yields

$$\begin{aligned} &\left[\frac{1}{\gamma_0^{(l)}}\left({}^{d}\mathsf{M}^{(l)}\mathsf{A}(\cdot)\ {}^{i}\mathsf{M}^{(l)}\right)^{-1}\mathsf{M}^{(l)} - \frac{1}{\gamma_1^{(l)}}\left({}^{d}\mathsf{M}^{(l)\partial}\mathsf{A}(\cdot)\ {}^{i}\mathsf{M}^{(l)}\right)^{-1}\mathsf{M}^{(l)\partial}\right]\mathbf{d}^{(l)} \\ &= \left[\frac{1}{\gamma_0^{(l)}}\left({}^{d}\mathsf{M}^{(l)}\mathsf{A}(\cdot)\ {}^{i}\mathsf{M}^{(l)}\right)^{-1} - \frac{1}{\gamma_1^{(l)}}\left({}^{d}\mathsf{M}^{(l)\partial}\mathsf{A}(\cdot)\ {}^{i}\mathsf{M}^{(l)}\right)^{-1}\right]\left(-\mathbf{e}^{(l)} - \sum_{\substack{m=1 \\ m\neq l}} \mathsf{T}^{(l,m)}\mathbf{d}^{(m)}\right) \end{aligned} \tag{3.84}$$

where

$$\mathsf{A}(\cdot) = \mathsf{A}\left(q_k^{(l)}; {\gamma^{(l)}}^2 q_k^{(l)}\right). \tag{3.85}$$

With

$$\mathsf{X}^{(l)} = \left[\frac{1}{\gamma_0^{(l)}}\left({}^{d}\mathsf{M}^{(l)}\mathsf{A}(\cdot)\ {}^{i}\mathsf{M}^{(l)}\right)^{-1}\mathsf{M}^{(l)} - \frac{1}{\gamma_1^{(l)}}\left({}^{d}\mathsf{M}^{(l)\partial}\mathsf{A}(\cdot)\ {}^{i}\mathsf{M}^{(l)}\right)^{-1}\mathsf{M}^{(l)\partial}\right] \tag{3.86}$$

$$\mathsf{Y}^{(l)} = \left[\frac{1}{\gamma_0^{(l)}}\left({}^{d}\mathsf{M}^{(l)}\mathsf{A}(\cdot)\ {}^{i}\mathsf{M}^{(l)}\right)^{-1} - \frac{1}{\gamma_1^{(l)}}\left({}^{d}\mathsf{M}^{(l)\partial}\mathsf{A}(\cdot)\ {}^{i}\mathsf{M}^{(l)}\right)^{-1}\right] \tag{3.87}$$

we can write the N equations $1 \leq l \leq N$ as

$$\mathsf{X}^{(l)}\mathbf{d}^{(l)} = \mathsf{Y}^{(l)}\left[-\mathbf{e}^{(l)} - \sum_{m\neq l} \mathsf{T}^{(l,m)}\mathbf{d}^{(m)}\right]. \tag{3.88}$$

Iterative solution

The iterative approach to solve (3.88) starts with the single-scattering solutions $\mathbf{d}_0^{(l)}$ for every scatterer. The equivalent of (3.50) for the l'th scatterer may be written in the form of (3.88) as

$$\mathsf{X}^{(l)}\mathbf{d}_0^{(l)} = -\mathsf{Y}^{(l)}\mathbf{e}^{(l)}. \tag{3.89}$$

In these vectors, the index 0 denotes the 'order' of the approximation. The single-scattering approximation which neglects all the interactions between the scattering bodies will be called order 0. Now, we take the zero-order outgoing waves $\mathbf{d}_0^{(m)}$ of all the cylinders and form a new incoming wave for the l'th cylinder with partial wave coefficients $\mathbf{f}_0^{(l)}$.

$$\mathbf{f}_0^{(l)} = \sum_{m\neq l} \mathsf{T}^{(l,m)}\mathbf{d}_0^{(m)} \tag{3.90}$$

Now, this yields a first-order approximation for the coefficients $\mathbf{d}$:

$$\mathsf{X}^{(l)}\mathbf{d}_1^{(l)} = -\mathsf{Y}^{(l)}\mathbf{f}^{(l)}. \tag{3.91}$$

If we continue this process by taking now the $\mathbf{d}_1^{(l)}$ as incoming waves, we obtain a converging iterative scheme, starting with (3.89).

$$\mathsf{X}^{(l)}\mathbf{d}_{i+1}^{(l)} = -\mathsf{Y}^{(l)} \sum_{m\neq l} \mathsf{T}^{(l,m)}\mathbf{d}_i^{(m)}. \tag{3.92}$$

This scheme corresponds to a matrix inversion as described below. As for numerical computation the latter is much faster, we focus on the 'matrix-inversion technique' for solving the multiple scattering problem from now on.

Solution by solving the linear system

With the help of the extended vectors

$$\mathbf{d}^e = \left(\mathbf{d}^{(1)^T}, \ldots, \mathbf{d}^{(N)^T}\right)^T \tag{3.93}$$

$$\mathbf{e}_{\mathsf{Y}}^e = \left(\left(\mathsf{Y}^{(1)}\mathbf{e}^{(1)}\right)^T, \ldots, \left(\mathsf{Y}^{(N)}\mathbf{e}^{(N)}\right)^T\right)^T \tag{3.94}$$

we eventually get a set of linear equations that may be solved with standard methods.

$$\mathsf{U}\mathbf{d}^e = \mathbf{e}_{\mathsf{Y}}^e \tag{3.95}$$

Here, U is given by

$$\mathsf{U} = \begin{pmatrix} \mathsf{X}^{(1)} & \mathsf{Y}^{(1)}\mathsf{T}^{(1,2)} & \ldots & & \mathsf{Y}^{(1)}\mathsf{T}^{(1,N)} \\ \mathsf{Y}^{(2)}\mathsf{T}^{(2,1)} & \mathsf{X}^{(2)} & \ldots & & \mathsf{Y}^{(2)}\mathsf{T}^{(2,N)} \\ \vdots & & \ddots & & \vdots \\ \mathsf{Y}^{(N-1)}\mathsf{T}^{(N-1,1)} & & \ldots & \mathsf{X}^{(N-1)} & \mathsf{Y}^{(N-1)}\mathsf{T}^{(N-1,N)} \\ \mathsf{Y}^{(N)}\mathsf{T}^{(N,1)} & \mathsf{Y}^{(N)}\mathsf{T}^{(N,2)} & \ldots & \mathsf{Y}^{(N)}\mathsf{T}^{(N,N-1)} & \mathsf{X}^{(N)} \end{pmatrix}. \tag{3.96}$$

Limiting cases

In the limit of Dirichlet scatterers, the boundary conditions (3.67) and (3.68) at the l'th obstacle simplifiy to

$$u_{\mathbf{k}}^{\text{in}}(\boldsymbol{\xi}_{l,0}^{(l)}) + \sum_{m=1}^{N} u_{\mathbf{k}}^{(m)}(\boldsymbol{\xi}_{l,0}^{(m)}) = 0\,. \tag{3.97}$$

Writing this explicitly we get

$$\frac{\mathrm{M}_{r_l}^{(3)}(\xi^{(l)}; q_k^{(l)})}{\mathrm{M}_{r_l}^{(1)}(\xi^{(l)}; q_k^{(l)})} d_{r_l}^{l} = -e^{i\mathbf{k}\cdot\mathbf{r}_0^{(l)}} e_{r_l}(\beta - \alpha^{(l)}; \rho^{(l)}, \psi^{(l)}) - \sum_{\substack{m=1 \\ m\neq l}}^{N} \sum_{p_m=-\infty}^{\infty} d_{p_m}^{(m)} B_{r_l,p_m}^{(3)}(\cdot), \tag{3.98}$$

where

$$B_{r,p}^{(j)}(\cdot) \equiv B_{r,p}^{(j)}(\boldsymbol{\rho}^{lm}, \alpha^{(l)} - \alpha^{(m)}, k, q_k^{(l)}, q_k^{(m)}). \tag{3.99}$$

In the same way as before this yields a matrix equation

$$\mathsf{U}^{D}\mathbf{d}^{e} = \mathbf{e}^{e} \tag{3.100}$$

where

$$\mathsf{U}^{D} = \begin{pmatrix} \mathsf{M}^{(1)} & \mathsf{T}^{(1,2)} & \dots & & \mathsf{T}^{(1,N)} \\ \mathsf{T}^{(2,1)} & \mathsf{M}^{(2)} & \dots & & \mathsf{T}^{(2,N)} \\ \vdots & & \ddots & & \vdots \\ \mathsf{T}^{(N-1,1)} & & \dots & \mathsf{M}^{(N-1)} & \mathsf{T}^{(N-1,N)} \\ \mathsf{T}^{(N,1)} & \mathsf{T}^{(N,2)} & \dots & \mathsf{T}^{(N,N-1)} & \mathsf{M}^{(N)} \end{pmatrix} \tag{3.101}$$

and

$$\mathbf{e}^{e} = \left(\left(\mathbf{e}^{(1)}\right)^{T}, \dots, \left(\mathbf{e}^{(N)}\right)^{T} \right)^{T}. \tag{3.102}$$

For Neumann scatterers, the boundary conditions (3.67) and (3.68) at the l'th obstacle simplifiy to

$$\frac{\partial}{\partial \xi^{(l)}} u_{\mathbf{k}}^{\text{in}}(\boldsymbol{\xi}_{l,0}^{(l)}) + \sum_{m=1}^{N} \frac{\partial}{\partial \xi^{(l)}} u_{\mathbf{k}}^{(m)}(\boldsymbol{\xi}_{l,0}) = 0\,. \tag{3.103}$$

Writing this explicitly we get

$$\frac{\frac{\partial}{\partial \xi^{(l)}}\mathrm{M}_{r_l}^{(3)}(\xi^{(l)}; q_k^{(l)})}{\frac{\partial}{\partial \xi^{(l)}}\mathrm{M}_{r_l}^{(1)}(\xi^{(l)}; q_k^{(l)})} d_{r_l}^{l} = -e^{i\mathbf{k}\cdot\mathbf{r}_0^{(l)}} e_{r_l}(\beta - \alpha^{(l)}; \rho^{(l)}, \psi^{(l)}) - \sum_{\substack{m=1 \\ m\neq l}}^{N} \sum_{p_m=-\infty}^{\infty} d_{p_m}^{(m)} B_{r_l,p_m}^{(3)}(\cdot), \tag{3.104}$$

where $B_{m,n}^{(j)}(\cdot)$ is again given by (3.99). In the same way as before this yields a matrix equation

$$\mathsf{U}^{N}\mathbf{d}^{e} = \mathbf{e}^{e} \tag{3.105}$$

where

$$\mathsf{U}^N = \begin{pmatrix} \mathsf{M}^{(1)\partial} & \mathsf{T}^{(1,2)} & \dots & & \mathsf{T}^{(1,N)} \\ \mathsf{T}^{(2,1)} & \mathsf{M}^{(2)\partial} & \dots & & \mathsf{T}^{(2,N)} \\ \vdots & & \ddots & & \vdots \\ \mathsf{T}^{(N-1,1)} & & \dots & \mathsf{M}^{(N-1)\partial} & \mathsf{T}^{(N-1,N)} \\ \mathsf{T}^{(N,1)} & \mathsf{T}^{(N,2)} & \dots & \mathsf{T}^{(N,N-1)} & \mathsf{M}^{(N)\partial} \end{pmatrix}. \tag{3.106}$$

Both (3.105) and (3.100) are sets of linear equations which may be solved with standard methods [15].

Asymptotic boundary condition

Another form of the addition theorem (cf. chapter 7), called *exterior addition theorem* is given by

$$\mathrm{M}_p^{(j)}(\xi^{(l)}; q_k^{(l)})\mathrm{me}_p(\eta^{(l)}; q_k^{(l)}) = \sum_{r=-\infty}^{\infty} A_r(\boldsymbol{\rho}^{lm}, \alpha^{(l)} - \alpha^{(m)}, k, q_k^{(l)}, q_k^{(m)}) \times \mathrm{M}_{r+p}^{(j)}(\xi^{(m)}; q_k^{(m)})\mathrm{me}_r(\eta^{(m)}; q_k^{(m)}). \tag{3.107}$$

This shows that the sum of outgoing scattered waves from all scatterers can be brought into the following form which is valid for ξ large enough (cf. chapter 7 again).

$$u^{\mathrm{sc}}(\xi, \eta) = \sum_{p=-\infty}^{\infty} d'_p \left(\mathbf{d}^{(l)}, \dots, \mathbf{d}^{(N)}\right) \mathrm{M}_p(\xi; q_k)\mathrm{me}_p(\eta; q_k) \tag{3.108}$$

Thus, all the outgoing waves from all the cylinders fulfill the asymptotic boundary condition as in (3.18). $u^{\mathrm{sc}}(\mathbf{x})$ has the asymptotic behaviour

$$u^{\mathrm{sc}}(\mathbf{x}) = \frac{e^{ikr}}{\sqrt{kr}} \left[u_\infty\left(\frac{\mathbf{x}}{r}\right) + O\left(\frac{1}{r}\right)\right] \tag{3.109}$$

The $\mathrm{M}_p^{(j)}$ are defined to fulfill $\mathrm{M}_p^{(j)}(\xi; q) \to Z_m^{(j)}(2\sqrt{q}\cosh\xi)$ for $\xi \to \infty$. With $2\sqrt{q}\cosh\xi \approx \sqrt{q}e^{\xi}$ for $\xi \gg 1$ and

$$H_m^{(1),(2)}(\xi) \to (-i)^m \sqrt{\frac{2}{\pi\xi}} e^{\pm i(\xi - \frac{\pi}{4})}$$

we get

$$\mathrm{M}_p^{(3,4)}(\xi; q) \to \frac{e^{\pm i\sqrt{q}e^{\xi}}}{\sqrt{\sqrt{q}e^{\xi}}} (-i)^m \sqrt{\frac{2}{\pi}} e^{\pm i\frac{\pi}{4}} \ . \tag{3.110}$$

So, we define a far-zone field for one scatterer

$$u_\infty(\eta) = (-i)^m \frac{1+i}{\sqrt{\pi}} \sum_{p=-\infty}^{\infty} d_p^{(m)} \mathrm{me}_p\left(\eta; q_k^{(m)}\right). \tag{3.111}$$

For several scatterers, we have $\mathbf{r} = \mathbf{r}_0^{(l)} + \mathbf{r}^{(l)}$. This means that $\mathrm{M}_p^{(j)}(\xi; q) \to Z_m^{(j)}(2\sqrt{q}\cosh\xi - k|\mathbf{r}_0^{(l)}|\cos(\eta - \psi^{(l)})$ for $\xi \to \infty$, therefore the far-zone field for several scatterers is

$$u_\infty(\eta) = \sum_{p=-\infty}^{\infty} \frac{1+i}{\sqrt{\pi}} \sum_{m=1}^{N} (-i)^m e^{-k|\mathbf{r}_0^{(m)}|\cos(\eta-\psi^{(m)})} d_p^{(m)} \mathrm{me}_p\left(\eta; q_k^{(m)}\right). \quad (3.112)$$

3.3 Summary

In this chapter, we considered time-independent scattering of electromagnetic waves by an array of elliptical cylinders. The mathematical model is formulated explicitly in elliptical geometry and solved by the separation of variables method. No a priori limitations are imposed on the number of scatterers, on the geometric parameters that fix their elliptical form, on their orientation, on their relative positions (except that overlap is forbidden), and on their material constants.

The solution is obtained in two steps: first, a solution of the single scattering problem (scattering by one elliptical cylinder) is obtained. By using the addition theorem for Mathieu functions (cf. chapter 7) two solution methods for the problem of several scatterers is then given for a given wave vector $\mathbf{k}$: first, an iterative approach which makes clear why the framework of solution for several scatterers is called *multiple scattering*. Second, a numerically more efficient approach is presented which is based on solving the set of linear equations directly.

Chapter 4

Scattering in a waveguide

This chapter deals with several scatterers in a two-dimensional waveguide where x is the longitudinal and y the transverse direction. This waveguide is described by Dirichlet boundary conditions at $y = 0$ and $y = W$. Note that this implies a modification of the asymptotic boundary condition. The physical meaning of these boundary conditions is a 'potential wall' of infinite height in quantum mechanics, an ideal conductor for the $\mathbf{E}_{\|}$ case in electrodynamics, and two infinite acoustically soft walls in acoustics. The waveguide contains several obstacles $O_i \subset \mathbb{R}^2$ whose shapes are parametrised by closed curves ∂O_i. See Fig. 4.1 for an illustration of the geometry. We demand that $u(\mathbf{x})$ satisfies Dirichlet boundary conditions on ∂O_i.

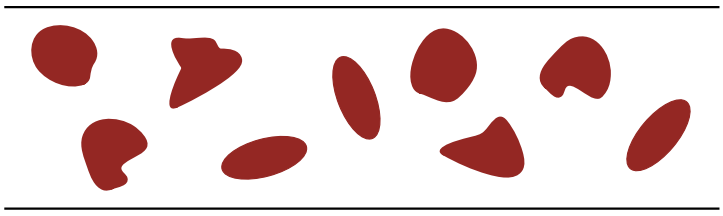

Figure 4.1: Obstacles in waveguide

Waveguide modes

Free solutions $u(x, y)$ in the waveguide without any obstacles must be solutions to the Helmholtz equation

$$\left(\Delta + k^2\right) u(x, y) = 0, \qquad \text{for } (x, y) \in D \tag{4.1}$$

in the domain

$$D = (-\infty, \infty) \times [0, W], \tag{4.2}$$

and fulfil the boundary conditions

$$u(x,0) = 0, \tag{4.3}$$
$$u(x,W) = 0. \tag{4.4}$$

The general free solution is given by

$$u^{\text{free}}(x,y;x_0) = \sum_{n=1}^{\infty} a_n \phi_n(y) e^{i\kappa_n(x-x_0)} + b_n \phi_n(y) e^{-i\kappa_n(x-x_0)}, \tag{4.5}$$

where

$$\phi_n(y) = \sqrt{\frac{2}{W}} \sin(k_n y), \tag{4.6}$$
$$k_n = \frac{n\pi}{W}, \tag{4.7}$$
$$\kappa_n = \sqrt{k^2 - k_n^2}\,. \tag{4.8}$$

The index n labels the *modes* of the waveguide. If κ_n is real, the mode is called *propagating*, if it is imaginary, it is called *evanescent*. Note that for a given k, there exist always only a finite number of propagating modes. The function (4.5) is well-behaved for any finite x. In order to calculate real scattering problems, we have to make sure that no exponentially growing waves are present for $x \to \pm\infty$.

4.1 Green's function formulation

In order to formulate an integral equation for the problem sketched in Fig. 4.1, we have to calculate the Green's function $G_k(\mathbf{x},\mathbf{x}')$, first. From its definition, it has to satisfy the inhomogeneous wave equation

$$\left(\Delta + k^2\right) G_k(\mathbf{x},\mathbf{x}') = -\delta(\mathbf{x}-\mathbf{x}') = -\delta(x-x')\delta(y-y'), \qquad (x,y) \in D. \tag{4.9}$$

Here, $\mathbf{x} = (x,y)$, $\mathbf{x}' = (x',y')$ and

$$D = (-\infty,\infty) \times (0,W). \tag{4.10}$$

The boundary conditions imposed on $G_k(\mathbf{x},\mathbf{x}')$ are:

1. Dirichlet boundary conditions on the walls

$$G_k(\mathbf{x},\mathbf{x}') = 0, \qquad \text{on } y = 0,\ y = W. \tag{4.11}$$

2. At infinity $G_k(\mathbf{x},\mathbf{x}')$ must consist of outgoing waves only.

$$\lim_{x\to+\infty} \left(\frac{\partial}{\partial x} - i\kappa_n\right) \int_0^W G(\mathbf{x},\mathbf{x}')\phi_n(y')\,\mathrm{d}y' = 0 \tag{4.12}$$
$$\lim_{x\to-\infty} \left(\frac{\partial}{\partial x} + i\kappa_n\right) \int_0^W G(\mathbf{x},\mathbf{x}')\phi_n(y')\,\mathrm{d}y' = 0 \tag{4.13}$$

In view of (4.11), let us make the ansatz

$$G_k(\mathbf{x},\mathbf{x}') = \sum_{n=1}^{\infty} \phi_n(y)\phi_n(y') f_n(x,x'). \tag{4.14}$$

Substituting this into (4.9), we obtain

$$\sum_{n=1}^{\infty} \left(\frac{\partial}{\partial x^2} + \kappa_n^2\right) \phi_n(y)\phi_n(y') f_n(x,x') = -\delta(x-x')\delta(y-y'). \tag{4.15}$$

Note that either $\kappa_n > 0$ or $\kappa_n = i\kappa_n'$ with $\kappa_n' > 0$. By applying a test function, we see that (4.15) is equivalent to the following differential equation for f_n.

$$\left(\frac{\partial}{\partial x^2} + \kappa_n^2\right) f_n(x,x') = -\delta(x-x')\frac{2}{W} \tag{4.16}$$

For $x \neq x'$, f_n satisfies the homogeneous one-dimensional wave equation so that we can write, using the radiation conditions (4.12) and (4.13),

$$f_n = \begin{cases} C_n e^{i\kappa_n}(x-x') & \text{for } x > x' \\ C_n e^{-i\kappa_n}(x-x') & \text{for } x < x'. \end{cases} \tag{4.17}$$

The amplitude C_n is the same for both cases, since G must be continuous across $x = x'$. In order to determine C_n, we integrate (4.16) once with respect to x. As

$$\begin{aligned} \lim_{\epsilon\to 0} \int_{x'-\epsilon}^{x'+\epsilon} \left(\frac{\partial}{\partial y^2} + \kappa_n^2\right) f_n(x,x')\,\mathrm{d}x &= \lim_{\epsilon\to 0} \frac{\partial f_n}{\partial x}\Big|_{x'-\epsilon}^{x'+\epsilon} \\ &= -\lim_{\epsilon\to 0} \frac{2}{W} \int_{x=x'-\epsilon}^{x=x'+\epsilon} \delta(x-x') = -\frac{2}{W} \end{aligned} \tag{4.18}$$

and as from (4.17) we see that the discontinuity of $\frac{\partial f_n}{\partial x}$ across the $x = 0$ plane is $2i\kappa_n C_n$, we see that

$$C_n = \frac{i}{\kappa_n W}. \tag{4.19}$$

Therefore, we obtain finally [16]

$$G_k(\mathbf{x},\mathbf{x}') = \frac{i}{W} \sum_{n=1}^{\infty} \frac{\sin\left(\frac{n\pi}{W}y\right)\sin\left(\frac{n\pi}{W}y'\right)}{\kappa_n} e^{i\kappa_n|x-x'|}. \tag{4.20}$$

4.1.1 Formulation of the problem

We outline some properties of the scattering solutions to the two-dimensional Helmholtz equation (4.1) for a single obstacle $O \subset D$ with the help of the *Green's function* (4.20). Given an integrable function $\psi(\mathbf{x})$, we define the single-layer potential [17]

$$[S\psi](\mathbf{x}) = \int_{\partial O} G_k(\mathbf{x},\mathbf{x}'(s))\psi(\mathbf{x}'(s))\,\mathrm{d}s, \qquad \mathbf{x} \in D \setminus O. \tag{4.21}$$

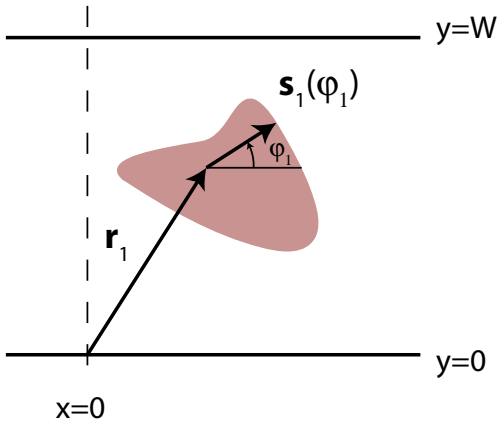

Figure 4.2: Coordinates for describing a scatterer in the waveguide

It is a solution to the Helmholtz equation in $D \setminus O$ and satisfies the same boundary and asymptotic conditions as $G_k(\mathbf{x}, \mathbf{x}')$ (4.11 - 4.13). For a given curve $\partial O \subset D$, which is parametrised by (cf. Fig. 4.2)

$$\mathbf{s}^1(\mathbf{r}_1, \varphi_1) = \mathbf{r}_1 + \mathbf{s}_1(\varphi_1), \qquad 0 \leq \varphi_1 < 2\pi, \tag{4.22}$$

we demand

$$u\left(\mathbf{s}^1(\mathbf{r}_1, \varphi_1)\right) = 0, \qquad \text{for } 0 \leq \varphi_1 < 2\pi. \tag{4.23}$$

A general solution for $u(\mathbf{x})$ is given by the sum of a given incident field

$$u^{\text{in}}(\mathbf{x}; x_0) = \sum_{n=1}^{\infty} a_n^{\text{in}} \phi_n(y) e^{i\kappa_n(x-x_0)} + b_n^{\text{in}} \phi_n(y) e^{-i\kappa_n(x-x_0)} \tag{4.24}$$

and the single layer potential of a yet unknown source distribution $\psi\left(\mathbf{s}^1(\mathbf{r}_1, \varphi_1)\right)$:

$$\begin{aligned} u(\mathbf{x}) &= u^{\text{in}}(\mathbf{x}; x_0) + [S\psi](\mathbf{x}) = u^{\text{in}}(\mathbf{x}; x_0) + u^{\text{sc}}(\mathbf{x}) \\ &= u^{\text{in}}(\mathbf{x}; x_0) + \int_0^{2\pi} G_k\left(\mathbf{x}, \mathbf{s}^1(\mathbf{r}_1, \varphi_1)\right) \psi\left(\mathbf{s}^1(\mathbf{r}_1, \varphi_1)\right) \left|\frac{\mathrm{d}s^1}{\mathrm{d}\varphi_1}\right| \mathrm{d}\varphi_1. \end{aligned} \tag{4.25}$$

4.2 Solution of the waveguide problem

Now, we make a Fourier ansatz for the unknown source distribution ψ on the boundary.

$$\psi\left(\mathbf{s}^1(\mathbf{r}_1, \varphi_1)\right) \left|\frac{\mathrm{d}s^1}{\mathrm{d}\varphi_1}\right| = \sum_{m=-\infty}^{\infty} j_m e^{im\varphi_1} \tag{4.26}$$

This leads to the field

$$u^{\text{sc}}(\mathbf{x}) = \sum_{m=-\infty}^{\infty} j_m u_m^{\text{sc}}(\mathbf{x}) \tag{4.27}$$

where

$$u_m^{\mathrm{sc}}(\mathbf{x}) = \frac{i}{W}\sum_{n=1}^{\infty}\frac{\phi_n(y)}{\kappa_n}\int_0^{2\pi}\phi_n(\mathbf{s}^1(\mathbf{r}_1,\varphi_1)\cdot\mathbf{e}_y)e^{i\kappa_n\left|x-\mathbf{s}^1(\mathbf{r}_1,\varphi_1)\cdot\mathbf{e}_x\right|}e^{im\varphi_1}\,\mathrm{d}\varphi_1. \tag{4.28}$$

In order to calculate the j_m, we multiply the boundary condition

$$u^{\mathrm{in}}\left(\mathbf{s}^1(\mathbf{r}_1,\varphi);x_0\right)+\sum_{m=-\infty}^{\infty}j_m u_m^{\mathrm{sc}}\left(\mathbf{s}^1(\mathbf{r}_1,\varphi)\right)=0 \qquad 0\le\varphi<2\pi \tag{4.29}$$

by $e^{in\varphi}$ and integrate it over φ from 0 to 2π. This yields for every $n\in\mathbb{Z}$ an equation

$$\sum_{l=1}^{\infty}\left[V_{n,l}^a(x_0)a_l^{\mathrm{in}}+V_{n,l}^b(x_0)b_l^{\mathrm{in}}\right]+\sum_{m=-\infty}^{\infty}U_{n,m}\,j_m=0, \tag{4.30}$$

where

$$U_{n,m}=\int_0^{2\pi}u_m^{\mathrm{sc}}\left(\mathbf{s}^1(\mathbf{r}_1,\varphi)\right)e^{in\varphi}\,\mathrm{d}\varphi, \tag{4.31}$$

$$V_{n,l}^a(x_0)=\int_0^{2\pi}\phi_l\left(\mathbf{s}^1(\mathbf{r}_1,\varphi)\cdot\mathbf{e}_y\right)e^{i\kappa_l(\mathbf{s}^1(\mathbf{r}_1,\varphi)\cdot\mathbf{e}_x-x_0)}e^{in\varphi}\,\mathrm{d}\varphi, \tag{4.32}$$

$$V_{n,l}^b(x_0)=\int_0^{2\pi}\phi_l(\mathbf{s}^1(\mathbf{r}_1,\varphi)\cdot\mathbf{e}_y)e^{-i\kappa_l(\mathbf{s}^1(\mathbf{r}_1,\varphi)\cdot\mathbf{e}_x-x_0)}e^{in\varphi}\,\mathrm{d}\varphi. \tag{4.33}$$

This is a linear set of equations. In vector and matrix notation, we obtain

$$\mathbf{j}=-U^{-1}\left[V_a\mathbf{a}^{\mathrm{in}}+V^b\mathbf{b}^{\mathrm{in}}\right]. \tag{4.34}$$

Several scatterers with overlap in x-direction

Next, we discuss the situation where several scatterers $O_k\subset D$, $1\le k\le N$, are present in the waveguide. With the unknown source distributions ψ^k, the general solution for the N scatterers is

$$\begin{aligned}u(\mathbf{x}) &= u^{\mathrm{in}}(\mathbf{x};x_0)+\sum_{k=1}^{N}\left[S\psi^k\right](\mathbf{x})=u^{\mathrm{in}}(\mathbf{x};x_0)+\sum_{k=1}^{N}u^{\mathrm{sc},k}(\mathbf{x})\\ &= u^{\mathrm{in}}(\mathbf{x};x_0)+\sum_{k=1}^{N}\int_0^{2\pi}G_k\left(\mathbf{x},\mathbf{s}^k(\mathbf{r}_k,\varphi_k)\right)\psi\left(\mathbf{s}^k(\mathbf{r}_k,\varphi_k)\right)\left|\frac{\mathrm{d}s^k}{\mathrm{d}\varphi_k}\right|\,\mathrm{d}\varphi_k.\end{aligned} \tag{4.35}$$

Similarly to (4.22), we parametrise ∂O_k by

$$\mathbf{s}^k(\mathbf{r}_k,\varphi_k)=\mathbf{r}_k+\mathbf{s}_k(\varphi_k), \qquad 0\le\varphi_k<2\pi. \tag{4.36}$$

We need functions

$$\psi^k(\left(\mathbf{s}^k(\mathbf{r}_k,\varphi_k)\right)\left|\frac{\mathrm{d}s^k}{\mathrm{d}\varphi_k}\right|=\sum_{m=-\infty}^{\infty}j_m^k e^{im\varphi_k} \tag{4.37}$$

on the surfaces ∂O_k of the scatterers. To solve the N boundary equations, on the surfaces ∂O_i, we introduce

$$u_m^{\mathrm{sc},k}(\mathbf{x}) = \frac{i}{W}\sum_{n=1}^{\infty}\frac{\phi_n(y)}{\kappa_n}\int_0^{2\pi}\phi_n(\mathbf{s}^k(\mathbf{r}_k,\varphi_k)\cdot\mathbf{e}_y)e^{i\kappa_n|x-\mathbf{s}^k(\mathbf{r}_k,\varphi_k)\cdot\mathbf{e}_x|}e^{im\varphi_k}\,\mathrm{d}\varphi_k. \tag{4.38}$$

The boundary equations read for $1\le i\le N$

$$\begin{aligned} 0 =\ & u(\mathbf{s}^i(\mathbf{r}_i,\varphi_i)) = u^{\mathrm{in}}(\mathbf{s}^i(\mathbf{r}_i,\varphi_i);x_0) + \sum_{k=1}^{N}\left[S\psi^k\right](\mathbf{s}^i(\mathbf{r}_i,\varphi_i)) \\ =\ & u^{\mathrm{in}}(\mathbf{s}^i(\mathbf{r}_i,\varphi_i);x_0) + \sum_{k=1}^{N}\sum_{m=-\infty}^{\infty} u_m^{\mathrm{sc},k}(\mathbf{s}^i(\mathbf{r}_i,\varphi_i))j_m^k, \qquad 0\le\phi_i<2\pi. \end{aligned} \tag{4.39}$$

Next, we multiply (4.39) by $e^{in\varphi_i}$, and integrate over φ_i from 0 to 2π. This yields for every $1\le i\le N$ and every $n\in\mathbb{Z}$ an equation

$$\sum_{l=1}^{\infty}\left[V_{n,l}^{a,i}(x_0)a_l^{\mathrm{in}} + V_{n,l}^{b,i}(x_0)b_l^{\mathrm{in}}\right] + \sum_{k=1}^{N}\sum_{m=-\infty}^{\infty}U_{n,m}^{i,k}\,j_m^k = 0, \tag{4.40}$$

where

$$U_{n,m}^{i,k} = \int_0^{2\pi} u_m^{\mathrm{sc},k}\left(\mathbf{s}^i(\mathbf{r}_i,\varphi_i)\right)e^{in\varphi_i}\,\mathrm{d}\varphi_i, \tag{4.41}$$

$$V_{n,l}^{a,i}(x_0) = \int_0^{2\pi}\phi_l\left(\mathbf{s}^i(\mathbf{r}_i,\varphi_i)\cdot\mathbf{e}_y\right)e^{i\kappa_l(\mathbf{s}^i(\mathbf{r}_i,\varphi_i)\cdot\mathbf{e}_x-x_0)}e^{in\varphi_i}\,\mathrm{d}\varphi_i, \tag{4.42}$$

$$V_{n,l}^{b,i}(x_0) = \int_0^{2\pi}\phi_l(\mathbf{s}^i(\mathbf{r}_i,\varphi_i)\cdot\mathbf{e}_y)e^{-i\kappa_l(\mathbf{s}^i(\mathbf{r}_i,\varphi_i)\cdot\mathbf{e}_x-x_0)}e^{in\varphi_i}\,\mathrm{d}\varphi_i. \tag{4.43}$$

This is again a linear set of equations. Using

$$\mathbf{j}^e = \left[\left(\mathbf{j}^1\right)^T,\left(\mathbf{j}^2\right)^T,\ldots,\left(\mathbf{j}^N\right)^T\right]^T, \tag{4.44}$$

and

$$V^{e,a} = \begin{pmatrix} V^{a,1}\\ V^{a,2}\\ \vdots\\ V^{a,N}\end{pmatrix}, \qquad V^{e,b} = \begin{pmatrix} V^{b,1}\\ V^{b,2}\\ \vdots\\ V^{b,N}\end{pmatrix}, \tag{4.45}$$

$$U^e = \begin{pmatrix} U^{1,1} & U^{1,2} & \cdots & U^{1,N}\\ U^{2,1} & U^{2,2} & \cdots & U^{2,N}\\ \vdots & & \ddots & \vdots\\ U^{N,1} & U^{N,2} & \cdots & U^{N,N}\end{pmatrix}, \tag{4.46}$$

we rewrite it as follows:

$$\mathbf{j}^e = -\left(U^e\right)^{-1}\left[V^{e,a}\mathbf{a}^{\mathrm{in}} + V^{e,a}\mathbf{b}^{\mathrm{in}}\right]. \tag{4.47}$$

4.3 Transfer Matrix

Take the two free solutions $u^L(\mathbf{x}; x_L)$ and $u^R(\mathbf{x}; x_R)$ defined to the left and to the right of the scatterer(s).

$$u^L(\mathbf{x}; x_L) = \sum_{n=1}^{\infty} a_n^L \phi_n(y) e^{i\kappa_n(x-x_L)} + b_n^L \phi_n(y) e^{-i\kappa_n(x-x_L)}, \quad -\infty < x \leq x_L, \tag{4.48}$$

$$u^R(\mathbf{x}; x_R) = \sum_{n=1}^{\infty} a_n^R \phi_n(y) e^{i\kappa_n(x-x_R)} + b_n^R \phi_n(y) e^{-i\kappa_n(x-x_R)}, \quad x_R \leq x < \infty. \tag{4.49}$$

Similarly to chapter 3, $\mathbf{a}$ will denote a vector with an infinite number of components $(a_1, a_2, \dots, a_N, a_{N+1}, \dots)$ and $\mathbf{a}_N$ the finite vector $(a_1, a_2, \dots, a_N)$. Now, in (4.25), set $u^{\text{in}}(\mathbf{x}; x_0) = u^L(\mathbf{x}; x_L)$, and $u(\mathbf{x}) = u^R(\mathbf{x}; x_R)$. With the source distributions given by (4.34) or (4.47), $u^R(\mathbf{x}; x_R)$ is then uniquely determined by the coefficients $\mathbf{a}^L$ and $\mathbf{b}^L$. The transfer matrix $\mathsf{T}(x_L, x_R)$ is defined as the matrix which describes this relation in the following way (cf. Fig. 4.3).

$$\begin{pmatrix} \mathbf{a}^R \\ \mathbf{b}^R \end{pmatrix} = \mathsf{T}(x_L, x_R) \begin{pmatrix} \mathbf{a}^L \\ \mathbf{b}^L \end{pmatrix}. \tag{4.50}$$

Note that once the transfer matrix is known for a given source distribution $\mathbf{j}$, we can calculate the solution for an arbitrary number of identical structures with the same source distribution by multiplying the free-wave coefficients on one side of the obstacles with the transfer matrix as often as necessary.

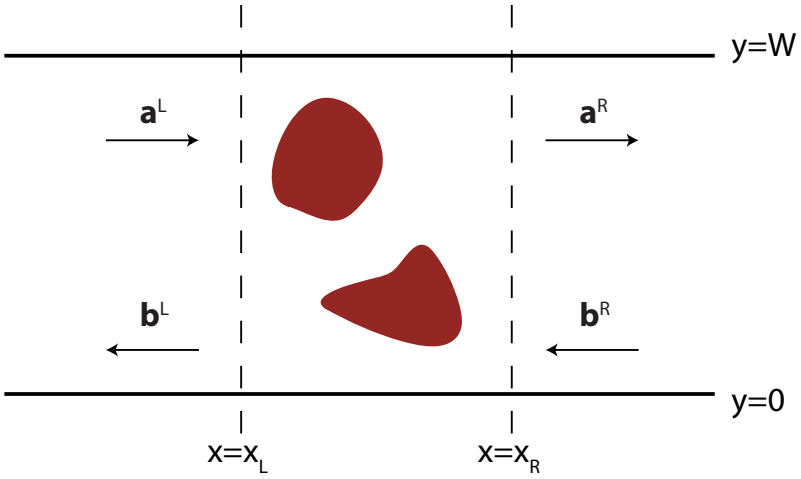

Figure 4.3: Transfer Matrix relating free solutions

4.3.1 Determination of the transfer matrix for one scatterer

Now, take (4.25) and its derivative, both with $u^{\text{in}}(\mathbf{x}; x_0) = u^L(\mathbf{x}; x_L)$, and $u(\mathbf{x}) = u^R(\mathbf{x}; x_R)$ and the source distribution (4.26) at a point $\mathbf{x}$ with $x > x_R$, and identify these functions with the free solutions (4.48 - 4.49) and its derivatives, respectively.

$$u^R(\mathbf{x}; x_R) = u^L(\mathbf{x}; x_L) + \sum_{m=-\infty}^{\infty} j_m u_m^{\text{sc}}(x, y) \tag{4.51}$$

$$\frac{\partial}{\partial x} u^R(\mathbf{x}; x_R) = \frac{\partial}{\partial x} u^L(\mathbf{x}; x_L) + \sum_{m=-\infty}^{\infty} j_m \frac{\partial}{\partial x} u_m^{\text{sc}}(x, y) \tag{4.52}$$

We multiply both equations by $\phi_l(y)$ and integrate them from 0 to W over y. This yields

$$\begin{aligned} a_l^R e^{i\kappa_l(x-x_R)} + b_l^R e^{-i\kappa_l(x-x_R)} = a_l^L e^{i\kappa_l(x-x_L)} + b_l^L e^{-i\kappa_l(x-x_L)} \\ + \sum_{m=-\infty}^{\infty} j_m \int_0^W \phi_l(y) u_m^{\text{sc}}(x, y) \ \mathrm{d}y, \end{aligned} \tag{4.53}$$

$$\begin{aligned} i\kappa_l \left[a_l^R e^{i\kappa_l(x-x_R)} - b_l^R e^{-i\kappa_l(x-x_R)} \right] = i\kappa_l \left[a_l^L e^{i\kappa_l(x-x_L)} - b_l^L e^{-i\kappa_l(x-x_L)} \right] \\ + \sum_{m=-\infty}^{\infty} j_m \int_0^W \phi_l(y) \frac{\partial}{\partial x} u_m^{\text{sc}}(x, y) \ \mathrm{d}y. \end{aligned} \tag{4.54}$$

With the definitions

$$X_{l,m}(x) = \int_0^W \phi_l(y) u_m^{\text{sc}}(x, y) \ \mathrm{d}y \tag{4.55}$$

$$X_{l,m}^d(x) = \frac{1}{i\kappa_l} \int_0^W \phi_l(y) \frac{\partial}{\partial x} \ u_m^{\text{sc}}(x, y) \ \mathrm{d}y \tag{4.56}$$

and $x = x_R$ equations (4.53) and (4.54) become

$$a_l^R + b_l^R = a_l^L e^{i\kappa_l(x_R - x_L)} + b_l^L e^{-i\kappa_l(x_R - x_L)} + \sum_{m=-\infty}^{\infty} X_{l,m}(x_R) j_m \tag{4.57}$$

$$a_l^R - b_l^R = a_l^L e^{i\kappa_l(x_R - x_L)} - b_l^L e^{-i\kappa_l(x_R - x_L)} + \sum_{m=-\infty}^{\infty} X_{l,m}^d(x_R) j_m. \tag{4.58}$$

In matrix notation, we obtain

$$\mathbf{a}^R + \mathbf{b}^R = T^{(1)}(x_R; x_L)\mathbf{a}^L + T^{(2)}(x_R; x_L)\mathbf{b}^L + X(x_R)\mathbf{j}, \tag{4.59}$$

$$\mathbf{a}^R - \mathbf{b}^R = T^{(1)}(x_R; x_L)\mathbf{a}^L - T^{(2)}(x_R; x_L)\mathbf{b}^L + X^d(x_R)\mathbf{j}, \tag{4.60}$$

where the elements of the diagonal matrices $T^{(1)}(x;x_0)$, $T^{(2)}(x;x_0)$ are defined by

$$T^{(1)}_{m,n}(x;x_L) = \delta_{m,n} e^{i\kappa_n (x-x_L)}, \tag{4.61}$$

$$T^{(2)}_{m,n}(x;x_L) = \delta_{m,n} e^{-i\kappa_n (x-x_L)}. \tag{4.62}$$

Now, knowing from (4.34)

$$\mathbf{j} = -U^{-1}\left[V^a \mathbf{a}^L + V^b \mathbf{b}^L\right] \tag{4.63}$$

from eq. (4.30), we end up with the following equations (in which we omit the arguments for brevity).

$$\mathbf{a}^R + \mathbf{b}^R = \left[T^{(1)} - XU^{-1}V^a\right]\mathbf{a}^L + \left[\, T^{(2)} - XU^{-1}V^b\right]\mathbf{b}^L \tag{4.64}$$

$$\mathbf{a}^R - \mathbf{b}^R = \left[T^{(1)} - X^d U^{-1}V^a\right]\mathbf{a}^L + \left[\, -T^{(2)} - X^d U^{-1}V^b\right]\mathbf{b}^L \tag{4.65}$$

To shorten the notation, we introduce now

$$M_1 = \left[T^{(1)} - XU^{-1}V^a\right], \tag{4.66}$$

$$M_2 = \left[\, T^{(2)} - XU^{-1}V^b\right], \tag{4.67}$$

$$M_3 = \left[T^{(1)} - X^d U^{-1}V^a\right], \tag{4.68}$$

$$M_4 = \left[\, -T^{(2)} - X^d U^{-1}V^b\right]. \tag{4.69}$$

Finally, we obtain with

$$\mathbf{a}^R + \mathbf{b}^R = M_1\mathbf{a}^L + M_2\mathbf{b}^L, \tag{4.70}$$

$$\mathbf{a}^R - \mathbf{b}^R = M_3\mathbf{a}^L + M_4\mathbf{b}^L, \tag{4.71}$$

the following solution for $\mathbf{a}^R$ and $\mathbf{b}^R$ in transfer matrix form:

$$\begin{pmatrix} \mathbf{a}^R \\ \mathbf{b}^R \end{pmatrix} = \frac{1}{2}\begin{pmatrix} M_1 + M_3 & M_2 + M_4 \\ M_1 - M_3 & M_2 - M_4 \end{pmatrix}\begin{pmatrix} \mathbf{a}^L \\ \mathbf{b}^L \end{pmatrix} \tag{4.72}$$

4.3.2 The transfer matrix for several scatterers

We perform a similar procedure in order to relate again u^L (4.51) and u^R (4.52) for N obstacles. We start again with the following equations derived from (4.25)

$$u^R(\mathbf{x};x_R) = u^L(\mathbf{x};x_L) + \sum_{k=1}^{N}\sum_{m=-\infty}^{\infty} j_m^k u_m^{\mathrm{sc},k}(x,y), \tag{4.73}$$

$$\frac{\partial}{\partial x}u^R(\mathbf{x};x_R) = \frac{\partial}{\partial x}u^L(\mathbf{x};x_L) + \sum_{k=1}^{N}\sum_{m=-\infty}^{\infty} j_m^k \frac{\partial}{\partial x}u_m^{\mathrm{sc},k}(x,y), \tag{4.74}$$

multiply these by $\phi_l(y)$ and integrate them from 0 to W over y. This yields with

$$X^k_{l,m}(x) = \int_0^W \phi_l(y) u^{\mathrm{sc},k}_m(x,y)\ \mathrm{d}y \tag{4.75}$$

$$X^{dk}_{l,m}(x) = \frac{1}{i\kappa_l}\int_0^W \phi_l(y)\frac{\partial}{\partial x}\ u^{\mathrm{sc},k}_m(x,y)\ \mathrm{d}y \tag{4.76}$$

and $x = x_R$ equations the following equations in matrix notation

$$\mathbf{a}^R + \mathbf{b}^R = T^{(1)}(x_R;x_L)\mathbf{a}^L + T^{(2)}(x_R;x_L)\mathbf{b}^L + X^e(x_R)\,\mathbf{j}^e, \tag{4.77}$$

$$\mathbf{a}^R - \mathbf{b}^R = T^{(1)}(x_R;x_L)\mathbf{a}^L - T^{(2)}(x_R;x_L)\mathbf{b}^L + X^{de}(x_R)\,\mathbf{j}^e. \tag{4.78}$$

Here,

$$X^e = \left(X^1, X^2, \ldots, X^n\right), \qquad X^{de} = \left(X^{d1}, X^{d2}, \ldots, X^{dn}\right). \tag{4.79}$$

Now, knowing from (4.47)

$$\mathbf{j} = -\left(U^e\right)^{-1}\left[V^{ea}\mathbf{a}^L + V^{eb}\mathbf{b}^L\right] \tag{4.80}$$

we obtain

$$\mathbf{a}^R + \mathbf{b}^R = \left[T^{(1)} - X^e\left(U^e\ \right)^{-1}V^{ea}\right]\mathbf{a}^L + \left[\ T^{(2)} - X^e\left(U^e\ \right)^{-1}V^{eb}\right]\mathbf{b}^L \tag{4.81}$$

$$\mathbf{a}^R - \mathbf{b}^R = \left[T^{(1)} - X^{de}\left(U^e\ \right)^{-1}V^{ea}\right]\mathbf{a}^L + \left[\ -T^{(2)} - X^{ed}\left(U^e\ \right)^{-1}V^{eb}\right]\mathbf{b}^L \tag{4.82}$$

We introduce now the matrices

$$M^e_1 = \left[T^{(1)} - X^e\left(U^e\ \right)^{-1}V^{ea}\right], \tag{4.83}$$

$$M^e_2 = \left[\ T^{(2)} - X^e\left(U^e\ \right)^{-1}V^{eb}\right], \tag{4.84}$$

$$M^e_3 = \left[T^{(1)} - X^{de}\left(U^e\ \right)^{-1}V^{ea}\right], \tag{4.85}$$

$$M^e_4 = \left[\ -T^{(2)} - X^{de}\left(U^e\ \right)^{-1}V^{eb}\right]. \tag{4.86}$$

With these, the transfer matrix for N obstacles is formally the same as for one scatterer. It is given by

$$\begin{pmatrix}\mathbf{a}^R\\ \mathbf{b}^R\end{pmatrix} = \frac{1}{2}\begin{pmatrix}M^e_1 + M^e_3 & M^e_2 + M^e_4\\ M^e_1 - M^e_3 & M^e_2 - M^e_4\end{pmatrix}\begin{pmatrix}\mathbf{a}^L\\ \mathbf{b}^L\end{pmatrix}. \tag{4.87}$$

4.3.3 General properties of the transfer matrix

Time reversal

Time-invariance of the time-dependent Helmholtz equation (2.1) means that if $u(\mathbf{x},t)$ is a solution, so is $u(\mathbf{x},-t)$. The Fourier transforms are $u(\mathbf{x},\omega)$ and

$u^*(\mathbf{x},\omega)$, respectively, and are both solutions to the Helmholtz equation (4.1). This means that the time-inversed counterparts to $u^L(\mathbf{x};x_L)$ and $u^R(\mathbf{x};x_R)$:

$$^{-}u^L(\mathbf{x};x_L) = u^{L^*}(\mathbf{x};x_L), \tag{4.88}$$

$$^{-}u^R_{-}(\mathbf{x};x_R) = u^{R^*}(\mathbf{x};x_R). \tag{4.89}$$

These are solutions for the free waveguide problem (4.1 - 4.4), too. Their components are denoted by $^{-}\mathbf{a}$ and $^{-}\mathbf{b}$, respectively. Comparison yields their relation to the components of (4.48) and (4.49) [18].

$$\begin{pmatrix} {}^{-}\mathbf{a}_R \\ {}^{-}\mathbf{b}_R \end{pmatrix} = \begin{pmatrix} 0 & \mathbb{I} \\ \mathbb{I} & 0 \end{pmatrix} \begin{pmatrix} \mathbf{a}^*_L \\ \mathbf{b}^*_L \end{pmatrix} = \mathsf{Q} \begin{pmatrix} \mathbf{a}^*_L \\ \mathbf{b}^*_L \end{pmatrix}. \tag{4.90}$$

Here, the matrix Q is defined by

$$\mathsf{Q} = \begin{pmatrix} 0 & \mathbb{I} \\ \mathbb{I} & 0 \end{pmatrix}. \tag{4.91}$$

As the vectors $^{-}\mathbf{a}$ and $^{-}\mathbf{b}$ have to be related by the same transfer matrix (4.50),

$$\begin{pmatrix} {}^{-}\mathbf{a}_R \\ {}^{-}\mathbf{b}_R \end{pmatrix} = \mathsf{T}(x_L,x_R) \begin{pmatrix} {}^{-}\mathbf{a}_L \\ {}^{-}\mathbf{b}_L \end{pmatrix}, \tag{4.92}$$

we obtain the time-reversal invariance requirement

$$\mathsf{T}^*(x_L,x_R) = \mathsf{Q}\,\mathsf{T}(x_L,x_R)\,\mathsf{Q}. \tag{4.93}$$

Flux conservation

The time-averaged flux density for the Helmholtz equation is (cf. chapter 2)

$$\langle \mathbf{j}(x,y)\rangle = \mathfrak{Re}\left\{ u(x,y)\left[\mathbf{e}_x \frac{\partial u^*(x,y)}{\partial x} + \mathbf{e}_y \frac{\partial u^*(x,y)}{\partial y}\right]\right\}. \tag{4.94}$$

As the total flux through every section $x = x_0$ has to be constant, we note that in the expression

$$F(x;w) = \int_0^w \langle \mathbf{j}(x,y)\rangle \cdot \mathbf{e}_x \,\mathrm{d}y, \tag{4.95}$$

the value of $F(x;W)$ is constant and independent of x. With the orthogonality relation

$$\int_0^W \phi_m(y)\phi_n(y)\,\mathrm{d}y = \delta_{m,n} \tag{4.96}$$

the total flow $F(x;W)$ of the free solution (4.5) is

$$F(x;W) = \mathfrak{Re}\left\{ \int_0^W u(x_0,y)\frac{\partial u(x_0,y)}{\partial x}\right\} = \mathfrak{Re}\left\{ \sum_{n=1}^{\infty} i\kappa_n \left[a_n a_n^* - b_n b_n^*\right]\right\}. \tag{4.97}$$

Thus, with $\sqrt{\mathsf{K}} = \text{Diag}\left(\sqrt{\kappa_1}, \sqrt{\kappa_2}, \ldots, \sqrt{\kappa_{N-1}}, \sqrt{\kappa_N}, \ldots\right)$ we get the expression

$$F(x;W) = \begin{pmatrix} \sqrt{\mathsf{K}} & 0 \\ 0 & \sqrt{\mathsf{K}} \end{pmatrix} \begin{pmatrix} \mathbf{a} \\ \mathbf{b} \end{pmatrix}^\dagger \begin{pmatrix} \mathbb{I} & 0 \\ 0 & -\mathbb{I} \end{pmatrix} \begin{pmatrix} \sqrt{\mathsf{K}} & 0 \\ 0 & \sqrt{\mathsf{K}} \end{pmatrix} \begin{pmatrix} \mathbf{a} \\ \mathbf{b} \end{pmatrix}. \tag{4.98}$$

If we compare now the flux of the free solutions (4.48) and (4.49), and use

$$\mathsf{W} = \begin{pmatrix} \mathbb{I} & 0 \\ 0 & -\mathbb{I} \end{pmatrix}, \tag{4.99}$$

we obtain

$$\begin{aligned} \begin{pmatrix} \mathbf{a}_L \\ \mathbf{b}_L \end{pmatrix}^\dagger \mathsf{W} \begin{pmatrix} \mathbf{a}_L \\ \mathbf{b}_L \end{pmatrix} &= \begin{pmatrix} \mathbf{a}_R \\ \mathbf{b}_R \end{pmatrix}^\dagger \mathsf{W} \begin{pmatrix} \mathbf{a}_R \\ \mathbf{b}_R \end{pmatrix} \\ &= \begin{pmatrix} \mathbf{a}_L \\ \mathbf{b}_L \end{pmatrix}^\dagger \mathsf{T}(x_L, x_R)^\dagger \, \mathsf{W} \, \mathsf{T}(x_L, x_R) \begin{pmatrix} \mathbf{a}_L \\ \mathbf{b}_L \end{pmatrix}. \end{aligned} \tag{4.100}$$

Thus, we obtain the flux conservation requirement

$$\mathsf{T}^\dagger(x_L, x_R) \, \mathsf{W} \, \mathsf{T}(x_L, x_R) = \mathsf{W}. \tag{4.101}$$

By multiplication with $\mathsf{T}^{\dagger -1}(x_L, x_R)$ from the left and with $\mathsf{T}(x_L, x_R)^{-1}$ from the right, and the observation $(\mathsf{W})^{-1} = \mathsf{W}$, we obtain the equivalent form

$$\mathsf{T}(x_L, x_R) \, \mathsf{W} \, \mathsf{T}^\dagger(x_L, x_R) = \mathsf{W}. \tag{4.102}$$

General form

If we suppose that the transfer matrix has the structure

$$\mathsf{T}(x_L, x_R) = \begin{pmatrix} a & b \\ c & d \end{pmatrix}, \tag{4.103}$$

where a, b, c and d denote $N \times N$ matrixes, then we see from (4.93) that

$$d = a^*, \qquad c = b^*, \tag{4.104}$$

so that (4.103) becomes

$$\mathsf{T}(x_L, x_R) = \begin{pmatrix} a & b \\ b^* & a^* \end{pmatrix}. \tag{4.105}$$

Flux conservation (4.101) yields

$$a^\dagger a - b^T b^* = \mathbb{I}, \tag{4.106}$$

$$a^\dagger b = b^T a^*. \tag{4.107}$$

The equivalent condition (4.102) yields in the same way

$$a^\dagger a - b b^\dagger = \mathbb{I}, \tag{4.108}$$

$$a b^T = b a^T. \tag{4.109}$$

The scattering matrix

The scattering matrix relates the outgoing to the incoming modes. Defining that a mode with exponential $e^{i\kappa_n x}$ 'runs to the right', we set $\mathbf{a}^L = \mathbf{a}^{\text{in}}$, $\mathbf{b}^L = \mathbf{b}^{\text{out}}$, $\mathbf{a}^R = \mathbf{a}^{\text{out}}$, and $\mathbf{b}^R = \mathbf{b}^{\text{in}}$. With these quantities, we define the scattering matrix

$$\begin{pmatrix} \mathbf{a}^{\text{out}} \\ \mathbf{b}^{\text{out}} \end{pmatrix} = \mathsf{S}(x_L, x_R) \begin{pmatrix} \mathbf{a}_{\text{in}} \\ \mathbf{b}_{\text{in}} \end{pmatrix} = \begin{pmatrix} S_{11} & S_{12} \\ S_{21} & S_{22} \end{pmatrix} \begin{pmatrix} \mathbf{a}_{\text{in}} \\ \mathbf{b}_{\text{in}} \end{pmatrix}. \tag{4.110}$$

Note that $\mathsf{S}(x_L, x_R)$ is related to the transfer matrix in the following way.

$$a = S_{11} - S_{12}S_{22}^{-1}S_{21} \tag{4.111}$$
$$a^* = S_{22}^{-1} \tag{4.112}$$
$$b = S_{12}S_{22}^{-1} \tag{4.113}$$
$$b^* = -S_{22}S_{21}^{-1} \tag{4.114}$$

By means of these equations, the scattering matrix may be calculated from the transfer matrix. It will be used during the numerical implementation in chapter (8) because its use presents some advantages over the transfer matrix.

4.3.4 Solution to the initial problem

In order to solve the problem initially proposed and depicted in Fig. 4.1, we cut the array of scatterers into non-overlapping slices to which we apply the transfer matrix method as sketched in Fig. 4.4. Then, in the given example,

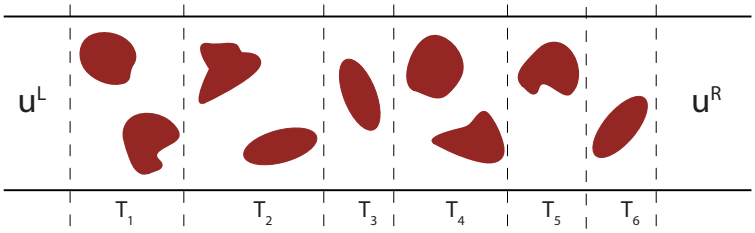

Figure 4.4: Transfer matrix method

the transfer matrix of the whole system is obtained by multiplication of the transfer matrices of the single 'slices'.

$$\begin{pmatrix} \mathbf{a}^R \\ \mathbf{b}^R \end{pmatrix} = T_6T_5T_4T_3T_2T_1 \begin{pmatrix} \mathbf{a}^L \\ \mathbf{b}^L \end{pmatrix} \tag{4.115}$$

Note that the numerical calculation is not straightforward. It is discussed in chapter 8.

4.4 Summary

In this chapter, we presented the problem of several Dirichlet scatterers in a waveguide where the projection of the scatterers normal to the infinite axis of the waveguide may be overlapping. For finite slices with a finite number of scatterers, we derive expressions for transfer matrices which may be used subsequently to calculate the solution for an arbitrary number of obstacles. In order to obtain these transfer matrices, an equation for the unknown source distribution at the boundary of the scatterer(s) in question is derived by a Green's function approach. An ansatz for this unknown function is made as a Fourier series and subsequently, a set of linear equations is derived which relates the coefficients of the series to the initial data given as the coefficients of an incoming wave that exists to the left of all scatterers.

Chapter 5

Scattering in one dimension

5.1 The problem

In order to understand the nature of localisation phenomena occurring with repulsive potentials, we look at the following one-dimensional model. Consider the Schrödinger equation

$$-\frac{\hbar^2}{2m}\frac{d^2}{dx^2}\psi(x) + V(x)\,\psi(x) = E\,\psi(x), \tag{5.1}$$

with a Dirac comb potential of variable height given by

$$V(x) = \sum_{n=-\infty}^{\infty} v_{2n+1}\,\delta(x-2n-1), \tag{5.2}$$

where $v_{2n+1} = v_{2n+1}^*$, $v_{2n} = 0$, and the comb is of finite length (one-dimensional 'finite crystal').

$$v_n = 0 \quad \text{for} \quad |n| > 2N \tag{5.3}$$

In the following, we use units where

$$\hbar^2/2m = 1.$$

The assumption $v_n \geq 0$ implies $E = k^2$ with $k = k^* \geq 0$. At a given point x in the 'cell' number with n, the wave function may be represented as a linear combination of plane waves with amplitudes A and B.

$$\psi(x) = A_{2n}\,e^{ik(x-2n)} + B_{2n}\,e^{-ik(x-2n)} \qquad \text{for } 2n-1 < x < 2n+1. \tag{5.4}$$

Since $V(x) = V(x)^*$, $\psi(x)$ may be chosen to be real, i.e.,

$$\psi(x) = \psi(x)^* \quad \Longleftrightarrow \quad B_{2n} = A_{2n}^*. \tag{5.5}$$

We abbreviate the coefficient vector as

$$\begin{pmatrix} A_{2n} \\ A_{2n}^* \end{pmatrix} = \mathbf{V}_{2n}. \tag{5.6}$$

From (5.4, 5.5), we obtain

$$2\,A_{2n} = \psi(2n) + i\,\varphi(2n) \quad \text{with} \quad \varphi(x) = \frac{1}{k}\,\frac{d\psi(x)}{dx}\,. \tag{5.7}$$

The coefficients of two adjacent cells are related by a transfer matrix

$$\mathbf{V}_{2n+2} = T_{2n+1}\,\mathbf{V}_{2n}, \tag{5.8}$$

where T_{2n+1} is of the form

$$T = \begin{pmatrix} s+it & y+iz \\ y-iz & s-it \end{pmatrix} \tag{5.9}$$

with

$$\det T = s^2 + t^2 - y^2 - z^2 = 1 \tag{5.10}$$

For $T = T_{2n+1} = T(\kappa, v)$ with $\kappa = 2k$ and $v = v_{2n+1}$, the functions appearing in the transfer matrix are given by

$$\begin{aligned} s(\kappa, v) &= \cos\kappa + (v/\kappa)\,\sin\kappa\,, && (5.11)\\ t(\kappa, v) &= \sin\kappa - (v/\kappa)\,\cos\kappa\,, && (5.12)\\ y(\kappa, v) &= 0\,, && (5.13)\\ z(\kappa, v) &= -\,v/\kappa. && (5.14) \end{aligned}$$

Note that $y = 0$ is a consequence of the fact that $v_{2n+1}\,\delta(x-2n-1)$ is symmetric with respect to the reflection $x - 2n - 1 \to -x + 2n + 1$.

As $\det T_{2n+1} = 1$ for all n, all vectors $\mathbf{V}_{2n}$ may be generated from a single one and if one of them vanishes, so do all of them.

5.1.1 Symmetric combs

We now make the simplifying assumption that all combs are symmetric.

$$v_{2n+1} = v_{-2n-1} \tag{5.15}$$

This entails the following

(i) $y = 0$ in the nondiagonal elements of the transfer matrix T which relates the free wave right of the crystal to the free wave left of it.

$$\mathbf{V}_{2N} = T\,\mathbf{V}_{-2N} = T_{2N-1}\;\ldots T_{-2N+1}\,\mathbf{V}_{-2N} \tag{5.16}$$

Proof by induction: The upper nondiagonal element of $T_{11} = T_1\,T_1$ is

$$iz_{11} = 2is_1z_1, \tag{5.17}$$

and that of $T_{212} = T_2\,T_1\,T_2$ is

$$iz_{212} = i(s_2^2z_1 + t_2^2z_1 + 2s_1s_2z_2 - 2t_1t_2z_2 + z_1z_2^2). \tag{5.18}$$

(ii) For every energy $E > 0$, the two linearly independent eigenfunctions may be chosen to be even ($p = 0$) and odd ($p = 1$), respectively.

$$\psi^p(x) = (-1)^p\,\psi^p(-x) \quad \Longleftrightarrow \quad A^p_{-2n} = (-1)^p\,(A^p_{2n})^* \tag{5.19}$$

Even and odd eigenfuctions are normalised such that for $-1 < x < 1$ we have $\psi^0(x) = 2\cos kx$ and $\psi^1(x) = 2\sin kx$. The vectors (5.6) for even and odd eigenfunctions can be expressed with the help of transfer matrices and the following coefficients in the cell with number 0.

$$\mathbf{V}^0_0(\kappa, v) = \mathbf{U}^0 = \begin{pmatrix} 1 \\ 1 \end{pmatrix} \quad \mathbf{V}^1_0(\kappa, v) = \mathbf{U}^1 = \begin{pmatrix} -i \\ i \end{pmatrix} \tag{5.20}$$

5.1.2 Transmission coefficient T

The transmission coefficient T is related to the transfer matrix T with elements $s \pm it$ and $\pm iz$ in the following way.

$$\mathsf{T} = (s^2 + t^2)^{-1} = (1 + z^2)^{-1} \tag{5.21}$$

$$\mathsf{T} = 1 \quad \Longleftrightarrow \quad z = 0 \tag{5.22}$$

Note that for asymmetric combs y does not vanish identically whence $\mathsf{T} = 1$ would imply both $y = y(\kappa) = 0$ and $z = z(\kappa) = 0$. To satisfy both conditions simulaneously is impossible in general.

The transmission coefficient is also related to the even and odd eigenfunctions in the following way. From (5.6), (5.9) with $y = 0$, and (5.16), we see that

$$\mathfrak{Re}\, A^0_{2N}(A^1_{2N})^* = -\,z\,\mathfrak{Im}\, A^0_{2N}(A^1_{2N})^*. \tag{5.23}$$

Setting $A^p_{2N} = |A^p_{2N}|\exp i\gamma_p$, we obtain

$$\mathsf{T} = \sin^2(\gamma_0 - \gamma_1). \tag{5.24}$$

This shows that $\mathsf{T} = 0$ if the even and odd wave functions outside the crystal have common nodes, and that $\mathsf{T} = 1$ if the distance between these nodes is half a wavelength.

5.1.3 Localisation

As a measure of the amplitude of the wave function in the interval $(2n-1, 2n+1)$, we take

$$2\,|\mathbf{V}_{2n}|^2 = 4\,|A_{2n}|^2 = |\psi(2n)|^2 + |\psi(2n)|^2. \tag{5.25}$$

Therefore

$$\Pi_{\text{in}} = 2\,|A_{-2N}|^2 + \sum_{n=-N+1}^{N-1} 4\,|A_{2n}|^2 + 2\,|A_{2N}|^2 \tag{5.26}$$

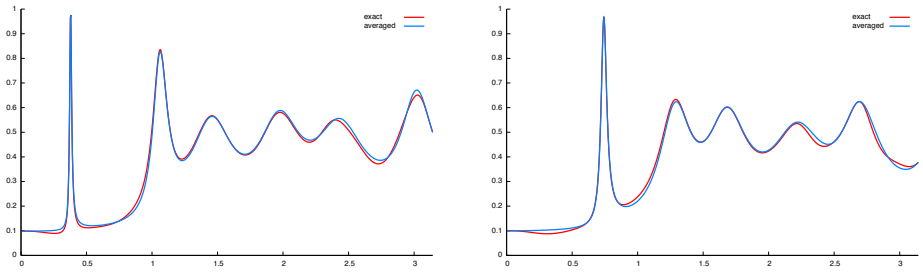

even wave functions odd wave functions

Figure 5.1: Comparison between exact norm of wave function inside the crystal and the approximation Π_{in}

is a (rough) measure for finding the particle inside the crystal and

$$\Pi_{\text{out}} = 4N\,|A_{-2N}|^2 + 4N\,|A_{2N}|^2 \tag{5.27}$$

is the corresponding measure for finding the particle in one of the two intervals to the left and to the right of the crystal, each of it being half as long as the crystal. We define the 'measure of localisation' as

$$\Lambda = \frac{\Pi_{\text{in}}}{\Pi_{\text{in}} + \Pi_{\text{out}}} \in (0,1). \tag{5.28}$$

It might seem more natural to define Π_{in} and Π_{out} by the corresponding integrals over $|\psi(x)|^2$. Fig. (5.1) shows a comparison between the exact integral, coloured in red, over the squared wavefunction from one end of the crystal to the other and corresponding approximation (5.26), coloured in blue. The figure shows clearly that (5.26) is a good approximation to the exact value of the integral.

5.1.4 Properties of the matrix $T(\kappa, v)$

The characteristic equation of the transfer matrix (5.9) is $\omega^2 - 2s\,\omega + 1 = 0$ whence the two eigenvalues of $T(\kappa, v)$ are given by

$$\omega(\kappa, v)^{\pm 1} = s(\kappa, v) \pm r(\kappa, v) \tag{5.29}$$

where for $n\pi < \kappa < (n+1)\pi$

$$r(\kappa, v) = \begin{cases} (-1)^n \sqrt{s(\kappa, v)^2 - 1} & \text{for} \quad s(\kappa, v)^2 > 1\,, \\ i\,(-1)^n \sqrt{1 - s(\kappa, v)^2} & \text{for} \quad s(\kappa, v)^2 < 1\,. \end{cases} \tag{5.30}$$

The sum of the two eigenvalues may be used to define band and gap regions of the crystal, painted in red and green in Fig. 5.2. The corresponding eigenvectors, defined by the equation

$$T(\kappa, v)\,\mathbf{W}^{\pm}(\kappa, v) = \omega(\kappa, v)^{\pm 1}\,\mathbf{W}^{\pm}(\kappa, v)\,, \tag{5.31}$$

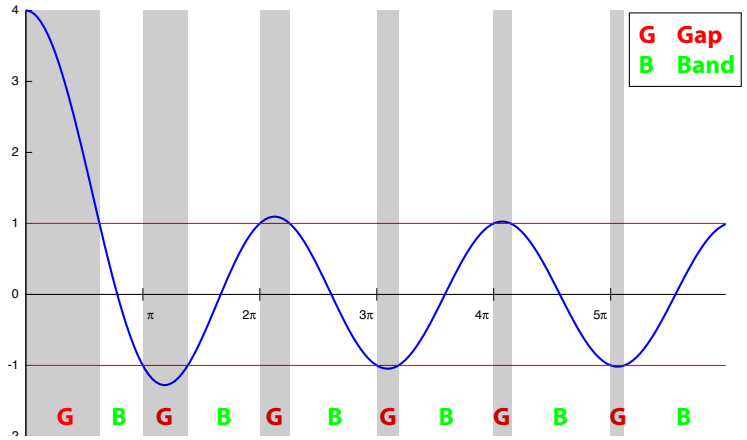

Figure 5.2: Band and gap regions for one-dimensional crystal

are

$$\mathbf{W}^{\pm}(\kappa, v) = \begin{pmatrix} \alpha(\kappa, v)^{\mp 1/2} \\ \alpha(\kappa, v)^{\pm 1/2} \end{pmatrix} , \tag{5.32}$$

with

$$\alpha(\kappa, v)^{\pm 1} = -\frac{t(\kappa, v) \pm i\, r(\kappa, v)}{z(\kappa, v)} . \tag{5.33}$$

Note that $r(\kappa, v)$, $\omega(\kappa, v)$, and $\alpha(\kappa, v)$ are continuous functions of κ and

$$\omega(\kappa, v) = \omega(\kappa, v)^*, \quad |\alpha(\kappa, v)| = 1 \quad \text{for} \quad s(\kappa, v)^2 > 1 , \tag{5.34}$$

$$|\omega(\kappa, v)| = 1, \quad \alpha(\kappa, v) = \alpha(\kappa, v)^* \quad \text{for} \quad s(\kappa, v)^2 < 1 . \tag{5.35}$$

The change between unimodular and real values occurs whenever

$$2\, r(\kappa, v) = \omega(\kappa, v) - \omega(\kappa, v)^{-1} = i\, z(\kappa, v)\big(\alpha(\kappa, v) - \alpha(\kappa, v)^{-1}\big) \tag{5.36}$$

becomes equal to zero. This happens at the 'upper band edges' $\kappa = n\,\pi$, $n = 1, 2, 3, \ldots$, and at the 'lower band edges' κ_n, $n = 1, 2 \ldots$, which satisfy $(n-1)\pi < \kappa_n < n\pi$ and

$$\frac{v}{\kappa} = \begin{cases} \tan \frac{\kappa}{2} & \text{for} \quad n \text{ odd}, \\ -\cot \frac{\kappa}{2} & \text{for} \quad n \text{ even}. \end{cases} \tag{5.37}$$

$$\kappa = \kappa_n : \quad \omega^{\pm 1} = s = (-1)^{n+1} , \quad \alpha^{\pm 1} = -t/z = (-1)^{n+1} \tag{5.38}$$

$$\kappa = n\,\pi : \quad \omega^{\pm 1} = s = (-1)^{n} , \quad \alpha^{\pm 1} = -t/z = (-1)^{n} \tag{5.39}$$

It follows from (5.31) and (5.32) that for integer n

$$T(\kappa, v)^n = A\, \mathrm{diag}(\omega^n, \omega^{-n})\, A^{-1} , \tag{5.40}$$

where A and A^{-1} are given by

$$A = \begin{pmatrix} \alpha^{-1/2} & \alpha^{+1/2} \\ \alpha^{+1/2} & \alpha^{-1/2} \end{pmatrix}, \quad A^{-1} = \frac{1}{\alpha^{-1} - \alpha} \begin{pmatrix} \alpha^{-1/2} & -\alpha^{+1/2} \\ -\alpha^{+1/2} & \alpha^{-1/2} \end{pmatrix}. \quad (5.41)$$

In these equations, $\alpha = \alpha(\kappa, v)$ and $\omega = \omega(\kappa, v)$.

5.2 Perfect comb

First, we examine the perfect comb with $2N$ delta spikes of equal height. In this case the matrix $T = T(\kappa, v)^{2N}$ of eq. (5.16) is of the form

$$T^{2N} = \frac{1}{\alpha^{-1} - \alpha} \begin{pmatrix} \alpha\omega^{-2N} - \alpha^{-1}\omega^{2N} & \omega^{2N} - \omega^{-2N} \\ \omega^{-2N} - \omega^{2N} & \alpha\omega^{2N} - \alpha^{-1}\omega^{-2N} \end{pmatrix}. \quad (5.42)$$

In the first gap region, $0 < \kappa < \kappa_1$, $\omega(\kappa, v) > 1$ and $\omega(\kappa, v)^{2N} \gg 1$ if v or/and N are large. In this case $\mathsf{T} \approx 0$ because of (5.21). In the first band region $\kappa_1 < \kappa < \pi$, $|\omega(\kappa, v)| = 1$ and its argument increases continuously from 0 to π, cf. (5.38), and (5.39). The argument of $\omega(\kappa, v)^{2N}$ increases therefore continuously from 0 to $2N\pi$, so that its imaginary part $(1/2)\left(\omega(\kappa, v)^{2N} - \omega(\kappa, v)^{-2N}\right)$ vanishes $2N + 1$ times, namely for $\omega(\kappa, v) = e^{im\pi/2N}$, $m = 0, 1, 2, \ldots, 2N$. For $m = 0$ and $m = 2N$, $\omega(\kappa, v) - \omega(\kappa, v)^{-1} = 0$ and $\alpha(\kappa, v) - \alpha(\kappa, v)^{-1} = 0$ but their ratio is different from zero, see (5.36). This leaves us with the well-known result that the first band region contains $2N - 1$ 'resonances' where the transmission coefficient assumes its maximum value $\mathsf{T} = 1$. These considerations are easily extended to higher energies.

In the perfect comb,

$$\mathbf{U}^0 = \frac{1}{\alpha^{1/2} + \alpha^{-1/2}}(\mathbf{W}^+ + \mathbf{W}^-), \qquad \mathbf{U}^1 = \frac{i}{\alpha^{1/2} - \alpha^{-1/2}}(\mathbf{W}^+ - \mathbf{W}^-), \quad (5.43)$$

where $W^{\pm}$ are the eigenvectors (5.32) of $T(\kappa, v)$. With (5.6 - 5.8), (5.20), (5.43), and (5.31), we obtain for $n = 0, \ldots, N$

$$\begin{aligned} \psi^0(2n) = &\quad \mathbf{U}^0 \cdot T^n \mathbf{U}^0 &&= \omega^n + \omega^{-n}, && (5.44)\\ \varphi^0(2n) = &\quad -\mathbf{U}^1 \cdot T^n \mathbf{U}^0 &&= -i\beta\left(\omega^n - \omega^{-n}\right), && (5.45)\\ \psi^1(2n) = &\quad \mathbf{U}^0 \cdot T^n \mathbf{U}^1 &&= i\,\beta^{-1}\left(\omega^n - \omega^{-n}\right), && (5.46)\\ \varphi^1(2n) = &\quad -\mathbf{U}^1 \cdot T^n \mathbf{U}^1 &&= \left(\omega^n + \omega^{-n}\right), && (5.47) \end{aligned}$$

where

$$\beta = \frac{\alpha - 1}{\alpha + 1}. \quad (5.48)$$

In the first gap $|\alpha| = 1$, $\beta = -\beta^*$, and $\omega = \omega^* > 1$. If $\omega^N \gg 1$ such that terms of order ω^{-2N} (relative to the leading term) may be neglected, then both

eigenfunctions increase, in essence, exponentially with the distance from the center of the crystal. In this case $\psi^1(x) \approx i\beta^{-1}\psi^0(x)$ for $x > 2N-1$ which implies $\mathsf{T} \approx 0$. In the first band $0 < \alpha = \alpha^* < 1$, $-1 < \beta = \beta^* < 0$, and

$$\tan\gamma_0 = \beta\,\frac{\omega^N - \omega^{-N}}{\omega^N + \omega^{-N}}\ , \quad \tan\gamma_1 = \beta\,\frac{\omega^N + \omega^{-N}}{\omega^N - \omega^{-N}}\ . \tag{5.49}$$

The nodes of the even and the odd eigenfunction outside the crystal are therefore shifted by half a wavelength if, and only if, $\omega^N = \omega^{-N}$ (even resonances) or $\omega^N = -\,\omega^{-N}$ (odd resonances).

In the first gap

$$4\,|A^p_{2n}|^2 = |\beta|^{-2p}\left[\big(1+|\beta|^2\big)\big(\omega^{2n}+\omega^{-2n}\big) + 2(-1)^p\big(1-|\beta|^2\big)\right] \tag{5.50}$$

so that

$$\Pi^p_{out} = 2N\,|\beta|^{-2p}\left[\big(1+|\beta|^2\big)\big(\omega^{N}+\omega^{-N}\big) + 2(-1)^p\big(1-|\beta|^2\big)\right]\ , \tag{5.51}$$

$$\Pi^p_{in} = |\beta|^{-2p}\left[\big(1+|\beta|^2\big)\,F_{2N}(\omega) + 4N(-1)^p\big(1-|\beta|^2\big)\right]\ , \tag{5.52}$$

$$F_{2N}(\omega) = \frac{\omega^{2N+1} - \omega^{-2N-1} + \omega^{2N-1} - \omega^{-2N+1}}{\omega - \omega^{-1}}. \tag{5.53}$$

For $\omega^N \gg 1$, $\Pi^p_{in} \approx (1/2N)\,\Pi^p_{out}$ and $\Lambda^p \approx (1/2N)$ which is consistent with the (average) exponential growth of the eigenfunctions $\psi^p(x)$ for $0 < x < 2N$.

In the first band

$$4\,|A^p_{2n}|^2 = \beta^{-2p}\ \left[4\beta^2 + \big(1-\beta^2\big)\,\big|\omega^{2n} + (-1)^p\omega^{-2n}\big|^2\right] \tag{5.54}$$

and hence

$$\Pi^p_{out} = 2N\,\beta^{-2p}\ \left[4\beta^2 + \big(1-\beta^2\big)\,\big|\omega^{2N} + (-1)^p\omega^{-2N}\big|^2\right]\ . \tag{5.55}$$

This is an oscillating function of ω, the minima and maxima being essentially given by those of $|\omega^{2N} + (-1)^p\omega^{-2N}|^2$ since β is slowly varying with ω. On the other hand, the oscillations of

$$\Pi^p_{in} = \beta^{-2p}\left[4N\,\big(1+|\beta|^2\big) + (-1)^p\big(1-\beta^2\big)\,F_{2N}(\omega)\right]\ . \tag{5.56}$$

are negligible so that the oscilations of Λ^p are determined by those of Π^p_{out}. In the vicinity of each resonance energy, where $\mathsf{T} = 1$, therefore one of the two functions Π^p_{out} has a local minimum and the corresponding function Λ^p a local maximum.

5.3 Comb with a gap

A comb with a gap is given by the symmetric potentials

$$v_{2n+1} = v_{-2n-1} = \begin{cases} v & \text{for} \quad 2L < 2n+1 < 2L+2M = 2N \\ 0 & \text{otherwise} \end{cases} \tag{5.57}$$

This means that the transfer matrix (5.16) is

$$T = T(v,\kappa)^M \, D(\kappa)^{2L} \, T(v,\kappa)^M, \tag{5.58}$$

where

$$D(\kappa) = T(0,\kappa) = \mathrm{diag}\,(e^{i\kappa}, e^{-i\kappa}). \tag{5.59}$$

With $T(v,\kappa)^M = T_2$, $D(\kappa)^{2L} = T_1$ (and hence $z_1 = 0$), we obtain from (5.18)

$$i\, z_{212} = 2i\, z_2\, (s_1 s_2 - t_1 t_2) = 2i\, z_2\, \Re e\, (s_1 + i\, t_1)(s_2 + i\, t_2) \tag{5.60}$$

From this equation, we see that the condition for full transmission, $\mathsf{T} = 1$, can only be fulfilled if $z_2 = 0$ or $\Re e\, (s_1 + i\, t_1)(s_2 + i\, t_2) = 0$.

(i) $z_2 = 0$. Resonances of a given comb are also resonances of a comb that consists of two such combs separated by a gap. (Obvious: T_2 is always diagonal, and if T_1 becomes so, so does $T_2 T_1 T_2$). There are $M - 1$ such resonances in each of the bands of the potential v.

(ii) $\Re e\, (s_1 + i\, t_1)(s_2 + i\, t_2) = 0$. These resonances result from the interaction of the two perfect combs.

$$(s_1 + i\, t_1)(s_2 + i\, t_2) = e^{2iL\kappa} f_M(v,\kappa) \tag{5.61}$$

$$\begin{aligned} f_M(v,\kappa) &= \frac{\alpha^{-1}\omega^M - \alpha\,\omega^{-M}}{\alpha^{-1} - \alpha} \\ &= \frac{1}{2}\,\frac{(\omega^M + \omega^{-M})(\alpha^{-1} - \alpha) + (\omega^M - \omega^{-M})(\alpha^{-1} + \alpha)}{\alpha^{-1} - \alpha} \\ &= \frac{1}{2}\,(\omega^M + \omega^{-M}) + i\,t \sum_{m=0}^{M-1} \omega^{M-1-2m} \end{aligned} \tag{5.62}$$

with $\alpha = \alpha(\kappa, v)$, $\omega = \omega(\kappa, v)$, and $t = t(\kappa, v)$. Both (5.61) and (5.62) are continuous functions of κ. We are especially interested in the argument of (5.61) because $\mathsf{T} = 1$ whenever it becomes equal to a half-integer multiple of π.

First gap

The first gap is given by $0 < \kappa < \kappa_1$. It follows from (5.62), (5.12), (5.14), and (5.38) that

$$f_M(v,\kappa) \to \frac{1}{2}\left(\omega(0,v)^M + \omega(0,v)^{-M}\right) + i\,(-\infty) \quad \text{for} \quad \kappa \to 0 \tag{5.63}$$

and

$$f_M(v,\kappa) \to 1 + i\,(Mv/\kappa_1) \quad \text{for} \quad \kappa \to \kappa_1\ . \tag{5.64}$$

The argument of $f_M(v,\kappa)$ increases continuously from $-\pi/2$ to

$$\delta_1 = \arctan(Mv/\kappa_1) \in (0,\pi/2) \tag{5.65}$$

(without assuming these values). As a consequence the argument of the function (5.61) increases continuously from $-\pi/2$ to $2L\kappa_1 + \delta_1$ and the number of resonances in the first gap is

$$G_1 = \sum_{n=0}^{\infty} \Theta\Big(2L\kappa_1 + \delta_1 - \big(n+\tfrac{1}{2}\big)\pi\Big)\ . \tag{5.66}$$

First band

The first band is given by $\kappa_1 < \kappa < \pi$. Here

$$f_M(v,\kappa) \to (-1)^M\left(1 - i\,(Mv/\pi)\right) \quad \text{for} \quad \kappa \to \pi. \tag{5.67}$$

Since now $0 < \alpha < 1$ and $\omega = \cos\phi + i\,\sin\phi$ with $0 < \phi < \pi$ the argument of the function

$$f_M(v,\kappa) = \cos(M\phi) + \frac{\alpha^{-1}+\alpha}{\alpha^{-1}-\alpha}\,\sin(M\phi) \tag{5.68}$$

increases continuously from δ_1 to $M\pi - \epsilon_1$ where

$$\epsilon_1 = \arctan(Mv/\pi) \in (0,\pi/2)\,. \tag{5.69}$$

Accordingly the argument of (5.61) increases continuously from $\delta_1 + 2L\kappa_1$ to $(2L+M)\pi - \epsilon_1$ and one obtains, in addition to the $M-1$ rsonances already found, another

$$B_1 = \sum_{n=0}^{\infty} \Theta\Big(\big(n+\tfrac{1}{2}\big)\pi - 2L\kappa_1 - \delta_1\Big)\Theta\Big((M+2L)\pi - \epsilon_1 - \big(n+\tfrac{1}{2}\big)\pi\Big) \tag{5.70}$$

resonances in the first band. Since $\epsilon_1 < \pi/2$ the total number of resonances in the range $\kappa \in (0,\pi)$ is the same as for a perfect comb of the same length.

$$G_1 + B_1 + (M-1) = 2L + 2M - 1 = 2N - 1 \tag{5.71}$$

Wave functions

For $0 \le n \le L$

$$\mathbf{V}^0_{2n} = \cos(\kappa n)\,\mathbf{U}^0 - \sin(\kappa n)\,\mathbf{U}^1\ , \quad \mathbf{V}^1_{2n} = \sin(\kappa n)\,\mathbf{U}^0 + \cos(\kappa n)\,\mathbf{U}^1, \quad (5.72)$$

whence for $0 \le m \le M$ we obtain

$$\begin{aligned} \mathbf{V}^0_{2L+2m} &= \frac{\cos(\kappa L)}{\alpha^{1/2}+\alpha^{-1/2}}\left(\omega^m\mathbf{W}^+ + \omega^{-m}\mathbf{W}^-\right) \\ &\quad - \frac{i\,\sin(\kappa L)}{\alpha^{1/2}-\alpha^{-1/2}}\left(\omega^m\mathbf{W}^+ - \omega^{-m}\mathbf{W}^-\right), \qquad (5.73) \\ \mathbf{V}^1_{2L+2m} &= \frac{\sin(\kappa L)}{\alpha^{1/2}+\alpha^{-1/2}}\left(\omega^m\mathbf{W}^+ + \omega^{-m}\mathbf{W}^-\right) \\ &\quad + \frac{i\,\cos(\kappa L)}{\alpha^{1/2}-\alpha^{-1/2}}\left(\omega^m\mathbf{W}^+ - \omega^{-m}\mathbf{W}^-\right). \qquad (5.74) \end{aligned}$$

Therefore

$$\begin{aligned} \psi^0(2N) &= \cos(\kappa L)\left(\omega^M+\omega^{-M}\right), -i\,\sin(\kappa L)\,\beta^{-1}\left(\omega^M-\omega^{-M}\right), \quad (5.75) \\ \varphi^0(2N) &= -\sin(\kappa L)\left(\omega^M+\omega^{-M}\right) - i\,\cos(\kappa L)\,\beta\left(\omega^M-\omega^{-M}\right), \quad (5.76) \\ \psi^1(2N) &= \sin(\kappa L)\left(\omega^M+\omega^{-M}\right) + i\,\cos(\kappa L)\,\beta^{-1}\left(\omega^M-\omega^{-M}\right), \quad (5.77) \\ \varphi^1(2N) &= \cos(\kappa L)\left(\omega^M+\omega^{-M}\right) - i\,\sin(\kappa L)\,\beta\left(\omega^M-\omega^{-M}\right). \quad (5.78) \end{aligned}$$

Provided that

$$\cos(\kappa L) - i\,\beta^{\pm 1}\sin(\kappa L) \not\approx 0 \quad (5.79)$$

and $\omega^M \gg 1$ we find in the first gap

$$\varphi^0(2N) \approx -i\,\beta\,\psi^0(2N) \approx \omega^M\left[-i\,\beta\,\cos(\kappa L) - \sin(\kappa L)\right] \quad (5.80)$$

$$\varphi^1(2N) \approx -i\,\beta\,\psi^1(2N) \approx \omega^M\left[-i\,\beta\,\sin(\kappa L) + \cos(\kappa L)\right] \quad (5.81)$$

which implies $\psi^0(x) \propto \psi^1(x)$ for $x > 2N$ and thus $\mathsf{T} \approx 0$. However, if

$$\cos(\kappa L) - i\,\beta^{-1}\sin(\kappa L) = 0 \quad \Longleftrightarrow\ \mathbf{V}^0_{2L} \propto \mathbf{W}^- \quad (5.82)$$

then

$$\frac{\varphi^0(2N)}{\psi^0(2N)} = -i\,\beta \approx -\frac{\varphi^1(2N)}{\psi^1(2N)} \quad (5.83)$$

and the transmission coefficient is essentially different from zero for those energies where (5.82) holds true. Comparison of (5.80), (5.81), and (5.83) shows that in the vicinity of these energies γ_0, the phase of A^0_{2N}, increases suddenly by π whereas γ_1, the phase of A^1_{2N}, remains essentially the same. Because of (5.24) T thereore assumes its maximum value 1 witin this narrow energy range. On the other hand, condition (5.82) means that the amplitude of the wave function $\psi^0(x)$, which is constant for $|x| < 2L$, decreases (on the average) exponentially for $2L < |x| < 2N$, a property that vanishes when the energy is even slightly

varied. If $\cos(\kappa L) - i\,\beta\,\sin(\kappa L) = 0$, the situation is esentially the same except that even and odd eigenfunctions change their roles. In both cases we find in the first gap $G1$ (5.66) sharp maxima of the transmission coefficient, and at essentially the same energies a maximum of one of the two localisation measures. Between these resonances $\mathsf{T} \approx 0$, both wavefunctions are exponentially growing at the ends of the comb, and the localisation measures are correspondingly small ($\Lambda^p \ll 0.5$).

5.4 Summary

A one-dimensional localisation model based on the Schrödinger equation and a finite Dirac-comb potential was formulated. The comparison of the transmission coefficient and a localisation measure for wave functions allows one to make predictions for the k-dependence of localised states. It can be seen that the transmission coefficient, which depends on the relative phase of the two linearly independent solutions outside the crystal, is related to the localisation coefficient which depends essentially on the magnitudes of these wave functions. This connection was shown analytically for two models, a finite Dirac comb of equal potential heights and a similar Dirac comb with a "hole"in the middle. The same phenomena were also observed in numerical studies of more general symmetric combs.

Chapter 6

Time dependent scattering

This chapter deals with solutions of the time-dependent Helmholtz equation (2.1) with a piecewise constant $\gamma(\mathbf{x})$ as in (2.7). The time-dependent solutions are obtained by a generalised inverse Fourier transform of time-independent wave functions in $\mathbf{k}$-space $u(\mathbf{k}, \mathbf{x})$ with a Gaussian weight factor. These $u(\mathbf{k}, \mathbf{x})$ were obtained in chapters 3, 4 and 5.

6.1 Scattering in vacuum

The time-dependent solution has the form

$$u(\mathbf{x}, t) = \frac{1}{2\,\pi} \int_{\mathbb{R}^2} u(\mathbf{k}, \mathbf{x}) \tilde{\psi}(\mathbf{k}, t)\, \mathrm{d}^2\mathbf{k}, \tag{6.1}$$

where

$$\tilde{\psi}(\mathbf{k}, t) = \tilde{\psi}_0(\mathbf{k}) e^{-i\omega(k)t}, \tag{6.2}$$

$$\tilde{\psi}_0(\mathbf{k}) \in L^2(\mathbb{R}^2), \tag{6.3}$$

and

$$\omega(k) = \alpha_1 k + \alpha_2 k^2. \tag{6.4}$$

Here, $\alpha_1 > 0$ and $\alpha_2 > 0$ depend on the model chosen. From chapter 2, we know that for electromagnetical and acoustical problems, $\alpha_1 = c$ and $\alpha_2 = 0$, as well as for quantum mechanical problems, $\alpha_1 = 0$ and $\alpha_2 = \frac{\hbar}{2m} k^2$.

A two-dimensional Gaussian wave packet which moves in the direction of the wave vector $\mathbf{k}_0$ is described by the weight factor

$$\tilde{\psi}_0(\mathbf{k}) = \sqrt{\frac{2\Gamma}{\pi}} e^{-\Gamma(\mathbf{k}-\mathbf{k}_0)^2}. \tag{6.5}$$

The normalisation is chosen to fulfil

$$\left\| \tilde{\psi}_0 \right\| = \left(\int_{\mathbb{R}^2} \tilde{\psi}_0(\mathbf{k}) \tilde{\psi}_0^*(\mathbf{k})\, \mathrm{d}^2\mathbf{k} \right)^{\frac{1}{2}} = 1. \tag{6.6}$$

A free plane wave is described by

$$u(\mathbf{k}, \mathbf{x}) = e^{i\mathbf{k}\cdot\mathbf{x}}. \tag{6.7}$$

The corresponding free wave packet takes the form of a two-dimensional Fourier integral:

$$\psi(\mathbf{x}, t) = \frac{1}{2\pi}\sqrt{\frac{2\Gamma}{\pi}} \int_{\mathbb{R}^2} e^{i\mathbf{k}\cdot\mathbf{x}} e^{-\Gamma(\mathbf{k}-\mathbf{k}_0)^2} e^{-i(\alpha_1 k + \alpha_2 k^2)t}\, \mathrm{d}^2\mathbf{k}, \tag{6.8}$$

This corresponds to the situation where we have a Gaussian wave packet with an initial wave vector $\mathbf{k}_0$ and a 'shape' constant Γ determining its spread in $\mathbf{k}$-space and $\mathbf{x}$-space, respectively. In general, only numerical solutions for (6.8) are available. The method how to obtain these numerical solutions is described in chapter 8.

6.1.1 Exact solutions

Analytic solutions for (6.8) are only available in special cases. Note that for all these, we tacitly assume that α_1, α_2 and Γ are real, as well as $\Gamma > 0$. The integrals may be evaluated using integral tables or standard software like Mathematica [19].

State at $t = 0$

The solution $\psi(\mathbf{x}, 0)$ reads

$$\begin{aligned}\psi(\mathbf{x}, 0) &= \frac{1}{2\pi}\sqrt{\frac{2\Gamma}{\pi}} \int_{-\infty}^{\infty} e^{ik_x x - \Gamma(k_x - k_{0,x})^2}\, \mathrm{d}k_x \int_{-\infty}^{\infty} e^{ik_y y - \Gamma(k_y - k_{0,y})^2}\, \mathrm{d}k_y, \\ &= \sqrt{\frac{1}{2\pi\Gamma}} e^{-\frac{1}{4\Gamma}\mathbf{x}^2 + i\mathbf{k}_0\cdot\mathbf{x}}. \end{aligned} \tag{6.9}$$

From the density

$$|\psi(\mathbf{x}, 0)|^2 = \frac{1}{2\pi\Gamma}\, e^{-\frac{1}{2\Gamma}\mathbf{x}^2} \tag{6.10}$$

and its plots (cf. Fig. 6.1.1) we see that Γ is a measure for the width of the wave packet at $t = 0$.

Quantum mechanical dispersion relation $\alpha_1 = 0$

The quantum-mechanical case $\alpha_1 = 0$, i.e., $\omega(k) \propto k^2$ is exactly solvable, too.

$$\begin{aligned}\psi(\mathbf{x}, t) &= \frac{1}{2\pi}\sqrt{\frac{2\Gamma}{\pi}} \int_{\mathbb{R}^2} e^{i\mathbf{k}\cdot\mathbf{x}} e^{-\Gamma(\mathbf{k}-\mathbf{k}_0)^2} e^{-i\alpha_2 k^2 t}\, \mathrm{d}^2\mathbf{k} \\ &= \sqrt{\frac{2\Gamma}{\pi}} \frac{1}{2(\Gamma + it\alpha_2)} e^{-\mathbf{k}_0^2\Gamma + \frac{(i\mathbf{x} + 2\Gamma\mathbf{k}_0)^2}{4(\Gamma + i\alpha_2 t)}} \end{aligned} \tag{6.11}$$

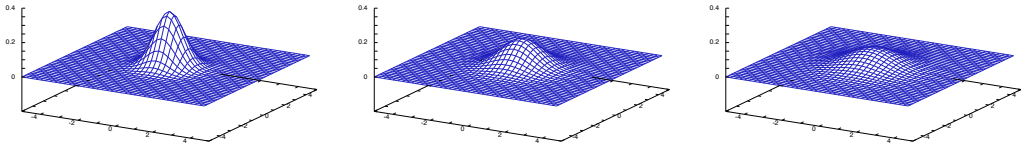

$\Gamma = \frac{1}{2}$ $\Gamma = 1$ $\Gamma = \frac{3}{2}$

Figure 6.1: Width of the two-dimensional wave packet for various Γ

The absolute value of $\psi(\mathbf{x}, t)$

$$|\psi(\mathbf{x}, t)| = \sqrt{\frac{2\Gamma}{\pi}} \frac{1}{2\sqrt{\Gamma^2 + \alpha_2^2 t^2}} e^{-\frac{\Gamma}{4(\Gamma^2+\alpha_2^2 t^2)}(\mathbf{x}-2\alpha_2 \mathbf{k}_0 t)^2} \tag{6.12}$$

shows that the 'quantum mechanical' wave packet travels with a speed proportional to $\mathbf{k}_0$. As well, the wave packet disperses for $\alpha_2 \neq 0$, i.e., for $\frac{\mathrm{d}^2\omega}{\mathrm{d}k^2} \neq 0$. This can be seen from the pre-factors in rftd:qma.

6.1.2 Approximate solutions

Asymptotics for the plane wave

With $\mathbf{k} = (k_x, k_y) = (k\cos\alpha, k\sin\alpha)$ and $\mathbf{x} = (x, y) = (r\cos\phi, r\sin\phi)$ we can write the plane wave (6.7) as [12]

$$e^{i\mathbf{k}\cdot\mathbf{x}} = e^{ikr\cos(\phi-\alpha)} = \sum_{m=-\infty}^{\infty} i^m J_m(kr) e^{im(\phi-\alpha)}. \tag{6.13}$$

From [20] we know the asymptotic form of $H_m^{(1),(2)}$:

$$H_m(z) \to \sqrt{\frac{2}{\pi z}}\, (\mp i)^m e^{\pm i(z-\frac{\pi}{4})}. \tag{6.14}$$

Assume now that $kr \gg m$. Then,

$$\begin{aligned} i^m J_m(kr) &= i^m \frac{1}{2}\left[\, H_m^{(1)}(kr) + H_m^{(2)}(kr)\right] \\ &= \frac{1}{2}\left[i^m H_m^{(1)}(kr) + (-1)^m i^{-m} H_m^{(2)}(kr)\right]. \end{aligned} \tag{6.15}$$

can be approximated by its asymptotic form. This yields for (6.13)

$$e^{i\mathbf{k}\cdot\mathbf{x}} \approx N_p \frac{1}{\sqrt{k}} \sum_{m=-\infty}^{\infty} \left[e^{i(kr-\frac{\pi}{4})} + e^{\pm im\pi} e^{-(kr-\frac{\pi}{4})}\right] e^{im(\phi-\alpha)}, \tag{6.16}$$

where

$$N_p = \sqrt{\frac{1}{2\pi r}}. \tag{6.17}$$

Asymptotics for the Gaussian weight factor

With the modified Bessel function of integer order $I_m(x) = i^{-m}J_m(ix)$ we obtain also in analogy to (6.13)

$$e^{2\Gamma k k_0 \cos\alpha} = \sum_{m=-\infty}^{\infty} I_m(2\Gamma k k_0) e^{im\alpha}, \tag{6.18}$$

thus we have the following series representation for $\tilde{\psi}_0$.

$$\tilde{\psi}_0(\mathbf{k}) = N e^{-\Gamma(k^2+k_0^2)} \sum_{m=-\infty}^{\infty} I_m(2\Gamma k k_0) e^{im\alpha}. \tag{6.19}$$

Here, N is the normalisation constant such that $\|\tilde{\psi}\| = 1$. The asymptotic form of the modified Bessel function $I_m(x)$ for large arguments x is given by [21]

$$I_m(x) \approx \frac{1}{\sqrt{2\pi x}} e^x \left[e^{-\frac{m^2}{2x}} + O\left(\frac{1}{x^4}\right)\right]. \tag{6.20}$$

Assume now that $k_0\sqrt{\Gamma} \gg 1$, and that $k\sqrt{\Gamma} \gg \frac{1}{2k_0\sqrt{\Gamma}}$, then

$$I_m(2\Gamma k k_0) \approx \frac{1}{\sqrt{4\pi\Gamma k k_0}} e^{2\Gamma k k_0} e^{-\frac{m^2}{4\Gamma k k_0}}. \tag{6.21}$$

As the factor $e^{-\Gamma(\mathbf{k}-\mathbf{k}_0)^2}$ has a sharp maximum around $\mathbf{k} \approx \mathbf{k}_0$, we set $k \approx k_0$ in the exponential of (6.21) and obtain for $\tilde{\psi}_0(\mathbf{k})$ the approximation

$$\tilde{\psi}_0(\mathbf{k}) = N' \frac{1}{\sqrt{k}} e^{-\Gamma(k^2-k_0^2)} \sum_{m=-\infty}^{\infty} e^{-\frac{m^2}{4\Gamma k_0^2} + im\alpha}. \tag{6.22}$$

For $k_0\sqrt{\Gamma} \gg 1$, we approximate the series with an integral:

$$\sum_{m=-\infty}^{\infty} e^{-\frac{m^2}{4\Gamma k_0^2} + im\alpha} \approx \int_{-\infty}^{\infty} e^{-\frac{m^2}{4\Gamma k_0^2} + im\alpha} \,\mathrm{d}m = \sqrt{4k_0^2\pi\Gamma} e^{-\Gamma k_0^2 \alpha^2}. \tag{6.23}$$

This yields finally an approximation for $\tilde{\psi}_0(\mathbf{k})$ which is separated in a radial and an angular part:

$$\tilde{\psi}_0 = N_k \tilde{\psi}_{0,k}(k) N_\alpha \tilde{\psi}_{0,\alpha}(\alpha) \tag{6.24}$$

where

$$\tilde{\psi}_{0,k}(k) = \frac{1}{\sqrt{k}} e^{-\Gamma(k-k_0)^2}, \tag{6.25}$$

$$\tilde{\psi}_{0,\alpha}(\alpha) = e^{-\Gamma k_0^2 \alpha^2}. \tag{6.26}$$

The normalisation factors are chosen such that

$$\left\| \tilde{\psi}_0 \right\|^2 = \int_0^\infty k \,\mathrm{d}k \int_{-\pi}^{\pi} \tilde{\psi}_0(\mathbf{k}) \psi_0^*(\mathbf{k}) = 1. \tag{6.27}$$

In particular,

$$\frac{1}{N_k^2} = \int_0^\infty e^{-2\Gamma(k-k_0)^2} = \sqrt{\frac{\pi}{2\Gamma}}\frac{1+\mathrm{erf}(\sqrt{2\Gamma}k_0)}{2}, \tag{6.28}$$

$$\frac{1}{N_\alpha^2} = \int_{-\pi}^{\pi} e^{-2\Gamma k_0^2\alpha^2} = \sqrt{\frac{\pi}{2\Gamma k_0^2}}\mathrm{erf}(\sqrt{2}\pi k_0\sqrt{\Gamma}\ ). \tag{6.29}$$

and as $k_0\sqrt{\Gamma} \gg 1$ and the error function converges very quickly towards its limit $\lim_{x\to\infty}\mathrm{erf}(x) = 1$, we can approximate the normalisation constants to

$$N_k = \left(\frac{2\Gamma}{\pi}\right)^{\frac{1}{4}}, \tag{6.30}$$

$$N_\alpha = \left(\frac{2\Gamma k_0^2}{\pi}\right)^{\frac{1}{4}}. \tag{6.31}$$

Stationary phase method

Next, we search for an approximation to the integral

$$\int_a^b A(k)e^{i\Phi(k)}\,\mathrm{d}k \tag{6.32}$$

where

1. $A(k)$ is changing slowly, and $\Phi(k)$ is changing fast, i.e.,

$$\frac{\mathrm{d}A}{\mathrm{d}k} \ll \frac{\mathrm{d}\Phi}{\mathrm{d}k} \qquad \text{almost everywhere in } (a,b). \tag{6.33}$$

2. $\Phi(k)$ is oscillating very quickly.

$$\frac{\Phi(b)-\Phi(a)}{2\pi} \gg 1 \tag{6.34}$$

The approximation presented here is called the *method of stationary phase*. It is applicable to integrals of the form (6.32 - 6.34). Under these circumstances, the major contribution to the integral is made in intervals J_i around values $\Phi(k) = \Phi(k_i)$ defined by $\frac{\mathrm{d}\Phi}{\mathrm{d}k}(k_i) = 0$. In Fig. 6.1.2 this argument is justified visually. We call the points k_i with this property *stationary points* and split the interval $[a,b]$ into the sum of the intervals $J = \cup J_i$ and a part $J_e = [a,b]\ \setminus \cup J_i$. We state that

$$\int_{J_e} A(k)e^{i\Phi(k)}\,\mathrm{d}k \approx 0. \tag{6.35}$$

An expansion of the remaining integral yields

$$\begin{aligned}\int_J A(k)e^{i\Phi(k)}\,\mathrm{d}k = \sum_i \int_{J_i}&\left[A(k_i) + \frac{\mathrm{d}A}{\mathrm{d}k}(k_i)(k-k_i) + \dots\right] \\ &\times e^{i\left[\Phi(k_i)+\frac{1}{2}\frac{\mathrm{d}^2\Phi}{\mathrm{d}k^2}(k_i)(k-k_i)^2+\dots\right]}\,\mathrm{d}k \qquad (6.36)\\ &\approx \sum_i A(k_i)e^{i\Phi(k_i)}\int_{J_i} e^{i\frac{1}{2}\frac{\mathrm{d}^2\Phi}{\mathrm{d}k^2}(k_i)(k-k_i)^2}\ \mathrm{d}k. \qquad (6.37)\end{aligned}$$

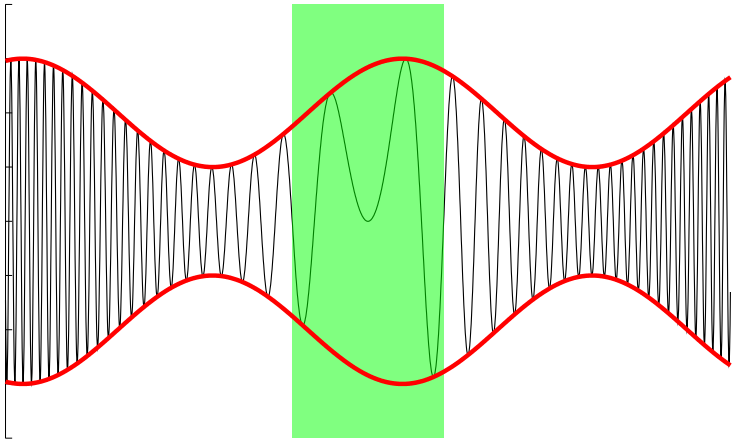

Figure 6.2: Stationary phase method

As all the contributions from $k \notin J_i$ are neglectable, we can write the integral as

$$\int_J A(k)e^{i\Phi(k)}\,\mathrm{d}k\,\mathrm{d}k = \sum_i A(k_i)e^{i\Phi(k_i)} \int_{-\infty}^{\infty} e^{i\frac{1}{2}\frac{\mathrm{d}^2\Phi}{\mathrm{d}k^2}(k_i)(k-k_i)^2}\,\mathrm{d}k. \tag{6.38}$$

The integral in (6.38) is a standard integral with a solution in closed form:

$$\int_{-\infty}^{\infty} \left[\cos ak^2 + i\sin ak^2\right] = \sqrt{\frac{\pi}{|a|}}\frac{1+\operatorname{sign} a}{\sqrt{2}} = \sqrt{\frac{\pi}{|a|}}e^{i\frac{\pi}{4}\operatorname{sign} a}. \tag{6.39}$$

Eventually, the stationary phase approximation reads

$$\int_a^b A(k)e^{i\Phi(k)}\,\mathrm{d}k \approx \sum_i A(k_i)\sqrt{\frac{2\pi}{\left|\frac{\mathrm{d}^2\Phi}{\mathrm{d}k^2}(k_i)\right|}}e^{i\left[\Phi(k_i)+\frac{\pi}{4}\operatorname{sign}\frac{\mathrm{d}^2\ \Phi}{\mathrm{d}k^2}(k_i)\right]}. \tag{6.40}$$

6.1.3 Free solutions

Now, take (6.1) in polar coordinates for $\mathbf{k} = (k, \alpha)$

$$u(\mathbf{x}, t) = \frac{1}{2\,\pi}\int_0^{\infty}\int_0^{2\pi} u(\mathbf{k}, \mathbf{x})\tilde{\psi}(\mathbf{k}, t)k\,\mathrm{d}k\,\mathrm{d}\alpha, \tag{6.41}$$

and insert (6.2), (6.24), (6.7) and (6.13). This yields

$$\begin{aligned} u(\mathbf{x}, t) =& N_k N_\alpha N_p \sum_{m=-\infty}^{\infty}\int_0^{\infty}\left[e^{i(kr-\frac{\pi}{4})} + e^{\pm im\pi}e^{-(kr-\frac{\pi}{4})}\right]e^{-\Gamma(k-k_0)^2}e^{-i\omega(k)t}\,\mathrm{d}k \\ &\times \sum_{n=-\infty}^{\infty} e^{-\frac{n^2}{4\Gamma k_0^2}+im\phi}\frac{1}{2\,\pi}\int_0^{2\pi} e^{i(n-m)\alpha}\,\mathrm{d}\alpha. \end{aligned} \tag{6.42}$$

Note that $-\pi < \phi < \pi$. Integration over α yields

$$u(\mathbf{x},t) = N_k N_\alpha N_p \Bigg\{ \sum_{m=-\infty}^{\infty} e^{-\frac{m^2}{4\Gamma k_0^2} + im\phi - i\frac{\pi}{4}} \int_0^\infty e^{-\Gamma(k-k_0)^2 - i\omega(k)t + ikr} + \sum_{m=-\infty}^{\infty} e^{-\frac{m^2}{4\Gamma k_0^2} + im(\phi\pm\pi) - i\frac{\pi}{4}} \int_0^\infty e^{-\Gamma(k-k_0)^2 - i\omega(k)t - ikr} \Bigg\}. \tag{6.43}$$

With (6.23), and

$$I_\sigma(r,t) = \int_0^\infty e^{-\Gamma(k-k_0)^2 - i(\alpha_1 k + \alpha_2 k^2)t + i\sigma kr}\,\mathrm{d}k, \tag{6.44}$$

$$N_s = \sqrt{4k_0^2\pi\Gamma}, \qquad \sigma = \pm 1, \tag{6.45}$$

we can approximate this as

$$u(\mathbf{x},t) = N_k N_\alpha N_p N_s \sum_{\sigma=\pm1} e^{-\Gamma k_0^2(\phi \mp \frac{\pi}{2} \pm \sigma\frac{\pi}{2})^2} I_\sigma(r,t). \tag{6.46}$$

Next, we approximate $I_\sigma(r,t)$ with the method of stationary phase. There is one stationary point

$$k_s = \frac{\sigma r - \alpha_1 t}{2t\alpha_2}, \tag{6.47}$$

and with (6.40) we obtain

$$I_\sigma(r,t) \approx \sqrt{\frac{\pi}{\alpha_2}} e^{-\frac{\Gamma}{4t^2\alpha_2^2}(r - \sigma\frac{\mathrm{d}\omega}{\mathrm{d}k}(k_0)t)^2} e^{i\left[-\omega(k_s) + \sigma k_s r + \frac{\pi}{4}\alpha_2\right]}. \tag{6.48}$$

According to (6.35), with the approximations made $I_\sigma(r,t) \approx 0$ for $r \not\approx \sigma\frac{\mathrm{d}\omega}{\mathrm{d}k}(k_0)t$. Finally, we obtain for the limits $t \to \pm\infty$ for $u(\mathbf{x},t)$ with $N = N_k N_\alpha N_p N_s \sqrt{\frac{\pi}{\alpha_2}}$

$$\lim_{t\to\infty} |u(\mathbf{x},t)| \approx N e^{-\Gamma k_0^2\phi^2} e^{-\frac{\Gamma}{4t^2\alpha_2^2}\left[r - \frac{\mathrm{d}\omega}{\mathrm{d}k}(k_0)t\right]^2}, \tag{6.49}$$

$$\lim_{t\to-\infty} |u(\mathbf{x},t)| \approx N e^{-\Gamma k_0^2(\phi\pm\pi)^2} e^{-\frac{\Gamma}{4t^2\alpha_2^2}\left[r + \frac{\mathrm{d}\omega}{\mathrm{d}k}(k_0)t\right]^2}. \tag{6.50}$$

From the form of these equations we deduce the following statements.

1. The free wave packets evolve asymptotically in a hyperbola whose envelope is given by $e^{-\Gamma k_0^2\phi^2}$ for positive times and by $e^{-\Gamma k_0(\phi\pm\pi)^2}$ for negative times (cf. Fig. 2.2).

2. The velocity of the peak of the wave packet travels with a speed which is given by the *group velocity* $\frac{\mathrm{d}\omega}{\mathrm{d}k}(k_0)$.

6.1.4 Scattered wave packet

In the presence of a scatterer, the time-independent solution has the form

$$u(\mathbf{k},\mathbf{x}) = e^{i\mathbf{k}\cdot\mathbf{x}} + u^{\mathrm{sc}}(\mathbf{k},\mathbf{x}), \tag{6.51}$$

where $u^{\mathrm{sc}}(\mathbf{k},\mathbf{x})$ is a solution which fulfills the Helmholtz equation (2.5), the boundary conditions (2.8 - 2.9) on the obstacle and the Sommerfeld radiation condition (3.5). Expansion of $u^{\mathrm{sc}}(\mathbf{k},\mathbf{x})$ in cylindrical coordinates yields

$$u^{\mathrm{sc}}(k,\alpha,r,\phi) = \sum_{m=-\infty}^{\infty} d_m(k)\mathrm{H}_m(kr)e^{im(\phi-\alpha)}. \tag{6.52}$$

For the time-dependent scattered field, we obtain after integration over α

$$u^{\mathrm{sc}}(r,\phi) = N' \underbrace{\int_0^{\infty} e^{-\,\Gamma(k-k_0)^2 - i\omega(k)t + ikr}}_{I_+(r,t)} \sum_{m=-\infty}^{\infty} \sqrt{\frac{2}{\pi r}} d_m(k_0) e^{-\frac{m^2}{4\Gamma k_0^2} + im\phi}. \tag{6.53}$$

Therefore, the scattered wave packet has the form

$$u^{\mathrm{sc}}(r,\phi) \approx I_+(r,t) W_+^{\mathrm{sc}}(\phi) \tag{6.54}$$

with

$$W_+^{\mathrm{sc}}(\phi) = N' \sqrt{\frac{2}{\pi r}} \sum_{m=-\infty}^{\infty} d_m(k_0) e^{-\frac{m^2}{4\Gamma k_0^2} + im\phi}. \tag{6.55}$$

The Sommerfeld radiation condition ensures that $u^{\mathrm{sc}}(\mathbf{r},t)$ is a linear combination of 'outgoing' waves $\mathrm{H}_m(kr)e^{im\phi}$. They are called 'outgoing' because $I_+(r,t) \approx 0$ for $t < 0$, and thus

$$u(\mathbf{x},t) \approx u^{\mathrm{free}}(\mathbf{x},t), \qquad \text{for } t < 0. \tag{6.56}$$

Note that outside of the hyperbola for $t > 0$, $\psi_t^{\mathrm{free}}(\mathbf{x},t) \approx 0$. In this region, the angular dependence of $u(\mathbf{x},t)$ is given by $W_+^{\mathrm{sc}}(\phi)$ and thus time-independent. These facts are illustrated by the right-hand side of Fig. 2.3 where the free wave packet is shown in blue and the area where $I_+(r,t)W_+^{\mathrm{sc}}(\phi) \not\approx 0$ in red.

6.2 Waveguide

For the waveguide model the time-dependent solutions have the form

$$u(\mathbf{x},t) = \sqrt{\frac{1}{2\pi}} \int_{-\infty}^{\infty} u(k,\mathbf{x})\tilde{\psi}(k,t)\,\mathrm{d}k, \tag{6.57}$$

where

$$\tilde{\psi}(k,t) = \tilde{\psi}_0(k)e^{-i\omega(k)t}, \tag{6.58}$$

$$\tilde{\psi}_0(k) = \sqrt{\frac{\pi}{\Gamma}}\, e^{-\Gamma(k-k_0)^2}. \tag{6.59}$$

Free wave packet

A free solution of the Helmholtz equation has the form

$$u^{\text{free}}(\mathbf{x},k) = \sum_{n=1}^{\infty} \sin(k_n y)\left[a_n e^{i\kappa_n(x-x_0)} + b_n e^{-i\kappa_n(x-x_0)}\right], \tag{6.60}$$

where

$$k_n = \frac{n\pi}{W}, \tag{6.61}$$

$$\kappa_n = \kappa_n(k) = \sqrt{k^2 - k_n^2}, \tag{6.62}$$

and the free wavepacket is therefore given by

$$u^{\text{free}}(\mathbf{x},t) = \sqrt{\frac{1}{2\pi}}\sqrt{\frac{\Gamma}{\pi}}\int_{-\infty}^{\infty} e^{-\Gamma(k-k_0)^2}\sum_{n=1}^{\infty}\sin(k_n y)\Big[a_n e^{i\kappa_n(x-x_0)} + b_n e^{-i\kappa_n(x-x_0)}\Big]e^{-i\omega(k)t}\,\mathrm{d}k. \tag{6.63}$$

Stationary points only exist for real κ_n, i.e., if the sum over n ends at $M = \left\lceil \frac{kW}{\pi} \right\rceil$, where $\lceil x \rceil$ denotes the first integer bigger or equal than x. We will call the remainder of the infinite sum, where n is such that κ_n is imaginary, $r(\mathbf{x},t)$.

$$r(\mathbf{x},t) = r_a(\mathbf{x},t) + r_b(\mathbf{x},t), \tag{6.64}$$

$$r_a(\mathbf{x},t) = N\int_{-\infty}^{\infty} e^{-\Gamma(k-k_0)^2}\sum_{n=M}^{\infty}\sin(k_n y)a_n e^{-|\kappa_n|(x-x_0)}e^{-i\omega(k)t}, \tag{6.65}$$

$$r_b(\mathbf{x},t) = N\int_{-\infty}^{\infty} e^{-\Gamma(k-k_0)^2}\sum_{n=M}^{\infty}\sin(k_n y)b_n e^{|\kappa_n|(x-x_0)}e^{-i\omega(k)t}. \tag{6.66}$$

Note that for $|x| \to \infty$, either the exponential of $r_a(\mathbf{x},t)$ or the exponential of $r_b(\mathbf{x},t)$ diverges. Thus, we require $a_n = 0$, and $b_n = 0$ for $M \le n < \infty$ for a free solution with infinite domain; in other words, a free solution with infinite domain may not contain evanescent waves[1]. In the following, we will therefore require that $r(\mathbf{x},t) = 0$.

For the search of stationary points, we make the approximation $k \approx k_0$ in the square root of κ_n. This is justified by the exponential factor $e^{-\Gamma(k-k_0)^2}$ in the integrand. A Taylor expansion of $\frac{\mathrm{d}}{\mathrm{d}k}\kappa_n$ around $k = k_0$ yields

$$\frac{\mathrm{d}}{\mathrm{d}k}\sqrt{k^2 - \left(\frac{n\pi}{W}\right)^2} = \frac{k_0}{\sqrt{k_0^2 - \left(\frac{n\pi}{W}\right)^2}} - \frac{\left(\frac{n\pi}{W}\right)^2}{\left(k_0^2 - \left(\frac{n\pi}{W}\right)\right)^{\frac{3}{2}}}(k-k_0) + O\left([k-k_0]^2\right). \tag{6.67}$$

[1] Another way to get rid of the exponentially growing waves is to split the infinite domain in two half-infinite domains at a point $x = x_0$, allowing for exponentially decaying waves in every direction like in (4.48) and (4.49).

As stationary points we obtain

$$k_{\sigma,n} \approx \frac{k_0}{\sqrt{k_0^2 - \left(\frac{n\pi}{W}\right)^2}} \frac{\sigma(x - x_0)}{2\alpha_2 t} - \frac{\alpha_1}{2\alpha_2}, \qquad \sigma = \pm 1. \tag{6.68}$$

The $\pm$ sign reflects the signs in the exponential which corresponds to the coefficients a_n and b_n, respectively. Thus, for the free wave packet, we obtain

$$\begin{aligned} u^{\text{free}}(\mathbf{x}, t) \approx N \sum_{n=1}^{M-1} a_n e^{-\frac{\Gamma}{2\alpha_2}\left[x - x_0 + \frac{\mathrm{d}\omega}{\mathrm{d}k}(k_0) t \frac{\sqrt{k_0^2 - \left(\frac{n\pi}{W}\right)^2}}{k_0}\right]} \\ \times \sqrt{\frac{2\pi}{\left|\frac{\mathrm{d}^2\Phi}{\mathrm{d}k^2}(k_{+,n})\right|}} \sin(k_n y) e^{i\sqrt{k_{+,n}^2 - k_n^2}(x - x_0) - i\omega(k_{+,n})t} \\ + N \sum_{n=1}^{M-1} b_n e^{-\frac{\Gamma}{2\alpha_2}\left[x - x_0 - \frac{\mathrm{d}\omega}{\mathrm{d}k}(k_0) t \frac{\sqrt{k_0^2 - \left(\frac{n\pi}{W}\right)^2}}{k_0}\right]} \\ \times \sqrt{\frac{2\pi}{\left|\frac{\mathrm{d}^2\Phi}{\mathrm{d}k^2}(k_{-,n})\right|}} \sin(k_n y) e^{i\sqrt{k_{-,n}^2 - k_n^2}(x - x_0) - i\omega(k_{-,n})t}. \end{aligned} \tag{6.69}$$

In these equations,

$$\frac{\mathrm{d}^2\Phi}{\mathrm{d}k^2}(k) = \frac{k_n^2}{(k^2 - k_n^2)^{\frac{3}{2}}} - 2\alpha_2 t. \tag{6.70}$$

We see that the for $|x - x_0| \not\approx \left|\frac{\mathrm{d}\omega}{\mathrm{d}k}(k_0) t \frac{\sqrt{k_0^2 - \left(\frac{n\pi}{W}\right)^2}}{k_0}\right|$, $u^{\text{free}}(\mathbf{x}, t) \approx 0$. Thus, we obtained a sum of travelling wave packets where a mode n travels with the speed $\frac{\mathrm{d}\omega}{\mathrm{d}k}(k_0) \frac{\sqrt{k_0^2 - \left(\frac{n\pi}{W}\right)^2}}{k_0}$.

Scattered wave

For the scattered wave, we start with

$$u(\mathbf{x}, t) = u^{\text{free}}(\mathbf{x}, t) + u^{\text{sc}}(\mathbf{x}, t). \tag{6.71}$$

Take a given source distribution $\psi(\mathbf{x}')$ as in chapter 4, then the scattered field is (4.21)

$$u^{\text{sc}}(\mathbf{x}) = \int_{\partial O} G_k(\mathbf{x}, \mathbf{x}'(s)) \psi(\mathbf{x}'(s)) \, \mathrm{d}s. \tag{6.72}$$

In this representation of the solution, the evanescent waves with κ_n imaginary cannot cause any problems because for $|x| \gg 1$, the exponential $e^{i\kappa_n |x - x'(s)|} \ll 1$. The time-dependent scattered wave for this source distribution is then given

by

$$u^{\mathrm{sc}}(\mathbf{x},t) = \sqrt{\frac{1}{2\pi}}\frac{i}{W}\sum_{n=1}^{\infty}\sin(k_n y)\int_{\partial O}\sin(k_n y'(s))\psi(x'(s)) \times \int_{-\infty}^{\infty}\frac{1}{\kappa_n}e^{-\Gamma(k-k_0)^2}e^{i\kappa_n|x-x'(s)\ |-i\omega(k)t}\,\mathrm{d}k\,\mathrm{d}s. \tag{6.73}$$

With the same approximation as for the free wave packet, we obtain for the stationary points

$$k_{s,n}(s) \approx \frac{k_0}{\sqrt{k_0^2-\left(\frac{n\pi}{W}\right)^2}}\frac{|x-x'(s)|}{2\alpha_2 t} - \frac{\alpha_1}{2\alpha_2}. \tag{6.74}$$

The stationary-phase approximation for the integral is therefore

$$u^{\mathrm{sc}}(\mathbf{x},t) = \sqrt{\frac{1}{2\pi}}\ \frac{i}{W}\sum_{n=1}^{M-1}\sin(k_n y)\frac{e^{-i\omega(k_{s,n})t}}{\sqrt{k_{s,n}^2-k_n^2}}e^{-\Gamma(k_{s,n}^2-k_0)^2}\sqrt{\frac{2\pi}{\left|\frac{\mathrm{d}^2\Phi}{\mathrm{d}k^2}(k_{s,n})\right|}} \times \int_{\partial O}\sin(k_n y'(s))\psi(x'(s))e^{i\sqrt{k_{s,n}^2-k_n^2}|x-x'(s)\ |+\frac{\pi}{4}\mathrm{sign}\,\frac{\mathrm{d}^2\Phi}{\mathrm{d}k^2}(k_{s,n})}\,\mathrm{d}s \tag{6.75}$$

We see that for the scattered wave, the modes travel with the same speed as for the free wave as $u^{\mathrm{sc}}(\mathbf{x},t)\approx 0$ for $|x-x'(s)| \not\approx \left|\frac{\mathrm{d}\omega}{\mathrm{d}k}(k_0)t\frac{\sqrt{k_0^2-\left(\frac{n\pi}{W}\right)^2}}{k_0}\right|$, where s parametrises the surface of the scattering body.

6.3 One-dimensional case

In one dimension, the time-dependent solution reads

$$u(\mathbf{x},t) = \sqrt{\frac{1}{2\ \pi}}\int_{-\ \infty}^{\infty}u(k,x)\tilde{\psi}(k,t)\,\mathrm{d}k, \tag{6.76}$$

with

$$\tilde{\psi}(k,t) = \tilde{\psi}_0(k)e^{-i\omega(k)t}, \tag{6.77}$$

$$\tilde{\psi}_0(k) = \left(\frac{\Gamma}{\pi}\right)^{\frac{1}{4}}e^{-\Gamma(k-k_0)^2}. \tag{6.78}$$

The one-dimensional normalisation is chosen such that

$$\left\|\tilde{\psi}_0\right\| = \left(\int_{-\infty}^{\infty}\tilde{\psi}_0(k)\tilde{\psi}_0^*(k)\,\mathrm{d}k\right)^{\frac{1}{2}} = 1. \tag{6.79}$$

The one-dimensional free plane wave is described by

$$u(k,x) = e^{ikx}. \tag{6.80}$$

The corresponding free wave packet is described by the integral

$$\psi(x,t) = \sqrt{\frac{1}{2\pi}}\left(\frac{\Gamma}{\pi}\right)^{\frac{1}{4}} \int_{-\infty}^{\infty} e^{ikx} e^{-\ \Gamma(k-\ k_0)^2} e^{-i\omega(k)t}\,\mathrm{d}k, \tag{6.81}$$

where

$$\omega(k) = (\alpha_1|k| + \alpha_2 k^2), \qquad \alpha_1 \geq 0, \alpha_2 \geq 0. \tag{6.82}$$

6.3.1 Exact solutions

The advantage of the one-dimensional case is that more analytical solutions are available as in the two-dimensional case. They are described below.

Free wave packet with $\alpha_1 = 0, \alpha_2 > 0$ (quantum mechanics)

The quantum-mechanical case $\alpha_1 = 0$, i.e. $\omega(k) \propto k^2$ is exactly solvable for all dimensions. The one-dimensional integral to be evaluated here is of the form

$$\begin{aligned}\psi_q^{\pm}(x,t) =& \sqrt{\frac{1}{2\pi}}\left(\frac{\Gamma}{\pi}\right)^{\frac{1}{4}} \int_{-\ \infty}^{\infty} e^{\pm ikx} e^{-\ \Gamma(k-\ k_0)^2} e^{-i\alpha_2 k^2 t}\,\mathrm{d}k \\ =& \left(\frac{\Gamma}{4\pi}\right)^{\frac{1}{4}} \frac{1}{\sqrt{\Gamma + it\alpha_2}} e^{-k_0^2\Gamma + \frac{(\pm ix + 2\Gamma k_0)^2}{4(\Gamma + i\alpha_2 t)}}\end{aligned} \tag{6.83}$$

Similarly to the two-dimensional case, the absolute value of $\psi(x,t)$ is given by

$$\left|\psi_q^{\pm}(x,t)\right|^2 = \left(\frac{\Gamma}{4\pi}\right)^{\frac{1}{2}} \frac{1}{\sqrt{\Gamma^2 + \alpha_2^2 t^2}} e^{-\frac{\Gamma}{2(\Gamma^2 + \alpha_2^2 t^2)}(\mp x + 2\alpha_2 k_0 t)^2}; \tag{6.84}$$

it shows that the quantum mechanical wave packet travels with a speed proportional to k_0 and disperses. For $t \to \pm\infty$, we observe two phenomena: first, the width of the wave packet, determined by the pre-factor $-\frac{\Gamma}{2\sqrt{\Gamma^2+\alpha_2^2 t^2}}$, becomes larger with increasing absolute values of t. Secondly, the peak of the wave packet travels at $x = \mp 2\alpha_2 k_0 t$ with the velocity $\frac{\mathrm{d}\omega}{\mathrm{d}k}(k_0)$. In particular, we note that for

$$k_0 > 0, \qquad \frac{\mathrm{d}\omega}{\mathrm{d}k}(k_0) = 2\alpha_2 k_0 > 0, \tag{6.85}$$

the following asymptotics hold true.

$$\psi_q^+(x, t \gg 1) \approx 0 \qquad \text{for } x < 0 \tag{6.86}$$

$$\psi_q^+(x, t \ll -1) \approx 0 \qquad \text{for } x > 0 \tag{6.87}$$

$$\psi_q^-(x, t \gg 1) \approx 0 \qquad \text{for } x > 0 \tag{6.88}$$

$$\psi_q^-(x, t \ll -1) \approx 0 \qquad \text{for } x < 0 \tag{6.89}$$

$$\max_x \psi_q^+(x, t \gg 1) \approx \frac{\mathrm{d}\omega}{\mathrm{d}k_0} t \gg 1 \tag{6.90}$$

$$\max_x \psi_q^+(x, t \ll -1) \approx \frac{\mathrm{d}\omega}{\mathrm{d}k_0} t \ll -1 \tag{6.91}$$

$$\max_x \psi_q^-(x, t \gg 1) \approx -\frac{\mathrm{d}\omega}{\mathrm{d}k_0} t \ll -1 \tag{6.92}$$

$$\max_x \psi_q^-(x, t \ll -1) \approx -\frac{\mathrm{d}\omega}{\mathrm{d}k_0} t \gg 1 \tag{6.93}$$

Thus, we see that $\psi_q^+(x,t)$ is a wave packet which travels from $-\infty$ to $+\infty$ and $\psi_q^-(x,t)$ travels in the opposite direction.

Free wave packet with $\alpha_1 > 0, \alpha_2 = 0$ (electromagnetism)

The integral may be written down with the help of the error function [20].

$$\begin{aligned}\psi_e^\pm(x,t) &= \sqrt{\frac{1}{2\pi}} \left(\frac{\Gamma}{\pi}\right)^{\frac{1}{4}} \int_{-\infty}^{\infty} e^{\pm ikx} e^{-\Gamma(k-k_0)^2} e^{-ic|k|t}\,\mathrm{d}k \\ &= \left(\frac{1}{4\pi\Gamma}\right)^{\frac{1}{4}} \left\{ e^{-\frac{1}{4\Gamma}(x-ct)^2 \pm ik_0(x-ct)} \left[1 \pm \operatorname{erf}\left(\frac{2\Gamma k_0 \pm i(x-ct)}{\sqrt{4\Gamma}}\right)\right] \right. \\ &\quad \left. + e^{-\frac{1}{4\Gamma}(x+ct)^2 \pm ik_0(x+ct)} \left[1 \mp \operatorname{erf}\left(\frac{2\Gamma k_0 \pm i(x+ct)}{\sqrt{4\Gamma}}\right)\right] \right\}\end{aligned} \tag{6.94}$$

Here, $\operatorname{erf}(z)$ is defined by

$$\operatorname{erf}(z) = \frac{2}{\sqrt{\pi}} \int_0^z e^{-t^2}\,\mathrm{d}t. \tag{6.95}$$

In this case, there is no dispersion of the wave packet: its width is always characterised by Γ. Note that $\psi_e^\pm(x,t) \approx 0$ for $x \not\approx \pm ct$, thus the main peak travels in the same direction as k_0 with the velocity $\frac{\mathrm{d}\omega}{\mathrm{d}k}(k_0)$. We assume now that $\sqrt{\Gamma}k_0 \gg 1$, i.e. the width of the wave packet (which is characterised by $\sqrt{\Gamma}$ is much bigger then the average wave length $\lambda_0 = \frac{2\pi}{k_0}$. Then, for $x \approx \mp ct$, $\operatorname{erf}(\dots)$ in (6.94) is given approximately by $\operatorname{erf}(\sqrt{\Gamma}k_0)$. As $\lim_{x\to\infty} \operatorname{erf}(x) = 1$ converges quickly, this is approximately 1. The asymptotic expressions for $\psi_e^\pm(x,t)$ with

$$k_0 > 0, \qquad \frac{\mathrm{d}\omega}{\mathrm{d}k}(k_0) = \alpha_1 \operatorname{sign} k_0 > 0 \tag{6.96}$$

are given by the following equations.

$$\psi_e^+(x, t \gg 1) \approx 0 \qquad \text{for } x < 0 \tag{6.97}$$

$$\psi_e^+(x, t \ll -1) \approx 0 \qquad \text{for } x > 0 \tag{6.98}$$

$$\psi_e^-(x, t \gg 1) \approx 0 \qquad \text{for } x > 0 \tag{6.99}$$

$$\psi_e^-(x, t \ll -1) \approx 0 \qquad \text{for } x < 0 \tag{6.100}$$

$$\max_x \psi_e^+(x, t \gg 1) \approx \frac{\mathrm{d}\omega}{\mathrm{d}k_0} t \gg 1 \tag{6.101}$$

$$\max_x \psi_e^+(x, t \ll -1) \approx \frac{\mathrm{d}\omega}{\mathrm{d}k_0} t \ll -1 \tag{6.102}$$

$$\max_x \psi_e^-(x, t \gg -1) \approx -\frac{\mathrm{d}\omega}{\mathrm{d}k_0} t \ll -1 \tag{6.103}$$

$$\max_x \psi_e^-(x, t \ll -1) \approx -\frac{\mathrm{d}\omega}{\mathrm{d}k_0} t \gg 1 \tag{6.104}$$

Again, we see that $\psi_e^+(x,t)$ is a wave packet whose peak of constant height travels from $-\infty$ to $+\infty$; as well, $\psi_e^-(x,t)$ travels in the opposite direction from $+\infty$ to $-\infty$.

6.3.2 Scattered wave packet

A scattering 'body' which may be described with a $\gamma(x)$ that is bounded to the interval $[-x_0, x_0]$ can be described outside of this interval by the sum of two related free solutions.

$$u(k,x) = u^{\mathrm{in}}(k,x) + u^{\mathrm{sc}}(k,x) \qquad \text{for } |x| > x_0 \tag{6.105}$$

$$u^{\mathrm{in}}(k,x) = a^{\mathrm{in}} e^{ikx} + b^{\mathrm{in}} e^{-ikx} \tag{6.106}$$

$$u^{\mathrm{sc}}(k,x) = \begin{cases} a^{\mathrm{sc}}(k) e^{ikx} & x > x_0 \\ b^{\mathrm{sc}}(k) e^{-ikx} & x < x_0 \end{cases}. \tag{6.107}$$

The *scattering matrix* relates the coefficients of the free solutions long before ($u^{-\infty}(k,x)$) and long after ($u^{\infty}(k,x)$) the scattering process.

$$\begin{pmatrix} a^{\infty} \\ b^{\infty} \end{pmatrix} = S(k) \begin{pmatrix} a^{-\infty} \\ b^{-\infty} \end{pmatrix} = \begin{bmatrix} S_{11}(k) & S_{12}(k) \\ S_{21}(k) & S_{22}(k) \end{bmatrix} \begin{pmatrix} a^{-\infty} \\ b^{-\infty} \end{pmatrix} \tag{6.108}$$

The free solutions are given by

$$u^{-\infty}(k,x) = a^{-\infty} e^{ikx} + b^{-\infty} e^{-ikx}, \tag{6.109}$$

$$u^{\infty}(k,x) = a^{\infty} e^{ikx} + b^{\infty} e^{-ikx}, \tag{6.110}$$

where the coefficients are related to the ones already defined by

$$\begin{aligned} a^{-\infty} &= a^{\mathrm{in}}, & b^{-\infty} &= b^{\mathrm{in}}, \\ a^{\infty} &= a^{\mathrm{in}} + a^{\mathrm{sc}}, & b^{\infty} &= b^{\mathrm{in}} + b^{\mathrm{sc}}. \end{aligned} \tag{6.111}$$

Conservation of the probability current leads for the scattering matrix to the relations

$$|S_{11}(k)|^2 + |S_{12}(k)|^2 = 1, \tag{6.112}$$

$$|S_{21}(k)|^2 + |S_{22}(k)|^2 = 1, \tag{6.113}$$

$$S_{11}(k) S_{12}^*(k) + S_{21}(k) S_{22}^*(k) = 0. \tag{6.114}$$

From these relations, we show that $S(k)$ and $S^T(k)$ are unitary. Time-reversal invariance signifies that if $u(x,t)$ is a solution and $\gamma(x)$ is real, then $u^*(x,-t)$ is also a solution of the same Helmholtz equation with the same $\gamma(x)$. Note that that this operation interchanges incoming and outgoing waves. In terms of the scattering matrix, this means

$$S(k) = S^T(k). \tag{6.115}$$

Furthermore, as for every $u(k,x)$ the function $u(k,x)^*$ is also a solution to the one-dimensional Helmholtz equations, the equation

$$S(-k) = S^\dagger(k) \tag{6.116}$$

holds. Finally, if the scattering potential is symmetric, i.e., $\gamma(x) = \gamma(-x)$, then $S(k)$ may be written as

$$S(k) = \begin{bmatrix} t(k) & -r^*(k) \\ r(k) & t^*(k) \end{bmatrix}, \tag{6.117}$$

where $r(k)$ and $t(k)$ are the reflection and transmission amplitudes. The corresponding reflection and transmission probabilities are given by $R(k) = r(k)r(k)^*$ and $T(k) = t(k)t(k)^*$. Note that $R(k) + T(k) = 1$. The scattered wave fulfills the Sommerfeld radiation condition in one dimension which states that at infinity, $u^{\mathrm{sc}}(x,k)$ must consist of outgoing waves only.

$$\lim_{x\to+\infty}\left(\frac{\partial}{\partial x} - ik\right) u^{\mathrm{sc}}(x,k) = 0 \tag{6.118}$$

$$\lim_{x\to-\infty}\left(\frac{\partial}{\partial x} + ik\right) u^{\mathrm{sc}}(x,k) = 0 \tag{6.119}$$

The scattered wave packet is given by the following integral.

$$\psi^{\mathrm{sc}}(x,t) = \begin{cases} \left(\dfrac{\Gamma}{4\pi^3}\right)^{\frac{1}{4}} \displaystyle\int_{-\infty}^{\infty} a^{\mathrm{sc}}(k) e^{ikx} e^{-\Gamma(k-k_0)^2} e^{-i(\alpha_1 k + \alpha_2 k^2)t}\,\mathrm{d}k & x > x_0 \\ \left(\dfrac{\Gamma}{4\pi^3}\right)^{\frac{1}{4}} \displaystyle\int_{-\infty}^{\infty} b^{\mathrm{sc}}(k) e^{-ikx} e^{-\Gamma(k-k_0)^2} e^{-i(\alpha_1 k + \alpha_2 k^2)t}\,\mathrm{d}k & x < x_0 \end{cases} \tag{6.120}$$

Because of the sharp peak of $e^{-\Gamma(k-k_0)^2}$ around $k \approx k_0$, we approximate $a^{\mathrm{sc}}(k)$ and $b^{\mathrm{sc}}(k)$ in the integrand with $a^{\mathrm{sc}}(k_0)$ and $b^{\mathrm{sc}}(k_0)$. Note that this approximation is not good enough to explain the two peaks in the time-dependent behaviour of wave packets hitting the one-dimensional model for localisation as shown in chapter 9. Now, omitting the subscript e or q for the electrodynamical or the quantum mechanical case, we rewrite $\psi^{\mathrm{sc}}(x,t)$ as follows.

$$\psi^{\mathrm{sc}}(x,t) \approx \begin{cases} a^{\mathrm{sc}}(k_0)\psi^+(x,t) & x > x_0 \\ b^{\mathrm{sc}}(k_0)\psi^-(x,t) & x < x_0 \end{cases} \tag{6.121}$$

In the usual situation $a^{\text{in}} = 1$, $b^{\text{in}} = 0$, the full wave packet may be written as follows.

$$\psi(x,t) \approx \begin{cases} t(k_0)\psi^+(x,t) & x > x_0 \\ r(k_0)\psi^-(x,t) + \psi^+(x,t) & x < x_0 \end{cases} \tag{6.122}$$

Looking at (6.86 - 6.93) and (6.97 - 6.104), we see that long before the scattering process, the wave packet is given by

$$\psi(x, t \ll -1) \approx \psi^+(x,t), \tag{6.123}$$

i.e., long before the scattering process, (6.122) describes the free solution $\psi^+(x,t)$ coming from $-\infty$ to hit the scattering potential. Long after the scattering process, the wave packet is given by the following expression.

$$\psi(x, t \gg 1) \approx \begin{cases} t(k_0)\psi^+(x,t) & x > x_0 \\ r(k_0)\psi^-(x,t) & x < x_0 \end{cases} \tag{6.124}$$

From this, we see that asymptotically long after the scattering process, we have a *transmitted wave packet* travelling in the direction of k_0 with the intensity $T(k_0)$ and a *reflected wave packet* which travels in the opposite direction with the intensity $R(k_0)$.

6.4 Summary

We have presented a method which may be used to obtain time-dependent wave packets as a weighted superposition of the time-independent solutions obtained in previous chapters. Analytic solutions as well as asymptotic expressions were given for scattering in vacuum, for waveguide scattering with and without scatterers, and for one-dimensional scattering. Only in one dimension, it is possible to find an analytic solution for free electrodynamical and acoustical wave packets. In higher dimensions, this is only possible in the quantum mechanical model. In vacuum, the evolution of the free wave packet in a hyperbola and its interaction with the scattering wave packet was described for asymptotically large times.

Chapter 7

Mathieu functions

Mathieu functions were introduced in 1868 [22]. They are needed whenever a separation of variables technique is used to solve the Helmholtz equation in elliptic coordinates [23]. For example, these functions are needed to describe the scattering of classical and quantum mechanical waves by elliptical objects [24]. The exact solution obtained this way can be used to test the accuracy of other numerical schemes [25].

7.1 Eigenvalues of the Mathieu equation

Floquet solutions of the Mathieu equation

First, we introduce Mathieu functions using a terminology that refers to the eigenvalues of these functions with respect to certain operators. Mathieu functions are solutions of the *Mathieu equation*

$$\hat{H}^q\, y(z) = -\, y''(z) + 2q \cos 2z\, y(z) = \lambda\, y(z)\ . \tag{7.1}$$

We consider only values $q > 0$ and ask for solutions that are normalizable in the following sense.

$$\int_0^\pi |y(z)|^2\, \mathrm{d}z = \|y(z)\|^2 < \infty \tag{7.2}$$

To classify these solutions it is useful to introduce two more operators, namely

$$\hat{T}_\pi\, y(z) = y(z+\pi) \tag{7.3}$$

and

$$\hat{S}_0\, y(z) = y(-z)\ . \tag{7.4}$$

Note that both $\hat{T}_\pi$ and $\hat{S}_0$ commute with $\hat{H}^q$,

$$\hat{S}_0\, \hat{H}^q = \hat{H}^q\, \hat{S}_0\ , \quad \hat{T}_\pi\, \hat{H}^q = \hat{H}^q\, \hat{T}_\pi\ , \tag{7.5}$$

but that

$$\hat{S}_0\, \hat{T}_\pi\, \hat{S}_0 = \hat{T}_\pi^{-1} = \hat{T}_{-\pi}\ . \tag{7.6}$$

In a quantum mechanical context, where $\hat{H}^q$ is the Hamiltonian, $\hat{T}_\pi$ and $\hat{S}_0$ are unitary operators that commute with $\hat{H}^q$ and generate a symmetry group of infinite order (dihedral group D_∞). Accordingly, the irreducible representations of this group may be used to label the eigenfunctions and eigenvalues of $\hat{H}^q$. To this end we first consider the eigenvalue equation

$$\hat{T}_\pi\, y(z) = e^{i\mu\pi}\, y(z) \quad \text{with} \quad \mu \in (-1, +1]\ . \tag{7.7}$$

A solution of (7.1) which satifies (7.7) is called *Floquet solution* of the Mathieu equation with *characteristc exponent* μ.

Characteristic exponent $\mu \in (0, 1)$

For given $\mu \in (0, 1)$ the functions satisfying both (7.7) and (7.2) span a separable Hilbert space where the scalar product of two elements $a(z)$ and $b(z)$ is defined by

$$(a, b) = \frac{1}{\pi} \int_0^\pi a^*(z) b(z)\, \mathrm{d}z \tag{7.8}$$

and the functions

$$u_{\mu,2r}(z) = e^{i(\mu+2r)z}\ , \quad r = 0, \mp 1, \mp 2, \dots\ . \tag{7.9}$$

constitute an orthonormal basis. The action of $\hat{H}^q$ onto the elements of this basis,

$$\hat{H}^q\, u_{\mu,2r}(z) = \sum_{r'} \left(H^q_\mu\right)_{r',r}\, u_{\mu,2r'}(z)\ , \tag{7.10}$$

is given by the matrix H^q_μ with elements

$$\left(H^q_\mu\right)_{r',r} = \left(u_{\mu,2r'}(z), \hat{H}^q\, u_{\mu,2r}(z)\right)\ . \tag{7.11}$$

H^q_μ is Hermitean and bounded from below.

The Floquet solutions of (7.1) with characteristic exponent $\mu \in (0, 1)$ may therefore be obtained by a two-step procedure (algebraic eigenvalue problem):

- determination of the eigenvalues of the Hermitean matrix

$$H^q_\mu = \begin{pmatrix} (\mu+0)^2 & q & q & 0 & 0 & \cdots \\ q & (\mu-2)^2 & 0 & q & 0 & \cdots \\ q & 0 & (\mu+2)^2 & 0 & q & \cdots \\ 0 & q & 0 & (\mu-4)^2 & 0 & \cdots \\ 0 & 0 & q & 0 & (\mu+4)^2 & \cdots \\ \vdots & \vdots & \vdots & \vdots & \vdots & \ddots \end{pmatrix} \tag{7.12}$$

  with row and column indices

$$r = 0, -1, +1, -2, +2, \dots\ . \tag{7.13}$$

The *eigenvalues* $\lambda^q_{\mu,n}$ of this matrix with

$$n = 0, 1, 2, \dots \tag{7.14}$$

are nondegenerate and bounded from below whence they may be ordered according to their magnitude.

$$\lambda^q_{\mu,0} < \lambda^q_{\mu,1} < \lambda^q_{\mu,2} < \dots \tag{7.15}$$

- calculation of the related *eigenvectors* by solving the equations

$$\sum_{r'} \left(H^q_\mu\right)_{r,r'} \left(C^q_{\mu,n}\right)_{r'} = \lambda^q_{\mu,n} \left(C^q_{\mu,n}\right)_r \quad . \tag{7.16}$$

To obtain a unique solution of (7.16), we impose the following conventions.

$$\left(C^q_{\mu,n}\right)_r = \left(C^q_{\mu,n}\right)^*_r , \tag{7.17}$$

$$\sum_r \left(C^q_{\mu,n}\right)^2_r = 1. \tag{7.18}$$

(7.16), (7.17) and (7.18) determine the eigenvectors $C^q_{\mu,n}$ up to a sign which is fixed by a convection, cf. equations (7.39), (7.51), (7.78) below.

The common *eigenfunction* of $\hat{H}^q$ and $\hat{T}_\pi$ related to the eigenvalues $\lambda^q_{\mu,n}$ and $e^{i\mu\pi}$ is then

$$\sum_r (C^q_{\mu,n})_r \, u_{\mu,2r}(z) = y^q_{\mu,n}(z) \, . \tag{7.19}$$

Because of (7.17) and (7.18) these functions satisfy

$$\int_0^\pi \mathrm{d}z \left| y^q_{\mu,n}(z) \right|^2 = \pi. \tag{7.20}$$

Characteristic exponent $\mu \in (-1, 0)$

The only difference in the approach outlined above is the sign of the characteristic exponent. Inspection of (7.12) shows that for $\mu \in (0, 1)$ the matrix $H^q_{-\mu}$ may be obtained from the matrix H^q_μ by the orthogonal transformation $H^q_{-\mu} = W_-^\dagger H^q_\mu W_-$ where

$$W_- = \begin{pmatrix} 1 & 0 & 0 & 0 & 0 & \cdots \\ 0 & 0 & 1 & 0 & 0 & \cdots \\ 0 & 1 & 0 & 0 & 0 & \cdots \\ 0 & 0 & 0 & 0 & 1 & \cdots \\ 0 & 0 & 0 & 1 & 0 & \cdots \\ \vdots & \vdots & \vdots & \vdots & \vdots & \ddots \end{pmatrix} ; \tag{7.21}$$

this corresponds to a permutation of rows and colums (indices 0,-1,+1,-2,+2, $\ldots \to$ 0,+1,-1,+2,-2,...). Therefore

$$\lambda^q_{\mu,n} = \lambda^q_{-\mu,n} \quad \text{for} \quad n = 0, 1, 2, \ldots \ . \tag{7.22}$$

Another way to derive this relation is to consider the function $\hat{S}_0\, y^q_{\mu,n}(z)$ where $y^q_{\mu,n}(z)$ is a Floquet solution with characteristic exponent $\mu \in (0, 1)$ and eigenvalue $\lambda^q_{\mu,n}$. It follows from (7.5) that $\hat{S}_0\, y^q_{\mu,n}(z)$ is also an eigenfunction of $\hat{H}^q$ with eigenvalue $\lambda^q_{\mu,n}$; but because of (7.6) this function has the characteristic exponent $-\mu \in (-1, 0)$. Since the eigenvalues of H^q_μ are nondegenerate and Floquet solutions with noninteger characteristic exponent are linearly independent it is possible to choose the normalization constants and phase factors in such a way that

$$y^q_{-\mu,n}(z) = \hat{S}_0 y^q_{\mu,n}(z) = y^q_{\mu,n}(-z) \quad \text{for} \quad 0 < |\mu| < 1 \ . \tag{7.23}$$

Characteristic exponent $\mu = 0$

In the space spanned by the functions $u_{0,2r}(z)$ the translation operator $\hat{T}_\pi$ becomes the identity operator so that it is possible to diagonalize $\hat{T}_\pi$, $\hat{S}_0$, and $\hat{H}^q$, simultaneously. Let W_0 be the unitary matrix

$$W_0 = \begin{pmatrix} 1 & 0 & 0 & 0 & 0 & \cdots \\ 0 & \frac{1}{\sqrt{2}} & \frac{i}{\sqrt{2}} & 0 & 0 & \cdots \\ 0 & \frac{1}{\sqrt{2}} & \frac{-i}{\sqrt{2}} & 0 & 0 & \cdots \\ 0 & 0 & 0 & \frac{1}{\sqrt{2}} & \frac{i}{\sqrt{2}} & \cdots \\ 0 & 0 & 0 & \frac{1}{\sqrt{2}} & \frac{-i}{\sqrt{2}} & \cdots \\ \vdots & \vdots & \vdots & \vdots & \vdots & \ddots \end{pmatrix} \tag{7.24}$$

with row index (7.13) and column index

$$sp = 0+, 1+, 1-, 2+, 2-, \ldots \ . \tag{7.25}$$

Then

$$W_0^\dagger\, H^q_0\, W_0 = \begin{pmatrix} 0^2 & \sqrt{2}q & 0 & 0 & 0 & \cdots \\ \sqrt{2}q & 2^2 & 0 & q & 0 & \cdots \\ 0 & 0 & 2^2 & 0 & q & \cdots \\ 0 & q & 0 & 4^2 & 0 & \cdots \\ 0 & 0 & q & 0 & 4^2 & \cdots \\ \vdots & \vdots & \vdots & \vdots & \vdots & \ddots \end{pmatrix} \sim H^q_{0+} \oplus H^q_{0-} \tag{7.26}$$

(row/column index (7.25)). The first submatrix

$$H^q_{0+} = \begin{pmatrix} 0^2 & \sqrt{2}q & 0 & 0 & 0 & \cdots \\ \sqrt{2}q & 2^2 & q & 0 & 0 & \cdots \\ 0 & q & 4^2 & q & 0 & \cdots \\ 0 & 0 & q & 6^2 & q & \cdots \\ 0 & 0 & 0 & q & 8^2 & \cdots \\ \vdots & \vdots & \vdots & \vdots & \vdots & \ddots \end{pmatrix} \tag{7.27}$$

with row and column index

$$s+ = 0+, 1+, 2+, \ldots \tag{7.28}$$

shows the action of $\hat{H}^q$ onto the following basis.

$$v_{2s+}(z) = \begin{cases} 1 & \text{for } s = 0 \\ \sqrt{2}\cos 2sz & \text{for } s > 0 \end{cases} \tag{7.29}$$

$$= \begin{cases} u_{0,0}(z) & \text{for } s = 0 \\ \frac{1}{\sqrt{2}} u_{0,-2s}(z) + \frac{1}{\sqrt{2}} u_{0,2s}(z) & \text{for } s > 0 \end{cases} \tag{7.30}$$

The eigenvalues of (7.27) are denoted as [20]

$$\lambda^q_{0,2m} = a^q_{2m} \tag{7.31}$$

$$m = 0, 1, 2, \ \ldots \tag{7.32}$$

and its eigenvectors are calculated according to

$$\sum_{s'=0}^{\infty} \left(H^q_{0+}\right)_{s,s'} \left(A^q_{2m}\right)_{s'} = a^q_{2m} \left(A^q_{2m}\right)_s \,, \tag{7.33}$$

$$\left(A^q_{2m}\right)_s = \left(A^q_{2m}\right)^*_s , \tag{7.34}$$

$$\sum_s \left(A^q_{2m}\right)^2_s = 1, \tag{7.35}$$

and

$$\sum_s \left(A^q_{2m}\right)_s > 0. \tag{7.36}$$

The related eigenfunctions read

$$y^q_{0,2m}(z) = \sum_{s=0}^{\infty} (A^q_{2m})_s \, v_{2s+}(z) = \sum_r \left(C^q_{0,2m}\right)_r u_{0,2r}(z) \,, \tag{7.37}$$

$$\left(C^q_{0,2m}\right)_0 = \left(A^q_{2m}\right)_0 , \quad \left(C^q_{0,2m}\right)_{\pm r} = \frac{1}{\sqrt{2}} \left(A^q_{2m}\right)_r \quad \text{for } r > 0 \tag{7.38}$$

and are normalized as the functions for $\mu \in (0,1)$, see eq. (7.20). The phase convention (7.36) is equivalent to

$$y^q_{0,2m}(0) > 0. \tag{7.39}$$

The second submatrix is

$$H^q_{0-} = \begin{pmatrix} 2^2 & q & 0 & 0 & 0 & \cdots \\ q & 4^2 & q & 0 & 0 & \cdots \\ 0 & q & 6^2 & q & 0 & \cdots \\ 0 & 0 & q & 8^2 & q & \cdots \\ 0 & 0 & 0 & q & 10^2 & \cdots \\ \vdots & \vdots & \vdots & \vdots & \vdots & \ddots \end{pmatrix}, \tag{7.40}$$

where row and column indices are given by

$$s- = 1-, 2-, 3-, \ldots . \tag{7.41}$$

The corresponding basis is

$$\begin{aligned} v_{2s-}(z) &= \sqrt{2}\,\sin 2sz & (7.42)\\ &= \frac{i}{\sqrt{2}} u_{0,-2s} - \frac{i}{\sqrt{2}} u_{0,2s} & (7.43) \end{aligned}$$

The eigenvalues of (7.40) are denoted as [20]

$$\lambda^q_{0,2m+1} = b^q_{2m+2}\,. \tag{7.44}$$

The eigenvectors are defined by

$$\sum_{s'=1}^{\infty} \left(H^q_{0-}\right)_{s,s'} \left(B^q_{2m+2}\right)_{s'} = b^q_{2m+2} \left(B^q_{2m+2}\right)_s\,, \tag{7.45}$$

$$\left(B^q_{2m+2}\right)_s = \left(B^q_{2m+2}\right)^*_s, \tag{7.46}$$

$$\sum_s \left(B^q_{2m+2}\right)^2_s = 1, \tag{7.47}$$

and

$$\sum_s s \left(B^q_{2m+2}\right)_s > 0. \tag{7.48}$$

The related eigenfunctions read

$$y^q_{0,2m+1}(z) = \sum_{s=1}^{\infty} (B^q_{2m+2})_s\, v_{(2s)-}(z) = \sum_r \left(C^q_{0,2m+1}\right)_r u_{0,2r}(z)\,, \tag{7.49}$$

$$\left(C^q_{0,2m+1}\right)_{\pm r} = \mp \frac{i}{\sqrt{2}} \left(B^q_{2m+2}\right)_r \quad \text{for } r > 0 \tag{7.50}$$

and are normalized as the functions for $\mu \in (0,1)$, see eq. (7.20). The phase convention (7.48) corresponds to

$$\left[\frac{\mathrm{d}}{\mathrm{d}z}\, y^q_{0,2m+1}(z)\right]_{z=0} > 0. \tag{7.51}$$

Characteristic exponent $\mu = 1$

In this case, the operator $\hat{T}_\pi$ becomes again a multiple of the identity operator, namely -1. Following the same procedure as in the case $\mu = 0$ we introduce the unitary matrix

$$W_1 = \begin{pmatrix} \frac{1}{\sqrt{2}} & \frac{-i}{\sqrt{2}} & 0 & 0 & \cdots \\ \frac{1}{\sqrt{2}} & \frac{i}{\sqrt{2}} & 0 & 0 & \cdots \\ 0 & 0 & \frac{1}{\sqrt{2}} & \frac{-i}{\sqrt{2}} & \cdots \\ 0 & 0 & \frac{1}{\sqrt{2}} & \frac{i}{\sqrt{2}} & \cdots \\ \vdots & \vdots & \vdots & \vdots & \ddots \end{pmatrix} \tag{7.52}$$

with row index (7.13) and column index

$$sp = 0+, 0-, 1+, 1-, 2+, 2-, \ldots . \tag{7.53}$$

Then

$$W_1^\dagger \, H_1^q \, W_1 = \begin{pmatrix} 1+q & 0 & q & 0 & 0 & 0 & \cdots \\ 0 & 1-q & 0 & q & 0 & 0 & \cdots \\ q & 0 & 3^2 & 0 & q & 0 & \cdots \\ 0 & q & 0 & 3^2 & 0 & q & \cdots \\ 0 & 0 & q & 0 & 5^2 & 0 & \cdots \\ 0 & 0 & 0 & q & 0 & 5^2 & \cdots \\ \vdots & \vdots & \vdots & \vdots & \vdots & \ddots & \end{pmatrix} \sim H_{1+}^q \oplus H_{1-}^q \, . \tag{7.54}$$

The first submatrix is

$$H_{1+}^q = \begin{pmatrix} 1+q & q & 0 & 0 & 0 & \cdots \\ q & 3^2 & q & 0 & 0 & \cdots \\ 0 & q & 5^2 & q & 0 & \cdots \\ 0 & 0 & q & 7^2 & q & \cdots \\ 0 & 0 & 0 & q & 9^2 & \cdots \\ \vdots & \vdots & \vdots & \vdots & \vdots & \ddots \end{pmatrix} . \tag{7.55}$$

where rows and columns refer to the indices $s+$, eq. (7.28). The corresponding basis is

$$v_{(2s+1)+}(z) = \sqrt{2}\cos(2s+1)z \tag{7.56}$$

$$= \frac{1}{\sqrt{2}} u_{1,2s} + \frac{1}{\sqrt{2}} u_{1,-2s-2} \tag{7.57}$$

The eigenvalues, eigenvectors, and eigenfunctions are given by the following equations.

$$\lambda_{1,2m+1}^q = a_{2m+1}^q \tag{7.58}$$

$$\sum_{s'=0}^{\infty} \left(H^q_{1+}\right)_{s,s'} \left(A^q_{2m+1}\right)_{s'} = a^q_{2m+1} (A^q_{2m+1})_s \tag{7.59}$$

$$\left(A^q_{2m+1}\right)_s = \left(A^q_{2m+1}\right)^*_s \tag{7.60}$$

$$\sum_s \left(A^q_{2m+1}\right)^2_s = 1 \tag{7.61}$$

$$\sum_s \left(A^q_{2m+1}\right)_s > 0 \tag{7.62}$$

$$y^q_{1,2m+1}(z) = \sum_{s=0}^{\infty} (A^q_{2m+1})_s v_{(2s+1)+}(z) = \sum_r \left(C^q_{1,2m+1}\right)_r u_{1,2r}(z) \tag{7.63}$$

$$\left(C^q_{1,2m+1}\right)_r = \frac{1}{\sqrt{2}} \left(A^q_{2m+1}\right)_r \quad \text{for } r \geq 0 \tag{7.64}$$

$$\left(C^q_{1,2m+1}\right)_r = \frac{1}{\sqrt{2}} \left(A^q_{2m+1}\right)_{-r-1} \quad \text{for } r < 0 \tag{7.65}$$

and are normalized as the functions for $\mu \in (0,1)$, see eq. (7.20). The phase convention (7.62) corresponds to

$$y^q_{1,2m+1}(0) > 0. \tag{7.66}$$

The last submatrix is

$$H^q_{1-} = \begin{pmatrix} 1-q & q & 0 & 0 & 0 & \cdots \\ q & 3^2 & q & 0 & 0 & \cdots \\ 0 & q & 5^2 & q & 0 & \cdots \\ 0 & 0 & q & 7^2 & q & \cdots \\ 0 & 0 & 0 & q & 9^2 & \cdots \\ \vdots & \vdots & \vdots & \vdots & \vdots & \ddots \end{pmatrix} \tag{7.67}$$

where rows and columns refer to the indices $s-$ given by eq. (7.41). The corresponding basis is now

$$v_{(2s+1)-}(z) = \sqrt{2}\,\sin(2s+1)z \tag{7.68}$$

$$= -\frac{i}{\sqrt{2}} u_{1,2s} + \frac{i}{\sqrt{2}} u_{1,-2s-2} \tag{7.69}$$

and the eigenvalues, eigenvectors, and eigenfunctions read as follows.

$$\lambda^q_{1,2m} = b^q_{2m+1} \tag{7.70}$$

$$\sum_{s'=0}^{\infty} \left(H^q_{1-}\right)_{s,s'} \left(B^q_{2m+1}\right)_{s'} = b^q_{2m+1} (B^q_{2m+1})_s \tag{7.71}$$

$$\left(B^q_{2m+1}\right)_s = \left(B^q_{2m+1}\right)^*_s \tag{7.72}$$

$$\sum_s \left(B^q_{2m+1}\right)^2_s = 1 \tag{7.73}$$

$$\sum_s (2s+1)\left(B^q_{2m+1}\right)_s > 0 \tag{7.74}$$

$$y^q_{1,2m}(z) = \sum_{s=0}^{\infty} (B^q_{2m+1})_s v_{(2s+1)-}(z) = \sum_r \left(C^q_{1,2m}\right)_r u_{1,2r}(z) \tag{7.75}$$

$$\left(C^q_{1,2m+1}\right)_r = -\frac{i}{\sqrt{2}}\left(B^q_{2m+1}\right)_r \quad \text{for } r \geq 0 \tag{7.76}$$

$$\left(C^q_{1,2m+1}\right)_r = \frac{i}{\sqrt{2}}\left(B^q_{2m+1}\right)_{-r-1} \quad \text{for } r < 0 \tag{7.77}$$

The functions (7.75) are again normalized according to (7.20). The phase convention (7.74) corresponds to

$$\left[\frac{\mathrm{d}}{\mathrm{d}z}\, y^q_{1,2m}(z)\right]_{z=0} > 0. \tag{7.78}$$

Characteristic exponent $\mu \notin (-1, 1]$

If the characteristic exponent is not in the interval $(-1, 1]$, we decompose it according to $\mu + 2k$ accordingg to $\mu \in (-1, 1]$ and $k \in \mathbb{Z}$. Looking at

$$H^q_{\mu+2k} = \begin{pmatrix} (\mu+2k)^2 & q & q & 0 & 0 & \cdots \\ q & (\mu+2k-2)^2 & 0 & q & 0 & \cdots \\ q & 0 & (\mu+2k+2)^2 & 0 & q & \cdots \\ 0 & q & 0 & (\mu+2k-4)^2 & 0 & \cdots \\ 0 & 0 & q & 0 & (\mu+2k+4)^2 & \cdots \\ \vdots & \vdots & \vdots & \vdots & \vdots & \ddots \end{pmatrix} \tag{7.79}$$

we see that it corresponds to H^q_μ if columns and rows are appropriately rearranged.

$$\left(H^q_{\mu+2k}\right)_{r,r'} = \left(H^q_\mu\right)_{r+k,r'+k} \tag{7.80}$$

We therefore relate the eigenvalues and eigenvectors of $H^q_{\mu+2k}$ to those of H^q_μ in the following way.

$$\lambda^q_{\mu+2k,n} = \lambda^q_{\mu,n} \tag{7.81}$$

$$\left(C^q_{\mu+2k,n}\right)_r = \left(C^q_{\mu,n}\right)_{r+k} \tag{7.82}$$

7.1.1 Recurrence relations

Line r of (7.16) corresponds to

$$\left[\lambda^q_{\mu,m} - (\mu+2r)^2\right]\left(C^q_{\mu,m}\right)_r - q\left[\left(C^q_{\mu,m}\right)_{r+1} + \left(C^q_{\mu,m}\right)_{r-1}\right] = 0. \tag{7.83}$$

Line s of (7.33) yields

$$a^q_{2m}\,(A^q_{2m})_0 - \sqrt{2}q\,(A^q_{2m})_1 = 0\,, \tag{7.84}$$

$$(a^q_{2m} - 4)\,(A^q_{2m})_1 - q\left[\sqrt{2}\,(A^q_{2m}\,)_0 + (A^q_{2m})_2\right] = 0\,, \tag{7.85}$$

$$\left[a^q_{2m} - (2s)^2\right](A^q_{2m})_s - q\left[(A^q_{2m})_{s-1} + (A^q_{2m})_{s+1}\right] = 0 \qquad s \geq 2\,. \tag{7.86}$$

Equivalently, from (7.59) we obtain

$$\left(a^q_{2m+1} - 1 - q\right)\left(A^q_{2m+1}\right)_0 - q\left(A^q_{2m+1}\right)_1 = 0\,, \tag{7.87}$$

$$\left[a^q_{2m+1} - (2s+1)^2\right]\left(A^q_{2m+1}\right)_s - q\left[\left(A^q_{2m+1}\right)_{s-1} + \left(A^q_{2m+1}\,\right)_{s+1}\right] = 0 \qquad s \geq 1\,. \tag{7.88}$$

(7.45) yields

$$\left(b^q_{2m+2} - 4\right)\left(B^q_{2m+2}\right)_0 - q\left(B^q_{2m+2}\right)_1 = 0\,, \tag{7.89}$$

$$\left[b^q_{2m+2} - (2s+2)^2\right]\left(B^q_{2m+2}\right)_s - q\left[\left(B^q_{2m+2}\right)_{s-1} + \left(B^q_{2m+2}\right)_{s+1}\right] = 0 \qquad s \geq 2\,, \tag{7.90}$$

and with (7.71) we finally obtain

$$\left(b^q_{2m+1} - 1 + q\right)\left(B^q_{2m+1}\right)_0 - q\left(B^q_{2m+1}\right)_1 = 0\,, \tag{7.91}$$

$$\left[b^q_{2m+1} - (2s+1)^2\right]\left(B^q_{2m+1}\right)_s - q\left[\left(B^q_{2m+1}\right)_{s-1} + \left(B^q_{2m+1}\right)_{s+1}\right] = 0 \qquad s \geq 2\,. \tag{7.92}$$

Terminology of Meixner and Schäfke

A very convenient notation is introduced in [26]. Its advantage is that all Mathieu functions can be considered as one single function, the distinction between the four cases being taken care of by the notation used. Following [26] we write for $m = 0, 1, 2, \ldots$

$$\frac{1}{\sqrt{2}}y^q_{0,2m}(z) \quad = \mathrm{ce}_{2m}(z;q) = \quad \frac{1}{\sqrt{2}}\mathrm{me}_{2m}(z;q)\,, \tag{7.93}$$

$$\frac{1}{\sqrt{2}}y^q_{1,2m}(z) \quad = \mathrm{ce}_{2m+1}(z;q) = \quad \frac{1}{\sqrt{2}}\mathrm{me}_{2m+1}(z;q)\,, \tag{7.94}$$

$$\frac{1}{\sqrt{2}}y^q_{1,2m+1}(z) \quad = \mathrm{se}_{2m+1}(z;q) = \quad \frac{i}{\sqrt{2}}\mathrm{me}_{-2m-1}(z;q)\,, \tag{7.95}$$

$$\frac{1}{\sqrt{2}}y^q_{0,2m+1}(z) \quad = \mathrm{se}_{2m+2}(z;q) = \quad \frac{i}{\sqrt{2}}\mathrm{me}_{-2m-2}(z;q)\,. \tag{7.96}$$

In [26], a one-index notation for the $(C^q_{\mu,n})_r$ coefficients is used which is denoted by $c^m_{2r}(q)$. For $m > 0$, it is related to the previously defined coefficients by

$$c^{2m}_{2r}(q) = \left(C^q_{0,2m}\right)_r , \tag{7.97}$$

$$c^{2m+1}_{2r}(q) = \left(C^q_{1,2m}\right)_r , \tag{7.98}$$

$$c^{-2m-1}_{2r}(q) = \left(C^q_{1,2m+1}\right)_r , \tag{7.99}$$

$$c^{-2m-2}_{2r}(q) = \left(C^q_{0,2m+1}\right)_r . \tag{7.100}$$

The index n of the functions $\mathrm{ce}_n(z;q)$ and $\mathrm{se}_n(z;q)$ is called the *order* of these Mathieu functions. The eigenvalues related to the eigenfunctions (7.93) - (7.96) are a^q_{2m}, a^q_{2m+1}, b^q_{2m+1}, b^q_{2m+2} and

$$a^q_0 < b^q_1 < a^q_1 < b^q_2 < a^q_2 < b^q_3 < a^q_3 < \dots . \tag{7.101}$$

Note that for $q \to 0$ we have

$$b^q_m \to a^q_m \quad \text{for } m > 0 \tag{7.102}$$

and

$$\lim_{q\to 0} \mathrm{ce}_n(z;q) \to \cos nz , \tag{7.103}$$

$$\lim_{q\to 0} \mathrm{se}_n(z;q) \to \sin nz . \tag{7.104}$$

7.2 The modified Mathieu functions

If we replace the variable z in the Mathieu equation (7.1) by iz we obtain the *modified Mathieu equation*

$$\frac{\mathrm{d}^2 y}{\mathrm{d}z^2} - (\lambda - 2q\cosh 2z)\, y = 0. \tag{7.105}$$

Solutions of (7.105) may be obtained from the previously defined Mathieu functions by substituting $z \to iz$. The functions obtained are series in $\cosh nz$ and $\sinh nz$, the coefficients being the same as for the Mathieu functions with real argument.

Although theoretically well-defined, this series representation is numerically inconvenient. It is more efficient to use a series representation in Hankel functions. The symbol Z_m with $m \in \mathbb{N}_0$ has the following meaning.

$$Z^{(j)}_m(z) = \begin{cases} J_m(z) & j = 1 \\ Y_m(z) & j = 2 \\ J_m(z) + iY_m(z) & j = 3 \\ J_m(z) - iY_m(z) & j = 4 \end{cases} \tag{7.106}$$

$J_m(z)$ is the Bessel function with

$$J_m(z) \to \sqrt{\frac{2}{\pi z}} \cos\left(z - \frac{m\pi}{2} - \frac{\pi}{4}\right) \qquad \text{for } z \to \infty\,, \tag{7.107}$$

$Y_m(z)$ is the Neumann function with

$$Y_m(z) \to \sqrt{\frac{2}{\pi z}} \sin\left(z - \frac{m\pi}{2} - \frac{\pi}{4}\right) \qquad \text{for } z \to \infty\,, \tag{7.108}$$

and $Z_m^{(3,4)}(z)$ are the related Hankel functions with asymptotic form [20]

$$Z_m^{(3)}(z) \to (-i)^m \sqrt{\frac{2}{\pi z}} e^{+i(z-\frac{\pi}{4})} \tag{7.109}$$

$$Z_m^{(4)}(z) \to (-i)^m \sqrt{\frac{2}{\pi z}} e^{-i(z-\frac{\pi}{4})}. \tag{7.110}$$

Using these functions, we introduce the following *modified Mathieu functions.*

$$\mathrm{Mc}_{2n}^{(j)}(z;q) = \frac{1}{\mathrm{ce}_{2n}(0;q)} \sum_{r=0}^{\infty} (-1)^{n-r} \left(A_{2n}^q\right)_r \mathrm{Z}_{2r}^{(j)}(2\sqrt{q}\cosh z) \tag{7.111}$$

$$\mathrm{Mc}_{2n+1}^{(j)}(z;q) = \frac{1}{\mathrm{ce}_{2n+1}(0;q)} \sum_{r=0}^{\infty} (-1)^{n-r} \left(A_{2n+1}^q\right)_r \mathrm{Z}_{2r+1}^{(j)}(2\sqrt{q}\cosh z) \tag{7.112}$$

$$\mathrm{Ms}_{2n+2}^{(j)}(z;q) = \frac{\tanh z}{\mathrm{se}'_{2n+2}(0;q)} \sum_{r=0}^{\infty} (-1)^{n-r} (2r+2) \left(B_{2n+2}^q\right)_r \mathrm{Z}_{2r+2}^{(j)}(2\sqrt{q}\cosh z) \tag{7.113}$$

$$\mathrm{Ms}_{2n+1}^{(j)}(z;q) = \frac{\tanh z}{\mathrm{se}'_{2n+1}(0;q)} \sum_{r=0}^{\infty} (-1)^{n-r} (2r+1) \left(B_{2n+1}^q\right)_r \mathrm{Z}_{2r+1}^{(j)}(2\sqrt{q}\cosh z) \tag{7.114}$$

The relation of these functions to the functions $\mathrm{me}_n(iz;q)$ is discussed in [26]. For $j > 1$, the following equivalent series representations [26] are more useful for numerical calculations (cf. chapter 8).

$$\mathrm{Mc}_{2n}^{(j)}(z;q) = \frac{1}{(1+\delta_{s,0})\left(A_{2n}^q\right)_s} \sum_{r=0}^{\infty} (-1)^{n+r} \left(A_{2n}^q\right)_r \times \begin{bmatrix} \mathrm{J}_{r-s}(\sqrt{q}e^{-z})\mathrm{Z}_{r+s}^{(j)}(\sqrt{q}e^{z}) \\ +\mathrm{J}_{r+s}(\sqrt{q}e^{-z})\mathrm{Z}_{r-s}^{(j)}(\sqrt{q}e^{z}) \end{bmatrix} \tag{7.115}$$

$$\mathrm{Mc}_{2n+1}^{(j)}(z;q) = \frac{1}{\left(A_{2n+1}^q\right)_s} \sum_{r=0}^{\infty} (-1)^{n+r} \left(A_{2n+1}^q\right)_r \times \begin{bmatrix} \mathrm{J}_{r-s}(\sqrt{q}e^{-z})\mathrm{Z}_{r+s+1}^{(j)}(\sqrt{q}e^{z}) \\ +\mathrm{J}_{r+s+1}(\sqrt{q}e^{-z})\mathrm{Z}_{r-s}^{(j)}(\sqrt{q}e^{z}) \end{bmatrix} \tag{7.116}$$

$$\mathrm{Ms}_{2n+2}^{(j)}(z;q) = \frac{1}{\left(B_{2n+2}^q\right)_s} \sum_{r=0}^{\infty} (-1)^{n+r} \left(B_{2n+2}^q\right)_r \times \begin{bmatrix} \mathrm{J}_{r-s}(\sqrt{q}e^{-z})\mathrm{Z}_{r+s+2}^{(j)}(\sqrt{q}e^{z}) \\ -\mathrm{J}_{r+s+2}(\sqrt{q}e^{-z})\mathrm{Z}_{r-s}^{(j)}(\sqrt{q}e^{z}) \end{bmatrix} \tag{7.117}$$

$$\mathrm{Ms}_{2n+1}^{(j)}(z;q) = \frac{1}{\left(B_{2n+1}^q\right)_s} \sum_{r=0}^{\infty} (-1)^{n+r} \left(B_{2n+1}^q\right)_r \times \begin{bmatrix} \mathrm{J}_{r-s}(\sqrt{q}e^{-z})\mathrm{Z}_{r+s+1}^{(j)}(\sqrt{q}e^{z}) \\ -\mathrm{J}_{r+s+1}(\sqrt{q}e^{-z})\mathrm{Z}_{r-s}^{(j)}(\sqrt{q}e^{z}) \end{bmatrix} \tag{7.118}$$

Note that in (7.115) - (7.118) $s = 0, 1, 2, \dots$ is a free index and $Z^{(j)}_{-m}(z) = (-1)^m Z^{(j)}_m(z)$. Finally, the functions $M^{(j)}_m(z;q)$ are defined in the following way.

$$M^{(j)}_m(z;q) = \mathrm{Mc}^{(j)}_m(z;q) \qquad (m = 0, 1, 2, \dots) \tag{7.119}$$

$$(-1)^m M^{(j)}_{-m}(z;q) = \mathrm{Ms}^{(j)}_m(z;q) \qquad (m = 1, 2, 3, \dots) \tag{7.120}$$

The asymptotic behaviour of these functions is given by [26]

$$M^{(j)}_m(z;q) \to Z^{(j)}_m(2\sqrt{q}\cosh z) \qquad \text{for } z \to \infty. \tag{7.121}$$

7.3 Eigenfunctions of the Helmholtz equation

With the Laplacian (3.13), the Helmholtz equation (2.5) with piecewise constant $\gamma(\mathbf{x})$ reads

$$-\frac{\partial^2 u}{\partial \xi^2} - \gamma^2 \frac{h^2 k^2}{2} \cosh 2\xi = \frac{\partial^2 u}{\partial \eta^2} - \gamma^2 \frac{h^2 k^2}{2}. \tag{7.122}$$

From the ansatz $u(\xi, \eta) = U(\xi)V(\eta)$ we obtain the following two ordinary differential equations with the separation constant λ and $q_k = \frac{h^2 k^2}{4}$ as in (3.22).

$$-U''(\xi) + \left(\lambda - 2\gamma^2 q \cosh 2\xi\right) U(\xi) = 0 \tag{7.123}$$

$$V''(\eta) + \left(\lambda - 2\gamma^2 q \cos 2\eta\right) V(\eta) = 0 \tag{7.124}$$

Eq. (7.124) is equivalent to (7.1) and (7.123) to (7.105). Thus, we know that we can write the general solution for given λ, called *partial wave*, for the Helmholtz equation in elliptic coordinates as sum of two linearly independent solution, e.g.,

$$u_p(\xi, \eta) = a_p \mathrm{M}^{(1)}_p(\xi; \gamma^2 q_k)\mathrm{me}_p(\eta; \gamma^2 q_k) + b_p \mathrm{M}^{(3)}_p(\xi; \gamma^2 q_k)\mathrm{me}_p(\eta; \gamma^2 q_k). \tag{7.125}$$

Smoothness around the x-axis

Note that the conditions (3.14 - 3.17) have to be fulfilled for a partial wave inside of a scattering body. For $p > 0$, the sign of $\mathrm{me}_p(\eta; \gamma^2 q_k)$ flips when going though $y = 0$; for $p < 0$, the sign of $\frac{\mathrm{d}}{\mathrm{d}\eta}\mathrm{me}_p(\eta; \gamma^2 q_k)$ flips. This jump is 'compensated' for the *regular partial wave* $M^{(1)}_p(\xi; \gamma^2 q_k)\mathrm{me}_p(\eta; \gamma^2 q_k)$ by the fact that, for $\xi \to 0$, $M^{(1)}_p(\xi; \gamma^2 q_k) \to 0$ for $p > 0$ and $\frac{\mathrm{d}}{\mathrm{d}\xi} M^{(1)}_p(\xi; \gamma^2 q_k) \to 0$ for $p < 0$. However, the ξ-derivatives of the *singular partial wave* $M^{(2)}_p(\xi; \gamma^2 q_k)$ do not become zero, thus $M^{(2)}_p(\xi; \gamma^2 q_k)\mathrm{me}_p(\eta; \gamma^2 q_k)$ is not continuous; therefore, it cannot be part of the solution (3.26) inside of a scattering body. This is illustrated in Fig. (7.3).

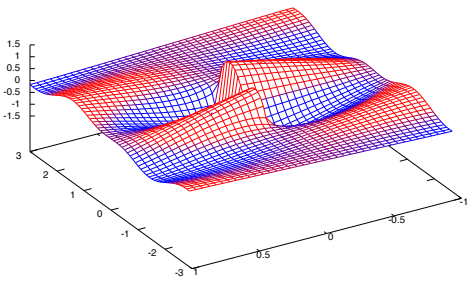

$-3 \leq x \leq 3, -1 \leq y \leq 1$

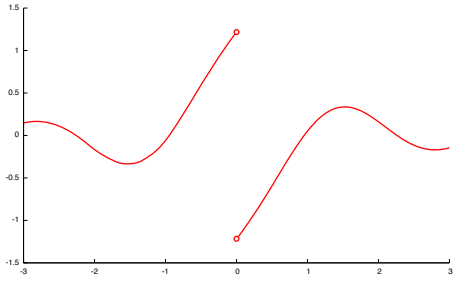

$x = 0.5, -3 \leq y \leq 3$

Figure 7.1: Discontinuity of the partial wave $\mathrm{M}_{-2}^{(2)}(\xi(x,y);2)\,\mathrm{me}_{-2}(\eta(x,y);2)$

7.4 Addition theorem for Mathieu functions

The addition theorem relates two solutions of the Helmholtz equation in different coordinate systems. It was used in chapter (3) to solve the scattering problem for N elliptical scatterers. We formulate it here for the two elliptical coordinate systems

$$\boldsymbol{\xi}^{(1)} = \boldsymbol{\Xi}\left(h^{(1)}, \mathsf{D}(-\alpha^{(1)})(\mathbf{x}-\mathbf{x}^{(1)})\right) = \boldsymbol{\xi}^{(1)}(\mathbf{x}), \tag{7.126}$$

$$\boldsymbol{\xi}^{(2)} = \boldsymbol{\Xi}\left(h^{(2)}, \mathsf{D}(-\alpha^{(2)})(\mathbf{x}-\mathbf{x}^{(2)})\right) = \boldsymbol{\xi}^{(2)}(\mathbf{x}), \tag{7.127}$$

where $\boldsymbol{\Xi}(h,\mathbf{x})$ is given by (3.9) and $\mathsf{D}(\alpha)$ by (3.59). The origins of the two coordinate systems are joined by the vector $\boldsymbol{\rho} = (\rho,\psi) = \mathbf{x}^{(1)} - \mathbf{x}^{(2)}$. We assume that the geometric parameters $\alpha^{(i)}$, $h^{(i)}$, and $h^{(i)}$ are all real. Formulas for complex parameters are similar, but the expansions are valid in more complicated regions [27]. For the description of the addition theorem coefficients, we will use the terminology (7.97 - 7.100). Now, the *exterior Addition theorem*

$$M_p^{(j)}(\xi^{(1)};q^{(1)})\mathrm{me}_p(\eta^{(1)};q^{(1)}) = \sum_{s=-\infty}^{\infty} A_s M_{p+s}^{(j)}(\xi^{(2)};q^{(2)})\mathrm{me}_{p+s}(\eta^{(2)};q^{(2)}), \tag{7.128}$$

$$A_s = \sum_{\substack{l=-\infty \\ r=-\infty}}^{\infty} (-1)^{l+s} c_{2r}^{p}(q^{(1)}) c_{2(r-l)}^{p+s}(q^{(2)}) e^{-i(p+2r)(\alpha_1-\alpha_2)} J_{2l-s}(k\rho) e^{i(2l-s)\psi}, \tag{7.129}$$

is valid in the region coloured in blue in Fig. 7.4

$$\xi^{(2)} > \xi_{\max}^{(2)}, \tag{7.130}$$

where

$$\xi_{\max}^{(2)} = \max\left[(\mathbf{x}^{(1)} + \mathsf{D}(\alpha^{(1)})\begin{pmatrix} h \\ 0 \end{pmatrix}, \mathbf{x}^{(1)} + \mathsf{D}(\alpha^{(1)})\begin{pmatrix} -h \\ 0 \end{pmatrix}\right]. \tag{7.131}$$

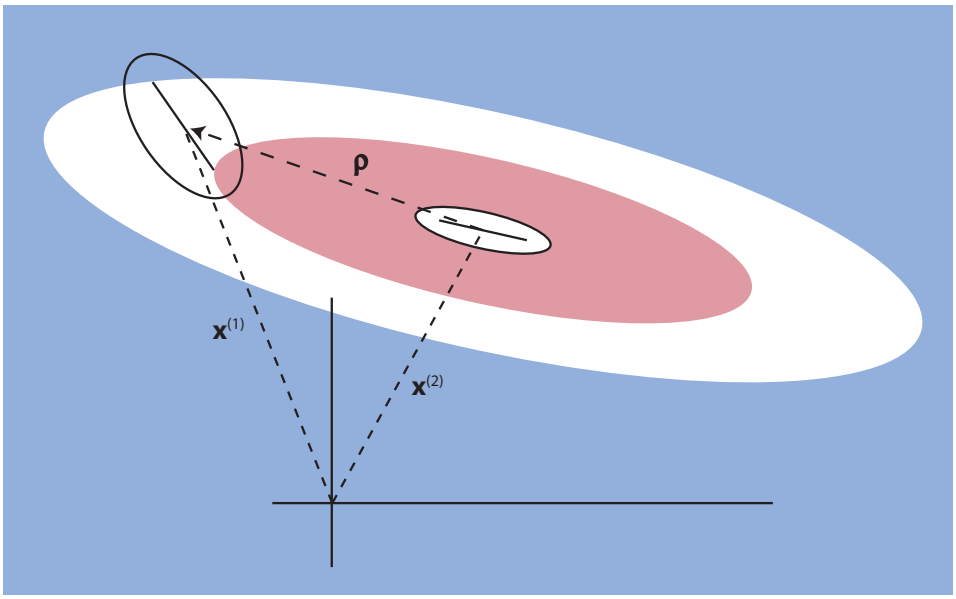

Figure 7.2: Range of addition theorem

The *interior Addition theorem*

$$M_m^{(j)}(\xi^{(1)};q^{(1)})\mathrm{me}_m(\eta^{(1)};q^{(1)}) = \sum_{r=-\infty}^{\infty} B_{r,m}^{(j)} M_r^{(1)}(\xi^{(2)};q^{(2)})\mathrm{me}_r(\eta^{(2)};q^{(2)}), \tag{7.132}$$

$$B_{r,m}^{(j)}(q^{(1)},q^{(2)}) = \sum_{\substack{f=-\infty \\ g=-\infty}}^{\infty} (-1)^{g-f+m} c_{2g}^m(q^{(1)}) c_{2f}^r(q^{(2)}) Z_{r-m+2(f-g)}^{(j)}(k\rho) \times e^{-i[r-m+2(f-g)]\psi} e^{-i(2g+m)\ (\alpha_1-\alpha_2)}, \tag{7.133}$$

is valid in the region coloured in red in Fig. 7.4

$$\xi^{(2)} < \xi_{\min}^{(2)}, \tag{7.134}$$

where

$$\xi_{\min}^{(2)} = \min\left[(\mathbf{x}^{(1)} + \mathsf{D}(\alpha^{(1)}) \begin{pmatrix} h \\ 0 \end{pmatrix}, \mathbf{x}^{(1)} + \mathsf{D}(\alpha^{(1)}) \begin{pmatrix} -h \\ 0 \end{pmatrix}\right]. \tag{7.135}$$

Note that in (7.133), the exponent of $(-1)^{g-f+m}$ differs from that in [28].

7.5 Summary

In this chapter, Mathieu functions were introduced as square-integrable eigenfunctions of commuting operators. The advantage of this approach is that the

labelling of Mathieu functions is clearly related to eigenvalue problems. This labelling is then related to the notation of Meixner and Schäfke [26] which excels in its simplicity all others, in particular the standard notation of [20]. The expansion coefficients of the Mathieu functions obtained in the first section are also used to define the Modified Mathieu functions and appear in the interior and exterior addition theorems for solutions of the Helmholtz equation in elliptic coordinates.

Chapter 8

Numerical Implementation

8.1 Mathieu Functions

Numerical routines for Mathieu functions are available, e.g. [29], [19], but the numerics of the addition theorem requires an implementation with supplementary precision. The approach presented here combines a well-known iterative approach [26] with matrix techniques [30], [31]; the matrix part is similar to the method used by Stamnes and Spjelkavik [32].

The Mathieu library implemented as described here allows the numerical calculation of the functions in the required precision. In addition it provides the user with a formalism [26] that is of comparable simplicity as calculations in spherical coordinates (cosine, sine, Bessel and Hankel functions).

The software presented here is written in an object-oriented language (C++) and organized around an 'object' which calculates and stores the Mathieu eigenvalues and eigenvectors. This object may then be used to calculate approximations for the eigenfunctions by truncating the corresponding series.

The object has to be initialized before Mathieu functions can be computed for various arguments (cf. fig. 8.1). The necessary subroutines are embedded in the object. The advantage of this object-oriented implementation is that the allocation, calculation and deallocation of the series coefficients is invisible to the user. As well, debugging is facilitated by the operator overloading feature of the language with which bounds checking may easily be introduced and then removed afterwards for performance reasons. The routines are designed for multiple evaluations of Mathieu functions with the same q. Thus, evaluation for different arguments is performed fast once the object is initialized.

The calculation of the coefficients is based on three public domain libraries: LAPACK [15] for the calculation of the eigenvalues of a tridiagonal matrix and GMP [33] for the iterative procudure which is performed in arbitrary precision. The Bessel and Hankel functions in the summation of the truncated series of the modified Mathieu functions are calculated with GSL [34]. To obtain Mathieu functions in arbitrary precision, one would just have to use Bessel and Hankel

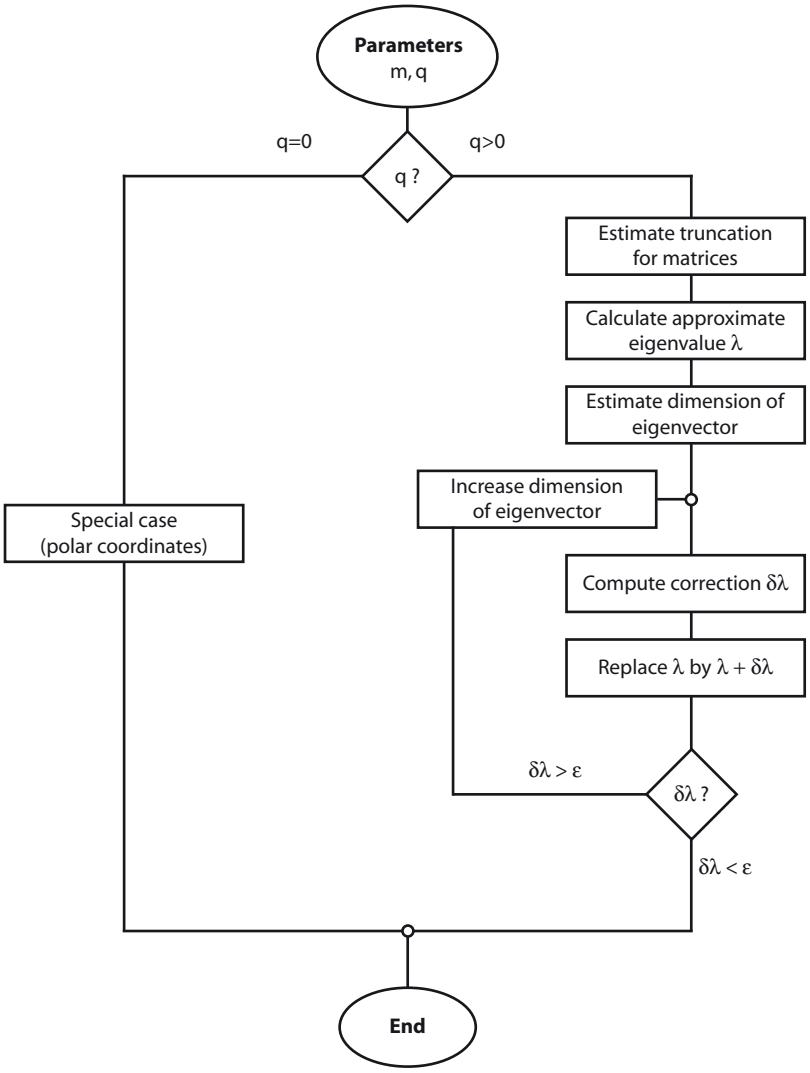

Figure 8.1: Flowchart of the initialization procedure

functions of the desired precision.

The case $q = 0$ is easily treated: the Mathieu functions become sine and cosine functions, and the modified Mathieu functions reduce to Bessel, Neumann and Hankel functions [26]. For $q > 0$, we first calculate an estimate for the eigenvalues $\lambda^q_{\mu,n}$ as described in section 8.1.1 below; afterwards in section 8.1.2 it is estimated how many components of the eigenvector will be needed. Finally in section 8.1.3 the estimate for $\lambda^q_{\mu,n}$ is iteratively refined.

8.1.1 Approximate eigenvalues

The eigenvalue problems that define the Mathieu functions are suited for automated calculation of an approximation to the characteristic values $\lambda^q_{\mu,n}$ (also for calculation of the eigenvectors C^q_m, but this will not be exploited here). To this end, we start from one of the matrices $H_{0+}, H_{0-}, H_{1+}, H_{1-}$, eqs. (7.27, 7.40, 7.55, 7.67). The infinite matrix is truncated at dimension $N(n, q)$ according to the following heuristic rule.

$$0 \leq n < 10 \qquad N = 20 \times \max(1, \log q) \tag{8.1}$$

$$n \geq 10 \qquad N = 2n \times \max(1, \log q) \tag{8.2}$$

Then, the real eigenvalues of the truncated matrix are calculated using the double precision routine *dstev* for tridiagonal symmetric matrices from CLAPACK [15].

8.1.2 Approximate eigenvectors

Next we need an estimate for the range $1 < s < S_{\max}$ such that $\left(A^q_m\right)_s < \epsilon$ or $\left(B^q_m\right)_s < \epsilon$ for $s > S_{\max}$. We know that for the converging solution of a three-term recursion

$$y_{k+1} - D_k y_k + y_{k-1} = 0 \qquad k = 1, 2, 3, \ldots \tag{8.3}$$

the following relation holds true [26].

$$|y_k| \leq \frac{1}{|D_k| - 1} |y_{k-1}| \tag{8.4}$$

For the components of the eigenvector A^q_{2n} this implies

$$\left|\left(A^q_{2n}\right)_s\right| \leq \frac{1}{\left|\frac{a^q_{2n} - (2s)^2}{q}\right| - 1} \left|\left(A^q_{2n}\right)_{s-1}\right| . \tag{8.5}$$

For an estimate of S that fulfills

$$\left(A^q_{2n}\right)_s < \epsilon \qquad \text{for} s > S, \tag{8.6}$$

we assume that the value of $\left(A^q_{2n}\right)_s$ at $s = 0$ is equal to 1. Then we use (8.5) to estimate the magnitude of the coefficients for increasing s. The typical behaviour of the coefficients is shown in fig. 8.1.2: there is only one maximum, after which the absolute value of the coefficients decreases with s according to (8.5).

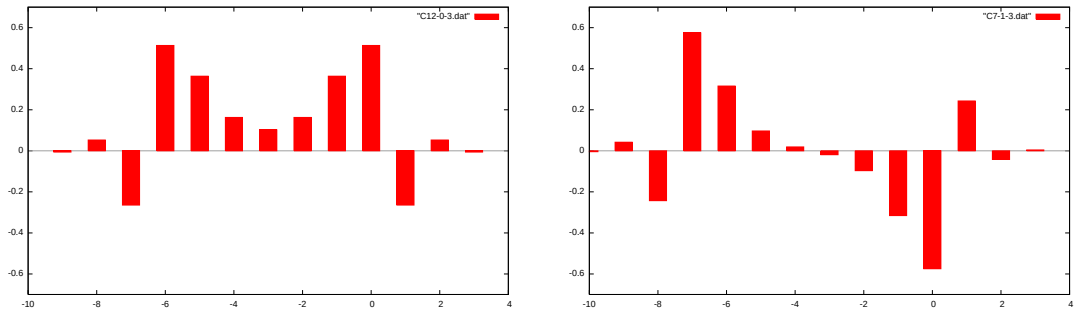

$C^{q=12}_{\mu=0,m=3}$ $C^{q=7}_{\mu=1,m=3}$

Figure 8.2: Typical values of $C^q_{\mu,m}$ coefficients

8.1.3 Iteration procedure for eigenvalues and eigenvectors

The core of the numerical calculation of Mathieu functions as proposed here is an iteration scheme which yields eigenvectors and eigenvalues with a prescribed precision. We use the iterative method of [26] because it is both efficient when good estimates for eigenvalues are available and easy to implement using an arbitrary precision library (in contrast to methods requiring equation solvers). As the original source [26] is written in German, the procedure will be briefly described here for a^q_{2n} and A^q_{2n}. The three other cases are treated analogously. If we set

$$\frac{(A^q_{2n})_{s+1}}{(A_{2n})_s} = N_s \tag{8.7}$$

in relations (7.84) - (7.86), we obtain

$$N_0 = \frac{a^q_{2n}}{\sqrt{2}q}, \tag{8.8}$$

$$\sqrt{2}\frac{1}{N_0} + N_1 = \frac{a^q_{2n} - 4}{q}, \tag{8.9}$$

$$\frac{1}{N_{s-1}} + N_s = \frac{a^q_{2n} - (2s)^2}{q} \qquad \text{for } s \geq 2\,. \tag{8.10}$$

It follows that

$$\lim_{S\to\infty} F(a^{q*}_{2n}, S) = 0 \tag{8.11}$$

if

$$F(a^q_{2n}, S) = \frac{a^q_{2n}}{q} - \frac{2}{\frac{a^q_{2n}-2^2}{q} -} \frac{1}{\frac{a^q_{2n}-4^2}{q} -} \frac{1}{\frac{a^q_{2n}-6^2}{q} -} \cdots \frac{1}{\frac{a^q_{2n}-(2S)^2}{q}}, \tag{8.12}$$

a^{q*}_{2n} is the exact eigenvalue, and $N_s \to 0$ for $s \to \infty$. The last condition follows from [26]

$$4s^2 N_s + q = q\,O\left(\frac{1}{s}\right) \qquad \text{for } s \to \infty\,. \tag{8.13}$$

We start the iteration from a given pair (a_{2n}^q, S) and use the magnitude of the function (8.12) as measure for the quality of the eigenvalue a_{2n}^q and the dimension S of the eigenvector.

In the beginning, we calculate the quotients $N_{0|L}, \ldots, N_{S|L}$ according to the recurrence relations (8.8) - (8.10). Here, L indicates that these recursions are relations that 'run from the left' (increasing s). Assuming N_S to vanish exactly we may use equations (8.10) and (8.9) to define a recursion that 'runs from the right'.

$$N_{S|R} = 0 \tag{8.14}$$

$$N_{S-1|R} = \frac{q}{a_{2n}^q - (2S)^2} \tag{8.15}$$

$$N_{S-2|R} = \frac{1}{\frac{a_{2n}^q - (2S-2)^2}{q} - N_{S-1|R}} \tag{8.16}$$

$$\cdots$$

$$N_{0|R} = \frac{1}{\sqrt{2}} \frac{1}{\frac{a_{2n}^q - 4}{q} - N_{1|R}} \tag{8.17}$$

If we change a_{2n}^q by δa_{2n}^q, the quotients N_s will change according to

$$\delta N_0 = \frac{\delta a_{2n}^q}{\sqrt{2} q} \tag{8.18}$$

$$\delta N_1 = \frac{\delta a_{2n}^q}{q} + \frac{\sqrt{2}}{N_0^2} \delta N_0 \tag{8.19}$$

$$\delta N_s = \frac{\delta a_{2n}^q}{q} + \frac{1}{N_{s-1}^2} \delta N_{s-1} \qquad \text{for } s \geq 2 \tag{8.20}$$

or

$$\delta N_s = N_s^2 \left[\delta N_{s+1} - \frac{\delta a_{2n}^q}{q} \right] \qquad \text{for } s \geq 2. \tag{8.21}$$

Therefore

$$\delta N_{t|L} = \frac{\delta a_{2n}^q}{q} \left[1 + \frac{1}{N_{t-1}^2} + \frac{1}{N_{t-1}^2 N_{t-2}^2} + \cdots + \frac{1}{N_{t-1}^2 N_{t-2}^2 \cdots N_1^2 N_0^2} \right] \tag{8.22}$$

and

$$\delta N_{t|R} = -\frac{\delta a_{2n}^q}{q} \left[N_t^2 + N_t^2 N_{t+1}^2 + \cdots + N_t^2 N_{t+1}^2 \cdots N_S^2 \right] . \tag{8.23}$$

If we require

$$N_{t|R} + \delta N_{t|R} = N_{t|L} + \delta N_{t|L} . \tag{8.24}$$

for an index $2 < t < S$ then δa_{2n}^q has to be determined from

$$N_{t|R} - N_{t|L} = \frac{\delta a_{2n}^q}{q} \Big[1 + \frac{1}{N_{t-1}^2} + \frac{1}{N_{t-1}^2 N_{t-2}^2} + \cdots + \frac{1}{N_{t-1}^2 N_{t-2}^2 \cdots N_1^2 N_0^2} + N_t^2 + N_t^2 N_{t+1}^2 + \cdots + N_t^2 N_{t+1}^2 \cdots N_S^2 \Big]. \tag{8.25}$$

We now choose t according to the condition

$$F(a^q_{2n} + \delta a^q_{2n}(a^q_{2n}, S, t), S) \to \min . \tag{8.26}$$

The magnitude of the right-hand side of (8.26) then determines whether the procedure has to be iterated or not. If yes, the pair $(a^q_{2n} + \delta a^q_{2n}, S + 1)$ is used as input in the next interation step.

8.1.4 Numerical validation

The tests performed are based on the calculation of the eigenvalue. If the value obtained is a good approximation to the true eigenvalue, so will be the related eigenvectors. It has turned out that in available standard packages the correct calculation of the eigenvalues is not always assured.

The quality of the eigenvalues is tested with $\delta = F(a^q_{2n}, S)$ (cf. eq. (8.12)) and analogous functions for the other eigenvalues. However, for some λ^q_n, (8.26) is very unstable, so it was necessary for testing purposes to obtain the eigenvalue up to a much higher precision than necessary for the use of the routines in vacuum scattering problems.

The eigenvalues listed in [20] are reproduced correctly by our calculation package. A selected list of eigenvalues not listed in [20] is shown in Table 8.1. The smallness of δ indicates the accuracy of the approximation.

μ, n	m	q	λ^q_n	δ
$1, 52$	-53	15	2809.04	1.43891×10^{-23}
$1, 52$	-53	150	2813.01	5.50336×10^{-73}
$1, 52$	-53	1500	3261.11	6.61372×10^{-151}
$1, 52$	-53	15000	-5744.58	1.38183×10^{-153}
$0, 7$	-8	20	67.2522	-1.54185×10^{-85}
$0, 7$	-8	200	-6.29144	-4.90374×10^{-88}
$0, 7$	-8	2000	-2687.24	-3.17698×10^{-85}
$0, 7$	-8	20000	-35785.8	-4.87859×10^{-87}
$1, 9$	9	10	81.6283	3.71361×10^{-124}
$1, 9$	9	100	126.396	8.32945×10^{-130}
$1, 9$	9	1000	-845.479	4.5954×10^{-126}
$1, 9$	9	10000	-16245.8	1.26889×10^{-125}
$0, 48$	48	13	2304.04	2.04218×10^{-34}
$0, 48$	48	130	2307.67	6.48867×10^{-81}
$0, 48$	48	1300	2729.32	8.02361×10^{-126}
$0, 48$	48	13000	-5129.57	3.2098×10^{-154}

Table 8.1: Numerical test of eigenvalue precision

Next we compare the eigenvalues given in Table 8.1 with the corresponding values obtained from other sources [29], [19].

μ, n	m	q	$\lambda^q_{\mu,n}$	Mathematica	Alhargan
$1, 52$	-53	15	2809.04	2809.04	2809.04
$1, 52$	-53	150	2813.01	2813.01	2813.01
$1, 52$	-53	1500	3261.11	*−2922.79*	3261.11
$1, 52$	-53	15000	−5744.58	−5744.58	*−5706.88*
$0, 7$	-8	20	67.2522	67.2522	67.2522
$0, 7$	-8	200	−6.29144	−6.29144	−6.29144
$0, 7$	-8	2000	−2687.24	−2687.24	*−2687.23*
$0, 7$	-8	20000	−35785.8	−35785.8	*−37959.83*
$1, 9$	9	10	81.6283	81.6283	81.6283
$1, 9$	9	100	126.396	126.396	126.396
$1, 9$	9	1000	−845.479	−845.479	−845.479
$1, 9$	9	10000	−16245.8	−16245.8	*−15768.42*
$0, 48$	48	13	2304.04	2304.04	2304.04
$0, 48$	48	130	2307.67	2307.67	2307.67
$0, 48$	48	1300	2729.32	*5350.44*	2729.32
$0, 48$	48	13000	−5129.57	−5129.57	*−5070.66*

Table 8.2: Comparison of eigenvalues obtained by different methods

Although Mathematica probably uses a similar routine for the determination of the eigenvalues, there seems to be a problem. As it is not possible to calculate a particular eigenvalue of a matrix, perhaps the error lies in choosing the right eigenvalue out of the list of all the eigenvalues. The issue is illustrated by Fig. 8.3.

8.2 Addition Theorem

For the numerical calculation of the interior addition theorem given by (7.132) and (7.133)

$$M_m^{(j)}(\xi^{(1)}; q^{(1)})\mathrm{me}_m(\eta^{(1)}; q^{(1)}) = \sum_{r=-\infty}^{\infty} B_{r,m}^{(j)} M_r^{(1)}(\xi^{(2)}; q^{(2)})\mathrm{me}_r(\eta^{(2)}; q^{(2)}), \tag{8.27}$$

$$B_{r,m}^{(j)}(q^{(1)}, q^{(2)}) = \sum_{\substack{f=-\infty \\ g=-\infty}}^{\infty} (-1)^{g-f+m} c_{2g}^m(q^{(1)}) c_{2f}^r(q^{(2)}) Z_{r-m+2(f-g)}^{(j)}(k\rho) \times e^{-i[r-m+2(f-g)]\psi} e^{-i(2g+m)\ (\alpha_1-\alpha_2)}, \tag{8.28}$$

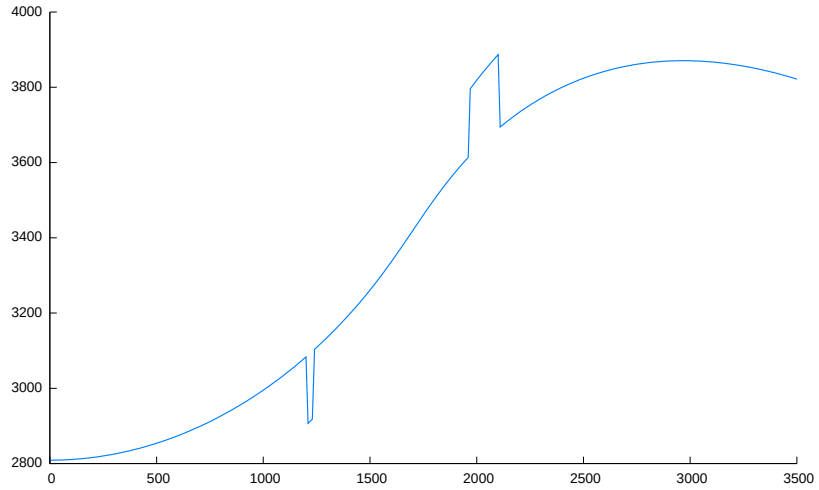

Figure 8.3: Eigenvalue $\lambda^q_{1,52}$ as calculated by Mathematica

we need to estimate the range of $f_{\min} \leq f \leq f_{\max}$ and $g_{\min} \leq g \leq g_{\max}$ which is used to truncate the series for (8.28). As well, for a given m, we need numbers $R_{\min}$ and $R_{\max}$ to truncate the summation over r in the right-hand side of (8.27).

To determine at which f, g we may stop the calculation the coefficient $B^{(3)}_{r,m}$, we look at the quantity

$$S^{(3)}_{r,m,F,G}(k\rho) = \frac{B^{(3)}_{r,m,F,G}(k\rho) + B^{(3)}_{r,m,-F,-G}(k\rho)}{\sum\limits_{\substack{f=-F \\ g=-G}}^{F,G} B^{(3)}_{r,m,f,g}(k\rho)} \tag{8.29}$$

where

$$\begin{aligned} B^{(3)}_{r,m,f,g}(k\rho)\mathrm{M}^{(1)}_r\left(\xi^{(2)};q^{(2)}\right) =& c^m_{2g}(q^{(1)})c^r_{2f}(q^{(2)})Z^{(j)}_{r-m+2(f-g)}(k\rho) \\ & \times \mathrm{M}^{(1)}_r\left(\xi^{(2)};q^{(2)}\right), \end{aligned} \tag{8.30}$$

The series abortion number X is chosen according to the following equation where δ is the desired relative precision.

$$\left|S^{(3)}_{r,m,X,X}\right| < \delta. \tag{8.31}$$

Typical numerical values are given in Fig. 8.4, where the X values for $\delta = 10^{-20}$ are plotted on a r, m grid where $-10 \leq r \leq 10$ and $-10 \leq m \leq 10$. The remaining parameters are $\mathbf{x}^{(1)} = (-4|0)$, $\alpha^{(1)} = 10°$ and $\mathbf{x}^{(2)} = (0|0)$, $\alpha^{(1)} = 30°$. We see that X values between 10 and 20 are sufficient for the desired precision. In the very same way, we proceed to an estimate for the truncation of (8.27)

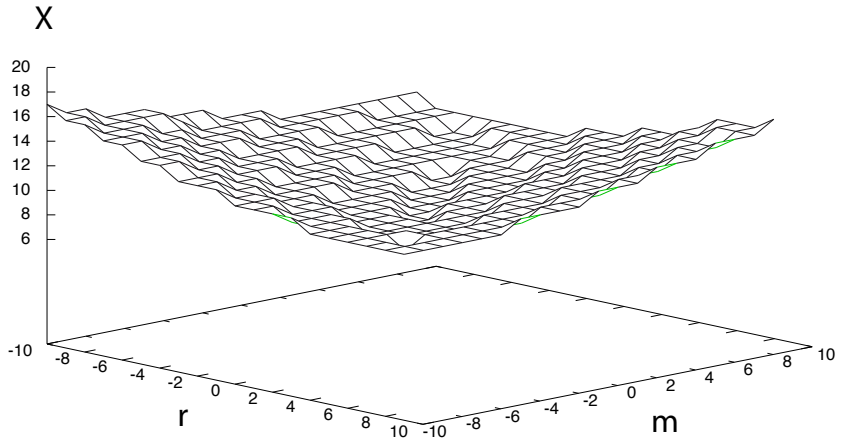

Figure 8.4: Flowchart of the initialization procedure

with the help of

$$T^{(3)}_{m,R}(\xi^{(2)}) = \frac{B^{(3)}_{R,m}\mathrm{M}^{(1)}_{R}\left(\xi^{(2)};q^{(2)}\right) + B^{(3)}_{-R,m}(k\rho)\mathrm{M}^{(1)}_{-R}\left(\xi^{(2)};q^{(2)}\right)}{\sum_{r=-R}^{R} B^{(3)}_{r,m}(k\rho)\mathrm{M}^{(1)}_{r}\left(\xi^{(2)};q^{(2)}\right)}. \tag{8.32}$$

We demand again $T^{(3)}_{m,R}(\xi^{(2)}) < \epsilon$ and series coefficients which are calculated with a precision of 10^{-20}. Looking for the same geometry at the point $\mathbf{x} = (-2|1)$, we see from table 8.3 that for a desired $\epsilon = 10^{-6}$, we need for this particular point a cutoff parameter between 32 and 64.

Note that when comparing the size of the $B_{R,m}$ and the size of $M^{(1)}_{R}$ that increasing m values demand a very high amount of precision of the Mathieu functions: e.g., any error made in $M^{(1)}_{13}$ is multiplied by 10^{30}.

8.3 Time-independent scattering in vacuum

For the numerical calculation of the scattered field (3.63) a cutoff parameter $P(\epsilon)$ is chosen such that the following a-posteriori estimate is fulfilled for every scatterer m.

$$S_P(a,b,\alpha,\beta,k) = \frac{d^{(m)}_{P(\epsilon)}(\beta,\mathbf{k})M^{(3)}_{P}(\xi^{(m)},q^{(m)}_{k}) + d^{(m)}_{-P}(\beta,\mathbf{k})M_{-P}(\xi^{(m)},q^{(m)}_{k})}{\sum\limits_{p=-P(\epsilon)} P(\epsilon)d^{(m)}_{p}(\beta,\mathbf{k})M^{(3)}_{p}(\xi^{(m)},q^{(m)}_{k})} < \epsilon. \tag{8.33}$$

For Dirichlet scatterers, the following alternative estimate works well. Since the Mathieu function $\mathrm{M}^{(2)}_{m}(\xi;q_k)$ typically has its maximum value around $\xi = 0$ (it behaves asymptotically for small q_k or large ξ like the Neumann function), an

m	R	$T^{(3)}_{m,R}(\xi^{(2)})$	$\lvert B_{R,m}\rvert + \lvert B_{-R,m}\rvert$	$\lvert M^{(1)}_{R}(\xi^{(2)})\rvert + \lvert M^{(1)}_{-R}(\xi^{(2)})\rvert$
-13	61	7.069×10^{-7}	6.827×10^{27}	5.919×10^{-34}
-12	61	7.409×10^{-7}	1.442×10^{27}	5.919×10^{-34}
-11	53	9.278×10^{-7}	1.616×10^{20}	1.642×10^{-26}
$\vdots$	$\vdots$	$\vdots$	$\vdots$	$\vdots$
-4	35	7.640×10^{-7}	9.736×10^{4}	5.676×10^{-12}
-3	29	1.205×10^{-7}	9.323×10^{1}	5.501×10^{-8}
-2	35	4.146×10^{-7}	2.218×10^{4}	5.676×10^{-12}
-1	35	3.593×10^{-7}	7.805×10^{3}	5.676×10^{-12}
0	32	3.308×10^{-7}	3.256×10^{2}	6.558×10^{-10}
1	32	4.359×10^{-7}	8.330×10^{2}	6.558×10^{-10}
2	32	4.814×10^{-7}	1.291×10^{3}	6.558×10^{-10}
3	32	6.176×10^{-7}	1.750×10^{3}	6.558×10^{-10}
4	33	2.076×10^{-8}	7.906×10^{3}	1.080×10^{-10}
$\vdots$	$\vdots$	$\vdots$	$\vdots$	$\vdots$
11	56	4.275×10^{-7}	2.849×10^{22}	3.405×10^{-29}
12	57	1.537×10^{-7}	1.026×10^{24}	4.392×10^{-30}
13	64	5.416×10^{-7}	1.870×10^{30}	8.345×10^{-37}

Table 8.3: Cutoff value for interior addition theorem

estimate for the maximum of $\left|d_m(\beta,\mathbf{k})\mathrm{M}^{(3)}_m(u;q_k)\right|$ is given by

$$\left[d_m\mathrm{M}^{(3)}_m(u;q_k)\right]_{u=u_0} \approx \mathrm{M}^{(1)}_m(u_0;q_k)\,. \tag{8.34}$$

The condition

$$R(\epsilon) = \left\{m : \mathrm{M}^{(1)}_m(u_0;q_k) < \epsilon\right\} \tag{8.35}$$

with $\epsilon \approx 10^{-15}$ yields reliable results.

In Tab. 8.4, the cutoff parameters $S_P(a,b,\alpha,\beta,k)$ for $\epsilon = 10^{-9}$ can be seen for the time-independent plots for one cylinder as shown in section (9.1). For brevity, S_P is denoted as $S^D_P(k)$ for Dirichlet scatterers with only k as parameter and $S^N_P(k)$ for Neumann scatterers.

Note that there is no difference between Dirichlet and Neumann scatterers. As to be expected, an increase in k demands more partial waves.

8.4 Waveguide Scattering

8.4.1 Calculation of the coefficients

The coefficients (4.31, 4.32, 4.33, 4.41, 4.42, 4.43, 4.55, 4.56, 4.75, 4.76) are all calculated with Gaussian quadrature rules as described in section 8.5.1.

b	$R^D(1)$	$R^N(1)$	$R^D(3)$	$R^N(3)$	$R^D(4)$	$R^N(4)$	$R^D(5)$	$R^N(5)$
0.99	10	10	15	15	17	17	20	21
0.95	20	21	15	15	17	17	20	21
0.9	20	20	15	15	17	17	20	20
0.75	20	20	14	15	16	16	20	20
0.5	18	18	13	14	15	15	18	18
0.25	16	17	12	13	14	14	16	17
0.1	15	16	12	12	13	13	15	16
0.05	15	16	12	12	13	13	15	16
0.01	15	14	11	12	13	12	15	14

Table 8.4: Cutoff values for single vacuum scatterers

8.4.2 Evanescent waves

For numerical calculation of eq. (4.20), it has to be truncated. Looking at an a-posteriori estimate of it, we examine for various $x-x'$ and $y-y'$ the function

$$S_{k,N}(\mathbf{x},\mathbf{x}') = \frac{\dfrac{\sin\left(\dfrac{N\pi}{W}y\right)\sin\left(\dfrac{N\pi}{W}y'\right)}{\kappa_N}e^{i\kappa_N|x-x'|}}{\displaystyle\sum_{n=1}^{N}\frac{\sin\left(\frac{n\pi}{W}y\right)\sin\left(\frac{n\pi}{W}y'\right)}{\kappa_n}e^{i\kappa_n|x-x'|}} \tag{8.36}$$

In our calculations, we limited the summation always to 20 evanescent waves: this way, numerical convergence was obtained for all parameter ranges used. However, it would be possible to reduce computational cost considerably with a more rigourous truncation condition.

8.4.3 Transfer matrix

The transfer matrix (4.50) is ill-conditionned. This can be measured by the condition number of the transfer matrix: for a linear equation system $A\mathbf{x} = \mathbf{b}$ with a disturbed matrix $A \to A + \Delta A$, an estimate of the relative error introduced by the disturbance is [35]

$$\frac{\|\Delta\mathbf{x}\|}{\|\Delta\mathbf{x}+\mathbf{x}\|} \leq K\frac{\|\Delta A\|}{\|\Delta A + A\|}, \tag{8.37}$$

where the condition number K is given by

$$K = \|A\|\|A^{-1}\|, \tag{8.38}$$

and the matrix-norm $\|\cdot\|$ for a matrix A with elements a_{ik}, is one of the following commonly used norms.

- The column-sum norm $\|A\|_1 = \max_{1\le i\le m} \sum_{i=1}^{m} |a_{ik}\ |$
- The spectral norm $\|A\|_2 = \max_{1\le k\le n} \sqrt{\max_{1\le k\le n}\{\lambda_i A^T A\}}$
- The line-sum norm $\|A\|_\infty = \max_{1\le k\le n} \sum_{i=1}^{m} |a_{ik}\ |$

Looking at the transfer matrix of vacuum,

$$\begin{pmatrix} a^R \\ b^R \end{pmatrix} = \begin{bmatrix} e^{i\kappa_1(x_R-x_L)} & & & & & & 0 \\ & \ddots & & & & & \\ & & e^{i\kappa_n(x_R-x_L)} & & & & \\ & & & e^{-i\kappa_1(x_R-x_L)} & & & \\ & & & & \ddots & & \\ 0 & & & & & & e^{-i\kappa_n(x_R-x_L)} \end{bmatrix} \begin{pmatrix} a^L \\ b^L \end{pmatrix}, \tag{8.39}$$

we see that its condition number $K_\infty = \|T\|_\infty \|T^{-1}\|_\infty$ is given by

$$K_\infty\,[T^{\text{vacuum}}\ ] = e^{2|\kappa_{\max}(z_R-z_L)}. \tag{8.40}$$

Typical condition numbers for circular obstacles are $K \approx 10^{13}$. The scattering matrix is, with typical condition numbers for the same situation $K \approx 10^{10}$, much better conditionned.

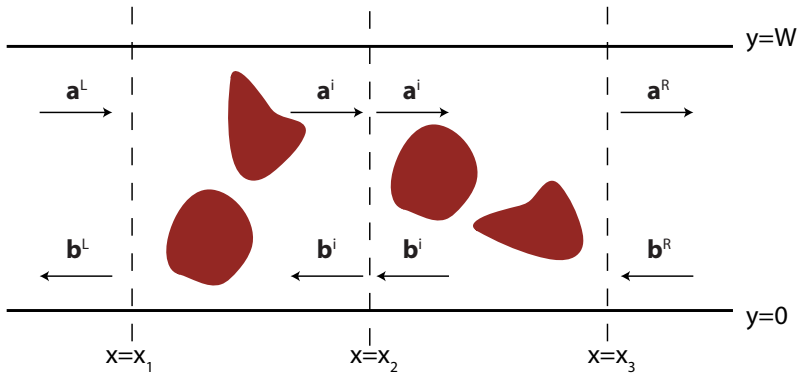

Figure 8.5: Combining two scattering matrices

Two scattering matrices

$$\begin{pmatrix} a^i \\ b^L \end{pmatrix} = \begin{bmatrix} S_{11}^{(1)} & S_{12}^{(1)} \\ S_{21}^{(1)} & S_{22}^{(1)} \end{bmatrix} \begin{pmatrix} a^L \\ b^i \end{pmatrix}, \qquad \begin{pmatrix} a^R \\ b^i \end{pmatrix} = \begin{bmatrix} S_{11}^{(1)} & S_{12}^{(1)} \\ S_{21}^{(1)} & S_{22}^{(1)} \end{bmatrix} \begin{pmatrix} a^i \\ b^R \end{pmatrix} \tag{8.41}$$

can be combined as shown in Fig. 8.5 to

$$\begin{pmatrix} a^R \\ b^L \end{pmatrix} = \begin{bmatrix} C_{11} & S_{12} \\ C_{21} & S_{22} \end{bmatrix} \begin{pmatrix} a^L \\ b^R \end{pmatrix}, \tag{8.42}$$

where

$$C_{11} = S_{11}^{(2)} \left[1 - S_{12}^{(1)} S_{21}^{(2)}\right]^{-1} S_{11}^{(1)}, \tag{8.43}$$

$$C_{12} = S_{11}^{(2)} \left[1 - S_{12}^{(1)} S_{21}^{(2)}\right]^{-1} S_{12}^{(1)} S_{22}^{(2)} + S_{12}^{(2)}, \tag{8.44}$$

$$C_{21} = S_{21}^{(1)} + S_{22}^{(1)} S_{21}^{(2)} \left[1 - S_{12}^{(1)} S_{21}^{(2)}\right]^{-1} S_{11}^{(1)}, \tag{8.45}$$

$$C_{22} = S_{22}^{(1)} S_{21}^{(2)} \left[1 - S_{12}^{(1)} S_{21}^{(2)}\right]^{-1} S_{12}^{(1)} S_{22}^{(2)} + S_{22}^{(1)} S_{22}^{(2)}. \tag{8.46}$$

8.5 Numerical Integration

In this section, we describe the methods used to obtain numerical approximations for one-dimensional integrals like

$$I^1_{[a,b]} f = \int_a^b f(x)\,\mathrm{d}x \tag{8.47}$$

or also two-dimensional integrals like

$$I^2_{[a,b]\times[c,d]} f = \int_a^b \int_c^d f(x,y)\,\mathrm{d}x\,\mathrm{d}y. \tag{8.48}$$

One-dimensional numerical integration is also called quadrature, two-dimensional integration cubature [35]. These methods are applied usually when analytic expressions for (8.47) or (8.48) cannot be given or when they are simply not needed. Usually, numerical integration approximates the integral with a weighted sum over the values of the integrand within the range of integration. The aim is to obtain the integrand as accurately as possible with the smallest number of evaluations of the integrand. An N-point quadrature rule of order n is a formula of the form

$$Q^1\text{–}[a,b] f = \sum_{k=1}^{N} w_k f(x_k) \tag{8.49}$$

with the nodes $a \le x_1 < x_2 < \cdots < x_n \le b$ and weights w_k chosen such that

$$Q^1 f_{[a,b]} = I^1_{[a,b]} f \tag{8.50}$$

is exact for all polynomials up to degree n. A rule which uses the value of the integrand at the endpoints, $f(a)$ or $f(b)$, is called a closed formula. If we cannot evaluate the integrand at the endpoints, e.g. because it has an integrable singularity there, we choose an open quadrature rule which only uses values $a < x_i < b$. Note that a higher order does not imply higher accuracy in practical calculations. In two dimensions, an N-point cubature rule of order n is given by [36]

$$Q^2_{[a,b]\times[c,d]} f = \sum_{k=1}^{N} w_k f(x_k, y_k). \tag{8.51}$$

Again, $a \le x_1 < x_2 < \cdots < x_n \le b$ and $c \le y_1 < y_2 < \cdots < y_n \le d$; the rest of the terminology is also the same.

8.5.1 Quadrature

For one-dimensional numerical integration, a variety of methods exist, e.g., the trapezoidal rule, Simpson's rule, "pulcherrima", and Milers rule denote the first four special cases of the so-called Newton-Côtes rules which are obtained by approximation of a function with a Lagrange polynomial and subsequent analytical integration of the polynomial [35]. Various methods exist for the approximation of oscillating integrands [37, 38, 39]. However, their use is limited for our applications because they usually work very well only for the integration of integrands which oscillate quickly with one frequency.

If we do not choose the abscissas in advance and calculate the corresponding weights afterwards, but take them also as degrees of freedom, we can achieve quadrature rules of higher degrees. In one dimension, a general form of optimal quadrature rules is known. This optimal quadrature rule is called *Gaussian Quadrature Rule* [35]; it integrates a polynomial of degree $2n + 1$ exactly with n points. The rules (up to 16 digits) which were used for this thesis are

- The 3-point rule

x_i	w_i
0	0.888888888888889
± 0.7745966692414833	0.5555555555555556

- The 5-point rule

x_i	w_i
0	0.5688888888888889
± 0.5384693101056830	0.4786286704993664
± 0.9061798459386639	0.2369268850561890

- The 7-point rule

x_i	w_i
0	0.4179591836734693
± 0.4058451513773971	0.3818300505051189
± 0.7415311855993944	0.2797053914892766
± 0.9491079123427585	0.1294849661688696

- The 9-point rule

x_i	w_i
0	0.3302393550012597
± 0.3242534234038089	0.3123470770400028
± 0.6133714327005903	0.2606106964029354
± 0.8360311073266357	0.1806481606948574
± 0.9681602395076260	0.0812743883615744 1

- The 11-point rule

x_i	w_i
0	0.2729250867779006
± 0.2695431559523449	0.2628045445102466
± 0.5190961292068118	0.2331937645919904
± 0.7301520055740493	0.1862902109277342
± 0.8870625997680952	0.1255803694649046
± 0.9782286581460569	0.05566856711617366

- The 15-point rule

x_i	w_i
0	0.2025782419255612
± 0.2011940939974345	0.1984314853271115
± 0.3941513470775633	0.1861610000155622
± 0.5709721726085388	0.1662692058169939
± 0.7244177313601700	0.1395706779261543
± 0.8482065834104272	0.1071592204671719
± 0.9372733924007059	0.0703660474881081
± 0.9879925180204854	0.03075324199611726

- The 21-point rule

x_i	w_i
0	0.1460811336496904
± 0.1455618541608951	0.1445244039899701
± 0.2880213168024011	0.1398873947910732
± 0.4243421202074388	0.1322689386333375
± 0.5516188358872198	0.1218314160537285
± 0.6671388041974123	0.1087972991671484
± 0.7684399634756779	0.09344442345603386
± 0.8533633645833173	0.07610011362837930
± 0.9200993341504008	0.05713442542685721
± 0.9672268385663063	0.03695378977085249
± 0.9937521706203895	0.01601722825777433

In this thesis, they were needed for the calculation of the time-dependent integrals as (6.1) and for the waveguide scattering coefficients (4.31, 4.32, 4.33, 4.41, 4.42, 4.43, 4.55, 4.56, 4.75, 4.76).

We use a combination of the following quadrature rules: 3-5, 7-9, 9-15, 15-21. The difference between the first and the second rule is always taken as an error estimate $e\ \left[\ Q^1 f\ \right]$. If the error estimate is acceptable, then the value of the higher order integration rule is taken as estimate for the true value of the integral. Note that using Gauss-Kronrod rules [40], one could reuse some points which are already calculated. However, in one-dimensional integration, calculation time was not such a concern as that this implementation was necessary.

8.5.2 Cubature

For higher-dimensional integration, the situation is more complicated [41, 42]. Some particular rules exist for which it is proven that they perform an integration of a polynomial up to a certain order exactly with the least number of points, but no general rule comparable to the Gaussian quadrature rules is available. Whenever for comparison purposes, arbitrary precision cubature rules were necessary and thus the nodes and points had to be recalculated, the formulas of [43] were used. All the rules we used and many more may be found in the a review on available cubature rules [44]. A particular cubature method which also specifies how the error estimate was obtained is always denoted by two number of points: N-M, where again each number specifies a cubature rule and the difference between the values obtained with rules is used as an error estimate. The value of the higher order rule is then used as an estimate for the integral in the particular subarea.

- The 4-7 rule (order 3 / order 5)
- The 7-10 rule (order 5 / order 6)
- The 7-12 rule (order 5 / order 7)
- The 10-12 rule (order 6 / order 7)
- The 10-17 rule (order 6 / order 9)
- The 17-24 rule (order 9 / order 11)
- The 24-33 rule (order 11 / order 13)
- The 33-44 rule (order 13 / order 15)
- The 44-60 rule (order 15 / order 17)
- The 60-72 rule (order 17 / order 19)

8.5.3 Adaptive integration procedure

We chose an adaptive approach [45] for the numerical calculation of integrals. This takes care of integrands which require a significantly higher concentration of points in some intervals than in others (cf. Fig. X). The following algorithm was used to obtain an approximation to the integral with a relative precision δ.

1. Calculation of $Q^1_{[a,b]}f$ as an approximation for $I^1 f$ and estimation of the error $e\left[Q^1_{[a,b]}f\right]$ of the approximation. If the error is smaller than δ, the process is terminated. Otherwise,
2. we define a set of subintervals which is initially $S = \{[a,b]\}$. Then, we set $x_1 = a$ and $x_2 = b$.

3. Calculate $Q^1_{\left[x_1,\frac{x_1+x_2}{2}\right]}f$ and $Q^1_{\left[\frac{x_1+x_2}{2},x_2\right]}f$ and their corresponding error estimates. Remove the interval $[x_1,x_2]$ from S and add the intervals $\left[[x_1,\frac{x_1+x_2}{2}\right]$ and $\left[\frac{x_1+x_2}{2},x_2\right]$ to it. If $e\left[Q^1_{\left[x_1,\frac{x_1+x_2}{2}\right]}f\right]+e\left[Q^1_{\left[\frac{x_1+x_2}{2},x_2\right]}f\right]<\delta$, accept the sum of all the estimates for the integrals of the subintervals as an approximation for I^1f. Otherwise,

4. S consists now of M subintervals L_i, $1\leq i\leq M$. Take the interval $L_j=[x_{j1},x_{j2}]\in S$ with the property e $\left[Q^1_{L_j}f\right]>e\left[Q^1_{L_i}f\right]$ for all $i\neq j$. Set $x_1=x_{j,1}$ and $x_2=x_{j,2}$ and proceed to 2) if the number of iterations does not exceed a defined limit.

The adaptive cubature algorithm works similarly with a subdivision of one area in four subareas of equal size.

8.6 1D scattering

8.6.1 Transfer matrix

The transfer matrices of the one-dimensional system were all calculated using arbitrary precision arithmetic [33]. In this manner, numerical problems were avoided at the expense of longer calculation times. However, in one dimension this is no essential problem.

8.6.2 Time-dependent scattering

The wave functions are implemented as functions returning complex double values which may be integrated by the routines of 8.5.1.

A comparison of the efficiency of these routines for the one-dimensional integration is given in Table 8.5. There, the integral (6.1) is evaluated for various paramteres k_0 and Γ. The rest of the parameters are $\alpha_2=\frac{3}{2}$, $t=1$ and $x=\alpha_2 t-\frac{1}{10\sqrt{(\Gamma)}}$. The integration interval $(-\infty,\infty)$ is approximated by $(-\frac{5}{\sqrt{\Gamma}},\frac{5}{\sqrt{\Gamma}})$. All the integrations reproduced the exact integral to a precision of 10^{-6} or slightly better.

8.7 Interpolation

For efficiency reasons, we interpolate the scattering coefficients, the radial Mathieu functions, and the angular Mathieu functions each on a two-dimensional grid as described below.

	3-5	7-9	9-15	15-21
$k_0 = 1,\ \Gamma = 1$	776	240	312	252
$k_0 = 1,\ \Gamma = 3$	552	208	168	180
$k_0 = 1,\ \Gamma = 6$	472	144	168	180
$k_0 = 2,\ \Gamma = 1$	1512	400	360	252
$k_0 = 2,\ \Gamma = 3$	984	272	360	252
$k_0 = 2,\ \Gamma = 6$	856	240	168	180
$k_0 = 3,\ \Gamma = 1$	3096	752	600	468
$k_0 = 3,\ \Gamma = 3$	2488	528	408	252
$k_0 = 3,\ \Gamma = 6$	1096	240	360	252
$k_0 = 4,\ \Gamma = 1$	6552	848	1080	540
$k_0 = 4,\ \Gamma = 3$	3608	560	744	252
$k_0 = 4,\ \Gamma = 6$	2184	400	312	252

Table 8.5: Necessary number of integration points for one-dimensional time-dependent scattering integral

8.7.1 Details of the interpolation procedure

Take a function $f(x, y)$ and a grid $\{x_1, \ldots, x_M\} \times \{y_1, \ldots, y_N\}$. The values $f(x_i, y_j)$ are denoted by $f_{i,j}$. For a given point (x, y), the indices $i = i(x, y)$ and $j = j(x, y)$ are the ones which fulfill

$$x_i \leq x \leq x_{i+1}, \tag{8.52}$$

$$y_j \leq y \leq y_{j+1}. \tag{8.53}$$

Then, the values at the four points surrounding this interior point are $f_{i,j}$, $f_{i+1,j}$, $f_{i,j+1}$, and $f_{i+1,j+1}$. The simplest interpolation in two dimensions is *bilinear interpolation* on the grid square [46]. For $i = i(x, y)$ and $j = j(x, y)$, its formulas are

$$t = \frac{x - x_i}{x_{i+1} - x_i}, \tag{8.54}$$

$$u = \frac{y - y_i}{y_{i+1} - y_i}, \tag{8.55}$$

and

$$f(x, y) \approx (1 - t)(1 - u)f_{i,j} + t(1 - u)f_{i+1,j} + tuf_{i,j+1} + (1 - t)uf_{i+1,j+1}. \tag{8.56}$$

We obtain a better approximation to the true value if we take into account not only the values $f_{i,j}$ at each grid point, but also the gradients $\frac{\partial f}{\partial x}(x_i, x_j) = f^x_{i,j}$, $\frac{\partial f}{\partial y}(x_i, x_j) = f^y_{i,j}$, and $\frac{\partial^2 f}{\partial x \partial y}(x_i, x_j) = f^{xy}_{i,j}$. To obtain such an approximation, we use an interpolation function which is cubic in the scaled coordinates t and u and fulfills the following requirements.

1. The values of the function and the specified derivates are reproduced exactly on the grid points.

2. The values of the function and the specified dedrivates change continuously as the interpolating point crosses from one grid square to another.

The interpolation method described in the following is called *bicubic interpolation* [46]. With

$$\mathsf{C}^{ij} = \begin{bmatrix} c_{00}^{ij} & c_{01}^{ij} & c_{02}^{ij} & c_{03}^{ij} \\ c_{10}^{ij} & c_{11}^{ij} & c_{12}^{ij} & c_{13}^{ij} \\ c_{20}^{ij} & c_{21}^{ij} & c_{22}^{ij} & c_{23}^{ij} \\ c_{30}^{ij} & c_{31}^{ij} & c_{32}^{ij} & c_{33}^{ij} \end{bmatrix}, \tag{8.57}$$

and

$$\mathbf{t} = \left(1, t, t^2, t^3\right)^T, \tag{8.58}$$

$$\mathbf{u} = \left(1, u, u^2, u^3\right)^T, \tag{8.59}$$

we make the following ansatz for the function and its derivative:

$$f(x,y) \approx g^{ij}(t,u) = \mathbf{t}^T \mathsf{C}^{ij}\, \mathbf{u}, \tag{8.60}$$

$$\frac{\partial f}{\partial x}(x,y) \approx g_x^{ij}(t,u) = \frac{\mathrm{d}\mathbf{t}^T}{\mathrm{d}t} \mathsf{C}^{ij}\, \mathbf{u}, \tag{8.61}$$

$$\frac{\partial f}{\partial y}(x,y) \approx g_y^{ij}(t,u) = \mathbf{t}\, \mathsf{C}^{ij} \frac{\mathrm{d}\mathbf{u}^T}{\mathrm{d}u}, \tag{8.62}$$

$$\frac{\partial^2 f}{\partial x \partial y}(x,y) \approx g_{xy}^{ij}(t,u) = \frac{\mathrm{d}\mathbf{t}^T}{\mathrm{d}t} \mathsf{C}^{ij} \frac{\mathrm{d}\mathbf{u}^T}{\mathrm{d}u}. \tag{8.63}$$

Now, the matrix C^{ij} has to be calculated from the values at the grid points. If we write the initial data as a vector $\mathbf{d}^{ij}$ and the coefficients of the matrix C^{ij} as a vector $\mathbf{c}^{ij}$,

$$\mathbf{c}^{ij} = \left(c_{00}^{ij}, c_{01}^{ij}, c_{02}^{ij}, c_{03}^{ij}, c_{10}^{ij}, c_{11}^{ij}, c_{12}^{ij}, c_{13}^{ij}, c_{20}^{ij}, c_{21}^{ij}, c_{22}^{ij}, c_{23}^{ij}, c_{30}^{ij}, c_{31}^{ij}, c_{32}^{ij}, c_{33}^{ij}\right), \tag{8.64}$$

$$\begin{aligned} \mathbf{d}^{ij} = \Big(& f_{i,j}, f_{i+1,j}, f_{i,j+1}, f_{i+1,j+1}, f_{i,j}^x, f_{i+1,j}^x, f_{i,j+1}^x, f_{i+1,j+1}^x, \\ & f_{i,j}^y, f_{i+1,j}^y, f_{i,j+1}^y, f_{i+1,j+1}^y, f_{i,j}^{xy}, f_{i+1,j}^{xy}, f_{i,j+1}^{xy}, f_{i+1,j+1}^{xy}\Big), \end{aligned} \tag{8.65}$$

we can relate them with the 16×16 matrix M defined by

$$\mathbf{c}^{ij} = \mathsf{M}\, \mathbf{d}^{ij}. \tag{8.66}$$

We obtain the matrix M by solving the 16 equations

$$\begin{bmatrix} g^{ij}(0,0) & g^{ij}(0,1) & g^{ij}(1,0) & g^{ij}(1,1) \\ g_x^{ij}(0,0) & g_x^{ij}(0,1) & g_x^{ij}(1,0) & g_x^{ij}(1,1) \\ g_y^{ij}(0,0) & g_y^{ij}(0,1) & g_y^{ij}(1,0) & g_y^{ij}(1,1) \\ g_{xy}^{ij}(0,0) & g_{xy}^{ij}(0,1) & g_{xy}^{ij}(1,0) & g_{xy}^{ij}(1,1) \end{bmatrix} = \begin{bmatrix} f_{ij} & f_{i+1,j} & f_{i,j+1} & f_{i+1,j+1} \\ f_{ij}^x & f_{i+1,j}^x & f_{i,j+1}^x & f_{i+1,j+1}^x \\ f_{ij}^y & f_{i+1,j}^y & f_{i,j+1}^y & f_{i+1,j+1}^y \\ f_{ij}^{xy} & f_{i+1,j}^{xy} & f_{i,j+1}^{xy} & f_{i+1,j+1}^{xy} \end{bmatrix}. \tag{8.67}$$

The solution is

$$\mathsf{M} = \begin{bmatrix}
1 & 0 & 0 & 0 & 0 & 0 & 0 & 0 & 0 & 0 & 0 & 0 & 0 & 0 & 0 & 0 \\
0 & 0 & 0 & 0 & 0 & 0 & 0 & 0 & 1 & 0 & 0 & 0 & 0 & 0 & 0 & 0 \\
-3 & 0 & 0 & 3 & 0 & 0 & 0 & 0 & -2 & 0 & 0 & -1 & 0 & 0 & 0 & 0 \\
2 & 0 & 0 & -2 & 0 & 0 & 0 & 0 & 1 & 0 & 0 & 1 & 0 & 0 & 0 & 0 \\
0 & 0 & 0 & 0 & 1 & 0 & 0 & 0 & 0 & 0 & 0 & 0 & 0 & 0 & 0 & 0 \\
0 & 0 & 0 & 0 & 0 & 0 & 0 & 0 & 0 & 0 & 0 & 0 & 1 & 0 & 0 & 0 \\
0 & 0 & 0 & 0 & -3 & 0 & 0 & 3 & 0 & 0 & 0 & 0 & -2 & 0 & 0 & -1 \\
0 & 0 & 0 & 0 & 2 & 0 & 0 & -2 & 0 & 0 & 0 & 0 & 1 & 0 & 0 & 1 \\
-3 & 3 & 0 & 0 & -2 & -1 & 0 & 0 & 0 & 0 & 0 & 0 & 0 & 0 & 0 & 0 \\
0 & 0 & 0 & 0 & 0 & 0 & 0 & 0 & -3 & 3 & 0 & 0 & -2 & -1 & 0 & 0 \\
9 & -9 & 9 & -9 & 6 & 3 & -3 & -6 & 6 & -6 & -3 & 3 & 4 & 2 & 1 & 2 \\
-6 & 6 & -6 & 6 & -4 & -2 & 2 & 4 & -3 & 3 & 3 & -3 & -2 & -1 & -1 & -2 \\
2 & -2 & 0 & 0 & 1 & 1 & 0 & 0 & 0 & 0 & 0 & 0 & 0 & 0 & 0 & 0 \\
0 & 0 & 0 & 0 & 0 & 0 & 0 & 0 & 2 & -2 & 0 & 0 & 1 & 1 & 0 & 0 \\
-6 & 6 & -6 & 6 & -3 & -3 & 3 & 3 & -4 & 4 & 2 & -2 & -2 & -2 & -1 & -1 \\
4 & -4 & 4 & -4 & 2 & 2 & -2 & -2 & 2 & -2 & -2 & 2 & 1 & 1 & 1 & 1
\end{bmatrix}. \tag{8.68}$$

8.8 Time-dependent scattering in vacuum

The calculation of the time-dependent integral (6.1) requires for every point in $\mathbf{x}$-space whose value is not equal to zero a grid of about 20000 points in $\mathbf{k}$-space for a relative precision of 10^{-2}; if the value of a point is zero, we cannot reasonably use an estimate of relative precision as this will lead to an explosion of calculation time. This is the main reason for the fact that the numerical approximation of the solution is so expensive, and the reason why calculation of the coefficients and their interpolation afterwards is separated. The cubature procedure used for the integral is the adaptive cubature algorithm described above with a 13-25 point rule.

8.8.1 Estimation of computational cost

The calculations were performed on an Athlon64 3500+ with 1GB of RAM. On this computer, the tabulation of the Mathieu functions with the grid described takes about 8 hours. The tabulation of the scattering coefficients on the chosen grid depends on the size of the scatterer and on the k values used; for one scatterer, it takes 3-6 hours with the chosen grid; for 2-3 scatterers one day. Once the scattering coefficients are calculated for a given system, the interpolation and integration procedure is relatively quick: a density plot of 50×50 is produced in about 2 hours with the precision and number of integration points described above.

A comparison with other numerical scattering methods, many of which are described in [9], is beyond the scope of this thesis: it would be necessary to calculate a numerical solution for a given system with several different methods.

Rule	Time (s)
4-7	15778
7-10	5776
7-12	5264
10-12	1185
10-17	1152
17-24	168
24-33	112
33-44	92
44-60	87
60-72	78

Table 8.6: Performance of cubature rules

In Tab. 8.6, we see a comparison of the time needed for the calculation of Fig. 8.6 according to (6.81) on a 80×80 points grid in $\mathbf{x}$-space with the parameters $\Gamma = 2$, $\mathbf{k}_0 = (1, 0)$, $\alpha_1 = 1$, $\alpha_2 = 0$, $t = 2$.

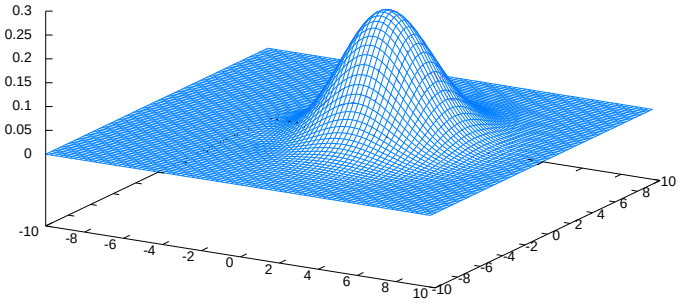

Figure 8.6: Free wave packet

We see very clearly, unlike the case of the cubature of the free wave packet in one dimension, that higher order cubature rules perform much better here.

8.9 Summary

Having formulated the algebraic eigenvalue problems for Mathieu functions in Section (7.1), we first present a package of subroutines which, due to the implementation in arbitrary precision, are more accurate than the ones presently

available. The iteration scheme used here depends on good initial values for the eigenvalues, which are obtained by formulating an eigenvalue procedure which is numerically solved with standard linear algebra routines. Numerical tests indicate that available routines can fail in extreme parameter regions.

Next, the chosen method for the numerical calculation of the Addition theorem was presented, based on an a-posteriori estimate of the truncation of the series. The procedure for the calculation of time-independent scattering is also based on a a posteriori error estimate. In the numerical solution of the waveguide scattering problem, the large magnitude of the condition number of the transfer matrix was pointed out. A remedy to this problem is the reformulation for several scatterers in terms of the scattering matrices. Finally, the numerical integration and interpolation methods used were briefly described.

Chapter 9

Numerical Results

9.1 Time-independent scattering in vacuum

For the time-independent plots in vacuum, we plot (3.111) in the following way. A plot for $0 \leq \eta \leq 2\pi$ would be seen in the left of Fig. 9.1. On the right-hand side, we see a curve plotted whose circular cylindric coordinates are given by $(|u_\infty(\eta)|, \eta)$. This type of plot is also called 'parametric plot'.

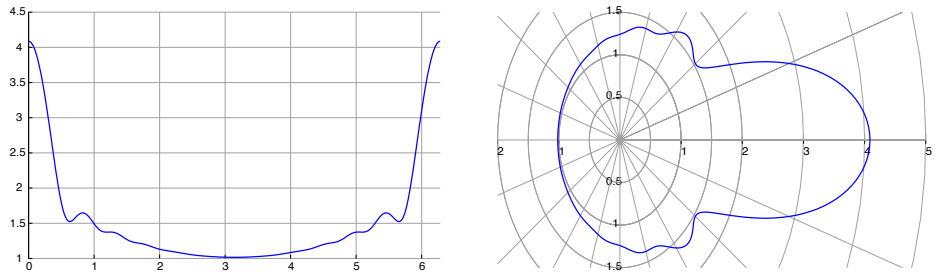

rectangular parametric

Figure 9.1: Angular intensity plot styles

9.1.1 One scatterer

The plots in Fig. 9.2 to 9.7 agree well with results known in literature [47].

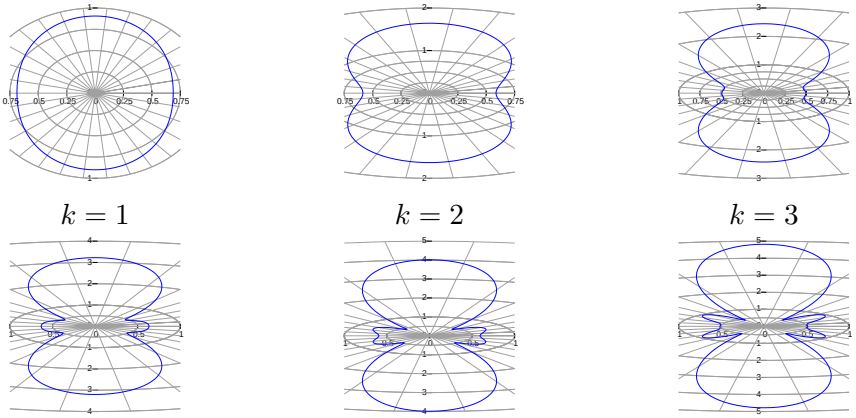

$k = 1$ $k = 2$ $k = 3$

$k = 4$ $k = 5$ $k = 6$

Figure 9.2: Angular intensity plot for Dirichlet scatterer with $a = 1$, $b = 0.01$, $\beta = 90°$

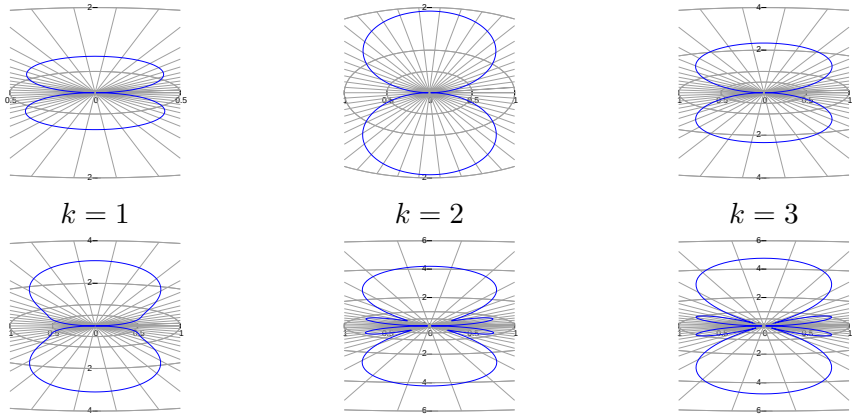

$k = 1$ $k = 2$ $k = 3$

$k = 4$ $k = 5$ $k = 6$

Figure 9.3: Angular intensity plot for Neumann scatterer with $a = 1$, $b = 0.01$, $\beta = 90°$

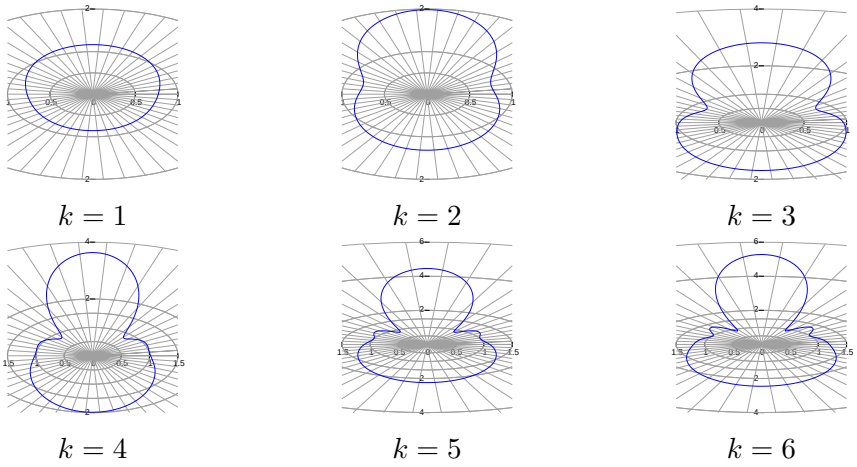

$k = 1$ $k = 2$ $k = 3$

$k = 4$ $k = 5$ $k = 6$

Figure 9.4: Angular intensity plot for Dirichlet scatterer with $a = 1$, $b = 0.5$, $\beta = 90°$

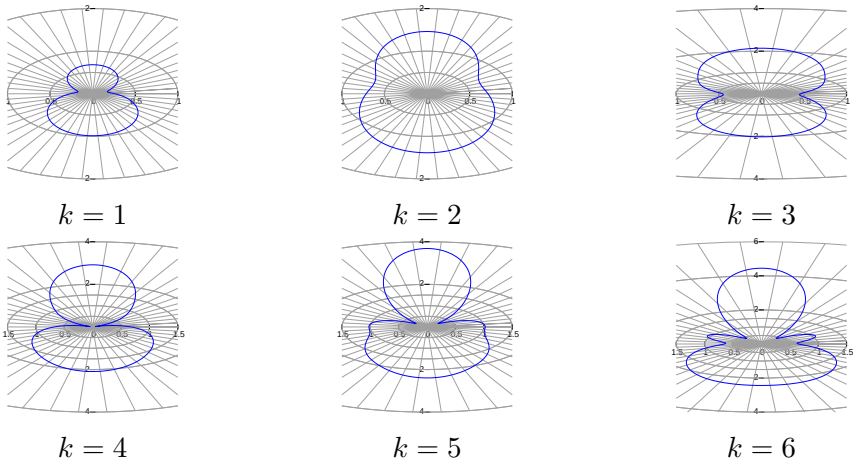

$k = 1$ $k = 2$ $k = 3$

$k = 4$ $k = 5$ $k = 6$

Figure 9.5: Angular intensity plot for Neumann scatterer with $a = 1$, $b = 0.5$, $\beta = 90°$

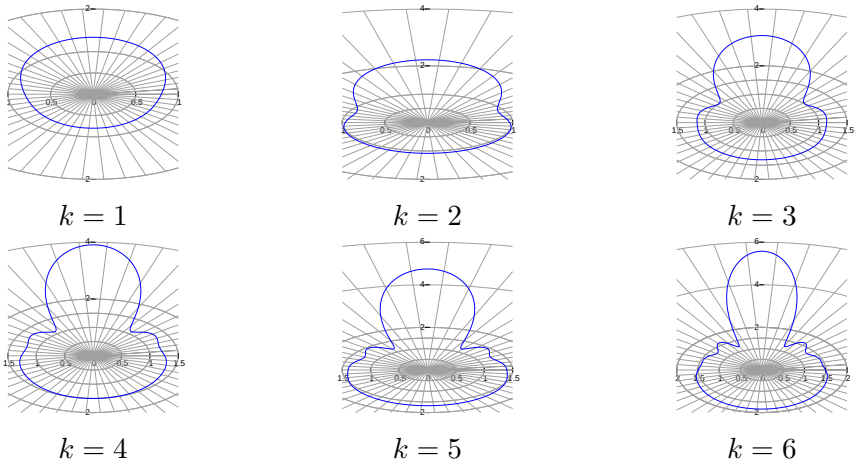

$k = 1$ $k = 2$ $k = 3$

$k = 4$ $k = 5$ $k = 6$

Figure 9.6: Angular intensity plot for Dirichlet scatterer with $a = 1$, $b = 0.9$, $\beta = 90°$

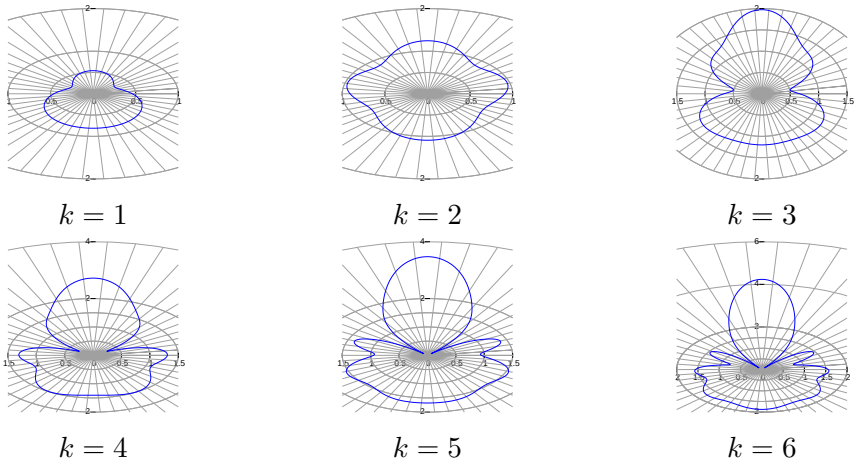

$k = 1$ $k = 2$ $k = 3$

$k = 4$ $k = 5$ $k = 6$

Figure 9.7: Angular intensity plot for Neumann scatterer with $a = 1$, $b = 0.9$, $\beta = 90°$

9.1.2 Several scatterers

The following configurations are examined:

Configuration 1 Two cylinders with $a = 2$, $b = 1$ at $(0, 2)$ and $(0, -2)$

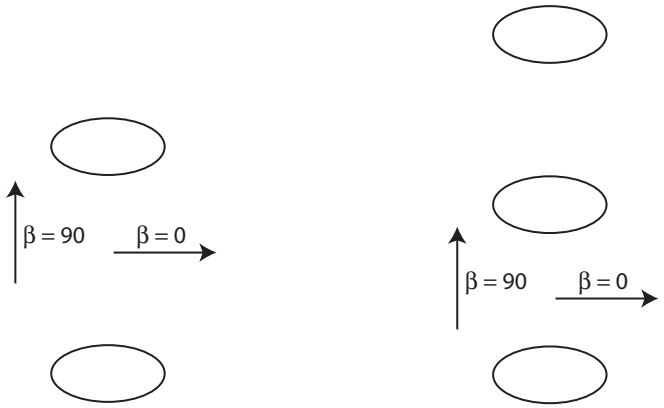

Configuration 1 Configuration 2

Figure 9.8: Time-independent multiple scattering configuarions 1 and 2

Configuration 2 Three cylinders with $a = 2$, $b = 1$ at $(0, 3)$, $(0, 0)$ and $(0, -3)$

Configuration 3 Four cylinders, all of them rotated by $\frac{\pi}{4}$ with axes $a = 3$, $b = 1$, placed at $(-4, -4)$, $(0, 4)$, $(4, -4)$, and $(8, 4)$.

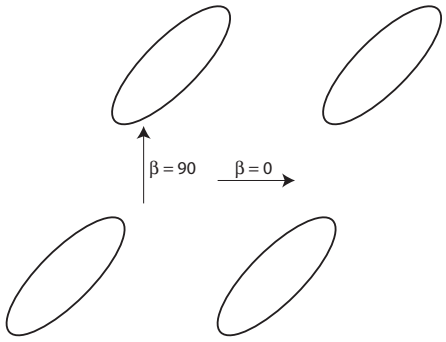

Figure 9.9: Time-independent multiple scattering configuarion 3

These results are interesting for comparison to other results in literature. They all fulfil numerically the prescribed boundary conditions at the obstacles; however, they do not agree completely with the results in [48]. We believe

that one possible explanation are the problems related to the numerical implementation of the addition theorem which led us to the implementation of the coefficient calculation routine in arbitrary precision as described in chapter 8. It is possible that in 1991, similar techniques were not available and thus the results do not agree.

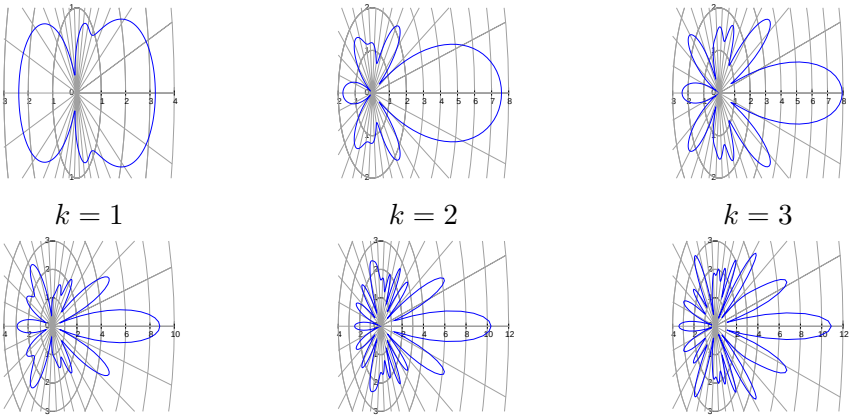

$k = 1$ $k = 2$ $k = 3$

$k = 4$ $k = 5$ $k = 6$

Figure 9.10: Multiple scattering configuration 1, Dirichlet b.c., $\beta = 0$

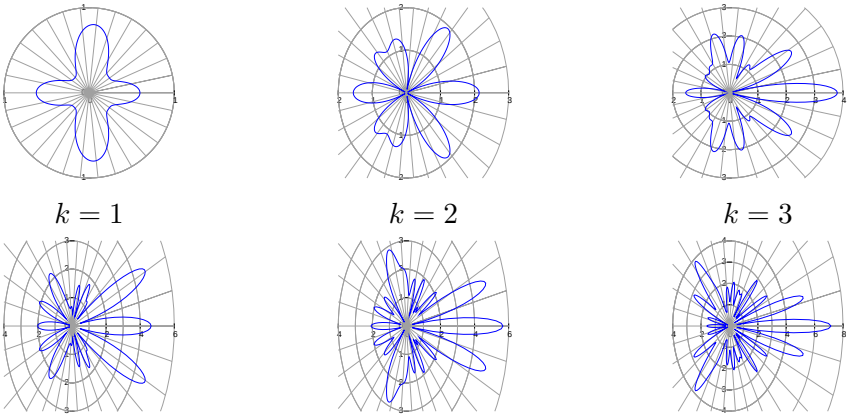

$k = 1$ $k = 2$ $k = 3$

$k = 4$ $k = 5$ $k = 6$

Figure 9.11: Multiple scattering configuration 1, Neumann b.c., $\beta = 0$

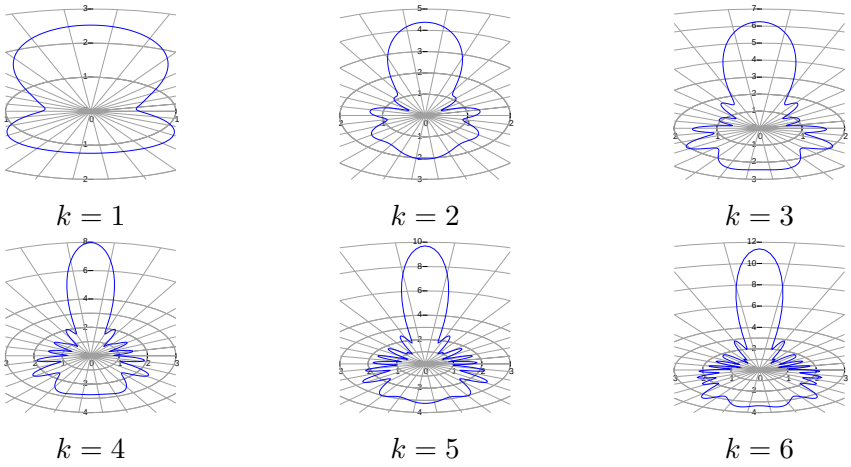

$k = 1$ $k = 2$ $k = 3$

$k = 4$ $k = 5$ $k = 6$

Figure 9.12: Multiple scattering configuration 1, Dirichlet b.c., $\beta = 90$

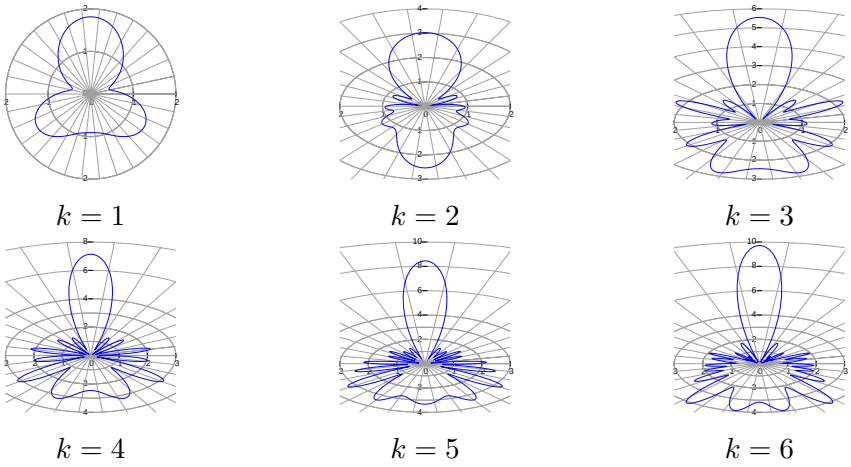

$k = 1$ $k = 2$ $k = 3$

$k = 4$ $k = 5$ $k = 6$

Figure 9.13: Multiple scattering configuration 1, Neumann b.c., $\beta = 90$

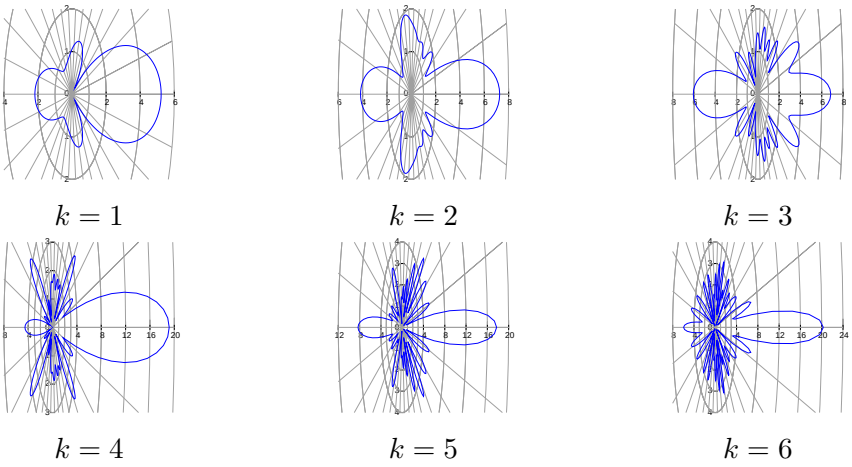

$k = 1$ $k = 2$ $k = 3$

$k = 4$ $k = 5$ $k = 6$

Figure 9.14: Multiple scattering configuration 2, Dirichlet b.c., $\beta = 0$

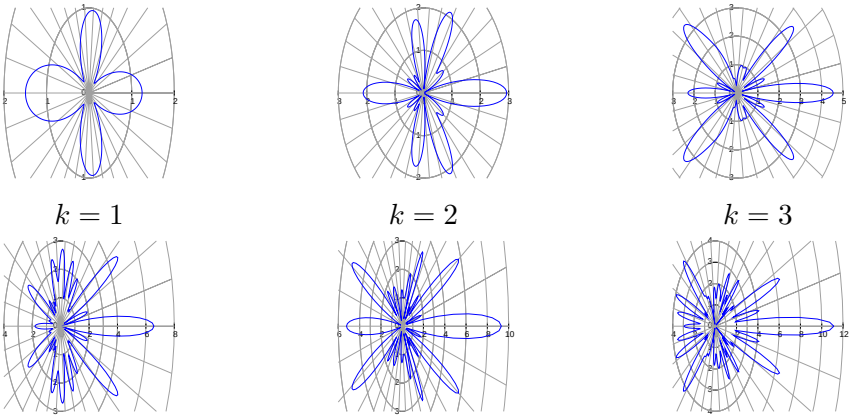

$k = 1$ $k = 2$ $k = 3$

$k = 4$ $k = 5$ $k = 6$

Figure 9.15: Multiple scattering configuration 2, Neumann b.c., $\beta = 0$

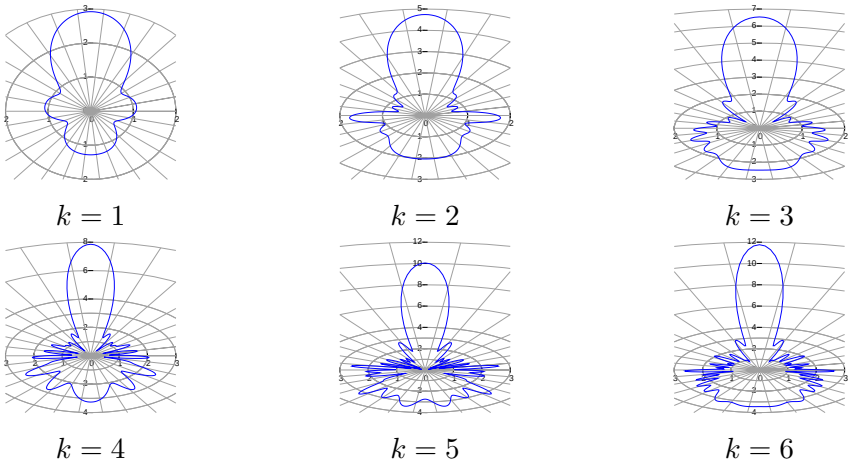

$k = 1$ $k = 2$ $k = 3$

$k = 4$ $k = 5$ $k = 6$

Figure 9.16: Multiple scattering configuration 2, Dirichlet b.c., $\beta = 90$

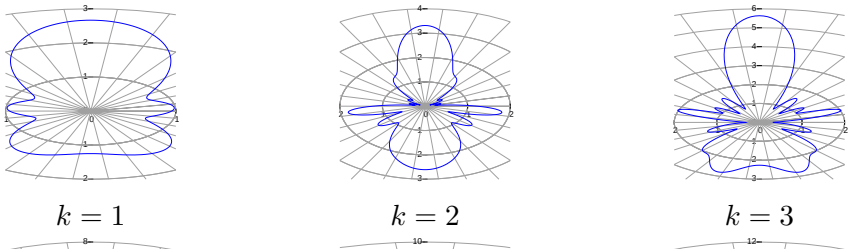

$k = 1$ $k = 2$ $k = 3$

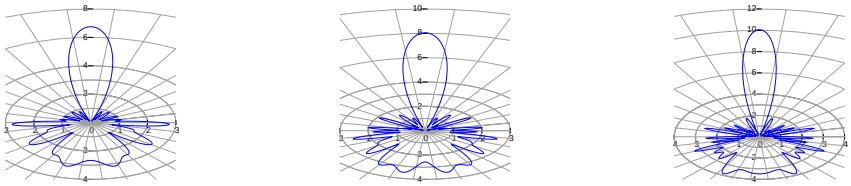

$k = 4$ $k = 5$ $k = 6$

Figure 9.17: Multiple scattering configuration 2, Neumann b.c., $\beta = 90$

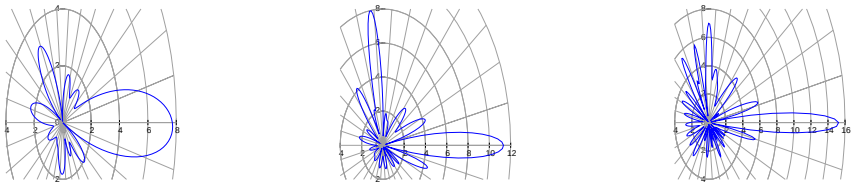

$k = 1$ $k = 2$ $k = 3$

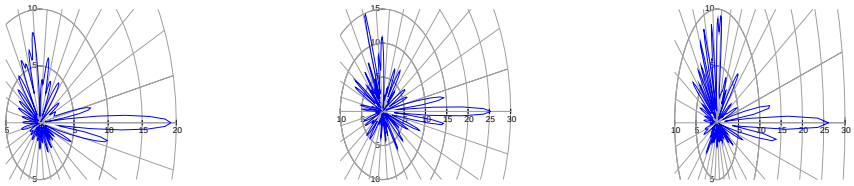

$k = 4$ $k = 5$ $k = 6$

Figure 9.18: Multiple scattering configuration 3, Dirichlet b.c., $\beta = 0$

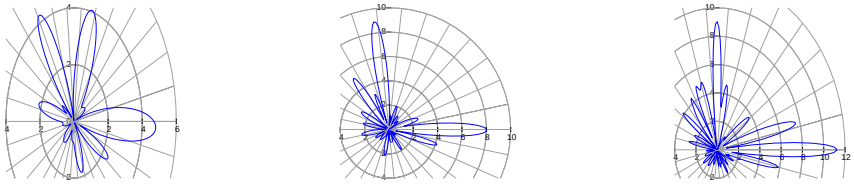

$k = 1$ $k = 2$ $k = 3$

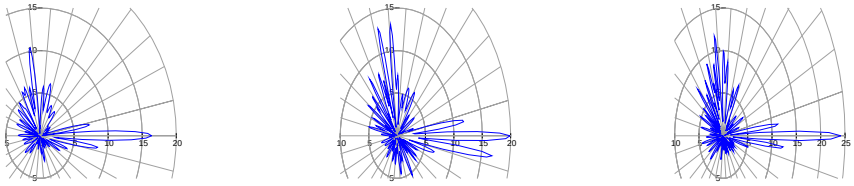

$k = 4$ $k = 5$ $k = 6$

Figure 9.19: Multiple scattering configuration 3, Neumann b.c., $\beta = 0$

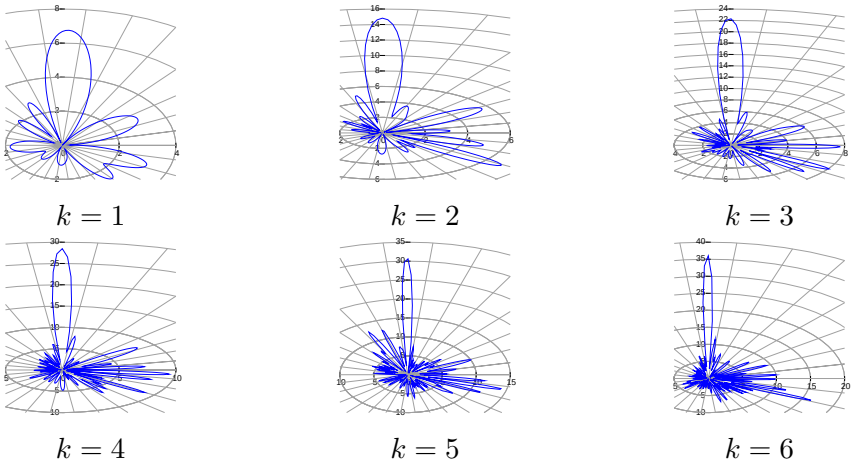

$k = 1$ $k = 2$ $k = 3$

$k = 4$ $k = 5$ $k = 6$

Figure 9.20: Multiple scattering configuration 3, Dirichlet b.c., $\beta = 90$

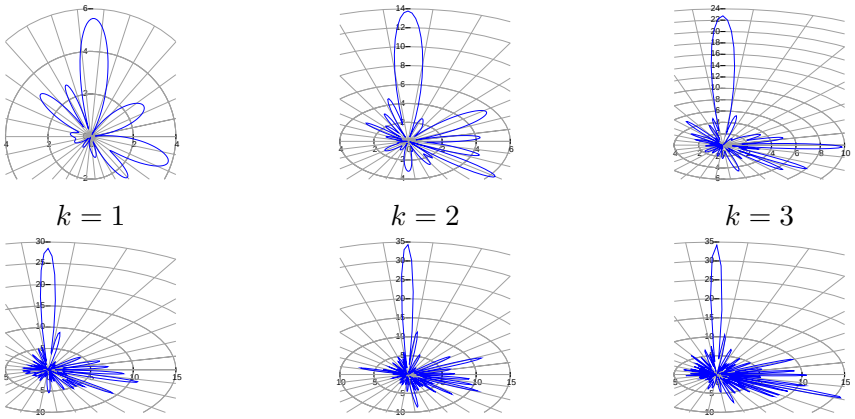

$k = 1$ $k = 2$ $k = 3$

$k = 4$ $k = 5$ $k = 6$

Figure 9.21: Multiple scattering configuration 3, Neumann b.c., $\beta = 90$

9.2 Time-dependent scattering in vacuum

Results of the time-dependent scattering code are displayed in figures 9.2 and 9.2. In these figures, we see a gaussian wave packet with parameters $\mathbf{k_0} = (0, 2)$ and $\gamma = 2$ travelling along the y axis from negative to positive values. It is scattered by three elliptical cylinders with axes $a = 1$, $b = \frac{1}{2}$ at positions $(0, 2)$, $(-2, 0)$, and $(2, 0)$, respectively. The latter two are rotated by $\frac{\pi}{4}$.

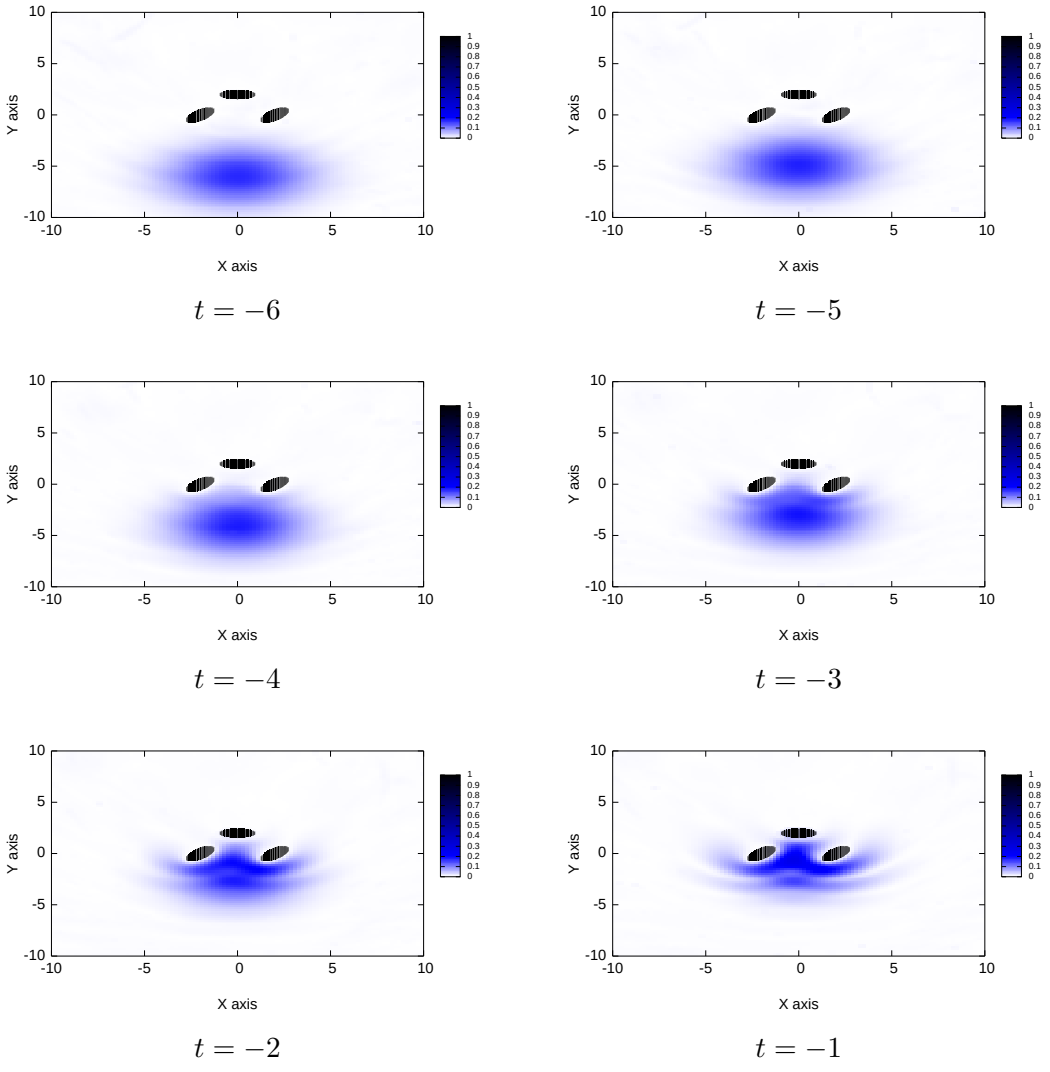

Figure 9.22: Density plot

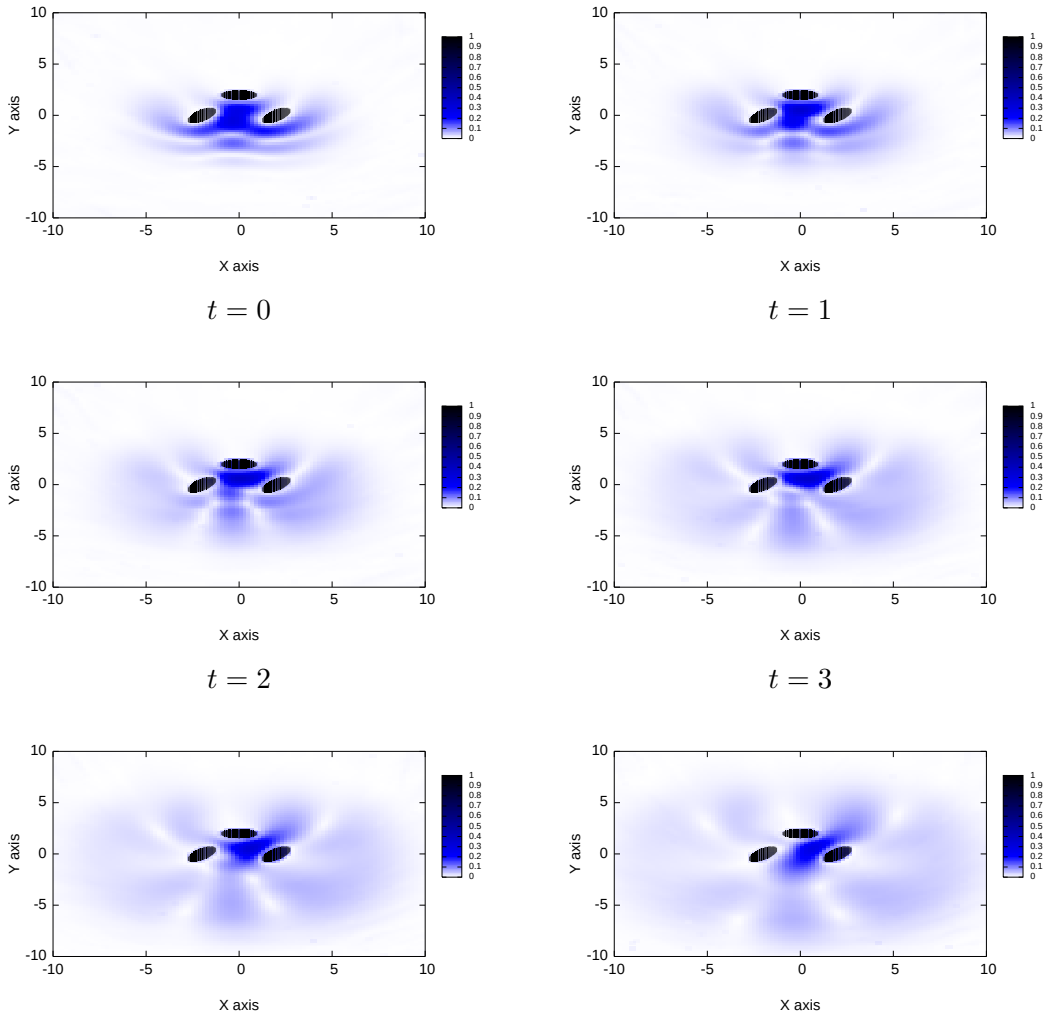

$t = 0$ $t = 1$

$t = 2$ $t = 3$

$t = 4$ $t = 5$

Figure 9.23: Density plot

9.3 Scattering in Waveguide

In the following figures, the absolute value of wave function inside a waveguide is plotted for various values of k and for varying circular cylinder radius. The other parameters are $W = 5$ and $L = 4$. To the left of every figure, we see a density plot of the wave function, and to the right, we see a plot of $F(x, y)$ as described in (4.95).

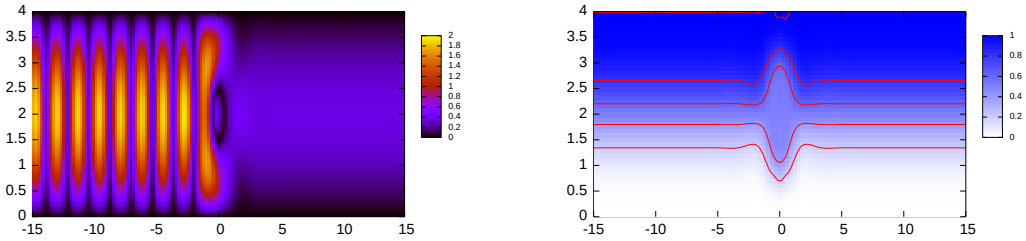

$|u(x, y)|$ $F(x, y)$

Figure 9.24: Waveguide: $N = 6, M = 6, d = 2, r = 0.5, k = 2$ and mode 1

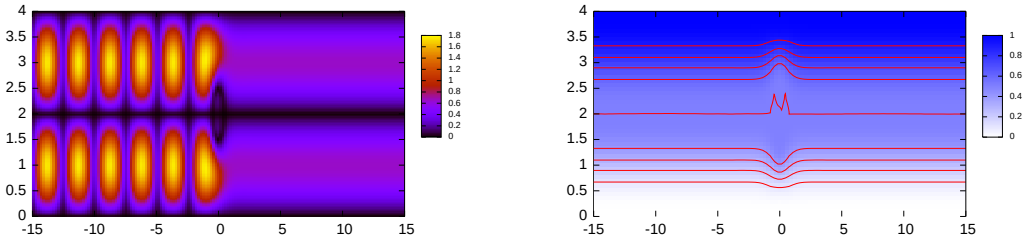

$|u(x, y)|$ $F(x, y)$

Figure 9.25: Waveguide: $N = 6, M = 6, d = 2, r = 0.5, k = 2$ and mode 2

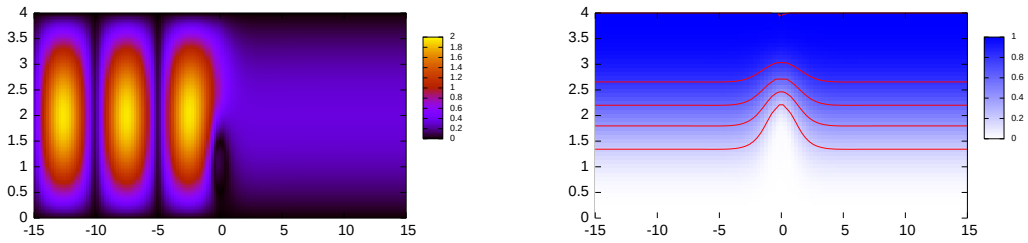

$|u(x,y)|$ $F(x,y)$

Figure 9.26: Waveguide: $N = 6, M = 6, d = 1, r = 0.5, k = 1$ and mode 1

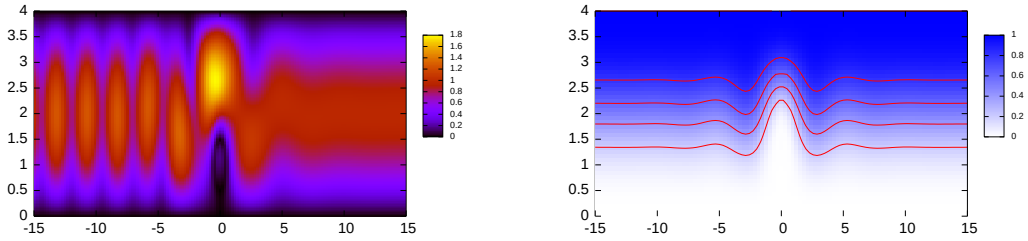

$|u(x,y)|$ $F(x,y)$

Figure 9.27: Waveguide: $N = 6, M = 6, d = 1, r = 0.5, k = 1.5$ and mode 1

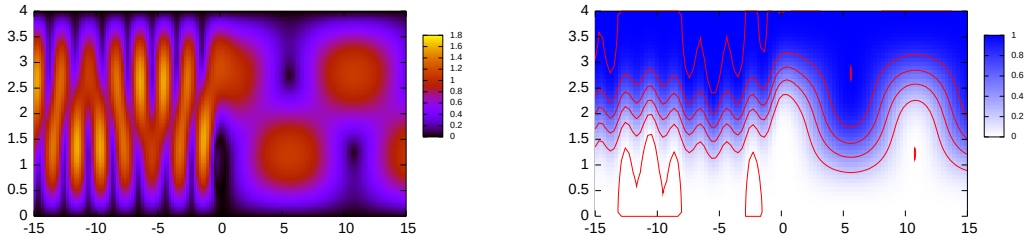

$|u(x,y)|$ $F(x,y)$

Figure 9.28: Waveguide: $N = 6, M = 6, d = 1, r = 0.5, k = 2$ and mode 1

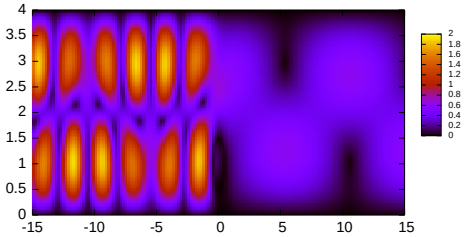

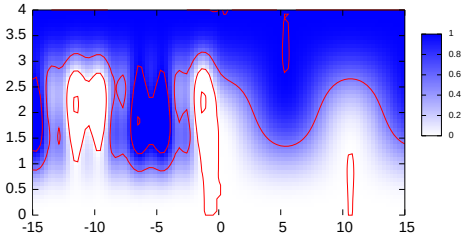

$|u(x,y)|$ $F(x,y)$

Figure 9.29: Waveguide: $N = 6, M = 6, d = 1, r = 0.5, k = 1$ and mode 2

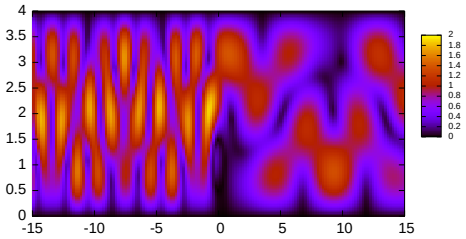

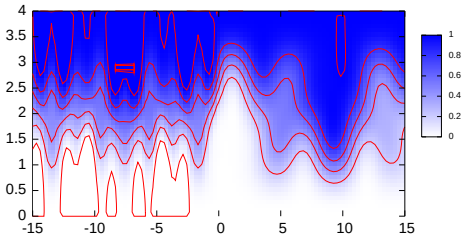

$|u(x,y)|$ $F(x,y)$

Figure 9.30: Waveguide: $N = 6, M = 6, d = 1, r = 0.5, k = 2.5$ and mode 1

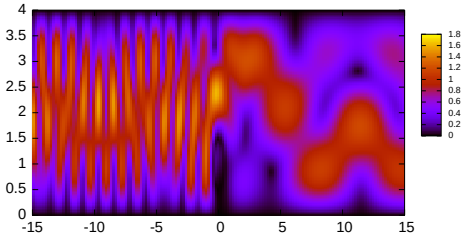

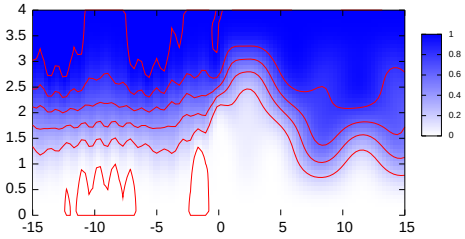

$|u(x,y)|$ $F(x,y)$

Figure 9.31: Waveguide: $N = 6, M = 6, d = 1, r = 0.5, k = 3$ and mode 1

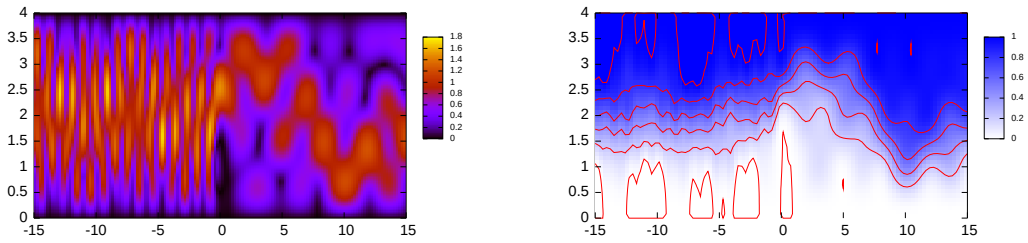

$|u(x,y)|$ $F(x,y)$

Figure 9.32: Waveguide: $N = 6, M = 6, d = 1, r = 0.5, k = 3.5$ and mode 1

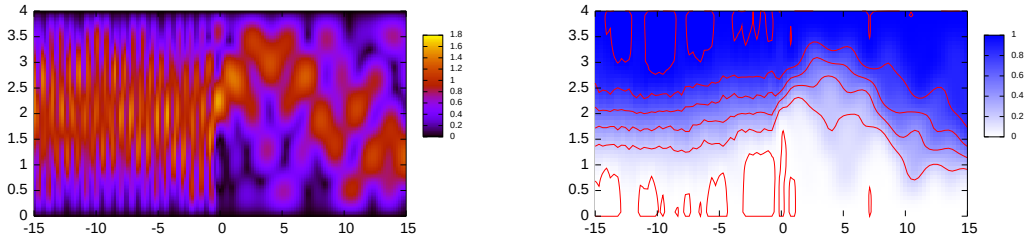

$|u(x,y)|$ $F(x,y)$

Figure 9.33: Waveguide: $N = 6, M = 6, d = 1, r = 0.5, k = 4.5$ and mode 1

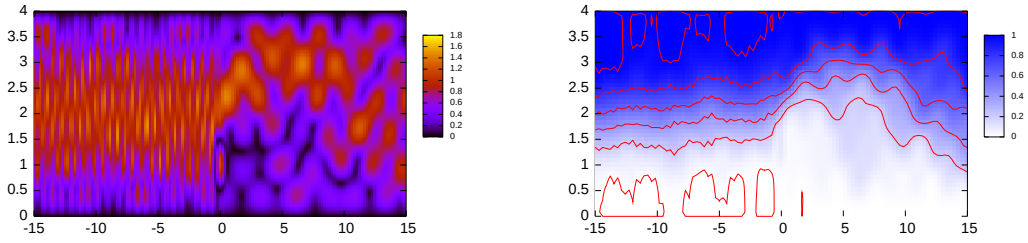

$|u(x,y)|$ $F(x,y)$

Figure 9.34: Waveguide: $N = 6, M = 6, d = 1, r = 0.5, k = 5.5$ and mode 1

9.4 Scattering in 1D

In this section, the phenomenon of time-dependent localisation is illustrated for a wave packet hitting a symmetric comb which consists of 12 evenly spaced delta potentials: 3 delta potentials with $V = 0.5$ followed by 6 delta-potentials of height 0, finally followed by again 3 delta potentials with $V = 0.5$ (cf. Fig. 9.4). The transmission and localisation coefficients for this system are displayed

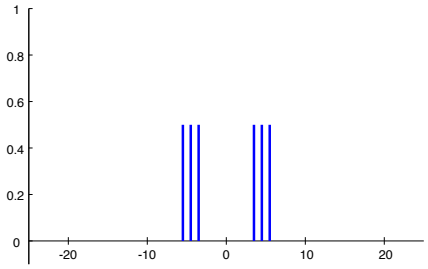

Figure 9.35: One-dimensional model for localisation

in Fig. 9.4. We see that the maxima of the transmission coefficient correspond

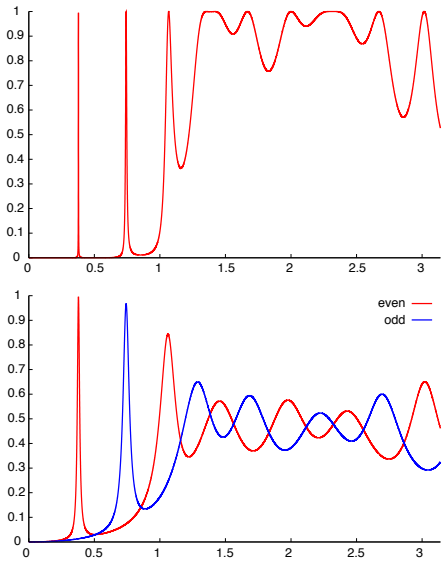

Figure 9.36: Transmission coefficient and localisation coefficient

to maxima of the localisation coefficient. Note that the latter is plotten for even (red) and odd (blue) wave functions. The numerical values for the first and the second maxima of the transmission coefficient are $k_1 = 0.3793000572532422$ and $k_2 = 0.7410735144813703$. The wave functions for these wavelength can be seen in Fig. 9.4 and Fig. 9.4 for the exact k values as well as for $k_{1,2} + 0.05$. The non-localisation of the wave function with a small deviance of the k value

is due to the sharpness of the maxima in the localisation coefficient.

In Fig. 9.39 and 9.40, a symmetric Gaussian wave packets with parameters $x_0 = \pm 800$, $\Gamma = 15000$, $c = 1$, and $k_0 = k_1$ (corresponding to the first even localised state as in Fig. 9.4) hits the finite Dirac comb as described above. To the left, the squared wave function is plotted, with a scale which permits to see the maxima of the wave packet evolving outside of the Dirac comb. To the right, the same wave function is plotted on a scale which permits to see the maximum of the wave function inside the 'crystal'. At $t = 2600$, we already see in the zoomed image to the right of the figure that a part of the wave gets 'trapped' inside the Delta potentials; while the parts of the wave which have k-values which are too far away from k_1 get reflected, the parts very near to the resonance wavelength get trapped. They lead to the formation of a second maximum (visible from $t = 4000$ on) in the free wave packet far away from the Dirac comb.

In Fig. 9.41, a similar situation is displayed for the odd localised state k_1. Note that the wave packet hitting the model is anti-symmetric; as the square of the wave function is plotted, this can not be seen in the figures – the corresponding symmetric wave packet is totally reflected.

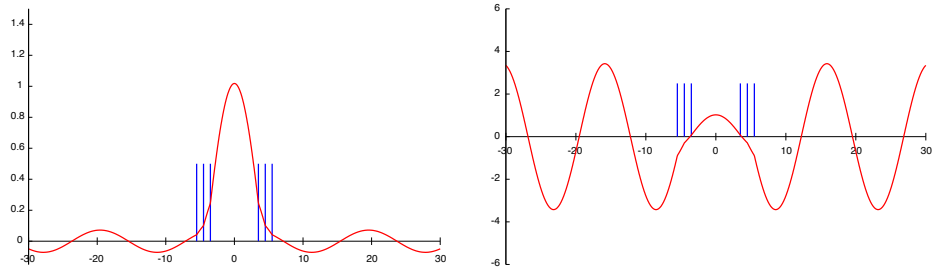

$k = k_1$ $\qquad$ $k = k_1 + 0.05$

Figure 9.37: Wave functions for 1st (even) localised state

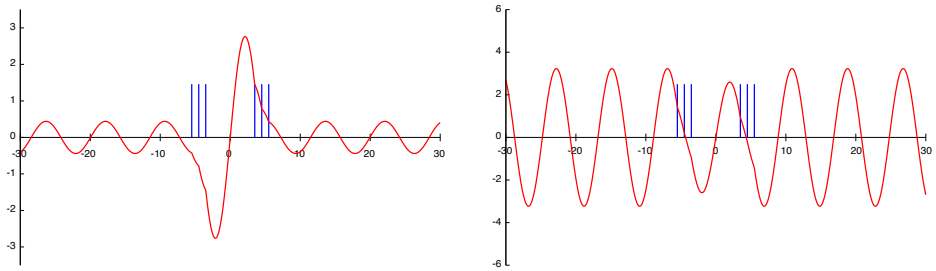

$k = k_2$ $\qquad$ $k = k_2 + 0.05$

Figure 9.38: Wave functions for 2nd (odd) localised state

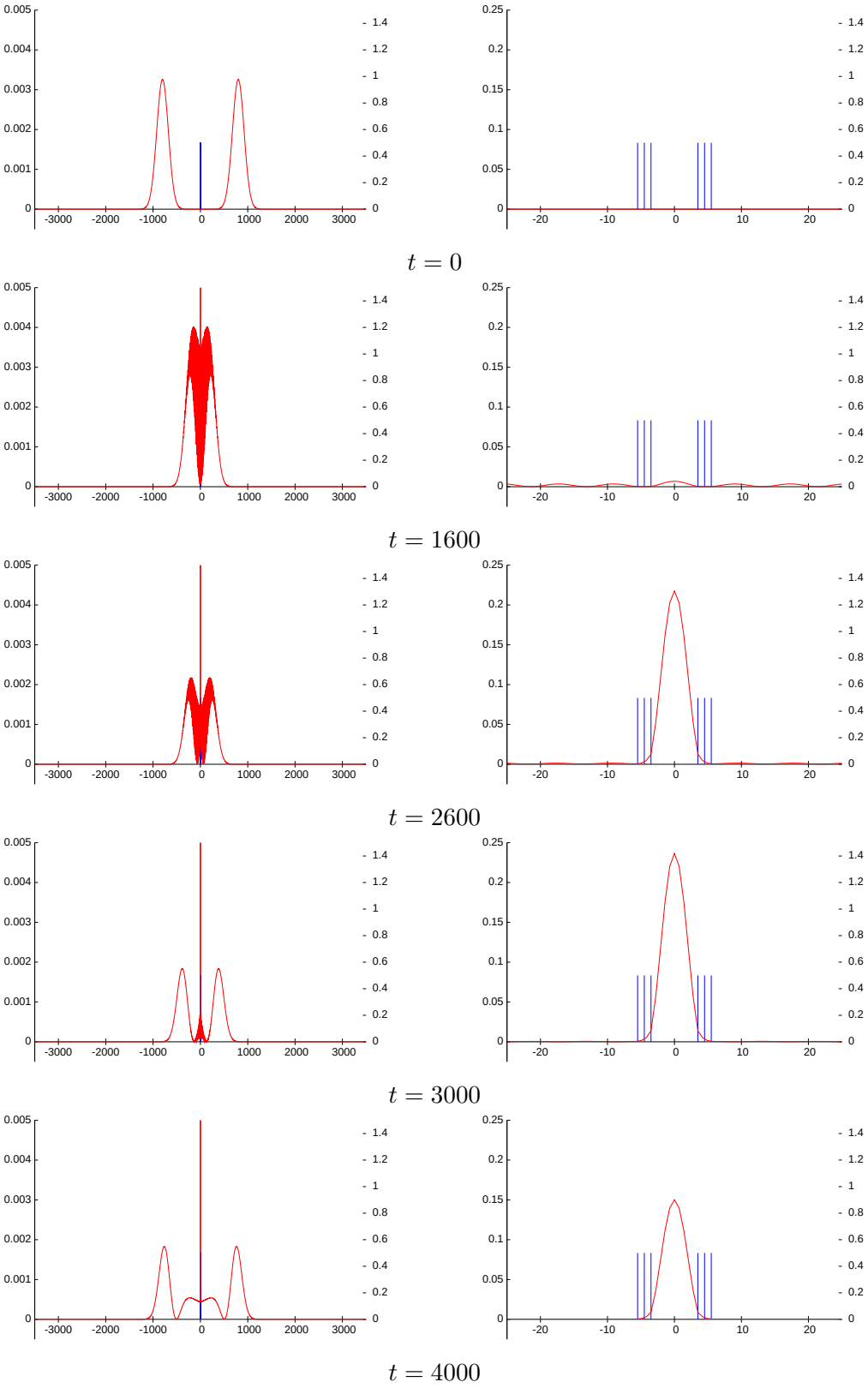

Figure 9.39: Symmetric wave packet / 1st even localised state

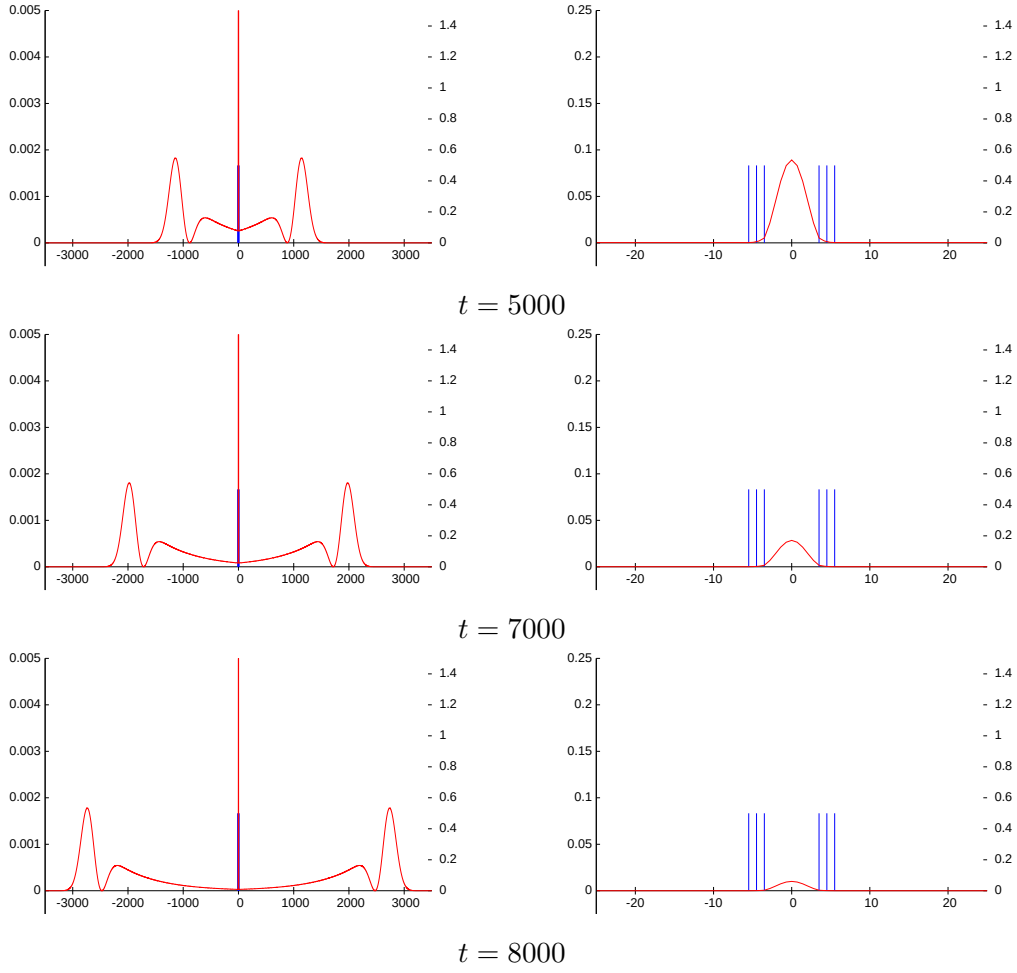

Figure 9.40: Symmetric wave packet / 1^{st} odd localised state

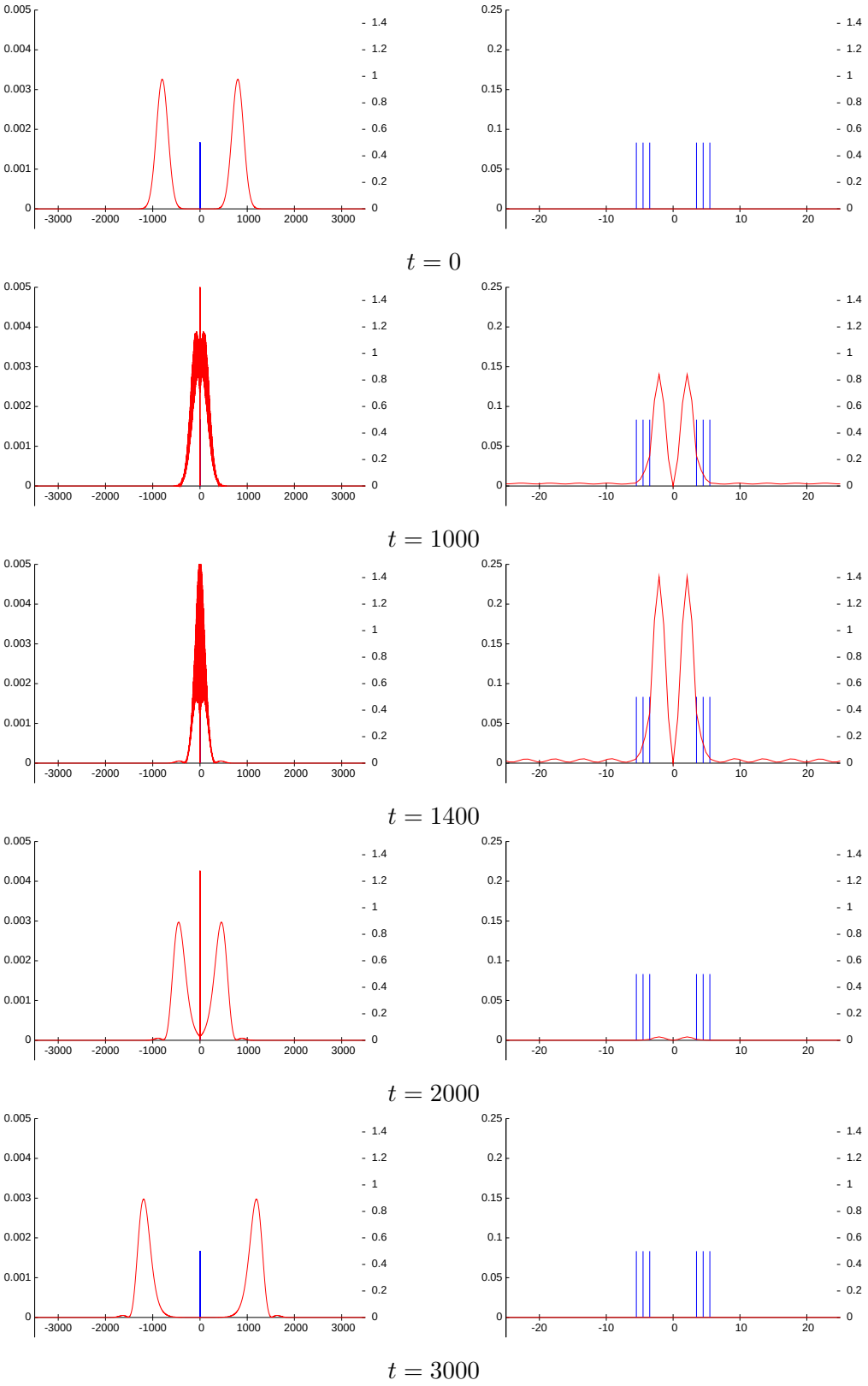

Figure 9.41: Antisymmetric wave packet / 1^{st} odd localised state

9.5 Summary

Results of the software packages for time-independent scattering in vacuum, time-dependent scattering in vacuum, time-independent scattering in a waveguide, and time-dependent localisation in one dimension were presented in this chapter. For the one-dimensional model, the time-dependent evolution of a wave packet which gets trapped inside a finite Dirac comb was shown.

Chapter 10

Conclusion

In this thesis, multiple scattering models were studied using the mathematical framework introduced in chapter 2. This framework is based on the Helmholtz equation, asymptotic boundary conditions at infinity, and boundary conditions for the obstacles. The solutions can be interpreted as two-dimensional electromagnetic, quantum mechanical, or acoustical problems.

Three models were studied: time-dependent scattering in vacuum by several elliptic cylinders, time-independent scattering in a waveguide by arbitrarily shaped objects, and time-dependent scattering and localisation in a one-dimensional Dirac comb model.

Scattering in vacuum

The solution for time-dependent scattering in vacuum by an array of elliptical cylinders is constructed in chapters 3, 6, 7 and 8: in chapter 3, time-independent scattering theory for elliptical scatterers in vacuum is introduced. No a priori limitations are imposed on the number of scatterers, on the geometric parameters that fix their elliptical form, on their orientation, on their relative positions (except that overlap is forbidden), and on their material constants. Here, time-independent scattering is formulated explicitly in elliptical geometry and solved by the separation of variables method.

The solution is obtained in two steps: first, a solution of the single scattering problem is calculated. By means of the addition theorem for Mathieu functions the outgoing field from one cylinder is then expressed in the vicinity of another cylinder as superposition of incoming fields. This is needed to fulfil the boundary conditions at all scatterers simultaneously. The procedure for the truncation of the series appearing in time-independent scattering theory is based on an a posteriori error estimate (cf. chapter 8).

To calculate the solution of the problem explicitly, we need the Mathieu functions which were introduced in chapter 7 as square-integrable eigenfunctions of commuting operators. The notation used here for the Mathieu functions [26]

excels all other notations in its simplicity, in particular the standard notation of [20]. Series for the Mathieu functions are derived; the expansion coefficients obtained in this way are used subsequently to define the Modified Mathieu functions and also to treat numerically the addition theorem for solutions of the Helmholtz equation in elliptic coordinates. In chapter 8, the details of a package of subroutines for the numerical calculation of Mathieu functions are presented. The coefficients are obtained with an iteration scheme which relies on good initial guesses for the eigenvalues; these guesses are obtained by formulating an eigenvalue procedure which is then numerically solved with standard linear algebra routines. As the calculation of these coefficients is implemented in arbitrary precision arithmetic, is is possible to obtain Mathieu functions with a higher precision than with other libraries publicly available. Note also that the routines present are not only more precise than others, but that numerical tests indicate that the available routines for the calculation of Mathieu functions fail in some parameter regions. However, this higher precision obtained here is a necessary requirement for the numerical convergence of the series in the addition theorem.

In chapter 6, the method used to obtain time-dependent wave packets as weighted superpositions of time-independent solutions which are already numerically available is presented. Analytic solutions as well as asymptotic expressions were given for scattering in vacuum; an exact analytic solution is only available for the evolution of a quantum mechanical wave packet. The evolution of this free wave packet and its interaction with the scattering wave packet is described for asymptotically large times. For the efficient calculation of numerical time-dependent solutions, it proved necessary to separate the calculation in two steps: first, the tabulation of Mathieu functions and expansion coefficients for the scattered fields; secondly, the interpolation and subsequent integration with cubature formulas to obtain the time-dependent solutions. The interpolation method as well as the performance of the cubature rules is discussed in chapter 8.

In chapter 9, results of time-independent theory are shown which agree with the ones given in literature. In addition, an application of the time-dependent code is shown: scattering by three elliptic Dirichlet cylinders.

Scattering in a waveguide

In chapter 4, we presented the problem of several Dirichlet scatterers in a waveguide where the projection of the scatterers normal to the infinite axis of the waveguide may be overlapping. For finite slices with a finite number of scatterers, we derive expressions for transfer matrices which may be used subsequently to calculate the solution for an arbitrary number of obstacles. In order to obtain these transfer matrices, an equation for the unknown source distribution at the boundary of the scatterer(s) in question is derived by a Green's function

approach. An ansatz for this unknown function is made as a Fourier series and subsequently a set of linear equations is derived which relates the coefficients of the series to the initial data given by the incident free wave which is defined left of all scatterers. In chapter 8, the important aspects of the numerical implementation chosen are discussed. In the numerical solution of the waveguide scattering problem, the large magnitude of the condition number of the transfer matrix was pointed out: a remedy to this problem is the reformulation for several scatterers in terms of the scattering matrices.

In chapter 9, we present examples of time-independent scattering in a waveguide for various wave numbers and shapes of scatterers.

One-dimensional scattering and localistion

In chapter 5, a one-dimensional localisation model based on the Schrödinger equation and a finite Dirac-comb potential was formulated. The definition of a localisation measure allows one to make predictions for the dependence of localised states on the wavelength of the incident field. In chapter 6, we have presented a method which may be used to obtain time-dependent wave packets as a weighted superposition of the time-independent solutions. Analytic solutions as well as asymptotic expressions were given: in one dimension, it is possible to find an analytic solution also for free electrodynamical and acoustical wave packets. Then, the evolution of the free wave packet and its interaction with the scattering wave packet was described for asymptotically large times in one dimension.

In chapter 9, we present an example of a time-dependent localisation phenomenon: one even and one odd 'localised' state inside a small finite one-dimensional structure are excited by a wave packet starting outside of this crystal.

Outlook

Is is intended to generalise the results from one-dimensional localisation to the two-dimensional waveguide model by formulating a transmission coefficient for various modes, defining a measure for localisation similar to the one in 1D, and finally searching for localised states for particular modes.

Bibliography

[1] P.A. Martin. Multiple scattering: an invitation. *Mathematical and Numerical aspects of wave propagation*, pages 1–15, 1995.

[2] F. Záviška. über die beugung elektromagnetischer wellen an parallelen, unendlich langen kreiszylindern. *Ann. Phys.*, 40:1024–1056, 1913.

[3] A.K. Hamid and M.I. Hussein. Iterative solution to the electromagnetic plane wave scattering by two parallel conducting elliptic cylinders. *J. of Electromagn. Waves and Appl.*, 17:813–828, 2003.

[4] J.D. Jackson. *Classical Electrodynamics*. John Wiley & Sons, New York, 1998.

[5] H. Hönl, A.W. Maue, and K. Westpfahl. Theorie der beugung. In S. Flügge, editor, *Crystal Optics, Diffraction*, page 218ff. Springer, Berlin, 1961.

[6] S.S.H. Naqvi. A comment on the use of te/tm polarization notation. *IEEE Transactions on Antennas and Propagation*, 38(4):584, 1990.

[7] E. Merzbacher. *Quantum Mechanics*. John Wiley & Sons, New York, 1963.

[8] P.M. Morse. Linear acoustic theory. In S. Flügge, editor, *Acoustics 1*, page 1ff. Springer, Berlin, 1961.

[9] M.F. Kahnert. Numerical methods in electromagnetic scattering theory. *J. Quant. Spectrosc. Radiat. Transfer*, 79-80:775–824, 2003.

[10] A.N. Tikhonov and A.A. Samarskii. *Equations of Mathematical Physics*. Pergamon Press, Oxford, 1963.

[11] A. Sommerfeld. Die greensche funktion der schwingungsgleichung. *Jahresber. Deut. Math. Ver.*, 21:309–353, 1912.

[12] J.A. Stratton. *Electromagnetic Theory*. McGraw-Hill, New York, 1941.

[13] P.M. Morse and H. Feshbach. *Methods of Theoretical Physics*, volume 1. McGraw-Hill, New York, 1953.

[14] P. Moon and D.E. Spencer. *Field Theory Handbook*. Springer, Berlin, 1961.

[15] E. Anderson, Z. Bai, C. Bischof, S. Blackford, J. Demmel, J. Dongarra, J. Du Croz, A. Greenbaum, S. Hammarling, A. McKenney, and D. Sorensen. *LAPACK Users' Guide*. Society for Industrial and Applied Mathematics, Philadelphia, PA, 1999.

[16] J. Schwinger and D.S. Saxon. *Discontinuities in Waveguides, Notes on Lectures by Julian Schwinger*. Gordon & Breach, New York, 1968.

[17] D. Colton and R. Kress. *Inverse Acoustic and Electromagnetic Scattering Theory*, volume 93. Springer, Berlin, 1998.

[18] P.A. Mello, P. Pereyra, and N. Kumar. Macroscopic approach to multichannel disordered conductors. *Ann. Phys.*, 181:290–317, 1988.

[19] Wolfram Research Inc. *Mathematica 5.1*. Wolfram Research, Inc., Champaign, Illinois, 2004.

[20] M. Abramowitz and I. Stegun. *Handbook of Mathematical Functions*, volume 55. National Bureau of Standards, 1972.

[21] P. Kasperkovitz. Asymptotic approximations for modified bessel functions. *J. Math. Phys.*, 21(1):6–13, 1979.

[22] É. Mathieu. Mémoire sur le mouvement vibratoire d'une membrane de forme elliptique. *J. math. pure appl.*, 13:137–203, 1868.

[23] L. Ruby. Applications of the mathieu equation. *Am.J.Phys.*, 64:39–44, 1996.

[24] J.J. Stamnes. Exact two-dimensional scattering by perfectly reflecting elliptical cylinders, strips and slits. *Pure Appl. Opt.*, 4:841–855, 1995.

[25] J. Piraux and B. Lombard. A new interface method for hyperbolic problems with discontinuous coefficients: one-dimensional acoustic example. *Journal of Computational Physics*, 168:227–248, 2001.

[26] J. Meixner and F. W. Schäfke. *Mathieusche Funktionen und Sphäroidfunktionen*. Springer, Berlin, 1954.

[27] G. Wolf. *Additionstheoreme Mathieuscher Funktionen*. PhD thesis, Universität Köln, Köln, 1969.

[28] K. Saermark. A note on addition theorems for mathieu functions. *ZAMP*, 10:426–428, 1959.

[29] A. Alhargan Fayez. Algorithm 804: subroutines for the computation of Mathieu functions of integer orders. *ACM Transactions on Mathematical Software*, 26(3):408–414, 2000.

[30] D. Frenkel and R. Portugal. Algebraic methods to compute mathieu functions. *J. Phys. A: Math. Gen.*, 34:3541–3551, 2001.

[31] L. Chaos-Cador and E. Ley-Koo. Mathieu functions revisited: matrix evaluation and generating functions. *Revista Mexiacana de Física*, 48:67–75, 2002.

[32] J.J. Stamnes and Bjørn Spjelkavik. New method for computing eigenfunctions (mathieu functions) for scattering by elliptical cylinders. *Pure Appl. Opt.*, 4:251–262, 1995.

[33] T. Granlund and al. *GNU Multiple Precision Arithmetic Library 4.1.4*. 2004.

[34] M. Galassi et al. *GNU Scientific Library Reference Manual*. 2004.

[35] J. Stoer and R. Bulirsch. *Introduction to Numerical Analysis*, volume 12. Springer, Berlin, 1992.

[36] G. H. Golub and J. H. Welsch. Calculation of gauss quadrature rules. *Math. Comput.*, 23:221–230, 1969.

[37] T. Sauter. Integration of highly oscillatory functions. *Comp. Phys. Comm.*, 125:119–126, 1999.

[38] D. Levin. Analysis of a collocation method for integrating rapidly oscillatory functions. *J. Comp. Appl. Math.*, 78:131–138, 1997.

[39] G.A. Evans. Multiple quadrature using highly oscillatory quadrature methods. *J. Comp. Appl. Math.*, 163:1–13, 2004.

[40] D. P. Laurie. Calculation of gauss-kronrod quadrature rules. *Math. Comput.*, 66:1133–1145, 1997.

[41] A.H. Stroud. *Approximate Calculation of Multiple Integrals*. Prentice-Hall, Englewood Cliffs, NJ, 1971.

[42] R. Cools. Constructing cubature formulae: the science behind the art. *Acta Numerica*, pages 1–54, 1997.

[43] T. Jankewitz. *Zweidimensionale Kubaturformeln*. PhD thesis, Friedrich-Alexander-Universität, Erlangen-Nürnberg, 1998.

[44] R. Cools. An encyclopaedia of cubature formulas. *J. Complexity*, 19:445–453, 2003.

[45] P. J. David and P. Rabinowitz. *Method of Numerical Integration*. Academic Press, London, 1984.

[46] W.T. Vetterling and B.P. Flannery. *Numerical Recipes in C++*. Cambridge University Press, Cambridge, 2002.

[47] J.J. Bowman, T.B.A. Senior, and P.L.E. Uslenghi. *Electromagnetic and Acoustic Scattering by Simple Shapes*. Hemisphere Publishing, New York, 1987.

[48] Sebak A. Transverse magnetic scattering by parallel conducting elliptic cylinders. *Can. J<. Phys.*, 69:1233–1241, 1991.

curriculum vitæ

Vienna, 8th February 2006

Martin Nigsch, born the 21st of January 1977 in Feldkirch, Austria

Danhausergasse 9/1
A-1040 Vienna

+43 650 7708850
martin@nigsch.com

Education

2003 – 2006	PhD Study at the Institute for Theoretical Physics, TU Vienna, Austria.
2005	Academic visitor at Imperial College, London, UK. Hosted by Prof. A. MacKinnon (Aug – Dec).
2001	Master of Theoretical Physics at the TU Vienna (with Distinction) Diploma from the École Centrale Paris in Applied Sciences
1997 – 99	TIME program at the École Centrale Paris
1997	1st degree in Applied Physics at the TU Vienna with Distinction

Professional Experience

2001 – 2003	Associate, then Consultant at The Boston Consulting Group
2000 – 01	TU Wien: Tutor for Physics beginner courses in 1st and 2nd year
before	various internships

Languages

German	Mother tounge
French	Fluent
English	Fluent
Spanish	Basic knowledge
Russian	Basic knowledge

Extracurricular Activities

Martial Arts (Wing-Tsun), Marathon running, Ballroom Dancing, Volleyball, Wining, Dining